IAHR AIRH

Supported by Spain Water and IWHR, China

IAHR 2017

37th IAHR WORLD CONGRESS

13-18 August, 2017

Kuala Lumpur, Malaysia

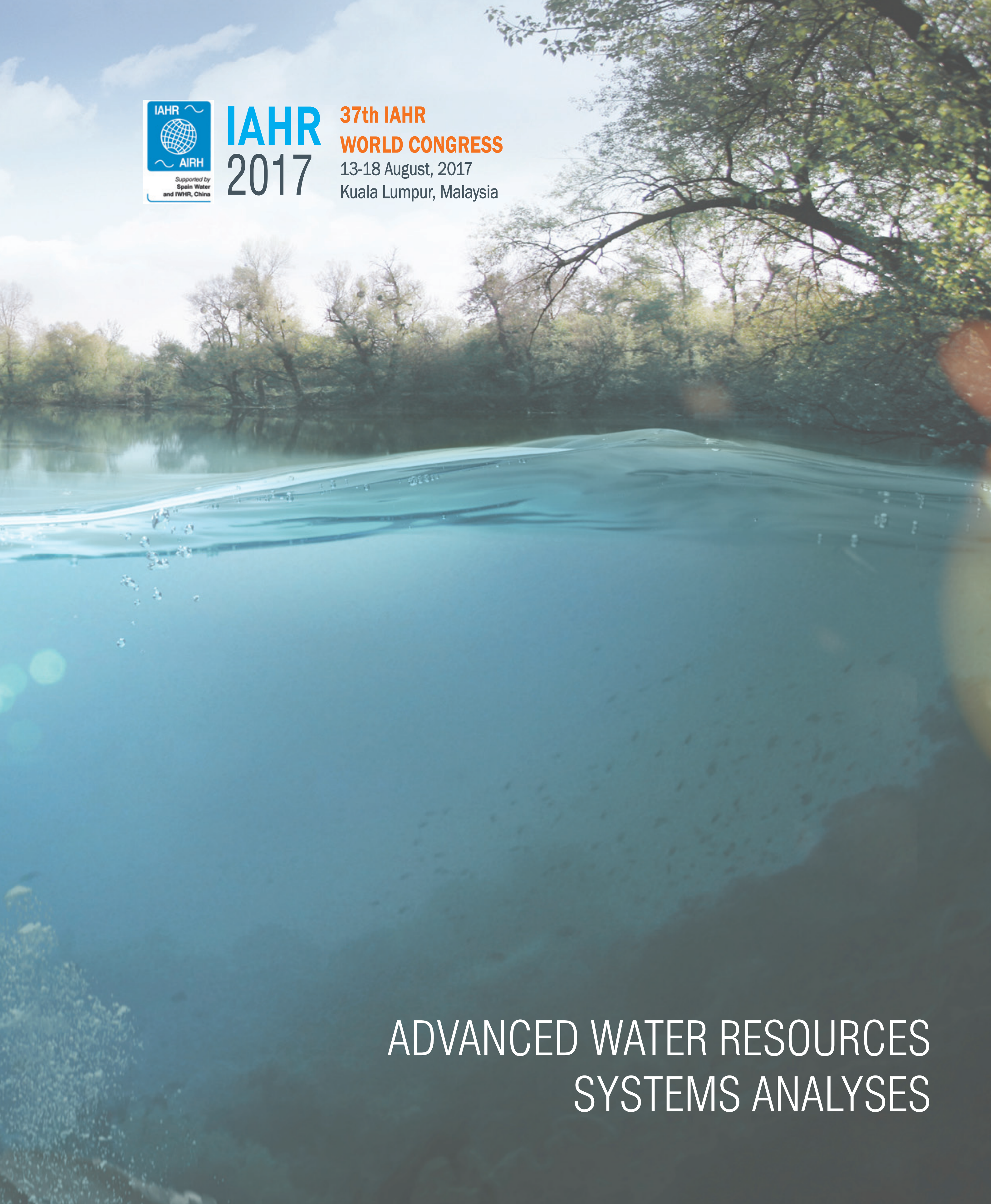

ADVANCED WATER RESOURCES SYSTEMS ANALYSES

COMPARISON ANALYSIS OF APPLICABILITY OF RUNOFF DATA EXTRACTED FROM GLDAS AND GRACE TO YARLUNG ZANGBO RIVER BASIN

HONG ZHANG(1), JIA LI(2), LINGLEI ZHANG(3), RUIDONG AN(4) & YUN DENG(5)

(1,2,3,4,5) State Key Laboratory of Hydraulics and Mountain River Engineering, College of Water Resource & Hydropower, Sichuan University, Chengdu 610065, PR China,
zhanghongsmile@yeah.net; lijia@scu.edu.cn; zhanglinglei@hotmail.com; anruidong@scu.edu.cn; dengyun@scu.edu.cn

ABSTRACT

Runoff change has a great influence on the pattern of global water cycle as well as the process of migration and transformation of biogenic matters in drainage basin. Yarlung Zangbo River is a typical lack-data basin, where the quantity of available runoff data is extremely limited and the spatial and temporal resolutions are very low. Combining total water storage variations from five data sources (*i.e.,* four models of Global Land Data Assimilation System (GLDAS), Gravity Recovery and Climate Experiment (GRACE)), precipitation and evapotranspiration from China meteorological data service center, runoff of Yarlung Zangbo River Basin are estimated by using the water balance equation. The regular of distribution, the variation trend, the continuity and mutability are comprehensively analyzed. And then, four statistical parameters (*i.e.,* Correlation coefficient (R), Mean bias (BIAS), Standard deviation of differences (σ_d), and Ratio of standard deviations (σ_r/σ_{obs})) are calculated to compare correlation and error between five data sources and in-situ measurements. At last, the Brunke ranking method is applied to comprehensively evaluate the data quality and applicability of the five data sources in Yarlung Zangbo River. The results reveal that the runoff estimated from GRACE can represent the runoff of Yarlung Zangbo River Basin better than other four models of GLDAS with a total ranking score of 2.00. This study carried out a helpful attempt on the hydrological study in lack-data basin by using several data source systems. In the matter of medium and long term, large and medium scale, the result is beneficial to deepen cognition and comprehend on the runoff characteristics of Yarlung Zangbo River, and settles foundation for setting up a data assimilation system, which is specifically aimed at Yarlung Zangbo River Basin, and then provides data, method and scientific reference for Yarlung Zangbo River Basin.

Keywords: Yarlung Zangbo River; runoff; GLDAS; GRACE; applicability analysis.

1 INTRODUCTION

Scientific management and regulation of water resource is based on the hydrologic cycle process, the system identification to its evolvement rule and the hydrologic forecast. In-situ observation data is a key basis of system identification to its evolvement rule and determines the precision of hydrologic forecast to a great extent (Zhao, 2009). However, there are a lot of lack-data basins in the world and the hydrologic forecast of these basins are facing huge difficulty and challenge. Hence, carrying out hydrological research in lack-data basins has great theoretical and practical significance.

Runoff is an important component of basin water cycle. The variation of runoff is influenced by precipitation, evapotranspiration, temperature, underlying surface condition, and human activities (Chen and Zhu, 2014). Using a variety of methods to get the runoff information has important scientific significance and social-economic benefit to get the spatial and temporal distribution regulation of runoff variation, understand the hydrologic process in large and medium scale, study regional climatic variation, manage water resource, and predict flood and draught disaster. For the moment, there are four main methods to obtain the runoff information. The first is traditional land surface observation station. The second is the radar and remote sensing. The third is hydrological models based on meteorological and hydrologic data (*i.e.,* GLDAS, Distributed Hydrologic Model, and Semi-Distributed Hydrologic Model). And, the last one is the use of GRACE (Zhong et al., 2009; Wahr et al., 1998; Luthcke et al., 2006). The land surface observation stations are distributed unevenly and a variety of internal and external conditions lead in-situ data not comprehensive. The radar and remote sensing can observe the surface runoff, but has low effect to sub-surface runoff. Meteorological and hydrologic data is not comprehensive and may affect result of distributed hydrologic model and semi-distributed hydrologic model. The GLDAS and GRACE are new methods to estimate total water storage, and combined with the water balance equation, we can easily calculate variation trend of runoff. This method provides new opportunity to the study of runoff.

At present, methods of GLDAS and GRACE to estimate total water storage have been proven in many basins. For instance, the Mississippi River, the Amazon River, Bay of Bengal, the Mekong River, the Irrawaddy River, the Nuking River, the Yangtze River, the Yellow River, the Haile River, and the Heike River

(Wahr et al., 2004; Yamamoto et al., 2007; Ma et al., 2011; Ni et al., 2014; Ren et al., 2013; Cao et al., 2012). But, study of combining GLDAS and GRACE data with meteorological data and hydrologic models to simulate basin runoff are seldom seen, mainly involve the Mississippi River, the Amazon River, the Columbia River, the Yangtze and Yellow River in China (Syed et al., 2005; Sproles et al., 2015; Ferreira et al., 2013; Qiong et al., 2016). The results show that the basin runoff spatial and temporal distribution can be well estimated by combining the water balance equation with GLDAS and GRACE data.

Yarlung Zangbo river basin is an important international river, which has the highest mean altitude (the mean altitude is above 4000 m) flowing through China, India and Bangladesh. The main stream in China is about 2057 km and ranges from 82°01′ E to 97°06′ E and from 27°40’ N to 31°17’ N. The control basin area is approximately 2.58 × 10^5 km^2, the mean stream flow is about 4.4 × 10^3 m^3/s, and the mean annual runoff is about 139.54 billion m^3, ranking third in China (Xu, 2013). The basin runoff variations will affect sustainable development of human life and social economy. Yarlung Zangbo River Basin locates on highland and cold area, so the in-situ observation runoff data is extremely lacking and the temporal and spatial resolutions are very low. Hence, in large and medium scale, and in medium and long term, study of runoff variations and trends by combining GLDAS and GRACE data with meteorological data to analyze the runoff temporal and spatial distribution is beneficial to deepen the cognition and comprehend on the runoff characteristics of Yarlung Zangbo River. The result settles foundation for setting up a data assimilation system, which is specifically aimed at Yarlung Zangbo River, and then provides data, method and scientific reference for Yarlung Zangbo River.

2 DATA AND METHODS

Combining total water storage variations from five data sources (*i.e.,* four models of GLDAS, GRACE), precipitation and evapotranspiration from China meteorological data service center, the runoff of Yarlung Zangbo River Basin were estimated by using the water balance equation. The regular of distribution, the variation trend, the continuity and mutability were comprehensively analyzed. The result settles foundation for setting up a data assimilation system, which was specifically aimed at Yarlung Zangbo River, and has a great theoretical significance and practical value to carry out hydrologic study in lack-data basin. The corresponding data and methods were as follows.

2.1 Data

2.1.1 In-situ runoff data of Yarlung Zangbo River Basin

In-situ observations of runoff data from Yarlung Zangbo River Basin were extremely lacking. At present, we got only several years of data from Nugget, Laze, Yongcun and Nuxia gauging stations locates on main stream of Yarlung Zangbo River. Based on the data from GRACE (from 2002 to 2016) and GLDAS (from 1979 to 2016), this study used in-situ runoff data of Nuxia gauging station from January 2009 to December 2013 to validate results. Figure 1a shows the water system map of Yarlung Zangbo River Basin. The control area of Yarlung Zangbo River Basin was approximately 1.9 × 10^5 km^2 and accounts for 74.21% of total basin in China, which can basically capture hydrological situation of Yarlung Zangbo River Basin. Figure 1b shows monthly runoff (R) from 2009 to 2013 of Nuxia gauging station.

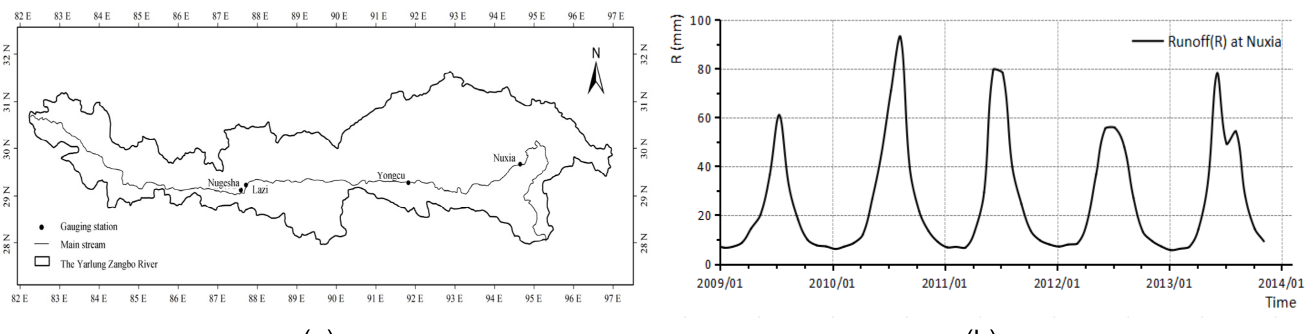

(a) (b)

Figure 1. (a) The water system map of Yarlung Zangbo River Basin and (b) Monthly runoff(R) from 2009 to 2013 of Nuxia gauging station.

2.1.2 Precipitation and evapotranspiration data

In this study, meteorological data (precipitation, evapotranspiration and temperature data) were obtained from China meteorological data service center (http://data.cma.cn). Monthly meteorological data from January 2009 to December 2013 of 38 meteorological stations in and near Yarlung Zangbo River Basin were downloaded. The 38 meteorological stations are distributed unevenly and unreasonably because of the limit of manpower, resource and natural environment. Hence, to get mean values of Yarlung Zangbo River Basin, related measures should be taken.

With the help of ArcGIS, Thiessen polygon method is used to calculate mean precipitation of a basin, which can be expressed in terms of the equation (1) as follows:

$$\overline{P} = \frac{p_1 f_1 + p_2 f_2 + \ldots + p_n f_n}{F} \qquad [1]$$

where p_1, p_2, ……, p_n is the precipitation of every single meteorological station, f_1, f_2, ……, f_n is the area of every single meteorological station, and F is the area of the whole basin.

To calculate the mean evapotranspiration of a basin, this study adopts a traditional but high precision method called Takahashi formula. The equation is as follows (Xu, 2013):

$$ET = \frac{3100 \cdot P}{3100 + 1.8 \cdot P^2 \cdot \exp\left(\frac{-34.4 \cdot T}{235 + T}\right)} \qquad [2]$$

where P is the monthly mean precipitation and T is the monthly mean temperature.

2.1.3 Computation of the total water storage(TWS) from GRACE

GRACE was developed jointly by NASA and DLR. Two satellites were launched in March 17th, 2002 in Russia. The mission is aimed at obtaining high precision medium-long wave of static earth gravitational field and determining the time variation characteristics for 15 to 30 days or even longer temporal scale of the earth gravitational field. The GRACE datasets are published by CSR (Center for Space Research, University of Texas at Austin), GFZ (German Research Center of Geo sciences) and JPL (Jet Propulsion Laboratories). We can get fully normalized spherical harmonic coefficients, $\overline{C_{lm}}$ and $\overline{S_{lm}}$, from their official website. Gravity potential and earth surface anomaly of every spatial domain can be calculated (Cao et al., 2011). The GRACE satellite mission has provided continuous satellite-based gravity data of the earth for nearly 14 years and has made a great contribution to Geophysics, Geodesy, Space science and Hydrology. The GRACE satellite can monitor high-precision hydrological signals, which has been widely studied and applied in mass balance of ice cover in polar region, mass balance of glacier in high mountains, variation of global sea level and the variation of terrestrial water storage.

In this study, 60 monthly average stokes coefficients from January 2009 to December 2013 are used, provided by RL-05 level-2 solutions from Screech monthly gravity field consists of fully normalized spherical harmonic coefficients, $\overline{C_{lm}}$ and $\overline{S_{lm}}$, to degree and order of 60. By using MATLAB, the total water storage can be successfully estimated by equivalently transform time variable earth gravity field which monitored by GRACE satellite to quality variations of earth surface, and then divide water density (Tapley et al., 2004). The calculation model is as follows (Wang, 2010):

$$\Delta \mathrm{h}(\theta,\varphi) = \frac{R\rho_{ave}}{3\rho_w} \sum_{lm} \frac{2l+1}{1+k_l} W_l P_{lm}(\cos\theta)[\Delta C_{lm}\cos(m\varphi) + \Delta S_{lm}\sin(m\varphi)] \qquad [3]$$

where l and m are the degree and order of spherical harmonics, respectively, R is the radius of the earth, ρ_{ave} is the mean quality of earth, ρ_w is the density of water, θ and φ are the co-latitude and longitude, respectively, K_l is the load love of l degree, r is the filtering radius, W_l is the smoothing kernel related to degree respectively, P_{lm} is the Legendre functions, and ΔC_{lm} and ΔS_{lm} are the variations of Stokes coefficients, respectively.

2.1.4 Computation of the total water-storage(TWS) from GLDAS

GLDAS is an off-line global land simulating system, which was developed jointly by GSFC of NASA and NCEP of NOAA. It coalesces the data both from land surface and satellite, and provides optimized land surface real-time state variable (Rodell et al., 2004; Wang. et al., 2013). GLDAS contains three land models called CLM, Noah and MOS, and one hydrology model called VIC. The four models provide 28 land surface process parameters (*e.g.,* soil moisture, surface temperature, snow water equivalent, surface and sub-surface runoff) from 1979 till now. The spatial resolution is 0.25°×0.25°and 1°×1° and the temporal resolution is 3 hours and 1 month (Hua, 2013). In this study, we used all the four models of GLDAS to provide monthly parameters of soil moisture and snow water equivalent with version-1 1.0° spatial resolution. The total water storage can be represented by soil moisture plus snow water equivalent (Xu, 2013).

2.2 Methods

2.2.1 Water balance equation

To estimate the monthly total runoff (both from surface and sub-surface) of Yarlung Zangbo River Basin, we used the water balance equation. Figure 2 is a schematic diagram for the water balance equation. Based on the monthly precipitation, evapotranspiration and variation of total water storage, we can estimate the runoff values and analyze the change rules of runoff during study period. The water balance equation is as follows:

$$P(t) — ET(t) — R(t) = \Delta S(t) \quad [4]$$

where P is the areal mean rate of precipitation, ET is the areal mean rate of evapotranspiration, R is the total basin runoff, ΔS is the total water storage variations of a basin, and t is the time.

The S estimated from GRACE Spherical Harmonic solutions were converted into the anomaly with respect to a mean gravity field of a selected period, called total water storage (TWS). In this study, while estimating the GRACE-based R(t) by water balance equation, the ΔS (t) is referred to a monthly scale value, called terrestrial water storage variations (TWSV). We used a brief and efficient way to calculate the TWSV following the method provided in Ramillien et al. (Ramillien et al., 2006). The TWSV can be denoted as:

$$TWSV\ (t) = \frac{TWS\ (t+1) - TWS\ (t-1)}{2} \quad [5]$$

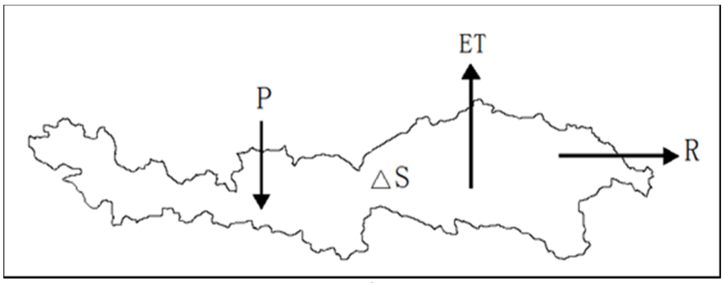

Figure 2. A schematic diagram for the water balance equation.

2.2.2 Data comparison and applicability analysis

The study calculates the total runoff of Yarlung Zangbo river basin by estimating GRACE and four models of GLDAS (CLM, Noah, MOS, and VIC) products. To analyze applicability of the five runoff products quantitatively, this paper compares these results with in-situ runoff data by four statistical quantities, (*i.e.,* correlation coefficient (R), mean bias (BIAS), standard deviation of differences (σ_d), and ratio of standard deviations (σ_r / σ_{obs})). The equations of each statistical quantity are as follows (Wei, 2007):

$$R = \frac{\frac{1}{N}\sum_{i=1}^{N}(M_i - \overline{M})(O_i - \overline{O})}{\sqrt{\frac{1}{N}\sum_{i=1}^{N}(M_i - \overline{M})^2}\sqrt{\frac{1}{N}\sum_{i=1}^{N}(O_i - \overline{O})^2}} \quad [6]$$

$$BIAS = \frac{1}{N}\sum_{i=1}^{N} D_i \qquad where \quad D_i = M_i - O_i \quad [7]$$

$$\sigma_d = \left(\frac{1}{N-1}\sum_{i=1}^{N} D_i^2\right)^{1/2} \quad [8]$$

$$\sigma_r / \sigma_{obs} = \frac{\left[\frac{1}{N-1} \sum_{i=1}^{N} (M_i - \overline{M})^2 \right]^{1/2}}{\left[\frac{1}{N-1} \sum_{i=1}^{N} (O_i - \overline{O})^2 \right]^{1/2}} \quad [9]$$

where M_i is the runoff data calculated from four models of GLDAS and CSR of GRACE, O_i is in-situ runoff data of Wuxia gauging station, $\overline{M}$ is the mean runoff data of study period from four models of GLDAS and CSR of GRACE, $\overline{O}$ is the mean runoff data of study period from in-situ runoff data of Wuxia gauging station, and N is the quantity of month during the study period.

The Brunke ranking method (Brunke et al., 2003) is applied to quantify the relative performance of the five datasets for each variable and statistical quantity. The method can comprehensively estimate quality and applicability of these five datasets of Yarlung Zangbo River Basin.

3 RESULTS AND DISSCUSSION

3.1 Precipitation and Evapotranspiration over Yarlung Zangbo River Basin

Based on the precipitation, evapotranspiration and temperature data from meteorological stations in and near Yarlung Zangbo river basin, the monthly mean precipitation and evapotranspiration during study period can be calculated by Thiessen polygon method and Takahashi formula. Figure 3a and 3b show the variation trends of monthly precipitation and evapotranspiration of Yarlung Zangbo River Resin from January 2009 to December 2013. The results show that the monthly mean precipitation and evapotranspiration both have obvious seasonal variability and the variation trends are relatively consistent. For precipitation, the monthly mean maximum values were common in July or August every year, whereas the minimum values were common in November, December and January every year. During the study period, the precipitation of July 2011 had a maximum value of 136.62 mm and the precipitation of December 2011 has a minimum value of 0.59 mm. For evapotranspiration, the monthly mean maximum values were common in July every year and July 2010 had a maximum value of 55.34 mm. The minimum values were common in December and January every year, and the evapotranspiration of December 2011 had a minimum value of 0.59 mm.

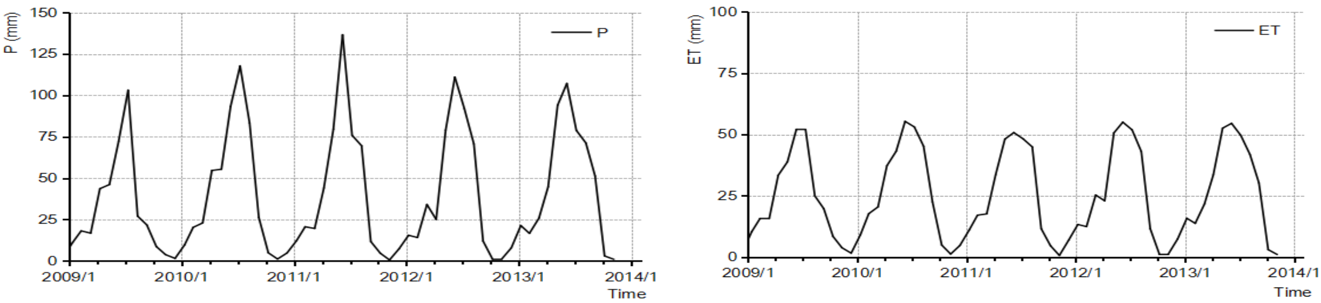

(a) (b)

Figure 3. Monthly precipitation and evapotranspiration of Yarlung Zangbo River Basin.

3.2 The TWSA over the Yarlung Zangbo River Basin

The results presented in Figure 4 show the process of total water storage anomaly calculated from four models of GLDAS (Mos, Noah, VIC, and CLM) and CSR version of GRACE. The results show similar fluctuations and all five results have significant seasonal variability in the study region. The total water storage trend of four models of GLDAS are in good agreement. Every year, the lowest TWS from GLDAS usually appear in August and September, whereas the highest TWS from GLDAS usually appear in March and April. However, TWSA calculated from GRACE has certain hysteresis. The lowest TWSA from GRACE usually appear around April, while the highest TWS from GRACE usually appear around August. The reason for this hysteresis is that the result of GRACE presented is a stable TWSA after a series of complex process, namely surface runoff, evapotranspiration, permeate, and sub-surface runoff. But, the result of GLDAS presented is not a stable TWSA as it has a link of infiltration (Liao, 2015). After linear fitting TWS during the study period, it was found that the four models of GLDAS indicate a persistent decreasing trend. TWSA declined 42 mm annually under GLDAS-MOS model, 33 mm under GLDAS-Noah model, 29 mm under GLDAS-VIC model, and declined 18 mm yearly under GLDAS-CLM model. However, TWSA of GRACE during the study period has a relative stable condition where the trend only has a slight rise.

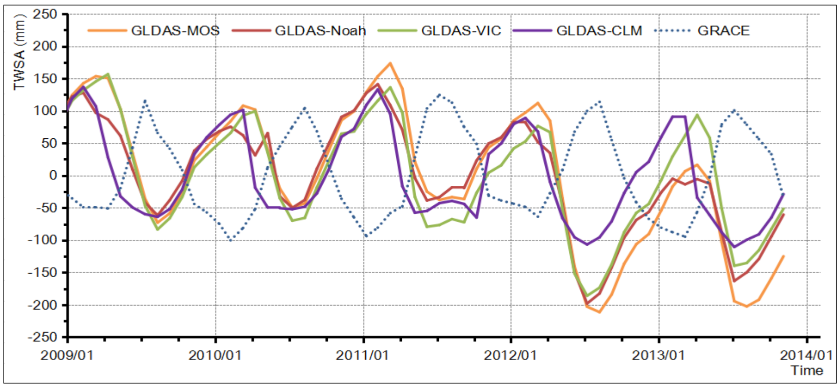

Figure 4. Monthly TWSA from GRACE and the 4 models of GLDAS.

3.3 Total runoff over Yarlung Zangbo River Basin

The total basin runoff can be estimated from the water balance equation while the basin is considered as a closed drainage system (Li et al., 2016). Yarlung Zangbo River Basin originates in northeast of Tibet Plateau and the snow melting in this area makes it one of the main runoff formation areas. Therefore, while calculating the runoff of the whole Yarlung Zangbo River basin, the snow melting from the river source should be considered. The Nugesha gauging station (NGS) is a control hydrological station on the Yarlung Zangbo River source and its catchment area is 1.06 $\times 10^5$ km^2. The runoff observed in NGS station partly represents the total runoff deduced by regional precipitation and snow melting. Thus, the runoff over Yarlung Zangbo River basin can be calculated as:

$$R_{NGS}(t) + P(t) - ET(t) - R(t) = \frac{TWSV(t+1) - TWSV(t-1)}{2} \quad [10]$$

Figure 5 presents the time series of runoff based on GRACE, four models of GLDAS (Mos, Noah, VIC, and CLM), and in-situ runoff of Nuxia gauging station. It can be seen from Figure 5 that the total runoff from five data source systems have similar fluctuations and significant seasonal variability in the study region as compared to the in-situ runoff of Nuxia gauging station. But, there were also some differences. The amplitudes of each runoff of GLDAS model are higher than the GRACE-based runoff. As for the limit values, the total runoff of four models of GLDAS (Mos, Noah, VIC, and CLM) are in good agreement. Every year, the lowest monthly runoff usually appears around November, whereas the highest monthly runoff usually appears in July and August. However, the lowest runoff from GRACE usually appears around June, while the highest runoff from GRACE usually appears in August and September. For in-situ runoff of Nuxia gauging station, the lowest runoff usually appears around February, whereas the highest runoff usually appears around August. The GRACE-based runoff data may have a more similar variation trend to the in-situ runoff data.

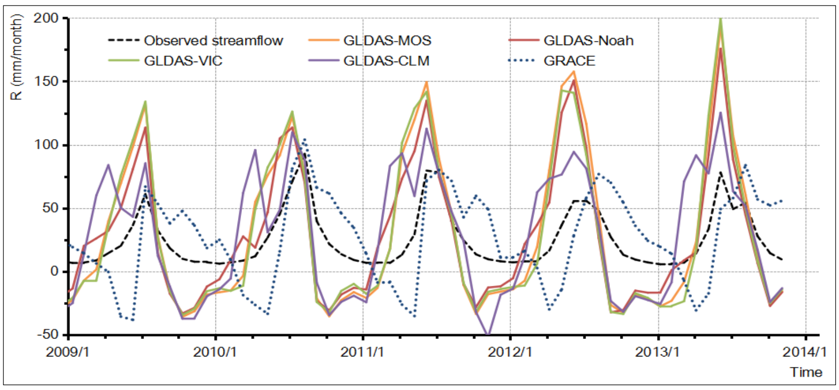

Figure 5. Monthly runoff from GLDAS, GRACE, and in-situ runoff of Nuxia gauging station.

3.4 Data comparison and applicability analysis

Using the Brunke ranking method (Liu et al., 2015), we can rank the five datasets from 1 to n (n presents the total number of datasets). If BIAS is the least (or σ_d is the least, or R is the largest), the ranking will be one. If BIAS is the largest (or σ_d is the largest, or R is the least), the ranking will be n. For σ_r/σ_{obs}, the value closest to 1 will be ranked one and the value that is the most furthest from one will be ranked n. At last, calculate arithmetic mean of each dataset from four statistical quantities rankings. We will then get the total ranking scores of these datasets.

Figure 7 present the correlation coefficient (R), mean bias (BIAS), standard deviation of differences (σ_d), and ratio of standard derivations (σ_r / σ_{obs}) between four models of GLDAS (MOS, Noah, VIC, and CLM), GRACE, and in-situ observations. Table 1 presents the average ranking scores of runoff data from four models of GLDAS and GRACE products. It can be seen from Figure 6 and Figure 7 that the correlation coefficient (R) between five datasets with in-situ runoff data have medium correlation, and R values are 0.76 ,0.73, 0.74, 0.60, 0.49, respectively. Products based GRACE has the lowest R as compared to in-situ runoff data. Based on the Brunke ranking method, the ranking score of GRACE is 5. It is the worst result. But, it was found that the products based GRACE have the best results in terms of mean bias (BIAS), standard deviation of differences (σ_d), and ratio of standard derivations (σ_r/σ_{obs}). According to the Brunke ranking method, the ranking scores of GRACE all are 1. From total ranking scores, it can be concluded that the runoff data based on GRACE is closer to in-situ runoff data of Nuxia gauging station than other four models of GLDAS. The results reveal the outcomes in Figure 5.

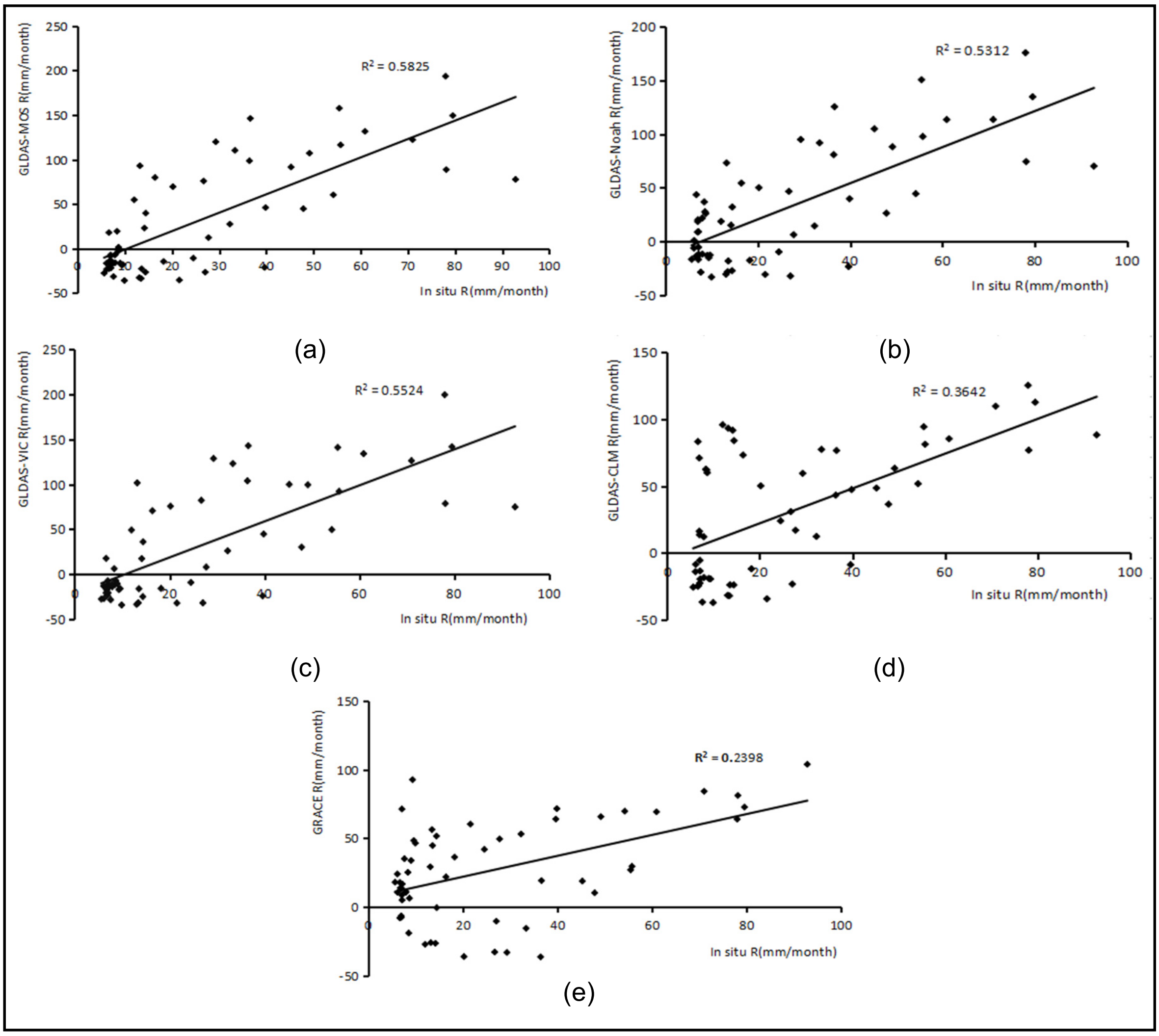

Figure 6. R between runoff data based GLDAS and GRACE with in-situ runoff data.

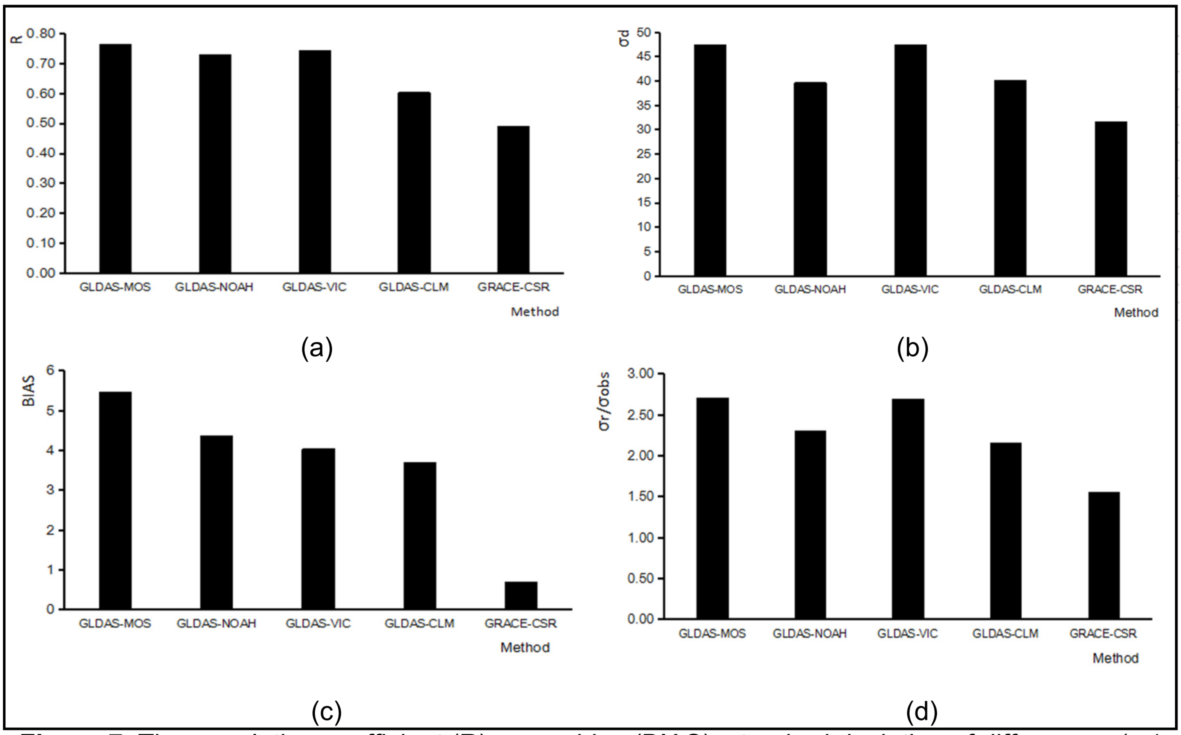

Figure 7. The correlation coefficient (R), mean bias (BIAS), standard deviation of differences (σ_d), ratio of standard derivations (σ_r/σ_{obs}) of GLDAS, GRACE, and in-situ observations.

Table 1. The average ranking scores of runoff data from four models of GLDAS and GRACE products.

Name	GLDAS-MOS	GLDAS-NOAH	GLDAS-VIC	GLDAS-CLM	GRACE
R	1	3	2	4	5
BIAS	5	4	3	2	1
σ_d	4	2	5	3	1
σ_r/σ_{obs}	5	3	4	2	1
Total ranking scores	**3.75**	**3.00**	**3.50**	**2.75**	**2.00**

4 CONCLUSIONS

In this paper, we calculate the total runoff of the Yarlung Zangbo River Basin on a monthly time scale from February 2009 to December 2013 based on the water balance equation. Combining the total water storage (TWS) variations estimated from Gravity Recovery and Climate Experiment (GRACE), four models of Global Land Data Assimilation System (GLDAS), precipitation and evapotranspiration data calculated from Thiessen polygon and Takahashi formula, and in-situ runoff data, the total runoff over the Yellow River Basin are estimated. To analyze the applicability of runoff in five datasets, four statistical parameters (*i.e.,* Correlation coefficient (R), mean bias (BIAS), standard deviation of differences (σ_d), and ratio of standard deviations (σ_r/ σ_{obs})) are calculated. And, the Brunke ranking method is applied to quantify the relative performance of the five datasets for each variable and statistical quantity.

Based on the results of comparison with in-situ runoff data of Nuxia gauging station, it can be concluded that the runoff data from four models of GLDAS can partially represent the runoff over the Yarlung Zangbo River Basin. The runoff data based on GRACE is closer to in-situ runoff data of Nuxia gauging station than other four models of GLDAS.

In conclusion, the Yarlung Zangbo River is a typical lack-data basin, where the quantity of available runoff data is extremely limited and the spatial and temporal resolutions are very low. The method we used can comprehensively estimate the quality and applicability of these five data sources of Yarlung Zangbo River Basin. The result settles foundation for setting up a data assimilation system, which is specifically aimed at Yarlung Zangbo River, and then provides data, method and scientific reference for Yarlung Zangbo River. We believe that the results will help to understand the global water cycle.

ACKNOWLEDGEMENTS

This work was funded by the National Natural Science Foundation of China (No. 91547211) and the National Key R&D Program of China (No. 2016YFC0502200). The authors also would like to thank the CSR providing the RL05 GRACE gravity data and the GES DISC providing GLDAS data. The work of these scientists is the basis for our investigations.

REFERENCES

Brunke, M.A., Fairall, C.W., Zeng, X., Eymard, L. & Curry, J.A. (2003). Which Bulk Aerodynamic Algorithms are Least Problematic in Computing Ocean Surface Turbulent Fluxes?. *Journal of Climate*, 16(4), 619-635.

Chen, H.L. & Zhu, K. (2014). Research Advance of Annual Runoff Characteristic and Prediction*. Agriculture and Technology*, 34(1), 162-164.

Cao, Y.P., Nan, Z.T. & Hu, X.L. (2012). Changes of Groundwater Storage in the Heihe River Basin Derived from GRACE Gravity Satellite Data*. Journal of Glaciology and Geocryology.* 34(3), 680-689.

Cao, Y.P. & Nan, Z.T. (2011). Applications of GRACE in Hydrology: A Review. *Remote Sensing Technology and Application,* 26(5), 543-553.

Ferreira, V.G., Gong, Z., He, X., Zhang, Y. & Andam-Akorful, S.A. (2013). Estimating Total Discharge in the Yangtze River Basin using Satellite-Based Observations. *Remote Sensing*, 5(7), 3415-3430.

Luthcke, S.B., Zwally, H.J., Abdalati, W., Rowlands, D.D., Ray, R.D., Nerem, R.S., ... & Chinn, D.S. (2006). Recent Greenland Ice Mass Loss by Drainage System from Satellite Gravity Observations. *Science*, 314(5803), 1286-1289.

Hua, L.R. (2013). *Read Me Document for Global Land Data Assimilation System Version1 (GLDAS-1),* [EB/OL].

Liu, C., Yu, Y., Xie, J., Zhou, X., Li, J.L. & Ge, J. (2015). Applicability of Soil Temperature and Moisture in Several Datasets over Qinghai-Xizang Plateau. *Plateau Meteorology*, 34(3), 653-665.

Liao, M.S. (2015). Change of Water Reserves in Recent Ten Years from GRACE and GLDAS in Dongting Lake Basin. Changsha: Hunan Normal University.

Li, Q., Zhong, B., Luo, Z. & Yao, C. (2016). GRACE-Based Estimates of Water Discharge over the Yellow River Basin. *Geodesy and Geodynamics*, 7(3), 187-193.

Ma, Q., Xie, Z.H., Chen, F., et al. (2011). Temporal and Spatial Distribution of Terrestrial W at Er Storage in the Yangtze River Basin during1982-2005*. Climatic and Environmental Research*, 16(4), 429-440.

Ni, S.N., Chen, J.L. & Li, J. (2014).Terrestrial Water Storage Change in the Yangtze and Yellow River Basin from GRACE Time Variable Gravity Measurements. *Journal of Geodesy and Geodynamics*, 34(4), 49-55.

Ren, Y.Q., Pan, Y. & Gong, H.L. (2013). Analysis of Underground Water Storage in the Haihe River Basin*. Journal of Capital Normal University*, 34(4), 49-55.

Rodell, M., Houser, P.R., Jambor, U.E.A., Gottschalck, J., Mitchell, K., Meng, C.J., ... & Entin*, J.K. (2004). The Global Land Data Assimilation System. *Bulletin of the American Meteorological Society*, 85(3), 381-394.

Ramillien, G., Frappart, F., Güntner, A., Ngo-Duc, T., Cazenave, A. & Laval, K. (2006). Time Variations of the Regional Evapotranspiration Rate from Gravity Recovery and Climate Experiment (GRACE) Satellite Gravimetry. *Water Resources Research*, 42(10), 1-8.

Syed, T.H., Famiglietti, J.S., Chen, J., Rodell, M., Seneviratne, S.I., Viterbo, P. & Wilson, C.R. (2005). Total Basin Discharge for the Amazon and Mississippi River Basins from GRACE and a Land‐Atmosphere Water Balance. *Geophysical Research Letters*, 32(24), 1-5.

Sproles, E.A., Leibowitz, S.G., Reager, J.T., Wigington Jr, P.J., Famiglietti, J.S. & Patil, S.D. (2015). GRACE Storage-Runoff Hystereses Reveal the Dynamics of Regional Watersheds. *Hydrology and Earth System Sciences*, 19(7), 3253-3272.

Tapley, B.D., Bettadpur, S., Ries, J.C., Thompson, P.F. & Watkins, M.M. (2004). GRACE Measurements of Mass Variability in the Earth System. *Science*, 305(5683), 503-505.

Wahr, J., Molenaar, M. & Bryan, F. (1998). Time Variability of the Earth's Gravity Field: Hydrological and Oceanic Effects and Their Possible Detection using GRACE. *Journal of Geophysical Research: Solid Earth*, 103(B12), 30205-30229.

Wahr, J., Swenson, S., Zlotnicki, V. & Velicogna, I. (2004). Time-Variable Gravity from GRACE: First Results. *Geophysical Research Letters*, 31(11), 1-4.

Wang, Y., Wang, S., Song, W. & Yang, S. (2013). Application of GLDAS Data to the Potential Evapotranspiration Monitoring in Weihe River Basin. *Journal of Arid Land Resources and Environment*, 27(12), 54-58.

Wei, F.Y. (2007). *Modern Climatic Statistical Diagnosis and Prediction Technology.* Beijing:Climate Press,1-298.

Wang, F. (2010). *Research of Region Water Storage based on the Gravity Satellite.* Chengdu:University of Electronic Science and Technology of China.

Xu, P.K. (2013). *Study on Glacier & Groundwater Mass Changes of Yarlung Zangbo River Basin in the Recent Years.* Nanjing: Nanjing University.

Yamamoto, K., Fukuda, Y., Nakaegawa, T. & Nishijima, J. (2007). Landwater Variation in Four Major River Basins of the Indochina Peninsula as Revealed by GRACE. *Earth, planets and space*, 59(4), 193-200.

Zhao, Z.X. (2009). *Prediction in Ungauged Basins (PUB) and It's Application on Flood Risk Elimination of Tangjiashan Barrier Lake.* Tianjin: Tianjin University.

Zhong, M., Duan, J.B., Xu, H.Z., et al. (2009). The Observation of China Terrestrial Water Storage Trend in Medium and Long Scale by the use of Gravity Satellite in Recent 5 Years. *Chinese Science Bulletin*, 54(9), 1290-1294.

SUSTAINABLE WATER RESOURCE MANAGEMENT AND THE UNCERTAIN ROLE OF SURFACE WATER IN LESS DEVELOPED COUNTRIES

MICHEL SOTO CHALHOUB[(1)]

[(1)]Department of Civil and Environmental Engineering, Notre Dame University, Louaizeh, Lebanon
Engineering Building, Rm 2074, mchalhoub@live.com

ABSTRACT

Developing countries face special challenges in water resource management including lack of environmental policies, technological gap, limited community involvement and demographic movement. The present research addresses an engineering component and a public policy component related to surface water and challenges due to the uncertainties of its flow in watercourses. A mathematical model is developed to illustrate the uncertainty in surface flow and the need for the statistical rather than deterministic approaches to account for the variability in its parameters. Upgrades in commonly used formulations are necessary to accommodate the peculiarities of medium to small streams. A second mathematical model is developed to analyze the empirical data for water policy recommendations. Field data was collected in Byblos County, Lebanon, in the East Mediterranean, which is endowed with high precipitation rates as compared to the region and yet, suffering from water shortage. In a multivariate linear regression analysis, a dependent variable was defined as the sustainability of surface water as a primary source of supply. Three independent variables were defined as X_1, the reliability of projections for surface flow given its uncertainty, X_2, the effectiveness of establishing a multi-decade surface water management program, and X_3, the effectiveness of transitioning to groundwater for processing and end-use. Results show that the first variable is statistically significant but negatively correlated, while the second and third variables are statistically significant and positively correlated. In addition, the secondary data confirms a continuous movement from rural to urban areas. Based on those results, it is recommended that a national water resource management plan is established with an environmentally sustainable multi-decade implementation program. The program needs to be intimately linked to the environmental protection policies that are starting to be applied in the country.

Keywords: Sustainable water resource management; surface watercourses flow; surface water policies; groundwater transition.

1 INTRODUCTION

In natural resource management, surface water is one of the most important components of the water cycle as it is supposed to offer the simplicity and accessibility as compared to subsurface fresh water or other sources (Lenton and Muller, 2009; Pidwirny, 2006). Yet, it has been an enduring concern that surface water suffers from mismanagement especially in developing countries (Turall, 1997; Grigg, 2002). For instance, in the Levant mountains of Lebanon, over 80% of surface water goes back to the Mediterranean without proper use (El-Fadel et al., 2000; Makdisi, 2007).

Surface water issues are numerous and are not only typical of developing countries as many developed countries face scarcity and have the need to establish environmental friendly and sustainable solutions to water demand (EPRI, 2009; Dourojeanni, 2001). Uncertainty is due to many factors especially the variability in precipitation, river flows, and air temperature. This makes the study of uncertainty even more important because it affects the physical phenomena as well as the decision making of policy (Grigg, 2016).

Water supply in most policy frameworks is carried out within a deterministic framework instead of a probabilistic methodology (Boucher et al. 2012). As such, boundary or reference values are set for inputs including the best estimates or the worst case scenarios are used as the key parameters, such as population growth, river flow, and local water demand (Wilks, 2006). Sources of uncertainty for water supply in this case are addressed only qualitatively in prioritizing solutions for decision making. Planning under uncertainty, on the other hand, improves the reliability of estimates and ensures that the results are neither overly conservative nor overly optimistic (Zhao et al., 2012).

Uncertainty in surface water affects groundwater and the dynamic interaction between the availability of groundwater and surface water supply poses additional challenges in simulating water resources (Yen and Riggins, 1991; Sophocleus, 2002). It is a common practice that simplified assumptions are made to reach a workable mathematical model. The uncertainty of surface water sources includes precipitation, physical processes, variability in river flows, and human use or interventions. Meanwhile, the uncertainty of groundwater sources includes dimensional effects in terms of natural reservoir, boundary conditions and associated recharge rates. River flows and aquifer are linked through a natural process but can also be actively managed if planned based on the consumption and demand. Water transfers to the stream if the aquifer level is greater than that of the stream and vice versa (Sophocleus, 2002). For that purpose, simulations such as Monte Carlo were applied to model surface-subsurface water interaction. Monte Carlo techniques require simplifying the assumptions but maintain the probabilistic nature of the input parameters (Peck et al., 1988).

2 FROM ENGINEERING TO PUBLIC SECTOR APPLICATIONS: NEED FOR UNCERTAINTYANALYSIS

Knowledge about the close and continuous interaction between the surface and ground water is not new, and the extraction of underground water is not a novel approach to public management in meeting the demand of communities. Over 3000 years ago, wells were dug in an inclined manner to compensate for drought and scarcity in surface water. Greeks and Romans had their share in executing works in ground water extraction and distribution to serve communities under public management (Baker and Horton, 1936; Todd and Mays, 2005). In Arabia, *Qanats*, or channels, were dug to extract ground water and distribute to districts (Lightfoot, 2000). Supported by the government, research on groundwater flourished in France in the 1600s and was extended in later centuries to address infiltration theory, the hydrologic cycle, and the mathematical modeling of seepage in soil media (Biswas, 1970). Darcy presented work on the water seepage in soil media, which became the basis of many computational packages used in our current days in analyzing subsurface water flow (Todd and Mays, 2005).

Between the 1950s and the 1980s, computational trends moved from the traditional water cycle studies to a decision support from the demand side, rather than studying the supply side (Thornthwaite and Mather, 1957, Burnash et al., 1973). The trend was also driven by concerning the global climate change (Nemec and Schaake, 1982; Gleick, 1987). As climate change gained priority on policy-makers agendas, the interest in turning to groundwater as a source of supply and its interaction with surface water was on the rise. In 1995, the United States Geologic Survey published data about the groundwater extraction reaching over 400,000 million gallons per day within the United States, accompanying an expansion between the 1940s and the 1990s in agricultural applications, automation of irrigation and cattle cleaning systems (Todd and Mays, 2005). The accelerated development in analysis tools and techniques for surface and subsurface water flow was supported by advancing in high speed computing technologies, but still, the main driver behind such analyses was the rising concern and increased the research interest on global environmental issues and climate change (EPRI, 2009, Salman and Bradlow, 2006). With the boom in computational techniques for water cycle studies, it was apparent that the accuracy in providing estimates required for the decision making of public sector would still benefit from a better handle in handling uncertainty in input parameters. As such, there is a need to mathematically and systematically account for uncertainty in models to set the reasonable expectations when an engineering analysis is presented to policy makers (Stave, 2002; Loucks and Van Beek, 2005).

3 DETERMINISTIC VERSUS STOCHASTIC WATER RESOURCE ESTIMATES

Communicating results with public decision makers and local communities would be more realistic, if uncertainty is properly included (Montanari, 2007). Setting expectations using uncertainty analysis would offer a more credible view on the river flow parameters than deterministic approaches (Beven, 2006). This becomes particularly important in basins where there is no direct measurement and hence, the mathematical models are critical in providing a relatively accurate means of extrapolating or interpolating field data results (Sivapalan et al., 2003).

There are many sources of uncertainty that we shall categorize as global, related to the general environment or pertaining to the major long term events such as climate change, and local, pertaining to specific regions and the characteristics of surface water in a restrained environment. Research on global issues such as potential greenhouse effect on the regional water resources addressed predictions for the twenty first century (Arnell and Reynard, 1993; 1996). Some use a general circulation model (GCM) to provide the climatic model inputs and study their effects on water resources (WMO, 1997). These sources of uncertainty buildup in the modeling process and provide a divergence in the final result. Goetzinger and Bardossy categorize the sources of uncertainty in three different groups pertaining to colleting observations, selecting parameters, and developing the mathematical model. They argue that the source of divergence is due to the parameter selection and mathematical modeling assumptions more so than from observations. It was confirmed that the uncertainty due to observation has less significant effects than the parameter selection and modeling (Goetzinger and Bardossy, 2008).

For example, if we consider the uncertainty related to the river discharge using the velocity-area method, with the relationship of $Q\ (s, t) = A\ (s, t).\ v\ (s, t)$, where Q is the discharge, A is the cross-sectional area, and v is the average velocity over the cross-section. All quantities vary as a function of location along the river bed, and time. In a deterministic mode, the quantities require to define a priori and the relationship becomes a simple multiplication. However, if uncertainty is accounted for all three quantities, Q, A, and v would be represented by a probability distribution of a given shape. A common shape used is the Gaussian distribution (Peck et al., 1988). The relationship is hence the one between three Gaussian curves rather than three simple parameters (Chalhoub and Jenkins, 1994). Uncertainty in the area and velocity propagates in the flow values. Clearly, the area cannot be exactly computed and the velocity may vary over the cross section. As far back as the 1980s,

  / ISSN 1562-6865 (Online) - ISSN 1063-7710 (Print)

researchers showed that depending on the number of sampling points where velocity is measured, the river discharge can vary between 8% and 20% with 95% confidence level (Pelletier, 1987).

Unsteady flow conditions induce uncertainty as well. This is particularly accentuated when the bed is weedy and does not lend itself to a single roughness value (Dottori et al., 2009). The roughness affects the values of flow in a one-on-one relationship due to the roughness coefficient presents in the denominator of the expression for *Q*. The roughness depends on the status of the vegetation, and that in turn, is affected by the season (Franchini et al., 1999). There have been diverging views as to whether the rating curves can be extrapolated beyond a certain range (Rantz et al., 1982; Pappenberger et al., 2006). It is therefore important to quantify the uncertainty in river flow, and the river flow data collected in the field, as part of hydrological processes (Montanari and Grossi, 2008).

4 ENGINEERING MATHEMATICAL MODEL OF SURFACE WATER IN OPEN CHANNELS

4.1 Limitations of common river-flow formulas

Open channel formulations are used to model surface water flowing in watercourses by simplifying the assumptions about the shape of the section, the roughness of the river bed, and the water particle velocity distribution (French, 1985). The shape of the channel cross-section is often over-simplified and modeled as a rectangular or trapezoidal shape. This approach may work for engineered canals built in a controlled

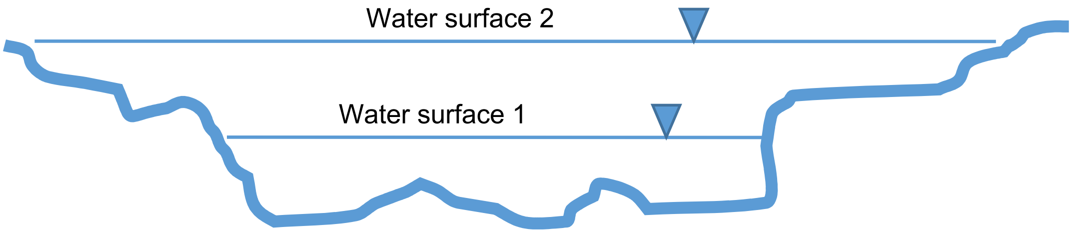

Figure 1a. Natural cross-section.

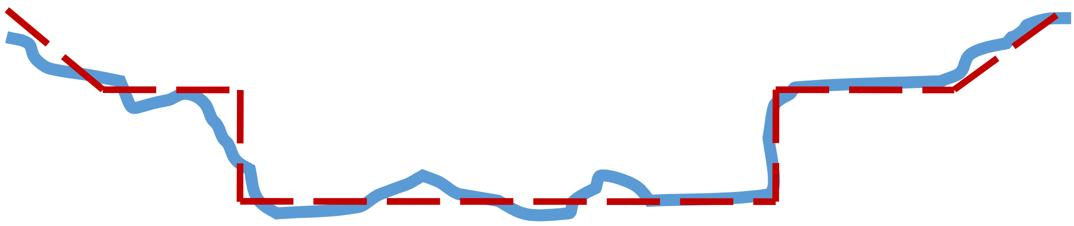

Figure 1b. Stylized cross-section.

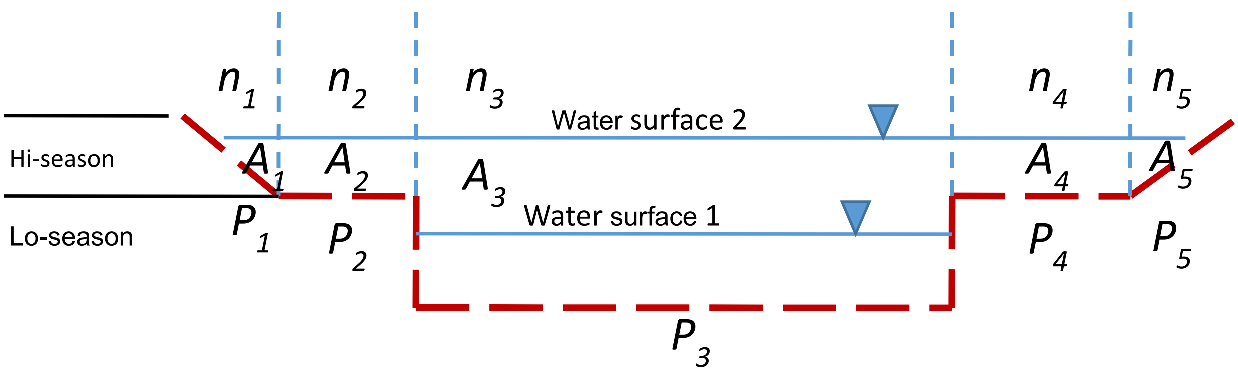

Figure 1c. Mathematical cross-sectional model.

environment, but results diverge from the reality when the shape is a natural result of water flow, erosion, and sediment transport. In the field, a large variation occurs in channel sectional shapes as you move along the longitudinal axis of the watercourse. The cross-sectional shape also varies in time depending on the season whereby water may occupy the middle section or may overflow across the river banks. The cross section is therefore a variable and a function of both time and space (Chalhoub, 2013).

River bed gradient has a high variability in most mountainous countries. In Lebanon, for example, all major rivers start with small waterways, streams and creeks in steep mountains overlooking the Mediterranean where the flow drastically decreases or disappears in summer and outbursts in winter and spring as snow melts. Weeds grow abundantly in the spring and cause significant changes in the river bed roughness coefficient, a parameter that is typically assumed constant in open channel flow problems (Chalhoub, 2013). In addition to vegetation, river beds typically contain boulders, large stones, and algae growth (Yalin, 1992). The majority of the mathematical models for open channels make plain assumptions about the steady-state behavior while they do not apply in areas of seasonal watercourses that may take several weeks to saturate the river bed before they appear above grade. The wavering nature of the river course also contributes to the divergence between the simplified formulae results and real life behavior. On a river bent, the water surface will take an inclined shape to compensate for the centrifuge force. As a result, the water depth would be larger on the outer side of the river bent than it would be on the inner side (Chalhoub, 2013).

The variations discussed above are better modeled with the stochastic parameters rather than deterministic. For this reason, accounting for uncertainty leads to better results and more reliable reporting, which in turn offer a more reasonable platform for policy decision making. We therefore propose that the roughness coefficient, denoted by *n*, should not be assumed to be constant for a given river bed material as tabulated in most open channel flow literature (Manning, 1891). The roughness coefficient will vary significantly with the geometry of the section, bents and the flow rate of an open channel (Chalhoub, 2013).

4.2 Mathematical modeling of roughness-flow rate interaction

The hydraulic radius, R is defined as the ratio of the cross-sectional area (A) to the wetted perimeter (P):

$$R = \quad A / P \qquad [1]$$

However, in natural watercourses or small rivers, the cross-sectional shape is seldom rectangular or trapezoidal. The area, the wetted perimeter, and the roughness coefficient change with the flow depth, which in turn depends on the season. During low season, the water flow is limited to the deeper middle section while in the high season, the river banks carry an additional flow (Figure 1a). The natural cross section can be stylized by breaking it down into simple geometric shapes, as shown by the dashed line overlaid on the cross section (Finnemore and Franzini, 2009). The total flow is computed as the sum of the sub-flows in each sub-section respectively (Figure 1b and 1c). Since the free water surface could be located at any depth depending on the season and the precipitation, a threshold is defined to separate low season flow from high season flow that corresponds to different roughness coefficients (Figure 1c). Manning coefficients may vary from n_3 around 0.033 for a well-charted relatively smooth natural stream bed up to n_1 or n_5 in the range of 0.15 for a weedy river bank, which is more than four times the resistance to water flow. The mathematical cross-sectional model is obtained by breaking down the flow into components where we can compute A_i, P_i, and R_i, with a corresponding n_i so that the flow can be computed as:

$$Q = \sum_{i=1}^{5} Q_i = \sum_{i=1}^{5} \frac{C\, A_i\, R_i^p\, S^r}{n_i} \qquad [2]$$

where C is a constant in the Manning equation that accounts for the system of units (e.g. $C = 1.486$ for a numerical application in US Customary units) and S is the slope at that particular location of the cross section. The hydraulic radius and the slope are raised to the power p and r, respectively. Through experiments, Manning concluded that for simple channel sections, which is the case of sub-sections where $i=1, \ldots, 5$, p could be taken as $2/3$ and r as $1/2$, respectively, with a reasonable agreement with scaled laboratory tests (Manning, 1891).

A numerical application was performed for a small river in Byblos County in Mount Lebanon that has a total river bed width ranging between 14 m and 20 m in the vicinity of the station used to measure flow velocity. During high season in 2016, the flow velocity measured between 0.85 and 1.1 m/s. The average high season water depth, away from the boulders and large depressions in its bed, was about 1.5 m. In the mathematical model, a 16 m river section width was used and was subdivided into 0.5 m, 2 m, 10 m, 2.5 m, and 1 m segments of horizontal projection for sections A_1, A_2, A_3, A_4, and A_5, respectively. A total water depth of 1.5 m was used in the middle section corresponding to A_3 and 0.5 m depth in the banks. The Manning coefficient was selected for each subsection independently whereby for the outer weedy sections $0.075 \le n_1 = n_5 \le 0.15$, for the river banks near the main bed, $0.045 \le n_2 = n_4 \le 0.06$, and for the main bed $0.025 \le n_3 \le 0.033$. The results are summarized in Table 1.

Table 1. Results from the subsection mathematical model.

Subsection	1	2	3	4	5	Total
ni-min	0.075	0.045	0.025	0.045	0.075	-
ni-max	0.150	0.060	0.033	0.060	0.150	-
Qi-min (m^3/s)	0.0069	0.2780	13.9550	0.0750	0.0163	14.33
Qi-max (m^3/s)	0.0139	0.3700	18.4210	0.1010	0.0325	18.94
$\mu\ (Q)$	0.0097	0.3199	15.9939	0.0868	0.0163	16.43
$\sigma\ (Q)$	0.0021	0.0290	1.3974	0.0079	0.0050	-

A second model based on a Gaussian distribution was used to compute the flow directly on the totality of the cross section without going through the subdivisions. The Manning coefficient mean value and standard deviation were found to be $\mu\ (n)\ =\ 0.029$ and $\sigma\ (n) =\ 0.0025$, respectively. The range for possible values of *n* was computed as $\{n_k\} =\ \mu\ (n)\ \pm\ 2\ \sigma\ (n)$, hence covering 95% of the probability distribution. The total flow was computed, its mean value and standard deviation were found to be $\mu\ (Q) = 14.7\ m^3/s$ and $\sigma\ (Q) = 1.63\ m^3/s$, respectively. This provides a range for possible values of total flow. If two standard deviations are used to cover 95% of the probability density, then *Q* would range between 11.44 m^3/s and 17.96 m^3/s.

Note that the results above from the two models are in the same range. However, the second model provides more reasonable values and takes into consideration the range that *Q* would cover based on the variability in bed roughness. Furthermore, the second model involved lesser parameters as it performs the analysis on the full section without subdividing it.

4.3 Mathematical modeling of roughness- water depth-flow rate interaction

The following modeling includes the variability in water flow depth, which would depend on the season. This is particularly critical in accounting for the uncertainty in flow given the wide fluctuations in precipitations from season to season. Considering *Q* as the total flow rate, as expressed in Equation [3] as a function of river cross sectional area (*A*), its hydraulic radius (R_h), the river bed slope (*S*), and the roughness coefficient (*n*), with power exponents (*p* and *r*) applied to R_h and *S* respectively:

$$Q = \frac{1}{n}\ A\ R_h^p\, S^r \qquad [3]$$

In the following derivation, we consider *p* and *r* in their general form, and *n* as a function of depth *y*. Denoting by *w* as the river width, expression [3] is rewritten as:

$$n\ (y) = \ \frac{w^{p+1}}{Q}\ \ S^r\ y\ \left[\frac{y}{w + 2\ y}\right]^p \qquad [4]$$

If we consider two streams of same width and carrying the same discharge, the variation in *n(y)* is the partial derivative of *n* with respect to *y*:

$$\frac{\partial n\ (y)}{\partial y}\ =\ K_{w,Q}\ \left[\frac{y}{w + 2y}\right]^p + p\ y\ \left[\frac{y}{w + 2y}\right]^{p-1} \left[\frac{w}{(w + 2y)^2}\right] \qquad [5]$$

where we define $K_{w,Q}$ as a function of river width and average flow. We make a first observation that small watercourses are typically shallow as one can observe the wavy effects exerted by the river bottom on the water free surface. The second observation was discussed earlier in that watercourses have variable bed geometry at any given control section, and that they are seasonal with a low flow or a dry river bed when off season. The third observation is that watercourses contain repeated bents along their flow line. The modeling of bents involves centrifuge forces that result in a rise in water surface on the outer side of the bent. This effect is outside the scope here and is treated in a separate working paper (Chalhoub, 2016). Numerical results from Eqs. [4] and [5] show that it is necessary to use the correction factors in computing watercourse flows, and that classical open channel theories, while they apply to less rugged open channel beds, fall short of representing the field behavior of such streams (Chalhoub, 2016). Introducing a function, $f\ (\partial n/\partial y)$, accounting for the simplifications defined above and the simplifications performed on the gradient of *n*, we integrate over the depth of the river to obtain the adjusted roughness coefficient, n^*.

$$n^*\ =\ \int_0^{y_{max}} f\ (\partial n(y)/\partial y)\ dy\ =\ \left[1 + \frac{\Delta n\ (\%)}{100}\right] n \qquad [6]$$

The adjustment factor on *n* is represented as a function of the flow depth for a given bed width. For a channel width, *w* = 20 m in the simulation model, *n* should be adjusted by 10% for a flow depth of 2 m, and by 35% for a flow depth of 0.10 m. The percentage by which *n* needs to be adjusted is a corrective factor that is expected to be higher as the depth gets lower. The mathematical model results are in reasonable agreement with field observations. For a small watercourse, given the same bed roughness and geometry, a deep water flow in the range of 2 m would have to overcome a lower frictional resistance than shallow waters flowing in the depth range of 0.1 to 0.2 m. Results are illustrated in Figure 2.

The adjustment derived here is also in agreement with the pipe flow theories that define *e/D*, where *e* is the irregularity or roughness on the interior surface of the pipe and *D* is the interior pipe diameter. Another simulation for a river width of 19 m and the flow depth varying between 0.05 m and 3 m was performed and similar conclusions were reached. Adjustments to *n* in this case ranged between 9% and 37%.

In light of the results above, the mathematical model can be rewritten in a simplified format by defining an exponential function for the case of *w* = 20 m and a depth varying between 0.05 m and 2 m. At a particular control section along the river reach, the adjustment over *n* is rewritten as a function of depth:

$$\frac{\Delta n\ (\%)}{100} = 0.3484\ e^{-0.518\ d} \qquad [7]$$

where *d* is the flow depth in meters and $\Delta n\ (\%)$ is the adjustment percentage. Expression [7] could be used for close values of the river bed width and still yield reasonable estimates within the field-related error margins. An exponential function for *w* = 19 m was also developed and found to be $\frac{\Delta n\ (\%)}{100} = 0.3893\ e^{-0.46\ d}$.

The mathematical models and the results above illustrate the uncertainty related to the variability in cross-sectional shapes, watercourse seasonality, among other input parameters (Chalhoub, 2016). The river bed coefficients that are typically tabulated in literature and used for open channel flow may underestimate the roughness of a meandering watercourse and therefore may cause an overly optimistic estimation of the flow carried by its stream. Such an overestimation of water flow has many implications on project planning and rural development expected outcomes.

5 Implications on Public Management Practices

Inefficiencies in public management and damage to natural resources have been long discussed in literature especially when it comes to developing countries (Hufschmidt and Tejwani, 1993). In several less developed countries, the trend of building dams in reservoir management lacked a long term strategic management, causing impairment, deterioration in ecosystems, and disequilibrium in the natural habitat (Takeushi, 1997). Research on the vertical integration of the water value chain whereby a given drainage basin would be folded under a single authority was considered to avoid fragmentation in decision making (UNDP, 2006). These considerations highlight the importance of closely coordinating runoff data with resource management as one single operation (UNESCO, 2008). This suggested approach becomes particularly challenging when the rivers go across national boundaries especially in developing countries where there was a lack of collaboration (McCaffrey, 1993, Dreischova et al., 2011). Note that the need for clear engineering input into public policy decisions is not only critical to developing countries, but also is the standard practice in developed countries (Liang et al., 2014; Chalhoub, 2016).

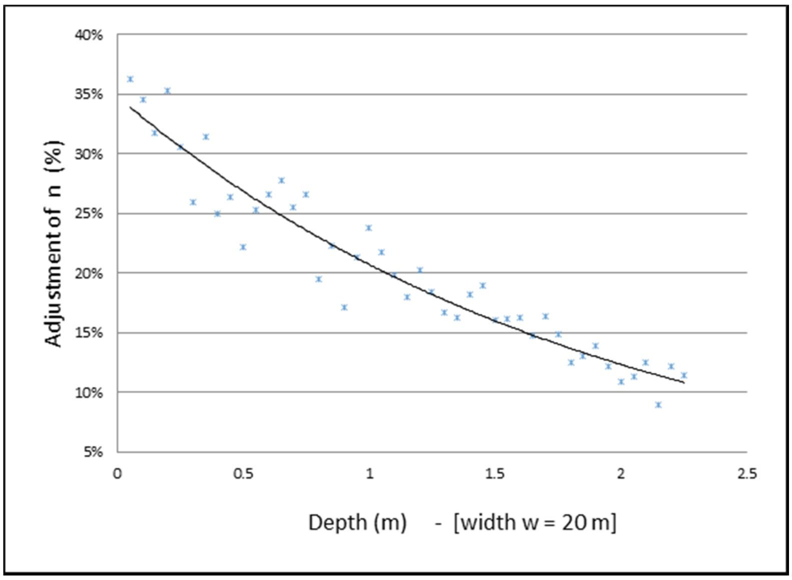

Figure 2. Percent adjustment to the roughness coefficient, *n*, as a function of flow depth (w = 20m).

5.1 Linear Regression - Mathematical Model

5.1.1 Model Definition and Rationale

A multivariate linear regression mathematical model is developed to address the water policies from the end-user perspective, based on the analysis of empirical data. Data collection was performed in Byblos County (Casa de Byblos), Lebanon, located in Mount Lebanon characterized by steep mountains overlooking the East Mediterranean. The paradox that such Counties are facing is that they have high precipitation rates relative to the rest of the region but suffer severe water shortage. A framework was developed and used as a basis for data collection in preparation for the linear multivariate linear regression analysis (Figure 3). The dependent variable was selected to represent the sustainability of using surface water as a primary source of supply. The model has three independent variables. The first variable, X_1, represents the extent to which projections for the surface flow are reliable given their inherent uncertainty. Variable X_2 represents the extent to which establishing a multi-decade surface water management program would be effective in solving the shortage issue. Variable X_3 represents the extent to which a transition to groundwater as a source of supply for the end-user would prove to be effective. The relationship is expressed in Eq. [8].

$$Y = \beta_0 + \beta_1 X_1 + \beta_2 X_2 + \beta_3 X_3 + o(X) \qquad [8]$$

with β_0 is the intercept of the regression, β_i ($i = 1, \ldots, 3$) are the regression coefficients, and $o(X)$ is an error term. The regression coefficients will be discussed along with their respective standard errors to determine the statistical significance of each independent variable in defining the dependent variable. The sign of the coefficient will also indicate whether the correlation is negative or positive.

The rationale behind the model is to involve the end-user in public decisions regarding the surface water resources. This is a subject of rising concern as water becomes a priority in conflict management in the region. From an engineering point of view, surface water in the East Mediterranean has untapped potential that requires a planned program in between central policy makers and local communities. As such, the choice of the first variable is in line with the past research about the negative effects of climate change on surface, and in-turn, groundwater. This requires further effort in involving the local communities in decision making in order to remedy or cope with this phenomenon. The second variable was selected because it is directly relevant to policy choices, where public attitudes towards the strategic planning and implementation of water resource management practices, or lack thereof, is critically relevant at both the planning and implementation levels. The third variable represents the ground water value chain as a potential substitute. Data collection was normalized on 1 to 5 Likert scale. The technical details of processing groundwater were left outside the scope of this paper and are part of future research, which would require more empirical data collection and follow-up. Many countries have turned public efforts to the harnessing of ground water more so than managing the surface water and runoff due to the economic and environmental reasons. The pollution of surface water, long and unforeseen drought periods of surface water flow and the thinning of medium to small river flow due to climatic developments are some of the reasons. However, similar concerns apply to groundwater especially in areas where the wastewater management is still under development and dwellings rely on untreated buried septic tanks. The use of groundwater supply would require further study especially that groundwater has its own range of environmental concerns related to ecosystems, water quality and public health threats.

5.1.2 Results and Interpretation

The linear regression analysis returned numerical values for the independent variable coefficients and their respective error values. The overall regression equation has an r^2 of 0.9 showing a good overall fit between the data and the model. All three independent variables were found to be statistically significant at α = 10% significance level. The relationship with the first independent variable shows a negative correlation with a coefficient, β_1 of -0.0539 and a standard error, $se_1 = 0.071 < 0.10$. This shows a positive relationship with the second variable with a coefficient, β_2= 0.5719 and a standard error, $se_2 = 0.0474 < 0.10$. The third variable also shows a positive correlation with β_3 = 0.4763 and a standard error, se_3 of $0.0524 < 0.10$. The resulting numerical relationship between Y and Xi, $i = 1, 2, 3,$ is represented in Eq. [9].

$$Y = -\ 0.0539\ X_1 + \ 0.5719\ X_2 + \ 0.4763\ X_3 \qquad [9]$$

Regression results were reasonably consistent with replies during focus interviews conducted in local communities in the exploratory phase. Due to a history of water shortage, local communities have little reliance on the surface water estimates. This is also consistent with the secondary data in the region, showing that over 80% of the surface water flows back to the seas unexploited. The positive correlation with the establishment of a multi-decade water resources management plan and the positive correlation with the use of groundwater were both expected. However, there were limitations in the data collection that most respondents were not aware of the technical challenges present in the use of groundwater as a main source of supply. In the past research, several techniques were developed to link the surface with groundwater in simplified models (Jones, 1997, Grayson et al., 1992, Polmann et al., 1991). There are several challenges related to the transition to groundwater supply as it is correlated with the surface water and has sources of uncertainty (Querner, 1996, Dettinger and Wilson, 1981). Still, the results for X_3 do confirm that the willingness of local communities to partake in a program on ground water exploration, extraction, treatment, and distribution.

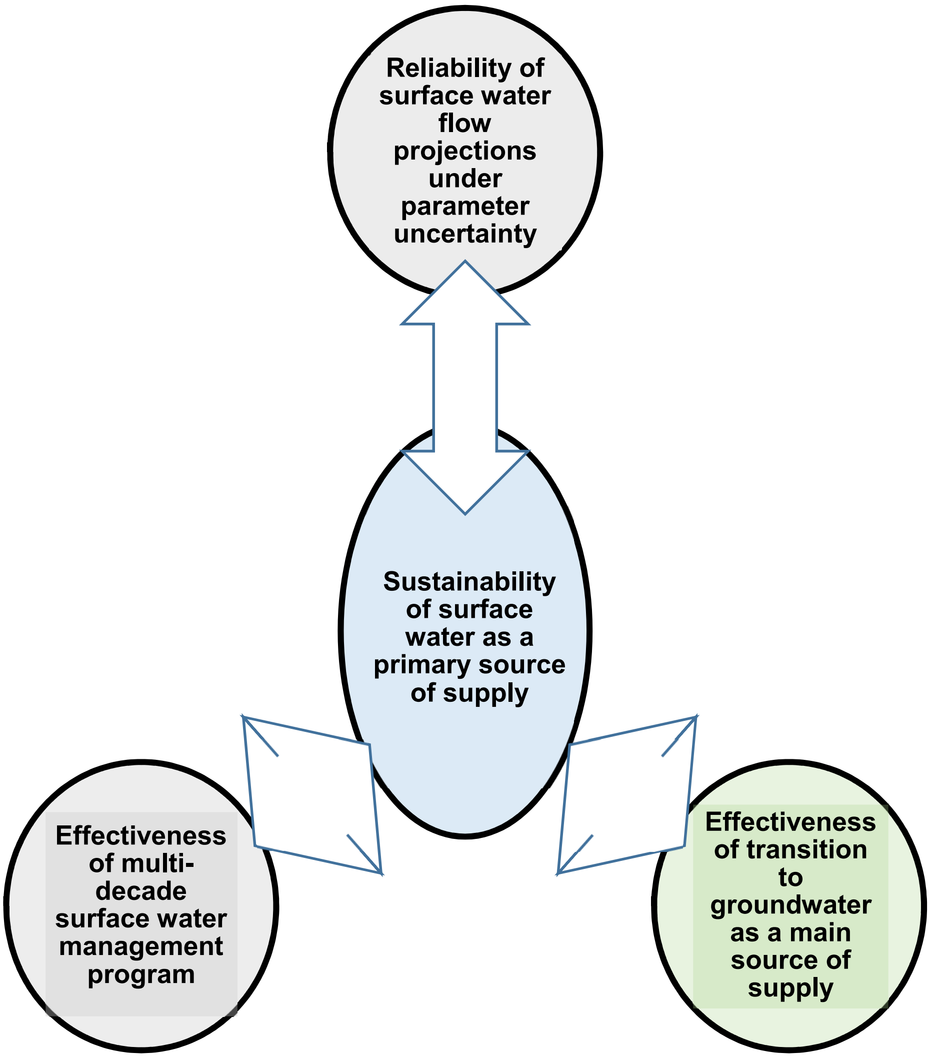

Figure 3. Framework used in empirical data analysis.

6 CONCLUSIONS

The use of surface water as a main source of supply is discussed along with the uncertainty about its input parameters as well as the classical formulas related to the surface watercourses. In several developing countries, pollution of the surface water and unforeseen drought periods due to the climatic developments have caused a severe drop in the flow of medium to small watercourses. Efforts turned to the harnessing of groundwater rather than managing the surface water and runoff due to the economic and environmental reasons. However, similar concerns apply to groundwater especially in areas where the wastewater management is still under development. An engineering mathematical model was developed and used to illustrate how uncertainty about the input parameters affects the surface water flow estimates and outcomes. It was found that the effects related to the cross-sectional geometry of the watercourse, location, flow depth, and hence seasonality, have significant effects on the accuracy of flow estimates. It was shown that a statistical approach would be more appropriate in computing estimates than a deterministic approach, in particular in relation to providing the input for public policy decisions. The paper presents a multivariate regression model that provides an insight into end-user input to public decision making. The results showed that the sustainability of surface water use as a primary source of supply to local communities is statistically significant and negatively correlated to the surface water flow estimates in their current form, while it is significantly but positively correlated with the prospects of establishing a multi-decade surface water management program, and the effectiveness of transitioning to groundwater exploration, extraction, treatment, distribution and end-use. Regression variables were selected based on their relevance to public management and policy choices, and the extent to which they illustrate public attitudes towards the need for strategic planning and implementation of water resource management practices at a national level. Details of the groundwater value chain were left out of the present scope for future research, empirical data collection and follow-up. Transitioning from surface to groundwater supply is a potential solution but it requires further study for reasons of surface water mismanagement, environmental concerns related to ecosystems, groundwater quality, and public health issues. It is recommended that a national water resource management plan be established with an environmentally sustainable multi-decade implementation program. The program needs to be closely linked to the environmental protection policies.

REFERENCES

Arnell, N. W. & Reynard, N. S. (1993). *Impact of Climate Change on River Flow Regimes in the United Kingdom*. Institute of Hydrology, Report to Department of the Environment, 130.

Arnell, N. W. & Reynard, N. S. (1996). The Effects of Climate Change Due to Global Warming on River Flows in Great Britain. *Journal of Hydrology*, 183(3-4), 397–424.

Baker, M. N. & Horton, R. E. (1936). Historical Development of Ideas regarding the Origins of Springs and Ground-Water. *Transactions American Geophysical Union*, 17(2), 395-400.

Beven, K. (2006). On Undermining the Science? Journal of Hydrological Processes. 20(14), 3141-3146.

Biswas, A. K. (1970). *History of Hydrology*. Elsevier, New York.

Boucher, M. A., Tremblay, D., Delorme, L., Perreault, L. & Anctil, F. (2012). Hydroeconomic Assessment of Hydrological Forecasting Systems. Journal of Hydrology, 416–417,133–144.

Burnash, R. J. C., Ferral, R. L. & Mcquire, R. A. (1973). *A Generalied Streamflow Simulation System Conceptual Model for Computer Simulation,*. US National Weather Service, Sacramento, California, USA.

Chalhoub, M.S. & Jenkins, G. (1994). *Monte Carlo Simulation Techniques for Project Appraisal in Water Resources.* Rpt. No. 93-02-25A, Harvard Institute for International Development, Program on Environmental Economics, Cambridge, MA.

Chalhoub, M. S. (2016).*Small River Hydraulics*: *Engineering and Environmental Issues*, Working paper, Notre Dame University, Louaize, Lebanon, 2016-17.

Dame University, Louaize, Lebanon, 2016-17.

Dettinger, M.D. & Wilson, J.L. (1981). First Order Analysis of Uncertainty in Numerical Models of Groundwater Flow, 1. Mathematical Development. *Water Resources Research*, 17(1), 149-161.

Dottori, F., Martina, M. L. V. & Todini, E. (2009). A Dynamic Rating Curve Approach to Indirect Discharge Measurement, *Hydrology and. Earth System. Sciences*. 13(6), 859–896.

Dourojeanni, A. (2001). *Water Management at the River Basin Level: Challenges in America.* United Nations, Rept. 187/2001, Santiago, Chile.

Dreischova, A. Fischhendler, I. & Giordano, M. (2011). The Role of Uncertainties in the Design of International Water Treaties: An Historical Perspective. *Climatic Change*, 105, 387–408.

Electric Power Research Institute - EPRI (2009). *Sustainable Water Resources Management, Volume 3, Case Studies on New Water Paradigm*, Palo Alto, California, Tetra Tech, 1020587.

El-Fadel, M., Zeinati, M. & Jamali, D. (2000). Water Resources in Lebanon: Characterization, Water Balance, and Constraints, *Journal of Water Resources Development*, 16, 619-642.

Finnemore, E. & Franzini, J. (2009). *Fluid Mechanics with Engineering Applications*. Tenth Ed. McGraw Hill Education. ISBN-10: 0072432020.

Franchini, M. Lamberti, P. & Di Giammarco, P. (1999). Rating Curve Estimation using Local Stages, Upstream Discharge Data and a Simplified Hydraulic Model. Hydrology and Earth System Sciences, 3(4), 541–548.

French, R. H. (1985). *Open-Channel Hydraulics*. McGraw-Hill Book Company. New York, 201-247.

Gleick, P. H. (1987). Global Climatic Changes and Regional Hydrology: Impacts and Responses. *The Influence of Climate Change and Climatic Variability on the Hydrologic Regime and Water resources*, 389-402.

Goetzinger, J. & Bardossy, A. (2008). Generic Error Model for Calibration and Uncertainty Estimation of Hydrological Models. Journal of Water Resource Research, 44(12), 1-18.

Grayson, R. B. Moore, I. D. & McMahon, T. A. (1992). Physically Based Hydrologic Modeling. 1. A Terrain Based Model for Investigative Purposes. *Water Resources Research*, 28(10), 2639-2658.

Grigg, N. S. (2016). *Integrated Water Resource Management: An Interdisciplinary Approach*. Springer, ISBN 978-1-137-57-6156, New York.

Grigg, N. S. (2002). *Water, Wastewater, and Stormwater Infrastructure Management*. Lewis Publishers, CRC Press, New York.

Hufschmidt, M. M. & Tejwani, K. G. (1993). *Integrated Water Resources Management: Meeting the Sustainability Challenge*, IHP Humid Tropics Program Series No. 5, UNESCO, Paris.

Jones, J. A. A. (1997). Pipeflow Contributing Areas and Runoff Response. *Journal of Hydrological Processes,* 11(1), 35-41.

Lenton, R. & Muller, M. (2009). *Integrated Water Resources Management in Practice: Better Water Management for Development.* Earthscan, London, United Kingdom.

Liang, H., Zeng, W. & Jiang, F. (2014). Investigation of Uncertainties in Surface Water Resource Assessment of Georgia's State Water Plan. *ASCE Journal of Water Resources Planning and Management*, 40(2), 228-237.
Lightfoot, D. R. (2000). The Origin and Diffusion of *Qanats* in Arabia: New Evidence from the Northern and Southern Peninsula, Geographic *Journal*, 166(3), 215-226.
Loucks, D. P. & Van Beek, E., with contributions from Stedinger, J. R., Dijkman, J. P. M., & Villars, M. T. (2005). *Water Resources Systems Planning and Management: An Introduction to Methods, Models and Applications*, Princeton Hall, Englewood Cliffs, New Jersey, USA, ISBN: 9231039989.
Makdisi, K. (2007). Towards a Human Rights Approach to Water in Lebanon: Implementation beyond Reform. *Journal of Water Resources Development*, 23(2), 369-390.
Manning, R. (1891). *On the Flow of Water in Open Channels and Pipes*, Transactions of the Institution of Civil Engineers in Ireland, 20, 177.
McCaffrey, S.C. (1993). *Water, Politics, and International Law in Water in Crisis: A Guide to the World's Fresh Water Resources*. P.H. Gleick (ed), Pacific Institute and Stockholm Environmental Institute. Oxford University Press, New York.
Montanari, A. (2007). What Do We Mean by Uncertainty? The Need for a Consistent Wording about Uncertainty Assessment in Hydrology. *Journal of Hydrological Processes*, 21(6), 841-845.
Montanari, A. & Grossi, G. (2008). Estimating the Uncertainty of Hydrological Forecasts: A Statistical Approach. *Water Resource Research*, 44, 1-9.
Nemec, J. & Schaake, J. (1982). Sensitivity of Water Resources Systems to Climate Variation. *Hydrology Science Journal*, 27(3), 327-343.
Peck, A., Gorelick, S., deMarsily, G., Forster, S. & Kovalevsky, V. (1988). *Consequence of Special Variability in Aquifer Properties and Data Limitations for Groundwater Modeling Practice*. IAHS Pub. No. 175, Washington DC.
Pappenberger, F., Matgen, P., Beven, K. J., Henry, J. B., Pfister, L. & de Fraipont, P. (2006). Influence of Uncertain Boundary Conditions and Model Structure on Flood Inundation Predictions. *Advance in Water Resource*, 29(10), 1430–1449.
Pelletier, M. P. (1987). Uncertainties in the Determination of River Discharge: A Literature Review. *Canadian Journal of Civil Engineering*, 15(5), 834–850.
Pidwirny, M. (2006). *The Hydrologic Cycle*. Fundamentals of Physical Geography, 2 nd Ed.
Polmann, D. J., McLaughlin, D., Gelhar, L. W. & Ababou, R., (1991). Stochastic Modeling of Large-Scale Flow in Heterogeneous Unsaturated Soils. *Water Resources Research*, 27(7), 1447-1458.
Querner, E. P. (1996). Description and Application of the Combined Surface and Groundwater Flow Model MOGROW. *Journal of Hydrology*, 192(1-4), 158-188.
Rantz, S. E. (1982). *Measurement and Computation of Streamflow*, US Geological Survey, and Water Supply Paper number 2175.
Salman, M. A. S. & Bradlow, D. D. (2006). *Regulatory Frameworks for Water Resources Management – A Comparative Study*. The International Bank for Reconstruction and Development and the World Bank, Washington DC.
Sivapalan, M., Bloschl, G., Zhang, L. & Vertessy, R. (2003). Downward Approach to Hydrological Prediction. *Journal of Hydrological Processes*, 17(11), 2101-2111.
Stave, K. A. (2002). Using System Dynamics to Improve Public Participation in Environmental Decisions. *System Dynamics Review*, 18(2), 139–167.
Takeushi, K. (1997). Least Marginal Environmental Impact Rule for Reservoir Development. *Hydrological Sciences Journal,* 42(4), 583-597.
Thornthwaite, G. M. & Mather, J. R. (1957). *Instructions and Tables for Computing the Potential Evapotranspiration and the Water Balance.* Drexel Institute Technology Publications in Climatology, Laboratory of Climatology, VII (3).
Todd, D. K. & Mays, L. W. (2005). *Groundwater Hydrology*. Third edition, John Wiley & Sons, Inc. NJ.
Turall, H., (1997). *Hydro Logic? Reform in Water Resources Management in Developed Countries with Major Agricultural Water Use Lessons for Developing Nations*. Overseas Development Institute, Portland House, London, 1-170.
UNESCO (2008). *Integrated Water Resource Management Guidelines at River Basin Level*, Part I, Principles.
Wilks, D. (2006). *Statistical Methods in the Atmospheric Sciences*. Academic, Cambridge, 100, 1-704.
World Meteorological Organisation, (1997). *Comprehensive Assessment of the Freshwater Resources of the World*. WMO, Geneva, 34.
Yalin, M. S. (1992). *River Mechanics.* Pergamon, Oxford.
Yen, B. C. & Riggins, R. (1991). Time Scale for Surface-Subsurface Flow Modeling. *Proceedings 1991 National Conference on Irrigation and Drain. Div., ASCE*, 351-358.
Zhao, T., Yang, D., Cai, X., Zhao. J, & Wang, H., (2012). Identifying Effective Forecast Horizon for Real-Time Reservoir Operation under a Limited Inflow Forecast. Water Resource Research, 48(1), 1-15.

RESEARCH ON ICE CONDITIONS IN THE MIDDLE YARLUNG ZANGBO RIVER BASED ON LANDSAT IMAGES

RUI CAO(1), YOUCAI TUO(2),YUN DENG(3), NAN LI(4) & LINGLEI ZHANG(5)

(1,2,3,4,5) State Key Laboratory of Hydraulics and Mountain River Engineering of Sichuan University, Chengdu, China, dengyun@scu.edu.cn

ABSTRACT

The Yarlung Zangbo River, located in Qinghai-Tibetan Plateau of China, has the characteristics of strong solar radiation and low air temperature in meteorology and canyon interlacing with wide valley in topography. These characteristics make the ice conditions special in the Yarlung Zangbo River Basin. However, due to the lack of existing ice observation data, it is unable to reflect the spatial and temporal ice variation in this region. In this paper, we interpreted the single-band satellite images from 2003 to 2016 using decision tree classification based on NDWI via ENVI software, and analyzed the temporal and planar spatial variations of ice, the influence of air temperature on the ice conditions, and the relationship between topography and ice distribution. These results showed that 1) the ice period was Dec. to Feb. In general, ice conditions had small inter-annual variation, and the freeze-up intensity, length of border ice and ice period duration decreased as the altitude decreases from west to east; 2) the Zangmu reservoir weakened the hydrodynamic conditions, resulting in the occurrence of ice in the downstream of the Lhasa River estuary; 3) 9 steady ice jam positions existed in the middle Yarlung Zangbo River, which had the planar topographic features of bend and narrowed channel; 4) ice cover distributed denser in wide valleys than in Canyons. The study enriched and expanded existing studies of ice condition in the Yarlung Zangbo River and is a contribution for water resource development and ecological environment protection of the Yalung Zangbo River Basin.

Keywords: Yarlung Zangbo River; remote sensing; ice condition; river net.

1 INTRODUCTION

The famous international river—Yarlung Zangbo River stretches about 2229 km with an average elevation of over 4500 m and a drop of 2600 m in China. The solar radiation is strong and the average air temperature is low and the change of meteorological elements is significant in the Yarlung Zangbo River basin, especially in the middle and upper reaches of it. Due to the unique meteorological and geographical elements, the Yarlung Zangbo River presents obvious ice characteristics contrasted with other rivers in the same latitude. The Chinese government always pays attention to the water resources and environmental protection of the middle and upper Yarlung Zangbo River. Ice has been one of the most important environmental factors, while the study of ice in the Yarlung Zangbo River Basin is insufficient now. Existing information and data were mainly from the hydrological station, which was set up in the main stream by the Tibet Hydrology Bureau. Liu (1993) analyzed the ice data from 11 hydrological stations in the Yarlung Zangbo River Basin from 1961 to 1992, and pointed out that the ice conditions in the downstream of the Yarlung Zangbo River were rare, while the middle reaches and the tributaries were common, and the ice period shortened as altitude decreased. It is difficult to fully reflect the ice variation of the whole basin as the existing researches were mainly based on observation data from some fixed-point hydrological station stations.

Satellite Remote Sensing is a new technology for ice observation with the advantage of large spatial scale, being timely and effective. It is now widely used for it is free from the human, financial or traffic factors, and it can be complementary with the traditional field observation. Since the 1980s, scholars used a variety of satellites data (e.g. Landsat, Terra satellites multi-spectral data, SMMR and other satellite passive microwave data, Radarsat satellite radar data) for the study of sea ice distribution and intensity (Steffen, 1991; Liu et al., 1999; Gloersen and Cavalieri, 1986). Nonaka et al. (2007) used the remote sensing method to reveal the average break-up of 18 lakes in Eurasian continents. In recent years, with the improvement of remote sensing image, the application of remote sensing technology in river ice research is increasing. Yang (2006) used multi-source remote sensing technology to carry out the flood monitoring from MODIS, landsat7, CBERS-02 and RADARSAT data to track the occurrence, development and ice-jam process in the Yellow River, China. Kääb et al. (2013) used the satellite images with the resolution of 15 m to track the ice conditions in the lower Lena River, Siberia, and studied the ice flux and water velocities. Li et al. (2016) classified the river ice in the Yellow River Sanhu estuary through the interpretation of landsat-8 images.

In this study, we used remote sensing classification technology to interpret the Landsat images from 2003-2016, figured out the temporal and spatial variation of ice in the middle Yarlung Zangbo River, and analyzed the influence factors and the relationship between ice condition and meteorology and topography.

2 STUDY AREA

The reach from Duobaixiang (110 km upstream from Lhaze town, 29°11′17.04″N, 86°50′53.95″E) to Zangmu dam (29°11′4.58″N, 92°31′0.48″E) has a total length of about 700 km. It is the main part of the middle Yarlung Zangbo River and it belongs to temperate semi humid semi-arid plateau monsoon climate zone. Along the study reach, it distributes the Lhaze, Shigatse, Gongga, and Giacha weather stations. The average air temperature of the basin is around 0 ºC during Nov. to Feb. (Wang et al., 2015). In this region, canyon and wide valley interlace each other and the riverbed elevation reduces from 4133 m to 3266 m.

Due to the change of air temperature and altitude, ice condition changes obviously from upstream to downstream. In this study, the middle Yarlung Zangbo River was divided into 9 small parts (Figure 1) according to the terrain characteristics and ice conditions. 1# (river reach 1# is abbreviated to 1#), 2#, 6#, 8# and 9# reaches lie in canyons, 3#, 4#, 5# and 7# reaches lie in wide valleys, and 3#, 5# and 7# reaches have the characteristic of river net.

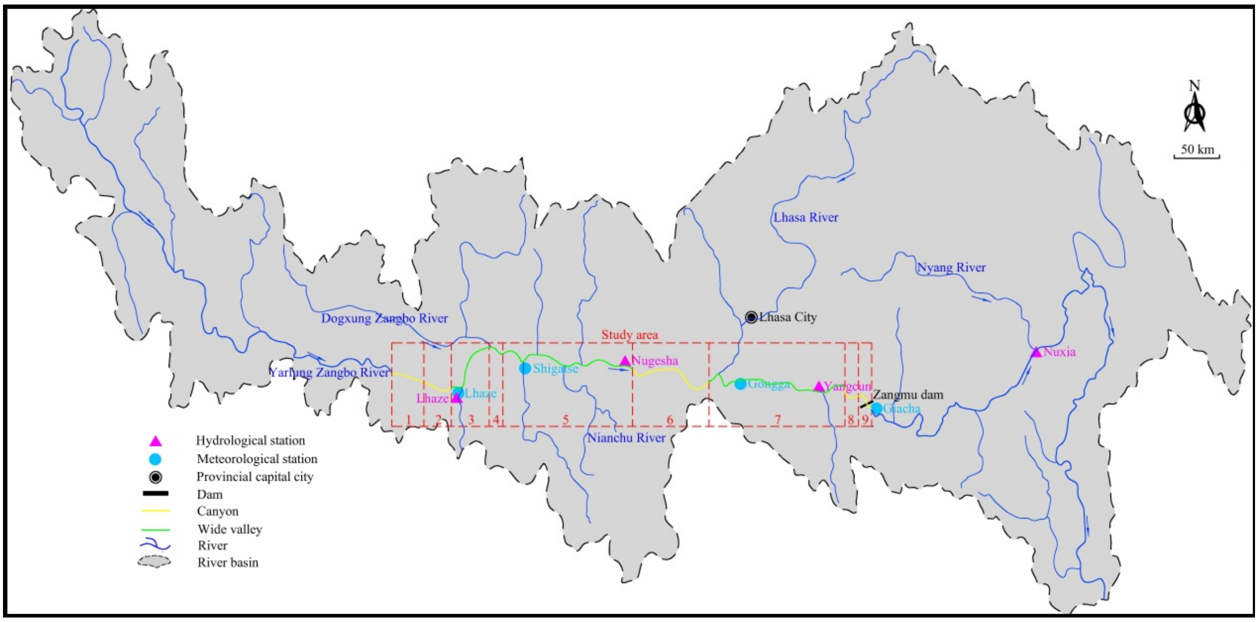

Figure 1. Location of the study area in the Yarlung Zangbo River Basin.

3 MATERIALS AND METHODS

3.1 Materials

The series of Landsat satellites (NASA, America) is widely used for earth observation. TM sensor and above version sensors have the spatial resolution of 30 m. Two satellites being in service at the same time makes the time resolution of data up to 8 days. Data during the winters of 2003-2015 from Landsat-5, Landsat-7 and Landsat-8 were obtained to analyze ice condition. Due to the large longitude span, 4 satellite images were needed to cover the whole study area at the same time. From west to east, the date acquired is 1 day later, but there is no effect on the observation especially for the stable ice period. Data collection is shown in Table 1.

Table 1. Remote sensing data used in this research.

Year	Satellite	Quantity	WRS Path/Row
2003-2008 (2005&2007 unavailable)	Landsat-5&Landsat-7	192	140/40,139/40, 138/40&137/40
2013-2015	Landsat-7&Landsat-8	144	

3.2 Methods

Generally, the basic method of recognizing ice and water in a piece of satellite image is to use the multi-spectral images. This study adopted the decision tree classification to divide ice from water and land bank (river beach).

Firstly, FLAASH atmospheric correction was performed to the multi-spectral image to weaken the negative impact from atmosphere and light to get the surface reflectance that is close to the real one. Secondly, the NDWI (Normalized Differences Water Index) was computed with the reflectance data. According to the false color composite and spectral reflectance curve, a certain amount of ice, water, and river beach samples were selected visually, then their NDWI range was compiled in statistics to form the classification rules. Then, the decision tree for classification was created and executed. At last, classification accuracy test was also executed via manual visual interpretation.

4 RESULTS AND ANALYSIS

Through the interpretation of the satellite images, the temporal and planar spatial information of ice in the middle Yarlung Zangbo River was obtained. Ice phenomena involve complex interactions between hydrodynamic, mechanical, and thermal processes (Shen, 2010). The influencing factors include meteorology, river topography and hydrodynamic characteristics. Considering the data collection of the above influencing factors, in this paper, ice conditions in the middle Yarlung Zangbo River were analyzed mainly from the following 3 aspects: the temporal and planar spatial variations of ice, the influence of air temperature on the ice conditions, and the relationship between topography and ice distribution.

4.1 The features of ice condition

(1) Temporal variations

The initial ice period in satellite image was in mid Nov. to mid Dec. The coverage of ice gradually increased since then and reached to the top in Jan., and gradually reduced till the ending date of the ice period which was generally in Feb. The ice period duration of the whole study area was 56 to 88 days.

It had a delaying trend for the initial ice period in the winters of 2003-2008, while the ending date of ice period was relatively stable, resulting in the shortening of ice period and decreasing of ice development degree. However, for the winters of 2013-2015, the ice development degree was enhanced, which was caused by the local climate change and hydrological characteristics.

Contrasting with these 9 reaches, the initial ice period of 3# to 6# was later than that of 1# to 2#, and the ending date of ice period was earlier than that of 1# to 2#, making the ice period of 3# to 6# shorter than that of 1# to 2#. The average ice period of 6# was about 24 days shorter than that of 1# (Figure 2). It can be observed that from upstream to downstream, the ice period was gradually shortened. No ice was observed downstream of 7# (except for the Zangmu reservoir). It is worth noting that the ice period of 4# was the shortest which was even shorter than that of 5# downstream of 4#. This phenomenon was related to the change of hydraulic condition caused by topographic features.

Overall, the ice period of the middle Yarlung Zangbo River gradually decreased with the decreasing of altitude. This is consistent with the research conclusion from Liu (1993) based on the observation data from hydrological stations.

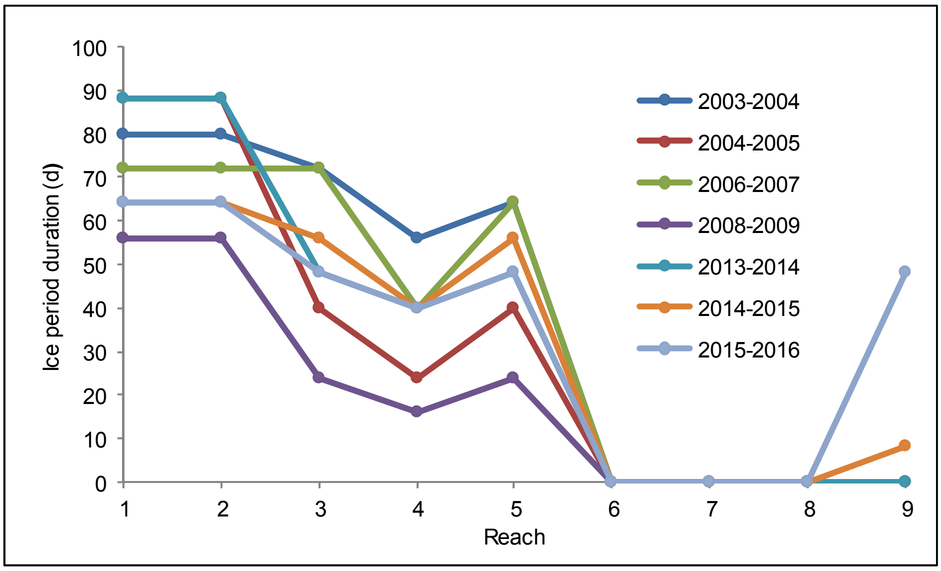

Figure 2. Ice period duration of each river reach.

(2) Spatial variations

Figure 3 shows the ice interpretation images of stable ice period during the winter of 2015-2016 when it reached to the maximum ice coverage (28/1/2016-31/1/2016) of the middle Yarlung Zangbo River. The main forms of ice in each reach are shown in Table 2.

1# (Duobaixiang to Zhuoricun), stretching for 40 km, was observed with the biggest ice area. With the average air temperature lower than 0 ºC, the reach upstream of 1# played its role of producing ice for 1#. Under suitable terrain conditions, ice accumulated and the ice edge kept going upstream, so 1# had a large amount of ice every winter. Affected by terrain conditions, ice jam occurred at many sections in 1#. The channel of 2# (Zhuoricun to Daju) was relatively straight and the hydraulic condition was simple. Border ice was the main ice form in this reach. Ice forms in 3# were mainly border ice and river net ice

 / ISSN 1562-6865 (Online) - ISSN 1063-7710 (Print)

cover. Particularly, the river net 10 km downstream Lhaze town had the densest distribution of river net ice cover. It was mainly due to the reducing of water power caused by the dispersion of water. 4# was the lower reach with single channel of Dogxung Zangbo River estuary. Its main ice form was border ice, but in some years two steady ice jam positions occurred (Table 3). Almost the whole reach of 5# is river net and its length doubles that of 3#. Inflows from the tributaries made the hydrodynamic condition more powerful. Added with higher average air

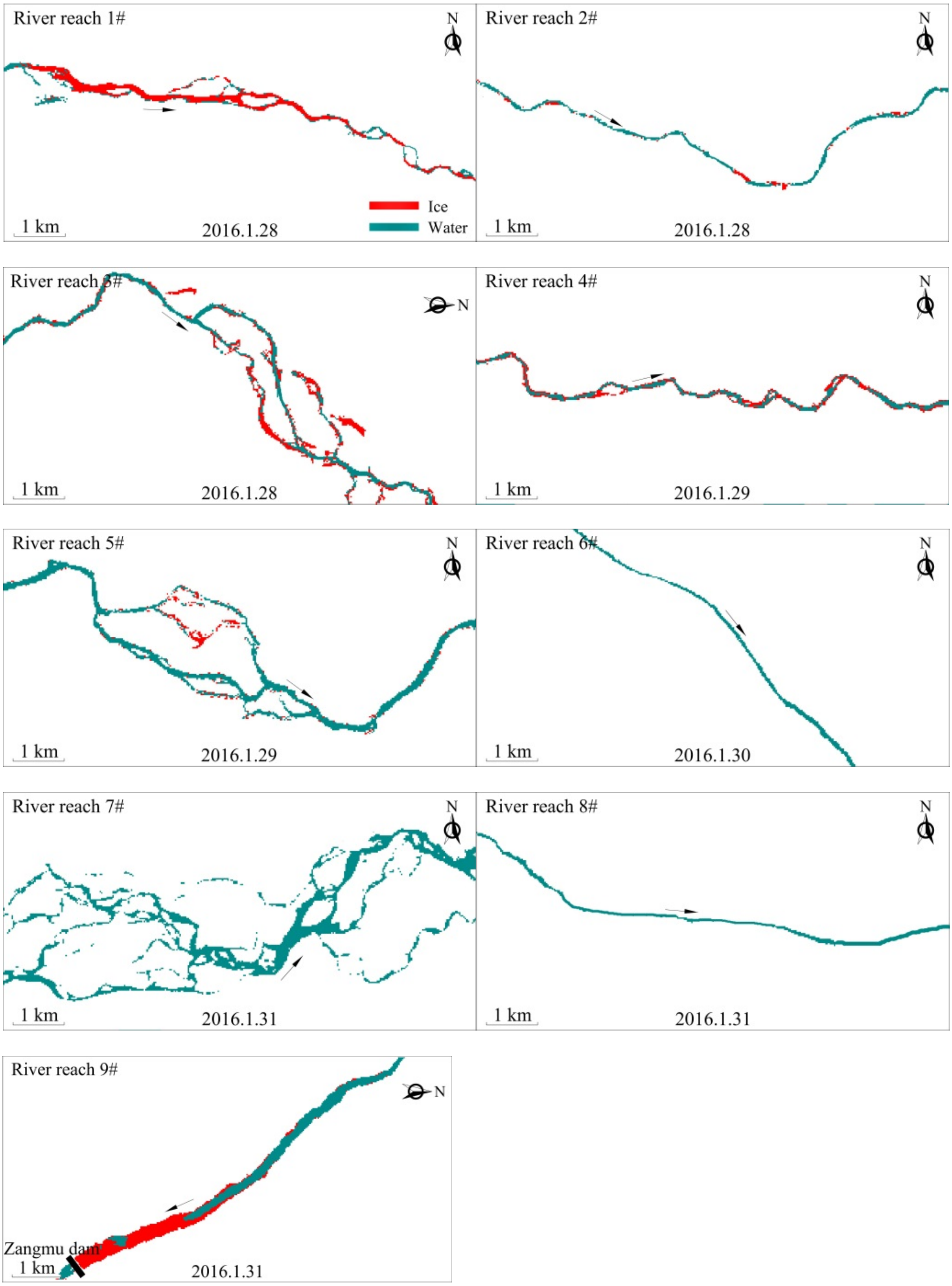

Figure 3. Ice images of each river reach in stable ice period of the winter of 2015-2016.

  / ISSN 1562-6865 (Online) - ISSN 1063-7710 (Print)

Temperature, the open water area was much larger than that in 3#. According to the data from Yangcun Hydrological Station (located within 6# to 8#), water temperature was above 0.8 ºC in winter, causing that in 6# to 8#, no ice was observed from satellite images. In 8#, ice was suspected to occur. However, after identification, the suspected ice was confirmed to be the splash of jet stream caused by the riverbed rocks or man-made structures. This phenomenon also existed in other seasons and these positions had never changed.

9# was the Zangmu reservoir. In Nov. 23, 2014, Zangmu hydropower station started working, and the maximum water depth in front of the dam was 60 m. In Jan. 28, 2015, a small piece of ice cover in front of the dam was observed from the Landsat image. Before the construction of the Zangmu Reservoir, ice never occurred in 9#. After the construction of the dam, the flow condition was weakened and a large piece of ice cover was observed in the winter of 2015-2016. The ice cover appeared between Dec. 12, 2015 and Dec. 20, 2015 and disappeared between Feb. 8, 2016 and Feb. 16, 2016 (about 58 days). The longest ice cover (7.5 km) was observed in Dec. 30, 2015.

In general, with the elevation's decrease from upstream to downstream in the middle Yarlung Zangbo River, freezing strength and border ice were gradually weakened. Except for 4#, ice positions and ice forms were inter-annually stable. Hydrodynamic conditions were weakened due to the construction of Zangmu reservoir, making it possible to form ice cover in winter.

Table 2. Main ice form of each river reach.

Ice Period	Reach									Mark
	1#	2#	3#	4#	5#	6#	7#	8#	9#	
12/2003-2/2004	●	○	●	○	●	-	-	-	-	●ice cover; ○border ice; -open channel.
12/2004-2/2005	○	○	●	○	●	-	-	-	-	
12/2006-2/2007	○	○	●	○	●	-	-	-	-	
12/2008-2/2009	○	○	●	○	●	-	-	-	-	
12/2013-2/2014	○	○	●	○	●	-	-	-	-	
12/2014-2/2015	●	○	●	○	●	-	-	-	●	
12/2015-2/2016	●	○	●	○	●	-	-	-	●	

4.2 Air temperature and ice conditions

Air temperature is the main factor affecting the process of ice development. The feature of multi-year average air temperature variation in the Yarlung Zangbo River Basin is consistent with altitude variation, that is, multi-year average air temperature gradually decreases from upstream to downstream (Zhang et al., 2011). Figure 4 shows the average air temperature during Dec. to Feb. of 2003-2016 from Lhaze, Shigatse, Gongga and Giacha weather stations. It shows that the average air temperature in winter was the lowest in Shigatse and highest in Giacha. On the whole, the cumulative negative air temperature and its cumulative days decreased from upstream to downstream. Air temperature in Qinghai-Tibetan Plateau fluctuates widely in a day and the difference can reach up to 20 ºC, and the ice formed in the night can easily decay in the daytime by solar radiation and higher air temperature (Liu, 1993). As a result, the cumulative amount of ice was relatively small. This is in accordance with the result of the main ice form of each reach in Table 2. Figure 5 shows the close relationship between ice period and negative air temperature and the correlation coefficient reaches 0.69 between ice period of river net in 3# and cumulative days of negative air temperature.

Due to the strong fluctuation of air temperature in ice period, the average daily air temperature can be above zero. Figure 6 compares the ice area of the 4 km-long river net near Jiandacun (located in 3#) and the daily air temperature of Lhaze weather station in the winter of 2015-2016. It showed a significant correlation between the process of ice development and air temperature. After Dec. 18, the average daily air temperature was negative and the river net ice cover was observed with an area of 250,000 m^2 in Dec. 19. After 5 days' accumulation of negative air temperature, ice area increased to 575,000 m^2. The rise of air temperature made the river ice to reduce from Jan. 4th. Ice area increased again after 8days of negative air temperature. Then, the air temperature gradually increased. Meanwhile, the ice area gradually decreased due to the other conditions (e.g. solar radiation and runoff) combined with air temperature.

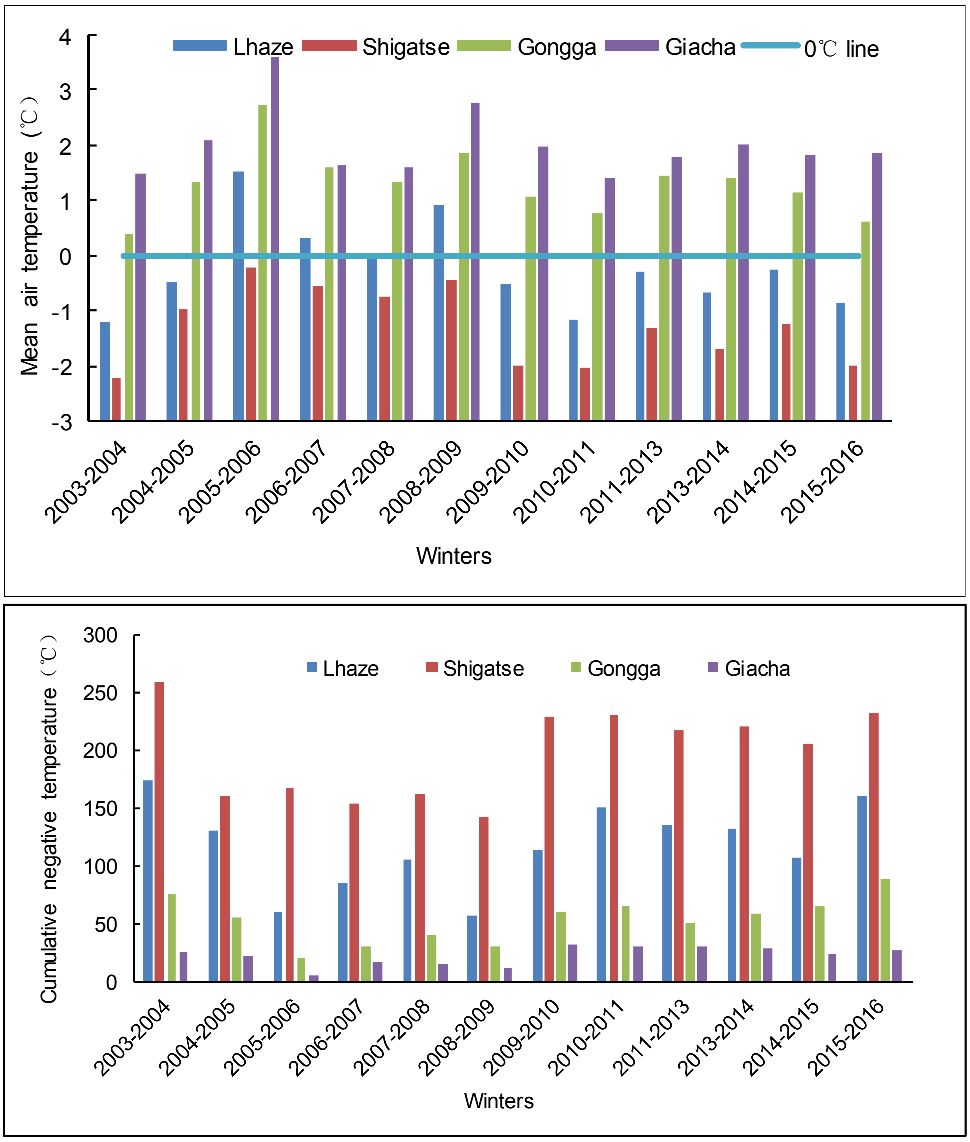

Figure 4. Mean air temperature of Dec. to Feb. along the middle Yarlung Zangbo River.

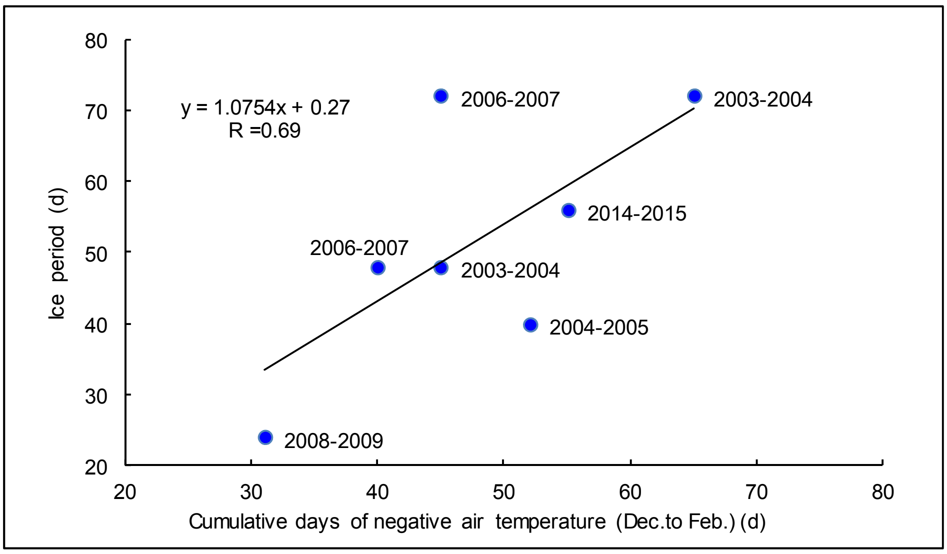

Figure 5. The Correlation analysis between ice period and cumulative days of negative air temperature.

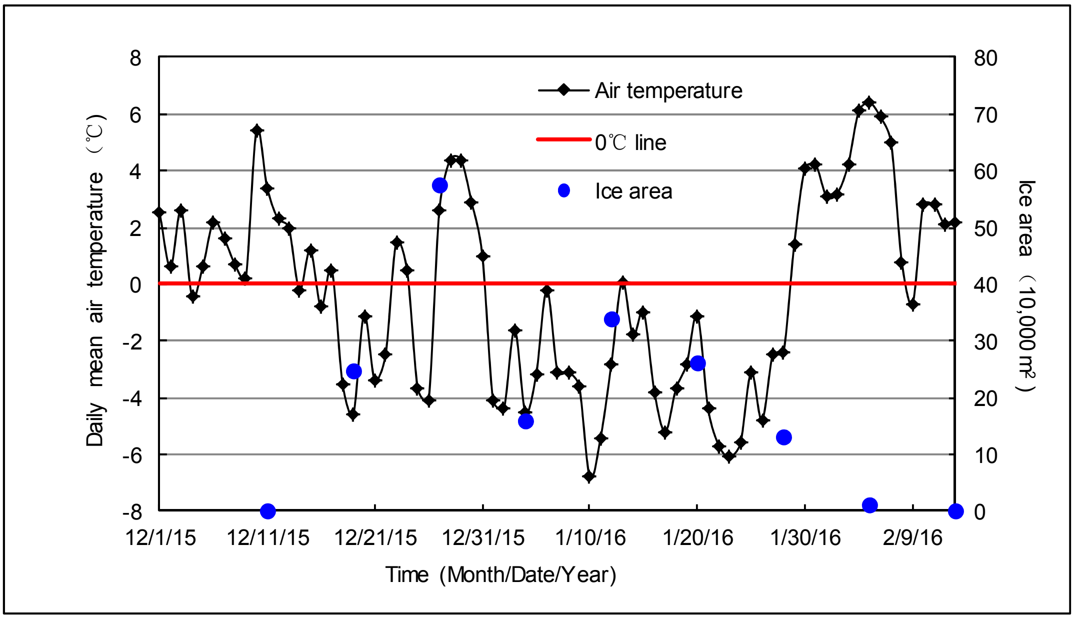

Figure 6. The variation of daily air temperature and ice area.

4.3 Topography and ice conditions

(1) Planar topographic features and steady ice jam positions

There were 9 steady ice jam positions in the middle Yarlung Zangbo River (Table 3). In 1# and 2#, there were 7 ice jam positions which first appeared and last disappeared in winters. In 4#, there were 2 ice jam positions which appeared in the winter of 2004, 2006 and 2008 and were stable during the ice period. The terrain features of ice jam positions contained at least one of the following two features: narrowed channel and bend channel. These channels blocked the slush ice and then were jammed.

Table 3. Information of steady ice jam positions.

River Reach	Latitude and Longitude	The Maximum Length of Ice Cover (km)	Planar Topographic Feature
1#	29°9′58.19″N,86°59′7.60″E	1.8~15.3	bend
	29°8′8.86″N,87°3′57.81″E	1.6	bend & narrow
	29°9′15.76″N,87°5′34.46″E	0.6	narrow
	29°9′44.54″N,87°8′14.21″E	0.3	narrow
	29°9′23.43″N,87°8′31.32″E	0.4	narrow
	29°8′58.81″N,87°9′25.27″E	1.0	narrow
2#	29°6′40.45″N,87°32′46.24″E	0.4	bend
4#	29°22′13.64″N,88°3′11.27″E	0.4	bend & narrow
	29°22′3.34″N,88°6′2.34″E	0.4	bend & narrow

Most of the ice jams occurred at bend channel. This was mainly due to the reduction of hydrodynamic and ice dynamic conditions. Slush ice easily accumulated there and then jammed when the ice accumulated was dense enough. Ice edge went upstream due to the bank resistance. Most of the ice jams occurred downstream of the bend (Figure 7).

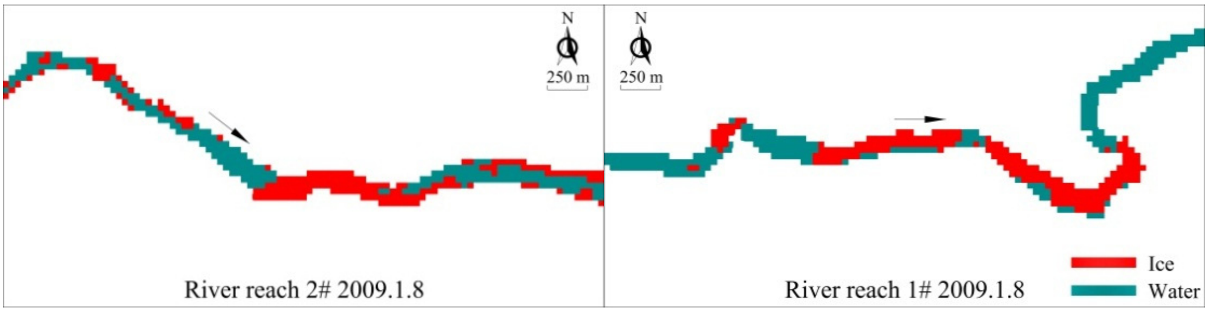

Figure 7. Steady ice jam positions at bends.

When the channel was getting narrower, the cross-section area was reduced, and it was easier to get jamming. Steep mountains formed the canyons, and alluvial fans were formed by the broken rock mass taken down by stream. The alluvial fans occupied a part of the riverbed, making the channel narrower and shallower. In these positions, ice was easily jammed, making them to be steady ice jam positions (Figure 8).

In addition, many unstable ice jam positions were observed in the middle Yarlung Zangbo River. The ice jams recurred during ice period at these positions affected by many influence factors such as topography and air temperature.

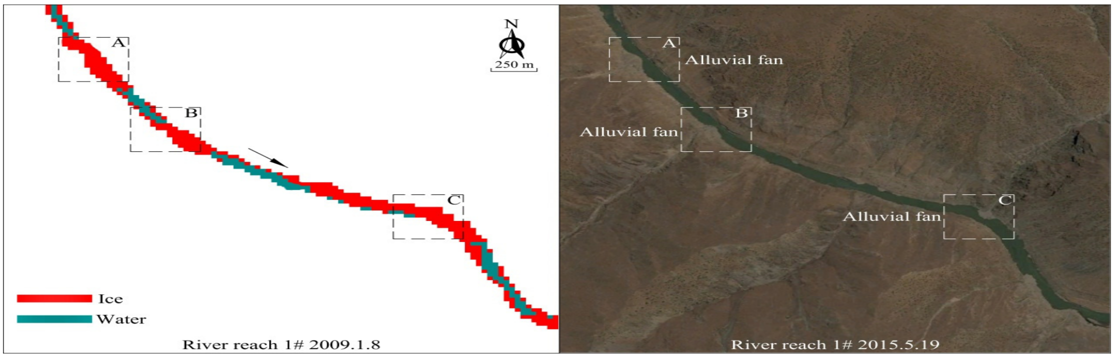

Figure 8. Steady ice jam positions resulted of alluvial fans.

(2) Topographic features and ice distribution

Canyons and wide valleys interlace in the study area. Reaches in canyons are single channels while in wide valleys mostly river nets (Shan, 2007).

Flow concentrated and made a strong hydrodynamic condition in single channel, while the flow was dispersed in river net and had weakened hydrodynamic condition. Small flow is more sensitive to low air temperature so it is easier for small flow to form ice cover. The channel of river net branches was narrow so that the slush ice was stuck easily. As water level dropped, many dead water zones were formed and they froze. 5# and 7# were in wide valleys with the channel form of river net and ice occurred (the ice condition in 7# was extremely weak and only existed upstream of it). 6# was in canyon with rapid flow in narrow single channel, so none of the ice was observed. The reach upstream Lhaze town (1# & 2#) was observed to be the most significant ice condition and downstream of it the ice form was mainly river net ice cover.

5 CONCLUSIONS

As altitude decreases, the Yarlung Zangbo River flows from west to east, forming straight stream channel, bend channel, river net, alluvial fan and other flat terrain features. The various flat terrain features together with unique meteorological features lead to special ice conditions in Yarlung Zangbo River. Based on the ENVI software and the single-band satellite images of the winters of 2003 to 2016, this paper interpreted and analyzed ice conditions in the 700 km-long middle Yarlung Zangbo River. The results indicate that: 1) the ice period was from Dec. to Feb. and the ice condition developed to its top-stage in Jan. Since the inter-annual variation of air temperature was relatively stable, the inter-annual variation of the ice conditions in the middle Yarlung Zangbo River was also stable. The newly built Zangmu reservoir weakened the hydrodynamic conditions, resulting in the occurrence of ice cover downstream of the Lhasa River estuary; 2) Ice occurred mainly in the 325 km-long upper reach of the study basin. Air temperature of the middle basin increased as the altitude decreased from upstream to downstream, leading to the weakening of ice development, total length of border ice, and ice period duration along stream; 3) There were 9 steady ice jam positions due to narrowed and bend channels in the study area. Due to the change of hydraulic characteristics and the reduction of ice dynamics, slush ice easily got jammed there. The ice edge developed upstream due to the riparian resistance; 4) Due to the difference in hydraulic conditions between river net and single channel, ice cover distributed denser in wide valleys than in Canyons.

ACKNOWLEDGEMENTS

This research was supported by the National Natural Science Foundation of China (Grant No. 91547211 and Grant No. 51309169).

REFERENCES

Gloersen, P. & Cavalieri, D.J. (1986). Reduction of Weather Effects in the Calculation of Sea Ice Concentration from Microwave Radiances. *Journal of Geophysical Research Oceans*, 91(C3), 3913–3919.

Kääb, A., Lamare, M. & Abrams, M. (2013). River Ice Flux and Water Velocities along a 600 km-long Reach of Lena River, Siberia, from Satellite Stereo. *Hydrology & Earth System Sciences Discussions*, 10(7), 9967-9997.

Li, C., Li, C.Y., Zhao, S.X. & Ji, H.L. (2016). Interpretation and Analysis of River Ice Process Based on Remote Sensing Data. *Advances in Science and Technology of Water Resources*, 36(3), 52-56.

Liu, J.Q., Wu, K.Q. & Huang, R.Y. (1999). The Monitoring of Sea Ice in the Bohai Sea with Radarsat SAR. *Marine Forecasts,* (3), 62-70.

Liu, T.C. (1993). The Yarlung Zangbo River Ice. *Journal of Tibet University,* (1), 37-42.

Nonaka, T., Matsunaga, T. & Hoyano, A. (2007). Estimating Ice Breakup Dates on Eurasian Lakes using Water Temperature Trends and Threshold Surface Temperatures Derived from Modis Data. *International Journal of Remote Sensing*, 28(10), 2163-2179.

Shan, J.P. (2007). Research on the Morphological Features of Yarlung Zangbo River Based on DEM, *Doctoral dissertation*. China University of Geosciences (Beijing).

Shen, H.T. (2010). Mathematical Modeling of River Ice Processes. *Cold Regions Science & Technology,* 62(1), 3-13.

Steffen, K. & Schweiger, A. (1991). NASA Team Algorithm for Sea Ice Concentration Retrieval from Defense Meteorological Satellite Program Special Sensor Microwave Imager: Comparison with Landsat Satellite Imagery. *Journal of Geophysical Research Oceans*, 96(C12), 21971–21987.

Wang, R., Yao, Z.J., Wu, S.S., Jiang, L.G. & Wang, L. (2015). Changes in Climate and Runoff in the Middle Course of the Yarlung Zangbo River Basin Area. *Resources Science*, 37(3), 619-628.

Yang, Z.H. (2006). The Research on the RS Dynamic Monitoring Mode of the Yellow River Icicle Hazard and the Ice Regime Information Extraction Model, *Doctoral dissertation*. China University of Geosciences (Beijing).

Zhang, X.X. (2011). Spatial-Temporal Evolutional Laws of the Key Hydrological Elements in Yarlung Zangbo River Basin, *Doctoral dissertation*. Beijing Forestry University.

Proceedings of the 37th IAHR World Congress
August 13 – 18, 2017, Kuala Lumpur, Malaysia

SEEKING THE OPTIMUM GROUNDWATER MONITORING NETWORK USING A GENETIC ALGORITHM APPROACH

MUSTAFA TAMER AYVAZ[(1)] & ALPER ELÇI[(2)]

[(1)] Department of Civil Engineering, Pamukkale University, Denizli, Turkey,
tayvaz@pamukkale.edu.tr
[(2)] Department of Environmental Engineering, Dokuz Eylul University, Izmir, Turkey,
alper.elci@deu.edu.tr

ABSTRACT

Planning and management of groundwater systems require appropriate monitoring data for groundwater quality and aquifer hydraulic head measurements. These data are usually collected from monitoring wells which are spatially distributed in the basin. Since monitoring of groundwater systems can be a time consuming and costly task, a minimum number of monitoring wells with an optimum spatial distribution is desired. Therefore, the conception of monitoring networks becomes an important engineering optimization problem. For this purpose, a genetic algorithm (GA) based optimization approach is proposed in this study for seeking the optimum groundwater quality monitoring network, starting with an already available set of monitoring wells. The goal of the proposed approach is to determine the optimum numbers and locations of the monitoring wells which provides equivalent amount of groundwater quality information with those obtained by using all available monitoring wells. This task was accomplished by representing each monitoring location with a binary bit in a GA chromosome to determine whether the associated location will be selected for the network. Then, the corresponding configuration fitness value was calculated by interpolating the associated water quality data over the field. The configuration fitness consists of the two objectives which are the maximization of the Nash-Sutcliffe model efficiency and the minimization of the number of monitoring wells in the newly generated configuration. Integration of these two objectives in an optimization framework results in best solutions with a minimum number of monitoring wells over the entire basin. Applicability of the proposed solution approach was evaluated by using groundwater quality data for the Gediz River Basin, a major basin located in western Turkey. The model results indicate that the proposed approach significantly reduced the number of monitoring wells with a relatively small deviation of the spatial distribution of the studied water quality parameter.

Keywords: Water resources; groundwater quality; monitoring network design; genetic algorithm; interpolation.

1 INTRODUCTION

The planning and management of groundwater require appropriate monitoring of groundwater quantity and quality. Data obtained from this kind of monitoring is typically collected by monitoring well networks, which may consist of more or less randomly distributed wells drilled in the studied aquifer system. The number and spatial distribution of wells in a monitoring network are important considerations that can affect the outcome in groundwater quality characterization studies. The configuration of a groundwater monitoring network that is used for groundwater sampling depends on several site-specific factors such as locations of already existing wells, suitability of a well for groundwater sampling, well configuration (number and depth of screens), accessibility, distance between wells, number of required groundwater samples, project budget and time, etc. Since groundwater sampling can become a time consuming and costly task, optimum design and assessment of the monitoring well network must be viewed as an important engineering optimization problem. Therefore, the main objective of this study is to propose a genetic algorithm (GA) based optimization approach (Goldberg, 1989) to solve this problem. The goal is to determine the optimum number and locations of the monitoring wells that provides an equivalent amount of groundwater quality information compared to the outcome of a network with the most available number of monitoring wells.

Previous studies dealt with the optimization of groundwater monitoring well networks to identify the distribution of contaminant plumes (Chadalavada and Datta, 2008; Kim and Lee, 2006), to identify unknown pollution sources (Jin et al., 2014; Bashi-Azghadi and Kerachian, 2010; Datta et al., 2009), and to reduce redundancy and minimize cost (Guo et al., 2011; Dhar and Datta, 2010; Baalousha, 2010; Wu et al., 2005). Methods used in these studies vary, however, most of them are based on nonlinear search and optimization methods used in combination with geostatistics (Chadalavada and Datta, 2008), flow and transport modeling (Wu et al., 2005; Reed et al., 2000) or groundwater vulnerability mapping (Baalousha, 2010).

The study presented in this paper focuses on finding a network with the fewest wells aiming to obtain sufficient information on groundwater quality. In the currently proposed approach, each monitoring well in the watershed is represented with a binary GA bit to evaluate if the corresponding monitoring well will be selected for the network. After determining the monitoring well distribution for each GA solution, their configuration fitness is calculated by interpolating the associated water quality data over the basin by using the minimum curvature interpolation approach. The proposed approach can solve the problem by simultaneously optimizing two conflicting objectives. The first objective is the maximization of the Nash-Sutcliffe model efficiency which is calculated by using the interpolated water quality data for the solutions with all available monitoring wells and the newly generated well configuration. The second objective deals with the minimization of the number of monitoring wells in the newly generated configuration by considering economic constraints.

2 STUDY AREA

The applicability of the proposed approach was evaluated on the groundwater monitoring wells of the Gediz River Basin (GRB) which is one of the most important river basins in Turkey (Figure 1). GRB has a drainage area of 17,146 km^2 and receives a total of 617 mm precipitation annually, based on long-term meteorological records. Main socio-economical activities in the basin are agriculture, animal husbandry, food industry, textile industry and mining. The agriculture sector is the most important water consumer in the GRB. Approximately 351,000 hectares of the basin area is subjected to extensive agricultural practices. Hydrogeology of the GRB consists of the 8 units which are sedimentary units (clay, sand, and gravel), limestone, clayey limestone (karst), detritic rocks, fractured rocks (volcanic), fractured limestone (karst), sandstone, shale, marble (karst), schist, and gneiss (DSI, 2014). A general location map of the GRB is provided in Figure 1.

Groundwater quality data set for the GRB was obtained from DSI (2014), which is a report for a comprehensive hydrogeological study conducted in the GRB. During the mentioned study, groundwater samples from 618 wells were collected for three monitoring periods which represented different seasons of the year (Mar – May 2013, Sep – Nov 2014, Mar – May 2014). All samples were analyzed for over 20 groundwater quality parameters. For this study, electrical conductivity (EC) is considered as the main groundwater quality parameter that is to be used in the optimization of the monitoring network. EC is a widely used indicator parameter to assess the general quality status of groundwater. For each monitoring period, spatial distributions of measured EC values are given in Figure 2.

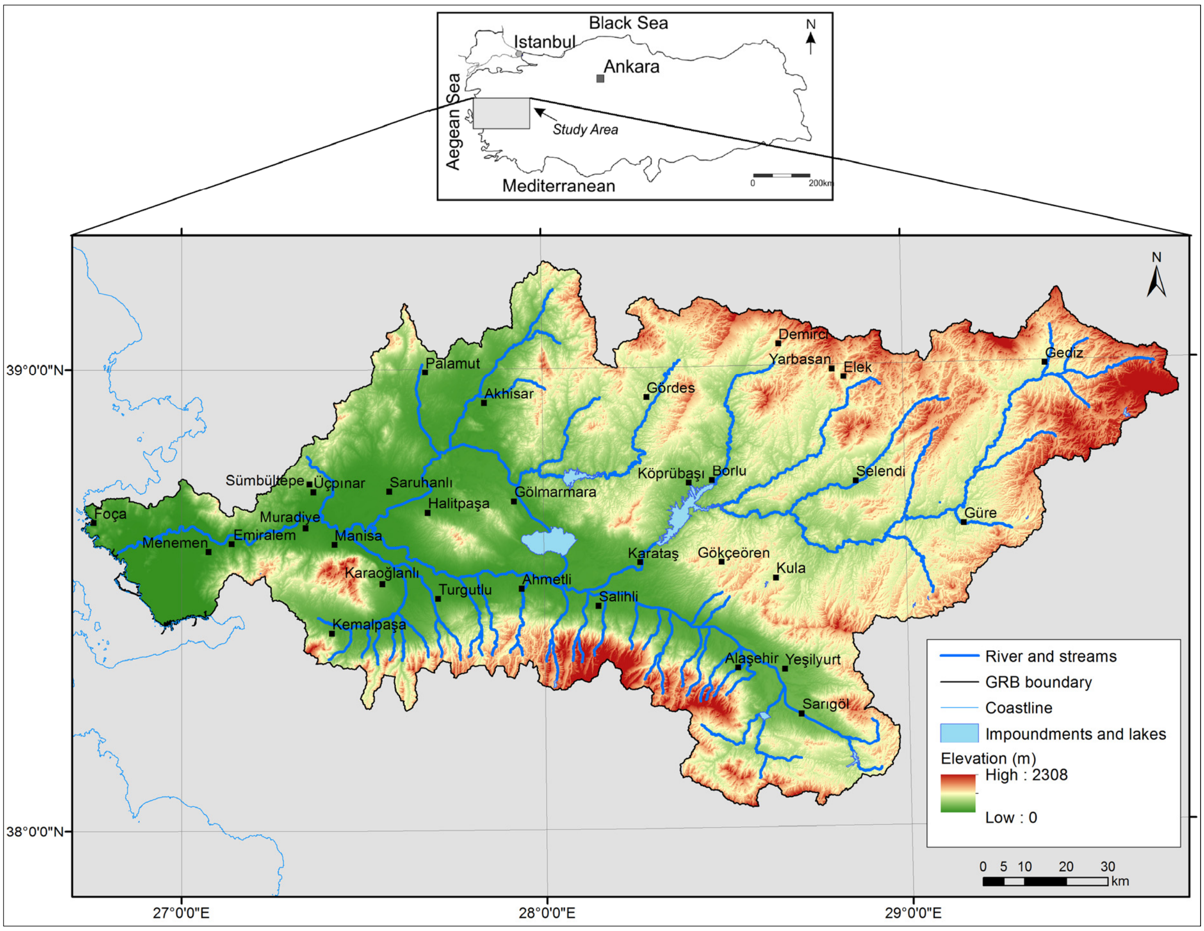

Figure 1. General location map of the Gediz River Basin (GRB).

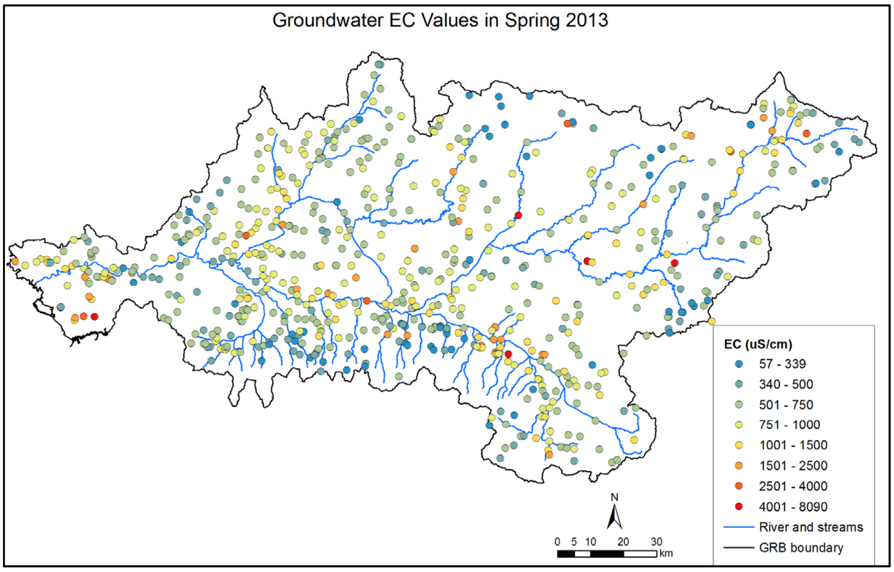

(a)

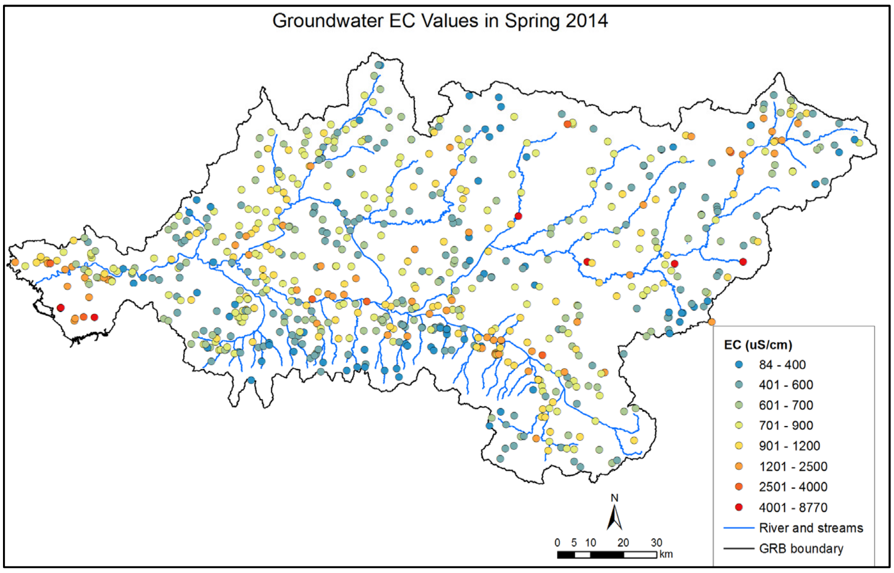

(b)

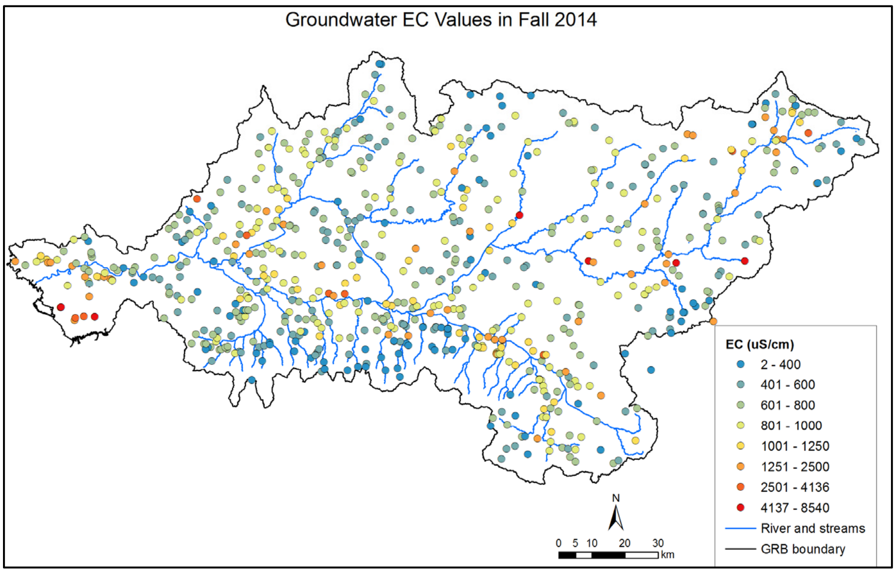

(c)

Figure 2. EC values in (a): Mar – May 2013; (b): Mar – May 2014; (c): Sep – Nov 2014.

GW Quality Parameter	Bits for Monitoring Wells									
	q_1	q_2	q_3	q_4	q_5	q_6	q_7	q_8	q_9	q_{10}
Bits for I_1	1	0	1	1	0	0	1	0	1	1
Bits for I_2	0	0	1	0	1	1	0	0	0	1

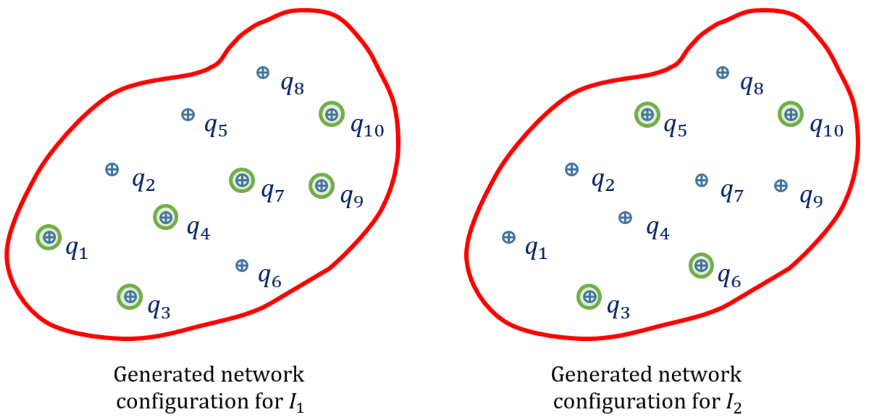

Figure 3. Random bits and their corresponding monitoring network configurations for $n_p = 2$ and $n_b = 10$.

3 OPTIMIZATION MODEL

As indicated previously, a GA-based optimization approach was proposed for seeking the optimum groundwater quality monitoring network. The objective of the proposed approach is to optimally determine the numbers and locations of the monitoring wells which provides an equivalent amount of groundwater quality information with those obtained by using all available monitoring wells in the field. The computational steps of the proposed GA-based optimization approach can be defined as follows:

Let n_p be the number of chromosomes in the GA population, n_b be the number of all available monitoring wells in the field, and I_c $\left(c = 1,2,3,\cdots,n_p\right)$ be the c^{th} GA chromosome in the population. I_c has a total of n_b bits and each of them corresponds to a monitoring well location such that a value of 1 means the corresponding monitoring well is active whereas a value of 0 means the well is not active in the generated network configuration. The first task is to generate the initial population which includes randomly generated $n_p \times n_b$ bits. As an example case, Figure 3 shows randomly generated GA chromosomes and their corresponding network configurations for an example basin model by considering $n_p = 2$ and $n_b = 10$.

As can be seen from Figure 3, for I_1 and I_2, 6 and 4 out of 10 monitoring wells are selected as the active wells to build up the network configurations. After this process, the groundwater quality information of q_k $(k = 1,2,3,\cdots,n_b)$ in the active well locations are interpolated over the field. The rationale for this operation is the conversion of point observations to a two dimensional parameter field. Then, interpolated parameter values within the watershed are separated from the all values to calculate the configuration fitness values. This optimization problem can be mathematically defined as follows:

$$z = \max(f_1 - \omega f_2) \qquad [1]$$

$$f_1 = 1 - \frac{\sum_{i=1}^{m_x \cdot m_y}(\tilde{q}_i - \tilde{q}_i^*)^2}{\sum_{i=1}^{m_x \cdot m_y}(\tilde{q}_i^* - \bar{\tilde{q}}^*)^2} \qquad [2]$$

$$f_2 = \frac{\tilde{\eta}}{n_b} \qquad [3]$$

subjected to

$$\tilde{q}_i = \begin{cases} \tilde{q}_i & \text{if } i^{\text{th}} \text{ grid point is located in the basin boundary} \\ 0 & \text{otherwise} \end{cases} \; ; \; i = 1,2,3,\cdots,m_x \cdot m_y \qquad [4]$$

$$\tilde{q}_i = \langle q_k, \tilde{\eta} \rangle_{m_x \cdot m_y} \ ; \ i = 1,2,3,\cdots, m_x \cdot m_y \ ; \ k = 1,2,3,\cdots, n_b \qquad [5]$$

$$\tilde{\eta} = \sum_{k=1}^{n_b} \eta_k \qquad [6]$$

$$\eta_k = \begin{cases} 1 & \text{if } k^{\text{th}} \text{ monitoring well is active} \\ 0 & \text{otherwise} \end{cases} \ ; \ k = 1,2,3,\cdots, n_b \qquad [7]$$

where q_k is the groundwater quality information in the k^{th} monitoring well $(k = 1,2,3,\cdots, n_b)$; η_k is an integer variable which takes a value of 1 if k^{th} monitoring well is active, otherwise it takes a value of 0; $\tilde{\eta}$ is the number of active wells which is calculated by taking the sum of all η_k values $(k = 1,2,3,\cdots, n_b)$; $\langle q_k, \tilde{\eta} \rangle_{m_x \cdot m_y}$ is the minimum curvature based interpolation model which converts the point measurements in the $\tilde{\eta}$ wells into two dimensional continuous surface with a dimensions of $m_x \times m_y$ where m_x and m_y are the number of grids in x and y directions, respectively; $\tilde{q}_i$ is the interpolated groundwater quality information in the i^{th} grid point $(i = 1,2,3,\cdots, m_x \cdot m_y)$; $\tilde{\mathfrak{q}}_i$ is the groundwater quality information value which takes a value of $\tilde{q}_i$ if i^{th} grid point is located within the watershed boundary $(i = 1,2,3,\cdots, m_x \cdot m_y)$, otherwise it takes a value of 0; $\tilde{\mathfrak{q}}_i^*$ is the groundwater quality information value in the i^{th} grid point $(i = 1,2,3,\cdots, m_x \cdot m_y)$ which is calculated by considering all available monitoring wells within the basin (n_b); and $\bar{\mathfrak{q}}^*$ is the mean of the all $\tilde{\mathfrak{q}}_i^*$ values in the field.

As can be seen from Eq. [1], the objective function (z) of the optimization model is composed of two different objectives. The first objective (f_1) deals with the maximization of the Nash-Sutcliffe model efficiency whose value changes from $-\infty$ to 1 such that a value of 1 corresponds to a perfect match between $\tilde{\mathfrak{q}}_i$ and $\tilde{\mathfrak{q}}_i^*$ for all the grid points in the watershed. The second objective (f_2) is related with the minimization of the ratio between the number of active and all available monitoring wells which is used due to the economic reasons. Note that these two objectives are integrated in a single objective function by using a weighting coefficient of ω which is used to adjust the importance of f_2 with respect to f_1. Note that different values of ω result with different optimum solutions. Therefore, a detailed sensitivity analysis should be conducted to determine the influence of ω to the model results.

After calculation of the configuration fitness (i.e. Eq. [1]) for each chromosome in the GA population, a new population is generated by means of the roulette wheel approach (Goldberg, 1989). Furthermore, the best solution in the population in terms of the calculated configuration fitness values is directly transferred to the next generation by means of the Elitism rule. Then, randomly selected chromosomes are subjected to crossover and mutation processes based on the probabilities of p_c and p_m. After completion of these computational steps, a new GA population is formed. By repeating these steps until satisfying the defined termination criterion (i.e. maximum number of generations), the problem of optimum groundwater monitoring network design can be solved by means of the proposed GA based optimization approach. The flowchart of the proposed GA based optimization approach is given in Figure 4.

4 IDENTIFICATION RESULTS

The proposed GA based optimization approach was executed to seek the optimum monitoring network in GRB by considering the EC values in the first monitoring period (i.e. Mar – May 2013). As indicated previously, the first objective is to maximize the Nash-Sutcliffe model efficiency which is determined by interpolating the EC values in the generated network configuration for each GA chromosome and all the available wells in the basin, respectively. The second objective is to obtain the best configuration by considering the minimum number of monitoring wells since each well needs to be visited to collect the samples. Since these two objectives are integrated into a single objective function by means of a weighting coefficient, ω, the identified results were evaluated for different ω values. Note that the total number of bits for each GA chromosome was assumed to be $n_b = 618$ since each well in GRB corresponds to a GA bit. As indicated previously, once the value of a bit is 1, the corresponding monitoring well was assumed to be active which means the EC value in the well was used during interpolation. On the other hand, the value of 0 for a bit means that the corresponding well is not active and its EC value was not used in the interpolation. Since the bit numbers for each GA chromosome was relatively high, the number of populations was taken as $n_p = 200$ to maintain the diversity in the population. The probabilities of crossover and mutation were taken as $p_c = 0.95$ and $p_m = 0.025$ and search process was terminated after 500 GA generations. For different ω values, the convergence plots of the proposed GA based optimization approach can be seen in Figure 5. As can be seen, for all the solutions, search processes were started from different initial solutions and objective function values were continuously improved through GA generations. It is clearly seen that when the values of ω increased from 0.20 to 1.00, the corresponding objective function values decreased as an expected behavior since the second objective of f_2 becomes more dominant for the higher ω values. Regarding this outcome, the identification results for different ω values are compared in Table 1.

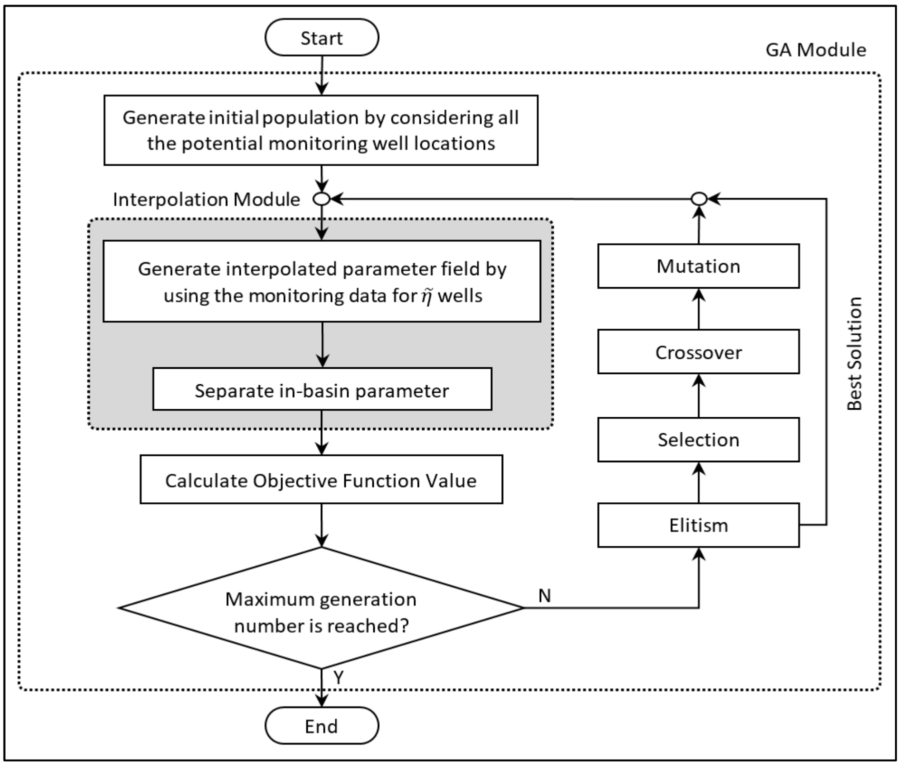

Figure 4. Flowchart of the proposed GA-based optimization approach.

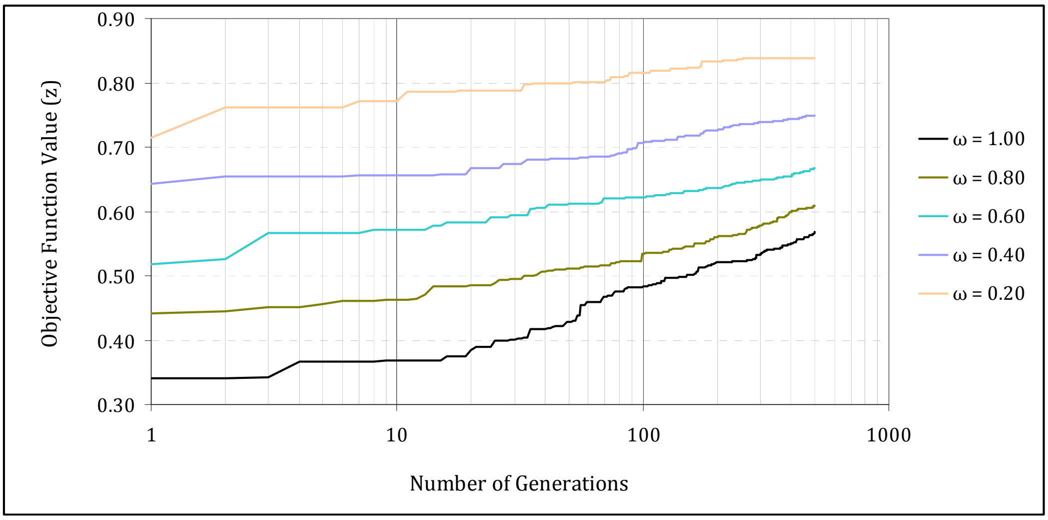

Figure 5. Convergence plots for different ω values.

Table 1. Identified results for different ω values.

Weighting Coefficient (ω)	Objective Function Value (z)	Nash-Sutcliffe Model Efficiency (f_1)	Ratio between the number of active and all available monitoring wells (f_2)	Number of Active Wells ($\tilde{\eta}$)
0.20	0.839	0.951	0.563	348
0.40	0.749	0.937	0.471	291
0.60	0.667	0.920	0.422	261
0.80	0.609	0.891	0.353	218
1.00	0.569	0.877	0.307	190

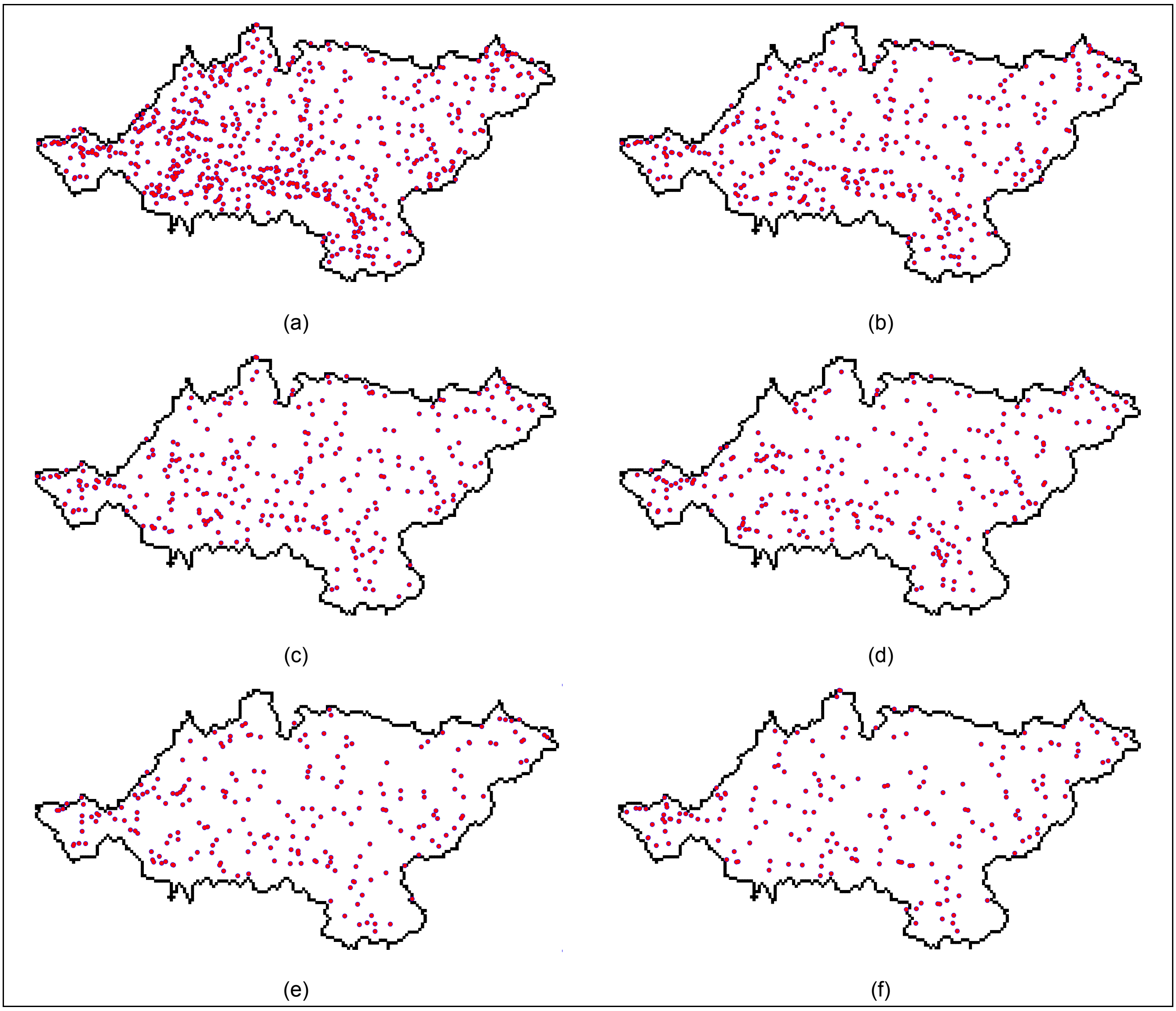

Figure 6. Identified monitoring well locations for different ω values (a): 618 monitoring wells; (b): $\omega = 0.2$; (c): $\omega = 0.4$; (d): $\omega = 0.6$; (e): $\omega = 0.8$; (f): $\omega = 1.0$.

As can be seen from Table 1, for $\omega = 0.2$, the final objective function value was obtained as 0.839 which corresponds to a Nash-Sutcliffe model efficiency of 0.951. This result was obtained by using 348 wells and this corresponds to 56.3% of all the monitoring wells in GRB. For $\omega = 1.00$, the objective function value was reduced from 0.839 to 0.569 and the same trend was also observed in the Nash-Sutcliffe model efficiency which was reduced from 0.951 to 0.877. However, this result was obtained by using the EC values in 190 wells which corresponds to 30.7% of all the monitoring wells. Generally speaking, the number of active wells monotonically decreased as the value of ω increased. As indicated previously, this result is associated with the dominant nature of the f_2 for the high ω values. For each solution in Table 1, the identified monitoring well locations are compared in Figure 6. It is clearly seen that all the identified well locations covers the entire area of the GRB.

It should be noted that the monitoring networks in Figure 6 were identified by considering the EC values in the first monitoring period (i.e. Mar – May 2013). After obtaining the model results, the next task was to validate the identified well configurations by considering the EC values in the second (i.e. Sep – Nov 2014) and the third (i.e. Mar – May 2014) monitoring periods. Note that the GA-based optimization model was not executed for the validation process. Instead, EC values in the corresponding well locations (Figure 6) for the second and the third monitoring periods were interpolated and the results were compared with those obtained by interpolating the EC values for the all available monitoring wells in the field. The validation results are given in Figure 7 in terms of the Nash-Sutcliffe model efficiency coefficient. As can be seen, for $\omega = 1.0$, the validation process resulted in the efficiency values over 0.90 and 0.88 for the second and the third monitoring periods, respectively. The trend of decrease in the model performance with increase of ω was also observed in the validation process.

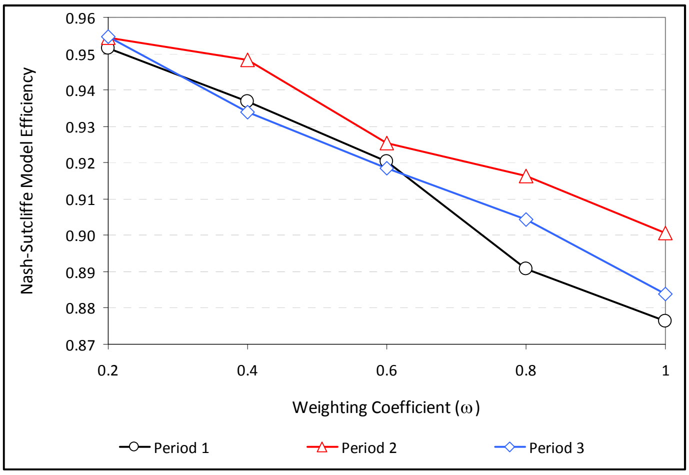

Figure 7. Validation results for different ω values.

5 CONCLUSIONS

In this study, a GA-based optimization approach is proposed for assessing and designing the groundwater quality monitoring networks. In the proposed approach, each monitoring well in the basin was represented with a binary GA bit to evaluate if the corresponding monitoring well location would be selected for the new network configuration. After determining the network configuration by means of the GA chromosomes, the corresponding parameter field was generated by using the Minimum Curvature interpolation approach. The proposed approach has two objectives: Maximization of the Nash-Sutcliffe model efficiency and minimization of the well numbers in the alternative network design and these two objectives are combined in a single objective function by means of a weighting coefficient. Integration of these two conflicting objectives in an optimization framework resulted with the best solutions that suggest a minimum number of monitoring wells over the entire watershed. Applicability of the proposed GA-based optimization approach was evaluated by using groundwater quality data from 618 groundwater monitoring wells in the Gediz River Basin, Turkey. Identified results indicated that the proposed optimization approach significantly reduced the number of monitoring wells with a relatively small change in the spatial concentration distribution of the selected groundwater quality parameter. Furthermore, since different values of this weighting coefficient provide different solutions, a detailed decision making analysis should be performed to determine which network configuration is the best alternative. All the analyses were performed by taking the electrical conductivity as the water quality parameter. Same model runs should also be performed for other parameters and the results of them should also be included in the decision making analysis which is considered as a future study.

REFERENCES

Baalousha, H. (2010). Assessment of a Groundwater Quality Monitoring Network using Vulnerability Mapping and Geostatistics: A Case Study from Heretaunga Plains, New Zealand. *Agricultural Water Management*, 97, 240-246.

Bashi-Azghadi, S.N. & Kerachian, R. (2010). Locating Monitoring Wells in Groundwater Systems using Embedded Optimization and Simulation Models. *Science of the Total Environment*, 408, 2189-2198.

Chadalavada, S. & Datta, B. (2008). Dynamic Optimal Monitoring Network Design for Transient Transport of Pollutants in Groundwater Aquifers. *Water Resources Management*, 22, 651-670.

Datta, B., Chakrabarty, D. & Dhar, A. (2009). Optimal Dynamic Monitoring Network Design and Identification of Unknown Groundwater Pollution Sources. *Water Resources Management*, 23, 2031-2049.

Dhar, A. & Datta, B. (2010). Logic-based Design of Groundwater Monitoring Network for Redundancy Reduction. *Journal of Water Resources Planning and Management*, 136(1), 88-94.

DSI. (2014). *Hydrogeological Study of the Gediz Watershed*, Main Report, Eser Project & Engineering Inc., Ankara.

Goldberg, D. (1989). *Genetic Algorithms in Search, Optimization, and Machine Learning*. Addison-Wesley, MA, 1-6.

Guo, Y., Wang, J.F. & Yin, X.L. (2011). Optimizing the Groundwater Monitoring Network using MSN theory. *Procedia Social and Behavioral Sciences*, 21, 240-242.

Jin, X., Ranjithan, R.S. & Mahintakumar, G. (2014). A Monitoring Network Design Procedure for Three-Dimensional (3D) Groundwater Contaminant Source Identification. *Environmental Forensics*, 15(1), 78-96.

Kim, K.H. & Lee, K.K. (2007). Optimization of Groundwater-Monitoring Networks for Identification of the Distribution of a Contaminant Plume. *Stochastic Environmental Research and Risk Assessment*, 21(6), 785-794.

Wu, J., Zheng, C. & Chien, C.C. (2005). Cost-Effective Sampling Network Design for Contaminant Plume Monitoring under General Hydrogeological Conditions. *Journal of Contaminant Hydrology*, 77, 41-65.

Proceedings of the 37th IAHR World Congress
August 13 – 18, 2017, Kuala Lumpur, Malaysia

OPERATIONAL DECISION SUPPORT SYSTEM FOR SUSTAINABLE WATER RESOURCE MANAGEMENT FOR SUNGAI SELANGOR

LEONORE BOELEE[(1)], RAZAK BAHROM[(2)], HASLINA AMIR[(3)], ZAMRI SONDOR[(4)], EMMA BROWN[(5)]
FAIZAH AHMAD[(6)] & GEOFF WILSON[(7)]

[(1, 5, 6, 7)] HR Wallingford Asia Sdn. Bhd., Kuala Lumpur, Malaysia.
l.boelee@hrwallingford.com; e.brown@hrwallingford.com; faizah.ahmad@hrwallingford.com; g.wilson@hrwallingford.com
[(2)] Servis EDA, Kuala Lumpur, Malaysia.
razak@serviseda.com
[(3, 4)] Lembaga Urus Air Selangor (LUAS), Selangor Darul Ehsan, Malaysia.
haslina@luas.gov.my; norzamri@luas.gov.my

ABSTRACT

The Selangor River lies on the west coast of Peninsular Malaysia, 70 km north of Kuala Lumpur. The Selangor catchment area is approximately 2000 km^2 and has two major dams located in the upstream part of the catchment: Sungai Selangor Dam and Sungai Tinggi Dam. Lembaga Urus Air Selangor (LUAS) is the Malaysian government agency responsible for water resources management of the Selangor catchment, with their main challenge being to balance an increase in water demand, whilst trying to manage the catchment's environmental state. The key to this is the amount of water that is released from the two reservoirs. The current manual decision-making process (based on staff experience) does not provide LUAS with the efficiency and accuracy that is required in a catchment where sustainability is key and water resources are not always abundant. A solution was required to improve the management of the current resources, thus reducing the need for the costly and environmentally contentious development of new infrastructure. The operational Decision Support System (DSS) for sustainable water resources management of the Sungai Selangor catchment is a non-structural tool developed to support LUAS in optimising the reservoir releases and water abstractions in the catchment. The DSS is a fully automated system that is driven by a combination of live, telemetered gauged data from various sources including the InfoBanjir telemetry database and Numerical Weather Prediction (NWP) rainfall forecasts from the Malaysian Meteorological Department (MMD). Simulations are carried out automatically on an hourly basis, to calculate and forecast whether water levels at the main abstraction location (SSP1) are being maintained at the required levels. If the required water levels at SSP1 are not met, being either too high or too low, the model is re-run using an adjusted reservoir release time series. The DSS should also be able to help LUAS in the future to increase the sustainability of management of water resources in the Selangor catchment. This paper describes the approach developed to support LUAS to meet this objective, in a manner that can be used in real-time, and can be transferred to other catchments in the future. The advantages and disadvantages of potentially expanding this system to use ensemble forecasts, data assimilation and optimization algorithms are discussed, along with suggestions for further research.

Keywords: Water resource management; operational systems; NWP; forecasting.

1 INTRODUCTION

In Malaysia, drought frequency is increasing and in recent years, a series of drought conditions has hit the country (Sanusi et al., 2015). Changes in global precipitation patterns may be causing increasing drought frequency in Malaysia (Ahmad and Low, 2003), in (Sanusi et al., 2015), (Ahmad and Hashim, 2010), in (Sanusi et al., 2015). In the region of Selangor, the most recent drought was in 2014. During this drought, the authorities were forced to ration water supplies for residential and business use, which disrupted daily activities. An important factor in the water shortage experience of 2014 was the increasing demand for water. The demand for water in Malaysia has increased 60% in the time period from 1995 to 2010. Predictions suggest an overall increase of 113% by 2020 (Department of Environment (DOE), 2003) in (Fulazzaky, 2013).

The Sungai Selangor catchment in Malaysia (Figure 1) provides water resources to the people and industries in the catchment as well as to four million people and industries in Kuala Lumpur, Petaling, Gombak and Julu Selangor (Department of Irrigation and Drainage (DID), 2007) in (Fulazzaky, 2013), (RBM Engineering consultant, 2014). In total, 60% of the water resources from the Selangor catchment are transferred for use outside of the catchment. Therefore, the Selangor catchment is of particular importance to the water resources of Malaysia.

To minimize water shortages in the future there are two main options: 1) increase water resource capacity; and 2) improve the management of the current resources. Increasing capacity through, for example, constructing new reservoirs is costly and has major environmental impacts. To cope with present and future demands it is essential to achieve optimization of the current supplies and improve the management of existing reservoirs (Ahmad et al., 2014).

One of the main aims of the Selangor Water Management Authority (Lembaga Urus Air Selangor: LUAS) is to improve the sustainability of water resource management within the Selangor catchment. LUAS have recognized the need to replace their manual reservoir release system with a decision-making system with increased efficiency and accuracy that will ensure minimum wastage of water resources.

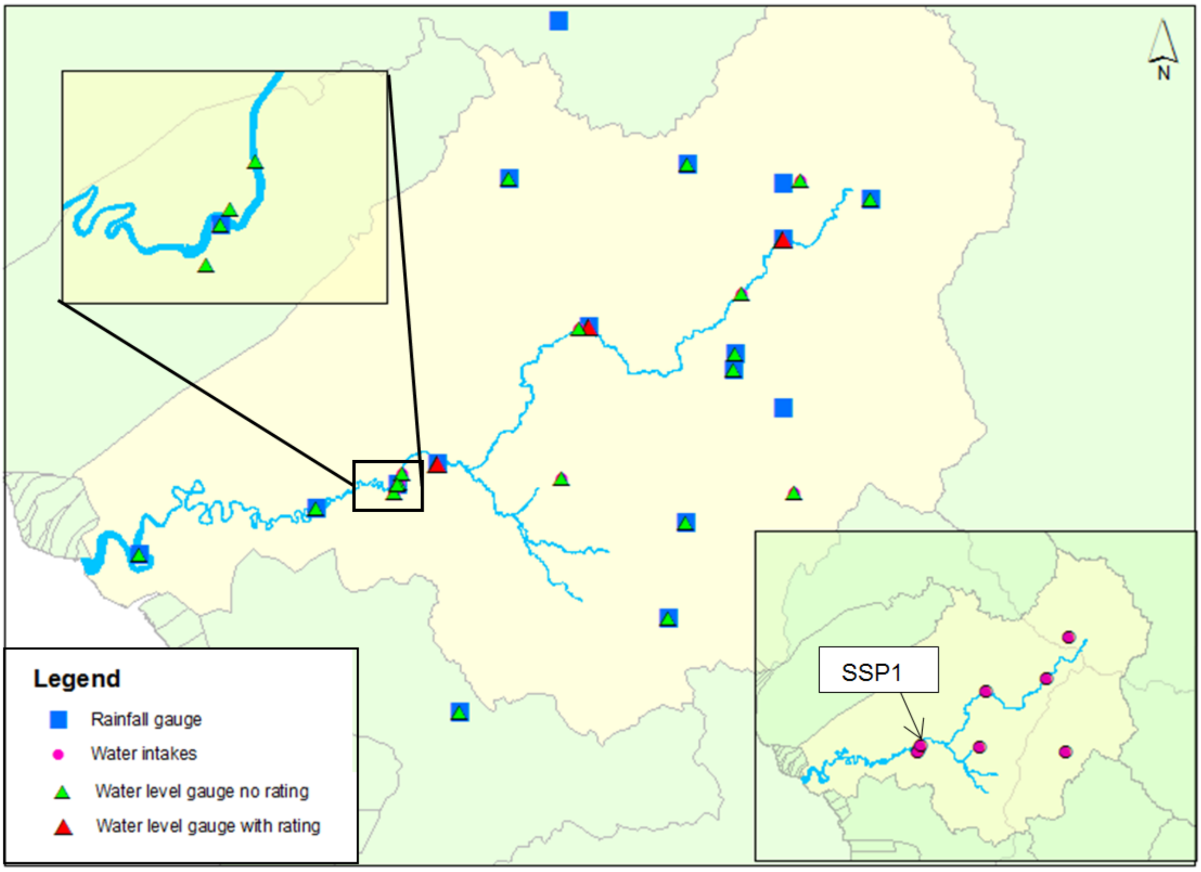

Figure 1. Map of the Sungai Selangor catchment, showing details of main abstract point SSP1 (inserts).

Research into how to optimize reservoir operations is plentiful, however there is a gap between the theoretical reservoir operation and the real-world implementation (Hejazi et al., 2008). In the research on reservoir release operations, there is a heavy focus on optimization algorithms but not enough focus on the needs of the reservoir operators who are looking for practical operational strategies (Ahmad et al., 2014). This gap is captured well in (Acreman, 2005) where different drivers of water managers and scientists are described. Water managers often have short time scales dictated by legislation, and seek simple consistent methods. In contrast, scientists often undertake long periods of study driven by innovation, and aim to produce replicable studies.

This paper provides an overview of an operational forecasting system where the best scientific solutions were matched to the needs, available data, facilities and resources of the reservoir managers at LUAS. Care was taken to consider the best solution in a holistic way, considering the whole forecast chain from the collection of real-time data and running the operational system, to communication and dissemination of warnings (WMO and GWP, 2013). Emphasis was placed on the needs and requirements of the operational staff in order to develop a user-friendly decision support tool. The new forecasting system provides short term dam release forecasts (3 days) and replaces the current manual reservoir release system. This new system aims to improve the sustainability of the water resources management. The advantages and disadvantages of potentially expanding this system to use ensemble forecasts, data assimilation and optimization algorithms are discussed.

2 BACKGROUND

2.1 Catchment description

The catchment of Sungai Selangor is located in the state of Selangor and is approximately 70 km north of Kuala Lumpur. The topography of the catchment is a mix of steep mountainous, hilly country and undulating low terrain (Hong and Hong, 2016). The climate in Selangor is tropical, with the southwest monsoon occurring in April and May and the northeast monsoon occurring in October to December. Dry periods dominate in January to March and June to September (Hong and Hong, 2016). The annual average rainfall in the state of Selangor is 2285 mm with a large proportion falling in the mountainous region rather than on the plains (Desa and Daud, 1999) in (Desa et al., 2001). Approximately 42% of the average annual rainfall occurs during the northeast monsoon season and 28% during the southwest monsoon season (Desa, et al., 2001).

Sungai Selangor has a length of 110 km with the river source located at the slopes near Fraser's Hill and Genting Highlands on the Main Range, from where it flows in a south-westerly direction to the Straits of Melaka (WWF Malaysia, 2000). The river has 19 tributaries and the total catchment size is approximately 2000 km^2. There are reservoirs formed by two dams in the upstream section of the catchment: Sungai Selangor Dam and Sungai Tinggi Dam. These two dams support water abstraction during the dry season (RBM Engineering consultant, 2014). Additional water resources are available to the catchment under the Hybrid Off-River Augmentation System (HORAS). Water from the HORAS system can be pumped into Sungai Selangor via the Operasi Pengepaman Air Kolam (OPAK). The flow of Sungai Selangor matches the rainfall patterns. High flows are recorded during the monsoons, with the northeast monsoon (October to December) resulting in the highest flow conditions. The lowest flows occur during the dry period of July and August (Fulazzaky, 2013).

The state of Selangor is one of the most populated regions in Malaysia; the estimated population of 2016 is 6,298,400 (Department of Statistics Malaysia, nd.). The land use is a combination of urban, jungle and plantations including rubber, oil palm, paddy, maize and vegetable cultivation (Hong and Hong, 2016). Land use has changed rapidly in Malaysia in recent decades. From 1950, increasing agricultural production has led to the loss of forested land to agricultural land, first focusing on rubber, and since the 1960s, focusing on palm oil (Abdullah and Nakagoshi, 2008). Malaysia has also seen a growth in manufacturing since the 1980s which has led to rapid industrialisation in the state of Selangor, with an associated increase in urbanization and a decrease in agricultural land (Erickson, 1995). In Selangor, the current land use is 57% natural forest, 22% agricultural, 17% urban and 4% water (RBM Engineering consultant, 2014). Urbanisation is expected to increase further to allocate housing, commercial and industrial activities. Changes in land use such as the loss of forested land and urbanisation, will affect the ecological processes, including the hydrological cycle. The exact effect of land use change on the hydrology is difficult to be predicted accurately, but deforestation is associated with an increase in runoff (Siriwardena et al., 2006) and increased urbanisation is associated with increases in peak flows (Hundecha and Bardossy, 2004). These factors should be taken into account when selecting calibration data for hydrological models, and indicate that there is a necessity to periodically update the calibration accordingly.

2.2 Current operational practice

Currently, observed data are being collected across the catchment and assessed manually by the operators who make decisions based on their assessment of the data and their experience. LUAS has seen an increase in water demand and has targets to reduce water wastage. This current method of decision making is not providing the accuracy and efficiency to meet the increase in demands and the minimum wastage targets.

3 METHODS

The goal of the new decision support system (DSS) is to forecast the water level at the main downstream abstraction point, referred to as SSP1 (Sungai Selangor Phase 1), as presented in Figure 1. There are minimum and maximum water level thresholds at SSP1, between which the water level needs to be maintained. This can be achieved by releases from the Selangor Dam and Tinggi Dam. To maintain an optimal level of water at SSP1, the DSS provides the dam operators at Selangor Dam and Tinggi Dam with recommended reservoir releases for the next 36 hours.

To meet the requirement of forecasting water levels, the DSS has a river model at its core. The DSS has further modules which: 1) process observed data; 2) process forecast data; 3) estimate the reservoir releases; and 4) send out warnings. The dissemination and communication of warnings is an important part of this system, but is not covered by the technical focus of this paper. ICMLive was selected as the software tool to bring all of these modules together and take care of the automated processes including checking for new data, triggering river model runs and sending out warnings. A schematic overview of the DSS is presented as Figure 2.

3.1 Coupled hydrological and hydraulic modelling

In selecting an appropriate model to forecast water levels at SSP1 the approach of (Booij, 2005) was taken: "find a model that is sufficiently detailed to capture the dominant process and natural variability, but not unnecessarily refined that computation time is wasted or data availability is limited." There are broadly two types of hydrological models to choose from: physically based models and data-driven models. Both types of models have advantages and disadvantages, the reader is referred to (Todini, 2007) for a comprehensive overview. In the case of the Selangor catchment, there are limited historical data available which would limit the training sets that could be created for a data-driven approach. Using a physically based model allows all *a priori* knowledge of the hydrological processes to be used in setting up the model, with the aim of reducing the uncertainty of the *a posteriori* forecasts (Todini, 2007).

A well-known simple physical river model is the hydrological model which represents the rainfall-runoff processes and often uses flow routing calculations to represent the river flow. In a hydrological model, the Saint Venant equations are simplified by removing the momentum conservation equation, for details the reader is referred to (Vorosmarty et al., 1989), (Listonet al., 1994), and (Coe et al., 2008). This results in important physical aspects of river hydraulics being lost, including backwater effects and looped stage-discharge relations (Paiva et al., 2013). In the case of Sungai Selangor, which has structures like bridges and weirs, the loss of the backwater effect would lead to unreliable results in critically important forecasting points. For instance, the backwater flow due to the barrage at SSP1 would not be captured by a simple flow routing model. A 1D hydraulic model would be able to represent these important processes whilst having low computational demands and a low data input requirement (Pappenberger et al., 2005). At the core of this, DSS is a lumped hydrological model (representing the rainfall-runoff processes) coupled to a 1D hydraulic model (representing the river processes).

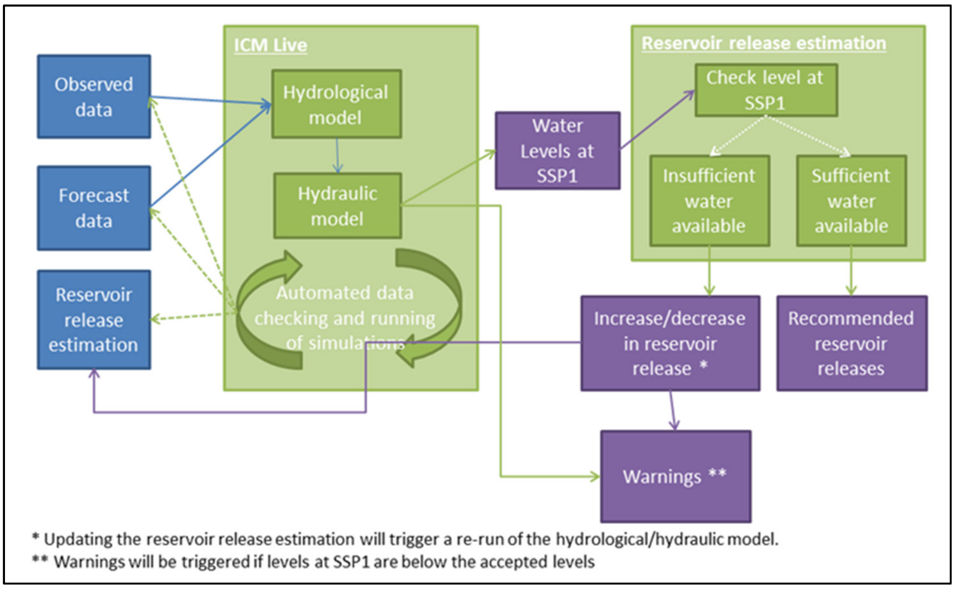

Figure 2. Schematic overview of the DSS with blue boxes for data, green boxes for modelling processes and purple boxes for outputs.

3.1.1 Probability Distributed Model (PDM)

In gauged catchments, the Probability Distributed Model (PDM), provides a pragmatic approach fitting between inherently complex, physically-based approaches, and simplified lumped modelling approaches; this probability-distributed approach considers the frequency of occurrence of certain hydrological variables used to derive algebraic expressions for the integrated flow response from the catchment (Moore, 1985). The PDM is a fairly general conceptual rainfall-runoff model which transforms rainfall and evaporation data to flow at the catchment outlet and was developed with operational applications in mind (Moore, 1985). The PDM model essentially distributes rainfall between runoff and recharge according to a soil moisture store. The runoff and recharge is routed via stores to the catchment outflow. One of the main advantages of the model is the use of a probability distribution rather than a single value for the soil moisture store. This represents the spatial variability in soil storage across the catchment and prevents threshold type behaviour. The model's short computational run time and continuous soil moisture accounting model makes it suited to continuous simulation using incoming telemetry data for flood forecasting. The model can also use observed flow data from telemetry to update its internal soil moisture values in a process known as state correction, which is important for maximising the accuracy of the model results.

3.1.2 Simple Runoff Model (SRM)

In the Sungai Selangor catchment, not all sub-catchments for which the rainfall-runoff process needs to be modelled are gauged. Although most of the catchments around the world are ungauged, setting up hydrological models for ungauged catchments remains a challenge (Bloschl, 2006). When no runoff data are available, keeping it simple is often the best solution. The Simple Runoff Model (SRM) is useful for deployment in catchments without any calibration data, or in urban areas if the runoff response is thought not to follow a soil moisture response. Eq. [1] presents the SRM equation in which the Effective Precipitation represents the runoff.

$$P_{eff} = P_c * RC * (1 - SMD) \quad [1]$$

where,

$$P_{eff} = Effective\ Precipitation$$
$$P_c = Catchment\ Precipitation$$
$$RC = Constant\ Runoff\ coefficient\ (0-1)$$
$$SMD = Soil\ Moisture\ Deficit\ Fraction\ (0-1)$$

In this approach, catchment rainfall is multiplied by a runoff fraction which is determined by the user and by a soil moisture deficit (SMD) fraction. The SMD fraction may be fixed, but for rural catchments, more accurate results are to be achieved if a time series is supplied. Soil moisture data are not available in this catchment, therefore, using the concept of hydrological similarity, it is assumed that catchments close to each other will behave hydrologically in a similar manner; this assumption is known as spatial proximity (Bloschl, 2006). Using these concepts, the soil moisture deficit time series from the PDM models in the gauged catchments can applied to the ungauged catchments. Although this method will increase the uncertainty of the forecasts, using calibration parameters from similar catchments in the same region is preferable over, for example, using parameters from donor catchments (Bloschl, 2006).

3.2 Observed data

Malaysia has an extensive network of gauging stations which include rainfall and water level stations (Department of Irrigation and Drainage Malaysia, 2017). In the LUAS catchment, there are 17 rainfall stations and 13 water level stations along the section of river that is being modelled. These data are available hourly at 15 minute intervals. There are rating curves available at the location of three water level stations, allowing the transformation from water level to flow. Further data are available for LUAS dam operators. For both dams, there are reservoir water level, dam spill and dam release data. These data are available as daily data. Water abstraction data are operationally available. The 17 rainfall stations and 13 water level stations are available operationally. The operational data is being provided to the LUAS server as simple text files. ICMLive checks for new data every hour (this can be increased if required) and before every run. In total, 76 gauges are connected to the live system of which 17 are rainfall gauges, 11 are water abstraction gauges, 4 provide reservoir data (spills and releases), 29 represent inflow water from the HORAS storage ponds and 15 water level gauges. An example of the observed flow, reservoir spills and observed rainfall data is presented in Figure 3.

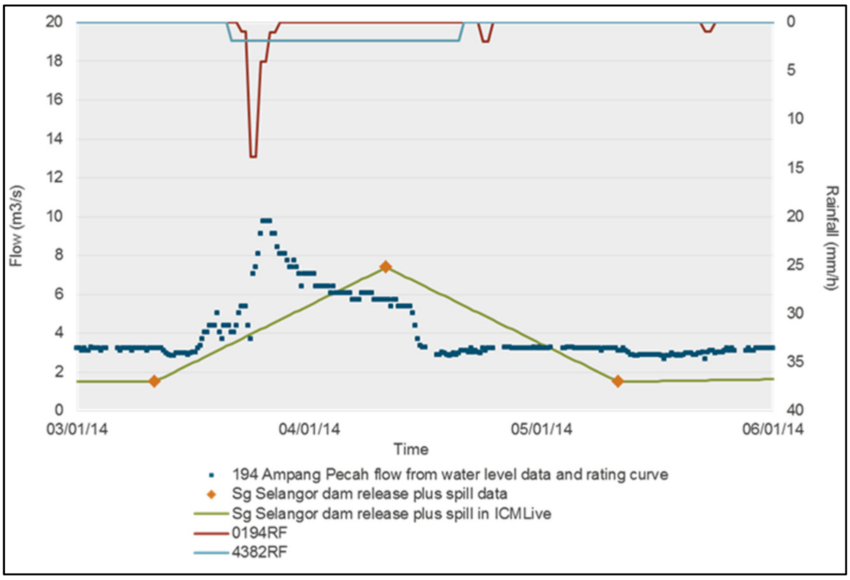

Figure 3. Example of the observed flow, reservoir spills and observed rainfall data for the Sungai Selangor catchment.

Challenges with the observed data include dealing with missing data. Missing data can occur due to various reasons such as instrument failure, power failure or communication line breakdown (Dastorani et al., 2010). Dealing with missing data is a challenge for both the calibration of the hydrological models and the running of the operational system. Another challenge with observed data is dealing with measurement errors. Errors in measurements are unpreventable and can be described as random errors, systematic errors and mistakes due to misreading an instrument or instrument malfunction (BSi, 1986). Errors in measurement will affect the calibration process and can yield biased parameter estimation (McMillan et al., 2010). To limit this, the data were cleaned of any constant systematic errors and mistakes where possible.

3.3 Forecast data

The Malaysian Meteorological Department (MMD) operationally runs the Weather Research and Forecasting model (WRF) (NCAR et al., 2017). The WRF model was first released in 2004 with one of its main objectives being to advance the understanding and prediction of mesoscale weather systems including precipitation systems. The wide user community and dissemination of the WRF model has been successfully advanced since the release date. Currently the user group has over 30,000 registered users in 150 countries (NCAR et al., 2017). The MMD has extensively tested the forecast performance of the WRF model for precipitation forecasts in Malaysia, for more information, the reader is referred to (Ibadullah et al., 2013). Currently, MMD are running WRF model version 2.2, a hydrostatic model at a horizontal resolution of 3km over a forecast time period of 5 days. The WRF model will be updated to a later version corresponding with the upgrade of the high performance computer (HPC). In preparation for this, extensive tests of the WRF model version and ensembles have been conducted (Subramaniam et al., 2010). MMD provides precipitation forecast data for the Sungai Selangor sub-catchments in gridded ASCII files. Forecasts are provided twice per day, at 00 hours and 12 hours. ICMLive automatically finds and loads the new forecast data and uses the first three days of the forecast in its water level predictions. An example of the NWP precipitation forecast is presented as Figure 4.

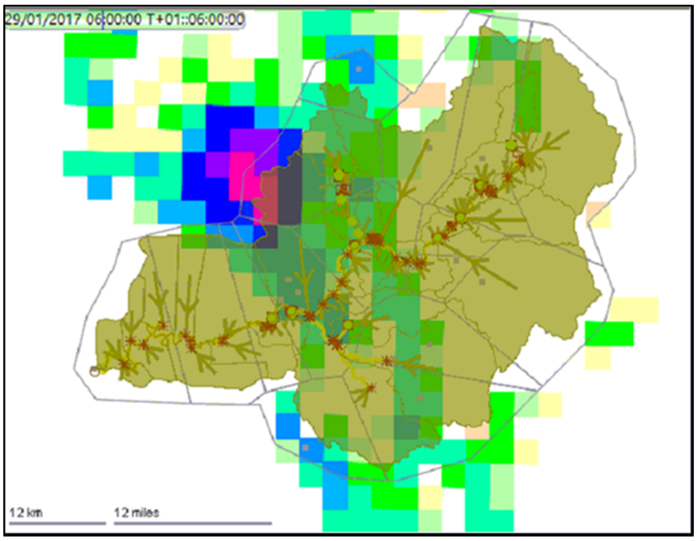

Figure 4. Example of the NWP precipitation loaded into the ICMLive system.

3.4 Estimation of reservoir releases (ERR)

As a starting point, the forecast reservoir releases of the previous day are supplied to the ICMLive system. The ICMLive system runs and produces forecasts of the water levels at SSP1 for the next 36 hours. The ERR compares the forecast water level with the optimal level and the tolerance level. If the forecast water levels at SSP1 drop beneath the threshold, the reservoir release time series is updated accordingly and this triggers a new ICMLive run. The newly produced forecast water levels at SSP1 are processed again by the ERR. If the levels are within the thresholds, the forecast reservoir release time series is then passed onto the reservoir operators as the recommended release. The ERR takes the minimum travel time of the water into account, which is 14 hours for the Tinggi dam, and 20 hours from the Selangor Dam to the barrage at SSP1 (RBM Engineering consultant, 2014).

4 RESULTS

4.1 Hydrological calibration

For the three locations where rating curves are available the PDM rainfall-runoff model was calibrated. Manual calibration was aided by using the automated PDM calibration tool. The calibration data were cleaned and prepared in calibration and validation sets. Low flow periods were prioritized whilst low flow simulation was continually checked. For all three locations, a calibration was achieved that met the standards set by LUAS. An example of the calibration for April 2013 is provided in Figure 5.

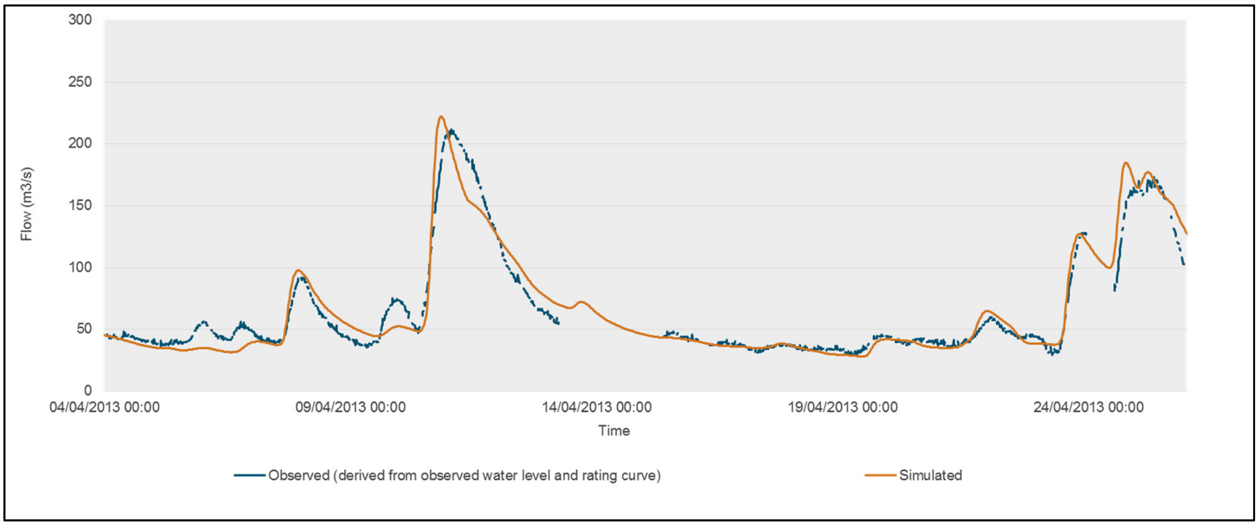

Figure 5. PDM calibration for April 2013.

4.2 Dealing with missing operational data

The ICMLive system needs to be robust in dealing with missing telemetry data. Especially during low flow periods, providing a realistic prediction of the water level at SSP1 is dependent on having accurate reservoir release telemetry data. To make sure that during these critical periods, the DSS can provide realistic results, when there are missing data, the ICMLive model is able to model the reservoir level and the abstractions using fallback data. These advanced backup systems make use of the real time control (RTC) available in the ICMLive software. The reservoir level was modelled and updated with the observations. When the observations were unavailable, the modelled levels were used instead. Figure 6 presents two examples of simulated and observed water levels in the Selangor reservoir.

Fallback systems have also been put in place for missing abstraction data, based on the design abstraction. The abstractions using the RTC system allow only the available water to be abstracted from the river, thus preventing model instability.

The model has been stress-tested for long periods of low flows and high flows to increase its robustness and provide LUAS with a DSS that meets its requirements for a robust operational system.

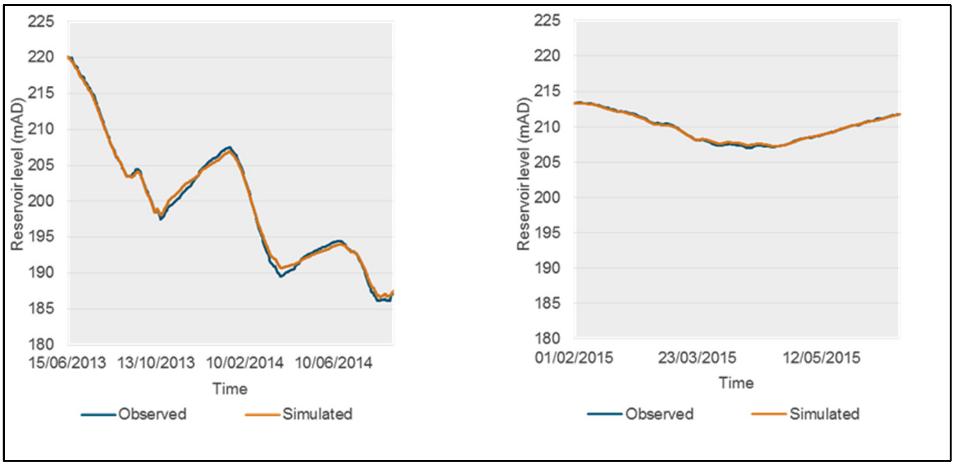

Figure 6. Simulation of Selangor reservoir levels for two events.

4.3 Forecasting levels at SSP1

The ICMLive model simulated water levels at SSP1 based on the observed data, outputs of the coupled hydrological-hydraulic model, and the forecast reservoir released from the ERR. The ICMLive operator client allows the operators to look at the model results and observed data and interrogate them in various ways including viewing results on the GIS plan view, in tables and as graphs. Figure 7 shows the hydrograph of the water levels at SSP1 from a live run.

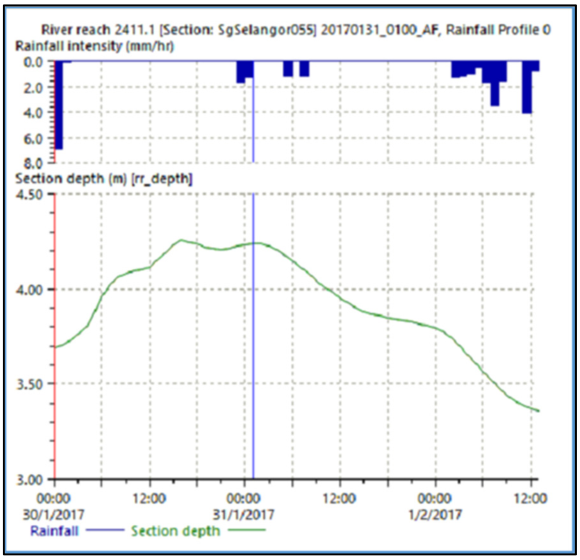

Figure 7. Modelled water level at SSP1 for the hindcast period (left of the vertical blue line) and the forecast period (right of the blue line), showing observed and forecast rainfalls (top hyetograph).

5 DISCUSSIONS

The DSS for Sungai Selangor has demonstrated how live data and forecasts from a range of sources can be combined with a simple reservoir optimization approach. The DSS has three main outputs: 1) The water level at SSP1; 2) Recommended dam release time series for the next 36 hours for Sungai Selangor Dam; and 3) Recommended dam release time series for the next 36 hours for Sungai Tinggi Dam. Using the outputs from the DSS, water levels in the reservoirs can be maintained at an optimal level and the target for minimum wastage can be met. The system is easily modifiable, to take account of changes in the catchment and in LUAS requirements, and can be scaled if necessary, so that a larger area can be represented. The DSS should also be able to help LUAS to manage extreme weather situations, such as floods and droughts, as well as their available water resources to meet increasing demands under a changing climate.

Operational models evolve over time to improve performance of the forecast, reflect changes in the catchment and meet the changing needs of the operators. The current ICMLive model provides a robust basis with a flexible setup suitable for evolving the model. Examples of evolving the model include updating and recalibrating the hydraulic and hydrological models if land use changes occur or additional data become available. For the future development of the LUAS DSS, three areas that could be explored are identified:

i. Expanding the ERR to include optimization algorithms;
ii. Data assimilation of observed water levels;
iii. Including uncertainty bands, in the forecasted levels.

The current ERR can be expanded to include state-of-the-art optimization algorithms. One of the most popular types of optimization algorithms are Genetic Algorithms, also referred to as Multi-Objective Evolutionary Algorithms (MOEAs) (Deb and Pratap, 2002; Hadka and Reed, 2013; Kasprzyk et al., 2012; Kollat and Reed, 2006; Paton et al., 2014; Wang et al., 2014). Using MOEAs could be combined with visualization tools like the Many-Objective Robust Decision Making (MORDM) (Herman et al., 2014), Many-Objective Visual Analytics (MOVA) (Fu et al., 2013) or Visually Interactive Decision-making and Design using Evolutionary multi-objective Optimization (VIDEO) (Kollat and Reed, 2007), which could aid decision making. MOEAs often rely on a high number of model reruns, which limits the application to the operational DSS due to computational and time restrictions. Research into the feasibility would be required and the benefits of an offline approach could be explored.

Data assimilation or model updating is a process where the observations are used to condition the model results, for example using water levels (Madsen and Skotner, 2005). Data assimilation can be applied in real time and will lead to increase in the performance of the forecast, by improving the initial condition. ICMLive offers the Kalman Filter data assimilation approach. For an overview on the topic of data assimilation, the reader is referred to (Liu et al., 2012).

To aid precautionary, proportional and robust decision making based on information from a forecast model, a representation of the uncertainty of that forecast can be helpful. The MMD will be issuing ensemble precipitation forecasts in the future, which allows the uncertainty of the precipitation forecast to be analyzed. To analyze the uncertainty arising from the hydrological and hydraulic models, it would be feasible to add an uncertainty quantification model to the current ICMLive setup. Examples of methods that could be considered are the Non-parametric data-based approach (Van Steenbergen and Willems, 2015) or the hydrological uncertainty processor (HUP) (Krzysztofwicz and Herr, 2001). For an overview on the topic of uncertainty, the reader is referred to (Klein et al., 2016).

6 CONCLUSIONS

The development of this DSS has shown how live data and forecasts from a range of sources can be combined with a simple reservoir optimization approach. In this way, water levels in the reservoirs can be maintained at an optimal level and the target for minimum wastage can be met. The DSS should be able to help LUAS to increase the sustainability of the management of water resources in the Selangor catchment. The approach can be applied to other catchments to manage water resources in real time.

REFERENCES

Abdullah, S.A. & Nakagoshi, N. (2008). Changes in Agricultural Landscape Pattern and its Spatial Relationship with Forestland in the State of Selangor, Peninsular Malaysia. *Landscape and Urban Planning*, 87, 147–155.

Acreman, M. (2005). Linking Science and Decision-Making: Features and Experience from Environmental River Flow Setting. *Environmental Modelling & Software*, 20, 99–109.

Ahmad, A., El-Shafie, A., Razali, S.F.M. & Mohamad, Z.S. (2014). Reservoir Optimization in Water Resources: A Review. *Water resources management*, 28(11), 3391-3405.

Ahmad, J. & Low, K. (2003). Droughts in Malaysia: A Look at Its Characteristics, Impacts, Related Policies and Management Strategies. *Water and Drainage Conference*, Kuala Lumpur.

Ahmad, S. & Hashim, N. (2010). *Perubahan Iklim Mikro di Malaysia (Micro Climate Change in Malaysia)*. Fakulti Sains Sosial dan University of Kebangsaan Malaysia, Bangi.

Bloschl, G. (2006). *Encyclopedia of Hydrological Sciences.* Part 11, 133 Rainfall-Runoff Modeling of Ungauged Catchments. John Wiley & Sons, Ltd.

Booij, M.J. (2005). Impact of Climate Change on River Flooding Assessed with Different Spatial Model Resolutions. *Journal of Hydrology*, 303, 176–198.

BSi. (1986). *Measurement of Liquid Flow in Open Channels.* Part 3 stream flow measurement, 524.

Coe, M.T., Costa, M.H. & Howard, E.A. (2008). Simulating the Surface Waters of the Amazon River Basin: Impacts of New River Geomorphic and Flow Parameterizations. *Hydrological Processes*, 22(14), 2542-2553.

Dastorani, M.T., Moghadamnia, A., Piri, J. & Rico-Ramirez, M. (2010). Application of ANN and ANFIS Models for Reconstructing Missing Flow Data. *Environmental monitoring and assessment*, 166(1), 421-434.

Deb, K., Pratap, A., Agarwal, S. & Meyarivan, T.A.M.T. (2002). A Fast and Elitist Multiobjective Genetic Algorithm: NSGA-II. *IEEE transactions on evolutionary computation*, 6(2), 182-197.

Department of Environment (DOE). (2003). *Water Quality Management in Malaysia*, Kuala Lumpur.

Department of Irrigation and Drainage (DID). (2007). *Selangor River Basin Management Plan 2007–2012*, Kuala Lumpur: Department of Irrigation and Drainage.

Department of Irrigation and Drainage Malaysia. (2017).The Official Web of Public Info Banjir. Available: http://publicinfobanjir.water.gov.my/ [Accessed 30/01/2017].

Department of statistics Malaysia. n.d., Population Quick Info (Jabatan perangkaan Malaysia), Population Quick Info (Jabatan perangkaan Malaysia). Available: http://pqi.stats.gov.my/searchBI.php [Accessed 01/12/2017].

Desa, M, Noriah, A.B. & Rakhecha, P.R. (2001). Probable Maximum Precipitation for 24h Duration over Southeast Asian Monsoon Region—Selangor, Malaysia. *Atmospheric Research*, 58(1), 41–54.

Desa, M.N. & Daud, Z. (1999). Interpretation of Spatial and Temporal Rainfall Properties of Annual and Monthly Rainfall in Selangor, Malaysia. *2nd International Colloquium on Hydrology and Water Management in the Humid Tropics*, Panama City: UNESCO, IHP and CATHALAC.

Erickson, D.L. (1995). Rural Land use and Land Cover Change Implications for Local Planning in the River Raisin in Watershed. *Land Use Policy*, 12(3), 223–236.

Fu, G., Kapelan, Z., Kasprzyk, J.R. & Reed, P. (2013). Optimal Design of Water Distribution Systems using Many-Objective Visual Analytics. *Journal of Water Resources Planning and Management*, 139(6), 624-633.

Fulazzaky, M.A. (2013). Assessing the Suitability of Stream Water for Five Different uses and Its Aquatic Environment. *Environmental Monitoring and Assessment*, 185, 523–535.

Hadka, D. & Reed, P. (2013). Borg: An Auto-Adaptive Many-Objective Evolutionary Computing Framework. *Evolutionary Computation*, 21(2), 231–259.

Hejazi, M.I., Cai, X. & Ruddell, B.L. (2008). The Role of Hydrologic Information in Reservoir Operation - Learning from Historical Releases. *Advances in Water Resources*, 31, 1636–1650.

Herman, J.D., Zeff, H.B., Reed, P.M. & Characklis, G.W. (2014). Beyond Optimality: Multistakeholder Robustness Tradeoffs for Regional Water Portfolio Planning under Deep Uncertainty. *Water Resources Research*, 50(10), 7692-7713.

Hong, D. & Hong, K.A. (2016). Drought Identification, Monitoring and Forecasting for Selangor River Basin', *International Journal of u- and e- Service, Science and Technology*, 9(3), 53–66.

Hundecha, Y. & Bardossy, A. (2004). Modeling of the Effect of Land use Changes on the Runoff Generation of a River Basin through Parameter Regionalization of a Watershed Model. *Journal of Hydrology*, 292, 281–295.

Ibadullah, W.M.W., Sammathuria, M.K. & Kwok, L.L. (2013). *Comparison of Performance of NWP Models WRFV2.2 and WRFV3.4 during a Heavy Rainfall Episode in Northeast Monsoon Season 2011*. 2/2013. Malaysian Meteorological Department (MMD), 5, 1-18.

Kasprzyk, J.R., Reed, P.M., Characklis, G.W. & Kirsch, B.R. (2012). Many-Objective De Novo Water Supply Portfolio Planning under Deep Uncertainty. E*nvironmental Modelling & Software*, 34, 87-104.

Klein, B., Meissner, D., Kobialka, H.-U. & Reggiani, P. (2016). Predictive Uncertainty Estimation of Hydrological Multi-Model Ensembles Using Pair-Couple Construction. *Water*, 8(4), 125.

Kollat, J.B. & Reed, P.M (2007). A Framework for Visually Interactive Decision-Making and Design using Evolutionary Multi-Objective Optimization (VIDEO). *Environmental Modelling & Software*, 22(12), 1691-1704.

Kollat, J. B. & P.M. (2006). Comparing State-of-the-Art Evolutionary Multi-Objective Algorithms for Long-Term Groundwater Monitoring Design. *Advances in Water Resources*, 29(6), 792-807.

Krzysztofwicz, R. & Herr, H.D. (2001). Hydrologic Uncertainty Processor for Probabilistic River Stage Forecasting: Precipitation-Dependent Model. *Journal of Hydrology*, 249, 46–68.

Liston, G.E., Sud, Y.C. & Wood, E.F. (1994). Evaluating GCM Land Surface Hydrology Parameterizations by Computing River Discharges using a Runoff Routing Model: Application to the Mississippi Basin. *Journal of Applied Meteorology*, 33, 394–405.

Liu, Y., Weerts, A.H., Clark, M., Hendricks Franssen, H.-J., Kumar, S., Moradkhani, H., Seo, D.-J., Schwanenberg, D., Smith, P., van Dijk, A.I.J.M., van Velzen, N., He, M., Noh, S.J., Rakovec, O. & Restrepo, P. (2012). Advancing Data Assimilation in Operational Hydrologic Forecasting: Progress, Challenges, and Emerging Oppertunities. *Hydrology and Earth System Sciences*, 16, 3863–3887.

Madsen, H. & Skotner, C. (2005). Adaptive State Updating in Real-Time River Flow Forecasting - A Combined Filtering and Error Forecasting Procedure. *Journal of Hydrology*, 308, 302–312.

McMillan, H., Freer, J., Pappenberger, F., Krueger, T. & Clark, M.P. (2010). Impacts of Uncertain River Flow Data on Rainfall-Runoff Model Calibration and Discharge Predictions. *Hydrological Processes*, 24(10), 1270-1284.

Moore, R.J. (1985). The Probability-Distributed Principle and Runoff Production at Point and Basin Scales. *Hydrological Sciences Journal*, 30, 273–297.

NCAR (2017). *The Weather Research & Forecasting Model*, WRF model. NCEP, FSL, AFWA, Naval Research Laboratory, the University of Oklahoma and FAA.

Paiva, R.C.D., Collischonn, W. & Buarque, D.C. (2013). Validation of a Full Hydrodynamic Model for Large-Scale Hydrologic Modelling in the Amazon. *Hydrological Processes*, 27, 333–346.

Pappenberger, F., Beven, K.J., Horritt, M. & Blazova, S. (2005). Uncertainty in the Calibration of Effective Roughness Parameters in HEC-RAS Using Inundation and Downstream Level Observations. *Journal of Hydrology*, 302(1–4), 46–69.

Paton, F.L., Maier, H.R. & Dandy, G.C. (2014). Including Adaptation and Mitigation Responses to Climate Change in a Multiobjective Evolutionary Algorithm Framework for Urban Water Supply Systems Incorporating GHG Emissions. *Water Resouces Research*, 50(8), 6285–6304.

RBM Engineering consultant. (2014). *RBM, Engineering Consultant*, Final Report, 173.

Sanusi, W., Jemain, A.A., Zin, W.Z.W. & Zahari, M. (2015). The Drought Characteristics using the First-Order Homogeneous Markov Chain of Monthly Rainfall Data in Peninsular Malaysia. *Water Resource Management*, 29, 1523–1539.

Siriwardena, L., Finlayson, B.L. & McMahon, T.A. (2006). The Impact of Land use Change on Catchment Hydrology in Large Catchments: The Comet River, Central Queensland, Australia. *Journal of Hydrology*, 326, 199–214.

Subramaniam, K., Kwok, L.L. & Hassan, W.A.W. (2010). *Performance of Ensemble Prediction for Malaysian Meteorological Department Numerical Weather Prediction Model*. 13/2010. MMD.

Todini, E. (2007). Hydrological Catchment Modelling: Past, Present and Future. *Hydrology and Earth System Sciences*, 11(1), 468–482.

Van Steenbergen, N. & Willems, P. (2015). Uncertainty Decomposition and Reduction in River Flood Forecasting: Belgian Case Study. *Journal of Flood Risk Management*, 8, 263–275.

Vorosmarty, C.J., Moore, B. & Grace, A.L. (1989). Continental Scale Models of Water Balance and Fluvial Transport: An Application to South. *Global Biogeochemical Cycles*, 3(3), 241–265.

Wang, Q., Guidolin, M., Savic, D. & Kapelan, Z. (2014). Two-Objective Design of Benchmark Problems of a Water Distribution System Via Moeas: Towards the Best-Known Approximation of the True Pareto Front. *Water Resouces Planning and Management*, 141(3), 1-14.

WMO & GWP (2013). *Flood Forecasting and Early Warning*. 19. World Meteorological Organization & Global Water Partnership.

WWF Malaysia (2000) *Land use in the Selangor River a study on the application and strategy for integrated river basin management*.

Proceedings of the 37th IAHR World Congress
August 13 – 18, 2017, Kuala Lumpur, Malaysia

DEALING WITH UNCERTAINTY IN DRINKING WATER SUPPLY SYSTEMS MANAGEMENT IN CASE OF DISASTERS

ALESSANDRO PAGANO(1), RAFFAELE GIORDANO(1), IRENE PLUCHINOTTA(2), ANNA BRUNA PETRANGELI(1) UMBERTO FRATINO(3) & MICHELE VURRO(1)

(1, 2, 4, 6) Water Research Institute – National Research Council (IRSA-CNR), Italy,
alessandro.pagano@ba.irsa.cnr.it
(3) LAMSADE, CNRS, Univ. Paris-Dauphine, PSL Research Univ., Paris, France
irene.pluchinotta@dauphine.fr
(5) DICATECh, Politecnico di Bari, Bari, Italy,
umberto.fratino@poliba.it

ABSTRACT

Drinking water availability and quality is crucial for the well-being and the safety of people, particularly in case a disaster occurs. In fact, the provision of critical services in general, particularly of drinking water after an emergency, may significantly contribute to limit the intensity and the duration of crises and support the resilience of the whole community. Among the main issues that contribute to make emergency management and decision-making into complex processes, it is worth to underline the role of uncertainty, which mainly representing the lack of reliable data and information related to the impacts of a disaster after its occurrence. Particularly focusing on drinking water supply systems, the development of tools capable of operating in a framework of uncertainty, quickly identifying the spatial location of the most critical elements of a complex infrastructure, assessing risk levels and suggesting potential strategies to cope with a disaster, may be crucial for decision-makers. The present article describes the implementation, using the potentialities of GIS systems, of a vulnerability assessment model for drinking water supply infrastructures based on Bayesian Belief Networks (BBNs). The tool is implemented in L'Aquila case study, which is particularly relevant in the recent history of emergencies related to natural hazards and contributes to stress the key role of either modeling or information of the uncertainty in the emergency management. BBNs are capable to integrate and manage different classes of data and categories of information, and to deal with information having a different level of uncertainty. Uncertainty, which is integral to Bayesian analysis, can be used to provide decision-makers with reliable information to select the most suitable strategies to manage emergencies. In the present work, a quantitative approach to uncertainty modeling is provided as well, and coupling with modeling results should support the effectiveness of decision-making processes.

Keywords: Bayesian belief networks (BBNs); vulnerability assessment; water supply systems; uncertainty management; disaster risk reduction (DRR).

1 INTRODUCTION

Infrastructural systems support the activities of modern societies, particularly in urban areas, and guarantee the well-being and the safety of citizens both in ordinary conditions and during emergencies (Pagano et al. 2014, Galvan and Agarwal 2015). In case of emergency, they represent key assets capable of providing critical services and of supporting the resilience of a community (Haimes et al 2005, Ertugay et al. 2016).

The need to protect drinking water from a wide variety of hazards has been emphasized by several authors (e.g. EPA 2015). The key requirement is to support management of infrastructural systems in order to ensure a minimum reliability level to the network (Fragiadakis and Christodoulou, 2014).

Risk cannot be fully eliminated, but it can be reduced (Zhou et al. 2014). Effective risk management strategies significantly depend on the understanding of risk dimensions, and particularly of vulnerability, which is often not well analyzed and understood. It can be basically defined as an expression of inherent states of the system that can adversely affect (cause harm or damage to) the system itself (Haimes 2006). Vulnerability reduction is thus a fundamental requirement in supporting decision processes to mitigate the impacts of potentially disastrous natural events (Pagano et al. 2014, Zhou et al. 2014).

Within these premises, the present article describes a vulnerability assessment tool for drinking water supply infrastructures, based on Bayesian Belief Networks (BBNs). The aim of the present work is to show how the tool can be used to provide information to decision-makers reducing the risk levels for drinking water supply infrastructures through a vulnerability assessment accounting also for data uncertainty. For this aim, BBNs potentialities have been integrated in GIS environment in order to support spatial modeling from data input until the visualization of the results. A criterion for an explicit analysis of uncertainty is discussed as well.

The vulnerability assessment tool was implemented in L'Aquila earthquake (2009) case study, with the cooperation of the local water utility. The case study represents a milestone in the history of natural disasters, and a valuable example on the importance of their impacts on infrastructural systems.

Within this framework, the paper will be structured as follows. After the present introduction, a comprehensive state of the art is provided, mainly focusing on the potentialities connected to the use of BBNs in such field, also taking into consideration spatial modeling and uncertainty management. A description of the architecture of the developed tool is then provided. The relevance of L'Aquila case study and the management of its complex drinking water supply infrastructure in emergency, is discussed in Section 4. At last, the main results are summarized, which are also through the identification of an indicator to explicitly express the uncertainty related to results.

2 STATE OF THE ART

Several successful applications of BBNs on drinking water supply infrastructures are mentioned in the scientific literature. BBNs were used to construct a model for pipe breaks based on learning from past breaks and covariate data, which proved insensitive to missing or incomplete data (Francis et al., 2014). A complex BBN-based integration of failure prediction models was proposed for water mains (Kabir et al., 2015). Pipe data, soil information and pipe breakage data were integrated into a GIS, which is used by the utilities for the visualization of results and for decision-making. A BBN-based model was developed to assess internal corrosion for oil and gas pipelines, integrating also the expert judgment (Shabarchin and Tesfamariam 2016). CBR risk related to a release of contaminants was examined as well as a consequence of physical damage. A decision support approach based on Fuzzy Bayesian Networks (FBNs) was proposed for assessing the state of existing pipelines in case of tunneling excavation (Zhang et al., 2016). A Bayesian model was also developed to assess infrastructural resilience (Hosseini and Barker, 2016). Different disruptive scenarios as well as potential strategies were simulated, and integrated with a sensitivity analysis of parameters.

BBNs are unable to natively provide a direct representation of the spatial relationships between variables. Nevertheless, they have been successfully used in recent years in many ecological and environmental applications (Gonzalez-Redin et al., 2016), and particularly in water resources management (Giordano et al., 2015; Phan et al., 2016).

Furthermore, one of the key features of BBNs is that they are capable to support reasoning from uncertain evidence to uncertain conclusion, analyzing the occurrence of specific consequences based on situational factors, which represent observable aspects of the system (John et al., 2016). Uncertainty represents the lack of exact knowledge (Refsgaard et al., 2007). Causes of uncertainty (either related to data or model reliability, ambiguity in the understanding of specific phenomena, etc.) imply limitations in the capability to describe efficiently a given system, and to forecast its behavioral evolution. The correct assessment of uncertainty is particularly crucial in case of emergency response, where decisions based on uncertain and complex information may have lasting and significant consequences (Cheong et al., 2016). The uncertainties can be explicitly treated in BBNs by propagating them throughout the network up to the final node (Uusitalo, 2007; Uusitalo et al., 2015) using the dispersion of its Posterior Probability Distribution (PPD) through specific metrics (Marcot, 2012).

The adoption of BBNs to support decision-making in emergency management is also useful for the following additional reasons. Firstly, the capability to integrate new variables, states or knowledge (Gonzalez-Redin et al. 2016; Landuyt et al., 2013; Haines-Young, 2011). Secondly, BBNs are capable to include various information (e.g. analytical models, expert knowledge, literature and historical data), as proved by several authors (e.g. Phan et al., 2016; Pagano et al., 2014; Chen and Pollino, 2012). At last, BBNs allow the probabilistic representation of interactions, which support to picture the explicit relationships between the variables of the models, thus facilitating communication to decision-makers.

3 DESCRIPTION OF THE TOOL

The probabilistic vulnerability assessment model aims at quantifying the vulnerability levels of drinking water supply systems with respect to both physical hazards (e.g. earthquakes, landslides) and CBR hazards (e.g. water contamination). As fully described in Pagano et al. (2014a) and Pagano et al. (2014b), the model is composed of a set of BBNs, used to assess both classes of vulnerability for all the elements of a drinking water supply infrastructure from the source to the tap. The BBN used to analyze the physical vulnerability of drinking water mains is shown in the following Fig. 1. Specific reference is made in the following to the proposed network, particularly in the discussion of the results of the case study. Vulnerability is interpreted as the results of four different mechanisms/causes (i.e. breaking, corrosion, joint extraction and security level). The variables in grey represent the 'parent' variables (input), whereas those in yellow are the 'child' variables (output). The state of the output variables is based on the propagation of probability (through the Conditional Probability Tables) from the state of the inputs.

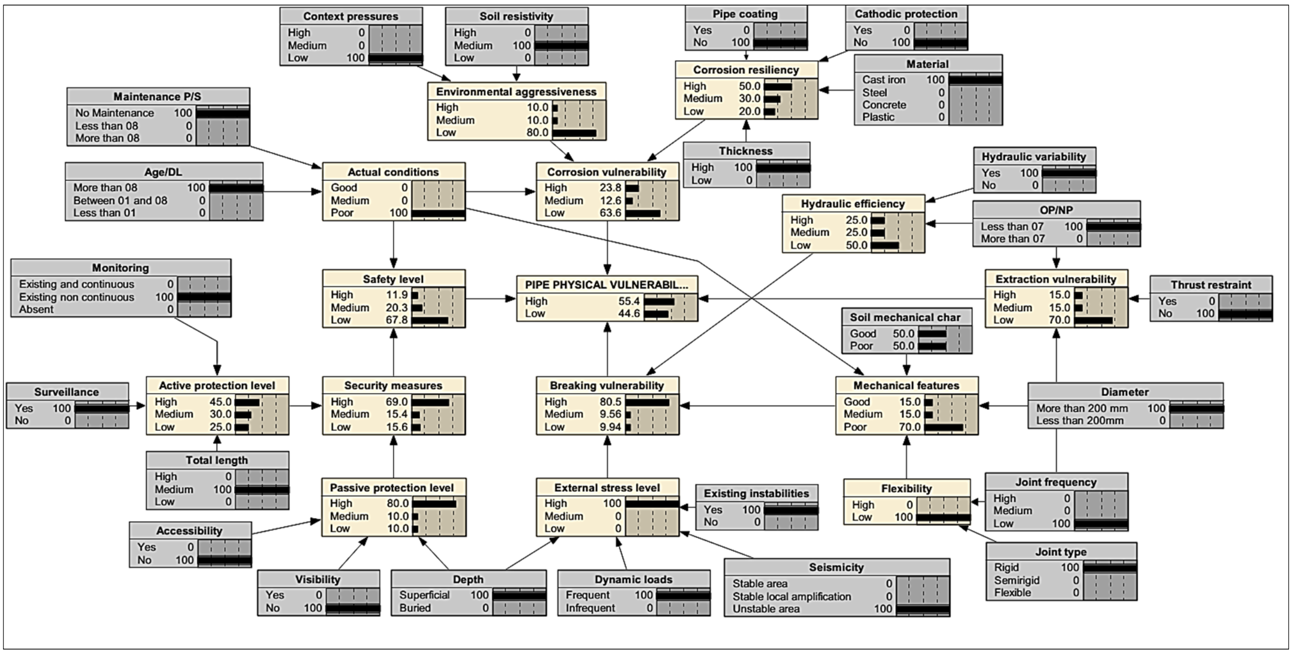

Figure 1. BBN used for the physical vulnerability assessment of water mains.

Performing the vulnerability analysis requires the integration of several data and information, belonging to three main classes (as summarized in the scheme proposed in Figure 2), which are the physical data (related to infrastructural characteristics), environmental data and operative data. The toolbox *G-Net*, was developed in ArcGIS ® in order to support the spatial implementation of the model, and to facilitate the mapping and interpretation of the results and related uncertainty. Firstly, the toolbox can be used for the collection, analysis and attribution of input data with a spatial dimension. Secondly, it can be used to visualize and map the outcomes of the vulnerability assessment, with the related uncertainty. The conceptual scheme of the adopted approach and the key interactions among the different tools are described in the Figure 2.

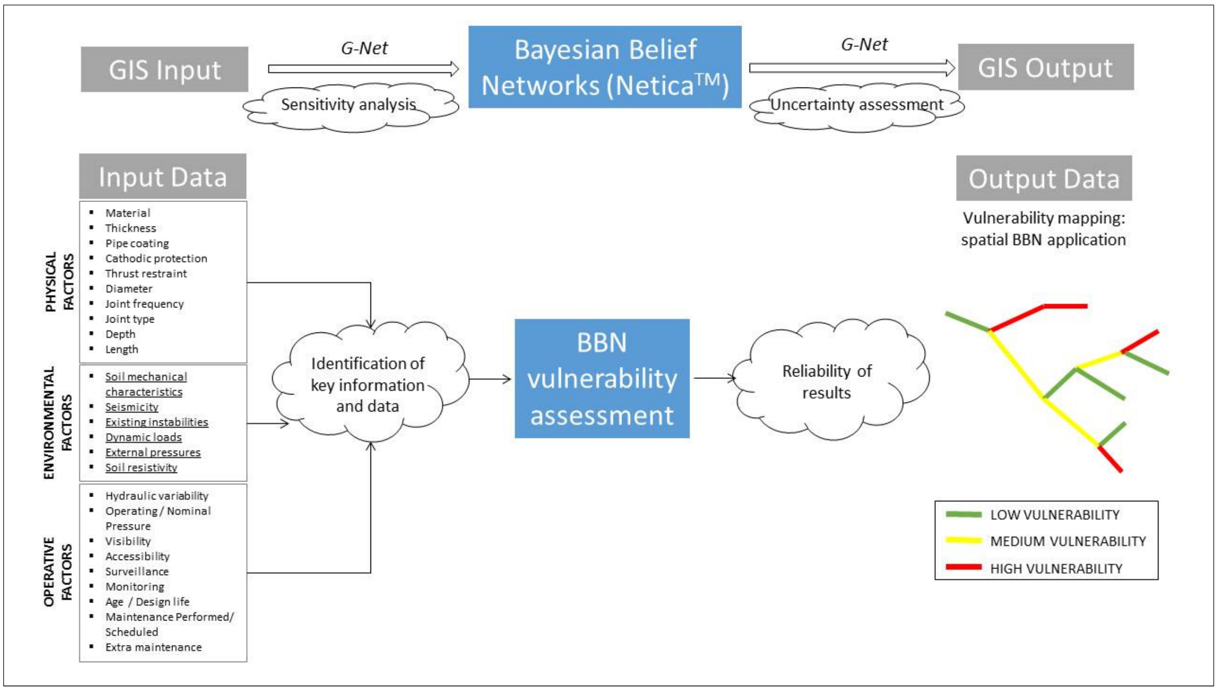

Figure 2. Spatial modeling procedure and uncertainty management.

Sensitivity analysis is an integral part of model description. It supports ranking and comparison of input variables in terms of variance or uncertainty reduction in a specified outcome variable. Sensitivity is calculated with input variables set to their default prior the probability distributions (Pagano et al., 2014) and represents a useful method for determining residual sensitivity behavior if one or more inputs are known.

Performing the sensitivity analysis supports in the identification of the most influential variables of the BBN. This means that the more sensitive to a variable the model is, the more important is to collect information related to it. Having reliable data on key variables is a crucial requisite to reduce the uncertainty related to model predictions.

The following Table 1 summarizes the main outcomes of the sensitivity analysis for the model, performed with respect to the variable 'breaking vulnerability'.

Table 1. Results of the sensitivity analysis performed with respect to the variable 'breaking vulnerability'.

Node	Mutual Info (Entropy Reduction)	Percent	Variance of Beliefs	Scenario
Breaking Vulnerability	1.3976	100	0.363296	
External stress level	0.19371	13.9	0.044494	
Mechanical features	0.09952	7.12	0.02237	
Physical vulnerability	0.04676	3.35	0.01062	
Seismicity	0.04403	3.15	0.010404	[1], [3]
Existing instabilities	0.02028	1.45	0.004848	[1], [3]
Actual conditions	0.01908	1.37	0.004305	
Soil mechanical characteristics	0.01267	0.907	0.002837	[3]
Hydraulic efficiency	0.01221	0.874	0.002945	
Safety level	0.00808	0.578	0.001839	
Extra-maintenance	0.0056	0.401	0.001275	[2], [3]
OP/NP	0.00312	0.223	0.000758	[2]
Dynamic loads	0.00269	0.193	0.000649	[1]
Flexibility	0.00212	0.152	0.000485	
Hydraulic variability	0.00138	0.0991	0.000338	
Age/Design life	0.00111	0.0797	0.000256	[2]
Joint extraction vulnerability	0.00084	0.0598	0.000204	
Maintenance: performed/scheduled	0.00077	0.0548	0.000175	[2]
Joint type	0.00063	0.0452	0.000145	[2]
Diameter	0.00059	0.0422	0.000137	[2]
Depth	0.0004	0.0283	9.49E-05	[2]
Joint frequency	0.00014	0.0102	3.25E-05	[2]
Corrosion vulnerability	0.00004	0.00251	0.000008	
Pipe coating	0.00003	0.00235	7.9E-06	
Cathodic protection	0.00001	0.000767	2.6E-06	
Thrust restraint	0	0	0	[2]

4 L'AQUILA CASE STUDY

L'Aquila was struck by a 6.3 magnitude earthquake on 6 April 2009. Despite the relatively moderate intensity, several damages to structures and infrastructures were detected over a broad area (Kongar et al., 2015). Drinking water supply infrastructures were significantly damaged as well (Pagano et al., 2017).

The water supply system of L'Aquila area is characterized by a significant complexity, described in details by Leopardi (2012). In order to fully understand the hydraulic behavior of the system and the functioning scheme, the staff of Gran Sasso Acqua S.p.A (GSA S.p.A), the local water utility, supported the research from a technical point of view. The local water supply system is constituted by multiple interconnected aqueducts, generally working for single municipalities or districts, but also highly interconnected to increase the flexibility of the whole system (Leopardi, 2012). An overview of the general scheme is proposed in the following Fig. 3.

Chiarino aqueduct (built in the 1920s) is the first *modern* system. It currently conveys a flow rate between 85 and 160 l/s. During the 1950s, the whole system was significantly re-designed, according to an increased water demand, and two new aqueducts were built, which are La Ferriera (approximately 240 l/s) and Acqua Oria (approximately 250 l/s). The most recent and relevant system, completed in 1997, is the Gran Sasso aqueduct with a mean discharge of 450 l/s. Acqua Oria aqueduct is the only one withdrawing water from wells, while all the others collect and convey water from springs.

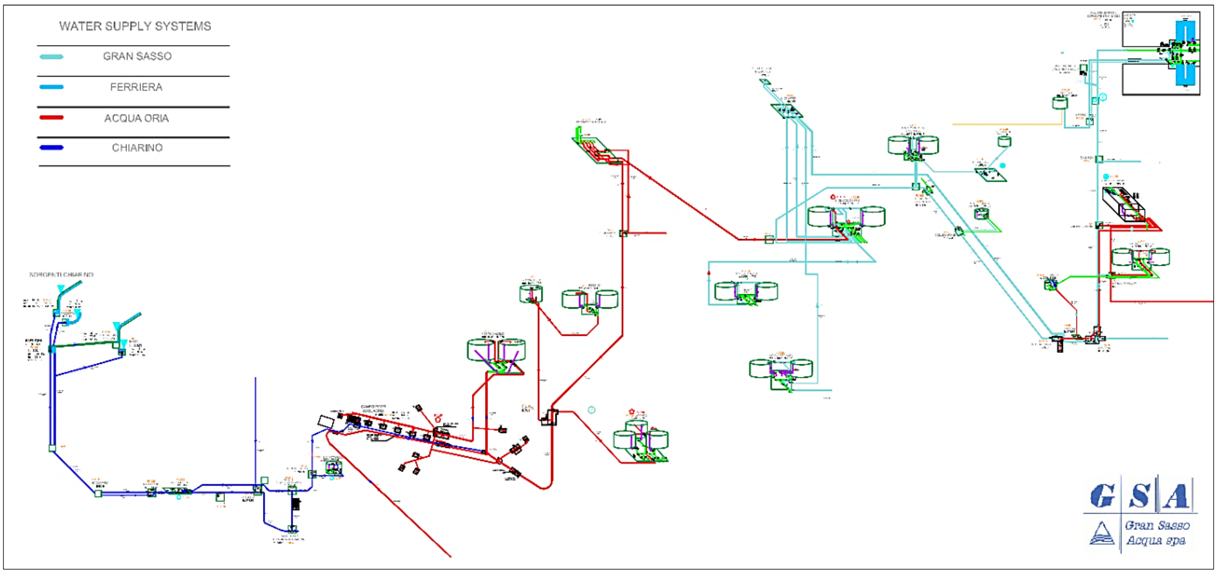

Figure. 3. Overview of the water supply system in L'Aquila area.

During the earthquake in 2009, Chiarino aqueduct was limitedly damaged mainly due to the stress induced at some weld joints by soil displacements. La Ferriera aqueduct also suffered limited damages, particularly on a reinforced concrete pipe, and at several weld joints. No damages occurred on other appurtenances of the water supply infrastructures (such as tanks or pumps). The major damage, instead, occurred on an important water pipe within the Gran Sasso aqueduct, which failed because crossing the surface trace of a fault activated during the earthquake (Rossetto et al., 2011; Dolce and Di Bucci, 2015; Leopardi, 2012, Pagano et al.; 2017). The steel joint of the pipeline (diameter 600 mm; pressure 25–30 atm) slipped off, and the cause of damage was identified as co-seismic rupture of Paganica fault crossing the pipe.

There were two main damages occurred on the Gran Sasso aqueduct in the aftermath of the earthquake. As a consequence, the operation of the whole system was interrupted. The complete closure of the system was needed to allow the restoration of infrastructural functionality; it also limited the problems originated by the widespread damages occurred in the city center. Nevertheless, this had strong impacts on the local community.

According to the interviews held with technicians involved during the emergency operations, the fragmented and uncertain knowledge available was a key limit in emergency operations. Infrastructural data were not readily available and most of the available data were often not reliable and directly usable, difficult to share and integrate. Emergency operators acknowledged the lack of reliable infrastructural information as a main issue hampering the effectiveness of emergency management strategies.

Based also on the lessons learned in L'Aquila earthquake, the tool was used to collect and integrate the main structural and environmental information related to the whole drinking water supply system of L'Aquila area, making them easily accessible to support emergency management.

5 RESULTS AND DISCUSSION

The main results of the vulnerability assessment procedure are represented in the following Fig. 4, which shows the most vulnerable elements of the network. It identifies the probability values associated with the state 'high' of the variable 'breaking vulnerability'.

The Fig. 4 shows the presence of a significant number of elements with values of 'breaking vulnerability' ranging from medium to high, and the support in the identification of the most vulnerable pipes. The highest value of 'breaking vulnerability' was associated to the pipe of the Gran Sasso Aqueduct that was primarily damaged during the earthquake. Other elements characterized by a significantly high 'breaking vulnerability' were identified as well, and this result was discussed with GSA S.p.A. In most cases, the model proved capable to locate well-known local vulnerabilities and criticalities; in other cases, it also supported in advising on other potential unknown weak points of the system. Globally, the implementation of the model resulted to be helpful for the water utility in building a knowledge framework on the conditions of the infrastructural system, and thus in the identification of its main criticalities. Although the model is primarily intended for emergency management, it can be used in ordinary conditions as well, mainly for scheduling and prioritizing maintenance activities.

The tool requires the integration of different classes of information, which should be collected well before the occurrence of a disaster. Not all the needed data might be readily available and accessible, and this may certainly require a pre-processing phase to increase the preparedness towards an extreme event. Nevertheless, one of the key features of BBNs is the capability to deal with data uncertainty. This means that the model can be run if some variables are unknown, and the loss of prediction quality and reliability is estimated accordingly.

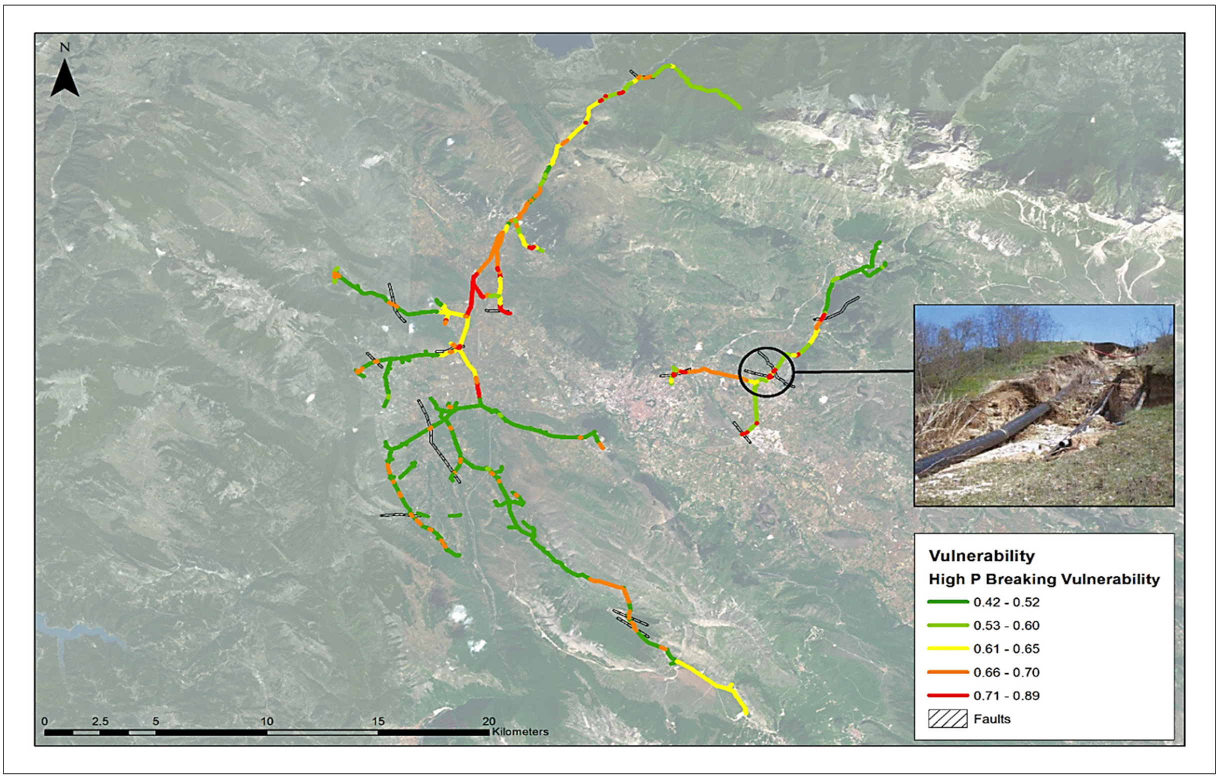

Figure 4. Results of the vulnerability assessment model in L'Aquila case study.

A correct estimation of uncertainty associated with the model results is fundamental for decision-makers, since the awareness of model output reliability supports in identifying the most suitable strategies. Particularly, the issue of input data uncertainty is crucial to identify the amount of additional information that would be needed in emergency conditions to understand system evolution and to provide coherent results. An approach to identify the root causes of uncertainty and quantify its entity in Bayesian models is described in the following.

We assume that a basic measure of uncertainty is related to the number of alternatives and the characteristic of the probability distribution over the states of a variable (Das 1999). The Shannon entropy $H(X)$ can be used for that purpose:

$$H(X) = -\sum_{i=1}^{n} P(x_i) \log P(x_i) \qquad [1]$$

H(X) measures the average information required in addition to the current knowledge to remove the ignorance associated to the probability distribution of the variable X. If the current state of knowledge is complete, then $H(X)$ =0. If it is total ignorance, the additional information required to pin down an alternative will be maximum. Higher values of $H(X)$ are representative of a uniform output probability distribution, which may lead to more uncertain decisions.

The Shannon entropy was used mainly in referring to the main output variable, i.e. the 'breaking vulnerability'. The values of $H(X)$ were computed for the whole network and plotted along with the results of the vulnerability assessment, in order to describe the spatial variation of uncertainty. This coupling (Fig. 5) supports the identification of the most critical elements of the system (high vulnerability associated with low uncertainty) and the areas where additional information would be primarily beneficial (medium-high vulnerability values coupled with high uncertainty).

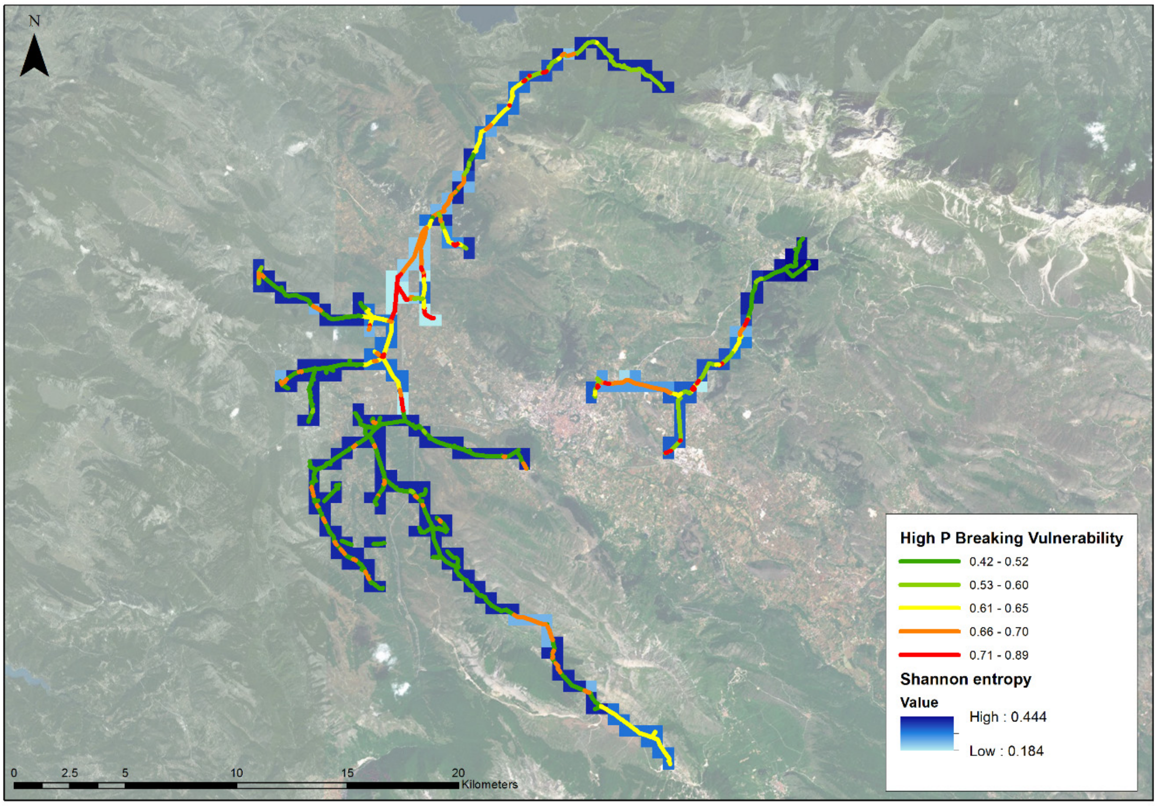

Figure 5. Coupled spatial representation of model results and related uncertainty

A key information for decision-makers operating in emergency conditions is related to the understanding of the impact of either information unavailability or uncertainty on results quality, and of the benefit associated to the potential introduction of additional data. The relevance of the Shannon entropy $H(X)$ for uncertainty assessment was tested through specific simulations, analyzing the impacts of the lack of important input information on model results. Based on the results of the sensitivity analysis (Tab. 1), the following scenarios were built under the assumption of missing information for a significant subset of input variables.

- U [1]: complete uncertainty is assumed for the variables identified with [1] in Tab. 1. Particularly, three highly influential environmental variables, i.e. ‘seismicity’, ‘existing instabilities’ and ‘dynamic loads’, are set to a uniform probability distribution, that is they are treated as unknown.
- U [2]: complete uncertainty is assumed for the input variables identified with [2] in Tab. 1. Both structural and operative features are set to a uniform probability distribution.
- U [3]: complete uncertainty is assumed for the input variables identified with [3] in Tab. 1. Four of the most relevant variables according to the sensitivity assessment (‘seismicity’, ‘existing instabilities’, ‘soil mechanical characteristics’ and ‘extra-maintenance’) are unknown.

The Shannon entropy $H(X)$ was then used in the cited scenarios to quantify the cumulative uncertainty related to unknown inputs. Following the ‘chain rule’ for entropy, the global entropy of a group of random variables was computed as the sum of conditional entropies. A summary of the results is proposed in the following Tab. 2:

Table 2. Shannon entropy values to assess uncertainty associated to the scenarios.

Scenario	**Shannon entropy (input variables)**
BASE	0
U [1]	0.067
U [2]	0.012
U [3]	0.083

The outcomes of the uncertainty analysis firstly suggest that although the scenario U [2] is characterized by a higher number of unknown variables, their impact on modeling results is lower if compared to both U [1] and U [3] scenarios, in which the main variables are unknown. Both U [1] and U [3] suggest that the knowledge related to environmental conditions is a key requirement to perform a reliable vulnerability assessment. Furthermore, referring particularly to the scenario U [3], the highest value of the Shannon entropy is the representative of a more critical condition, due to the highly uncertain set of available input data.

Coupling infrastructural vulnerability and uncertainty associated to the results is a key requirement to deal with emergency conditions. This information supports decision-makers to schedule (and prioritize) actions according to the vulnerability levels of the system. The results can be used in ordinary conditions as well, mainly to help water utilities in the selection of the most suitable strategies for DRR. The information related to the input uncertainty are particularly useful in order to identify the locations, where additional data and investigation would be of worth.

6 CONCLUSIONS

This work proposes a vulnerability assessment model for drinking water supply systems based on Bayesian networks, integrated in GIS. Specifically, the work shows how spatial analysis could support decision-makers during emergency management, in order to identify and select the most suitable strategies to cope with the impacts of disasters. To this aim, the tool has been implemented to assess the vulnerability of the water supply infrastructures in L'Aquila area, which was struck by an earthquake in 2009. The modeling activities were carried out in tight cooperation with both the Italian Department of Civil Protection and a group of engineers working for the local water utility. Although the model was mainly meant to support decision-makers in dealing with drinking water supply infrastructures emergencies in case of disasters, it proved useful for ordinary management as well.

The work discusses also the introduction and adoption of the Shannon entropy, a parameter computed considering the PPD of the output variable, as a measure of uncertainty. It defines the average information required in addition to the current knowledge to remove the ignorance associated to the probability distribution of the input variable. According to the results of the experiences described in this work, one of the main advantages related to the use of BBNs is directly related to the capability to deal with the uncertainty associated to the lack of input data, which is typical of emergency conditions (due to the difficulties in data collection), and to take it explicitly into account in the analysis of the results. Coupling the results of the model with an explicit measure of uncertainty support decision makers in properly taking into account the reliability of model predictions.

ACKNOWLEDGMENTS

The present research activity is partially developed within a research project funded by the Italian Department of Civil Protection ('Intesa Operativa del 19.12.2006 tra DPC e IRSA—Rep. 618'), and partially within the EU Horizon 2020 funded project 'EDUCEN' (Grant Agreement No 653874).

REFERENCES

Chen, S.H. & Pollino, C.A. (2012). Good Practice in Bayesian Network Modelling. *Environmental Modelling Software*, 37, 134-145.

Cheong, L., Bleisch, S., Kealy A., Tolhurst, K., Wilkening, T. & Duckham, M. (2016). Evaluating the Impact of Visualization of Wildfire Hazard upon Decision-Making under Uncertainty. *International Journal of Geographical Information Science*, 30(7), 1377-1404.

Das, B. (1999). Representing Uncertainty Using Bayesian Networks, Information Technology Division Electronics and Surveillance Research Laboratory DSTO-TR-0918.

Dolce, M. & Di Bucci, D. (2015). Comparing Recent Italian Earthquakes. *Bulletin of Earthquake Engineering*, 1-37.

EPA. (2015). Systems Measures of Water Distribution System Resilience. EPA 600/R-14/383.

Ertugay, K., Argyroudis, S. & Düzgün, H.S. (2016). Accessibility Modeling in Earthquake Case Considering Road Closure Probabilities: A Case Study of Health and Shelter Service Accessibility in Thessaloniki, Greece. *International Journal of Disaster Risk Reduction*, 17, 49–66.

Fragiadakis, M. & Christodoulou, S.E. (2014). Seismic Reliability Assessment of Urban Water Networks. *Earthquake Engineering Structural Dynamics*, 43, 357-374.

Francis, R.A., Guikema, S.D. & Henneman, L. (2014). Bayesian Belief Networks for Predicting Drinking Water Distribution System Pipe Breaks. *Reliability Engineering & System Safety*, 130, 1–11.

Galvan, G. & Agarwal, J. (2015). Community Detection and Infrastructure Criticality. Safety and Reliability of Complex Engineered Systems. *Proceedings of the 25th European Safety and Reliability Conference*, ESREL 2015, 1209-1217.

Giordano, R., D'Agostino, D., Apollonio, C., Scardigno, A., Pagano, A., Portoghese, I., Lamaddalena, N., Piccinni, A.F. & Vurro, M. (2015). Evaluating Acceptability of Groundwater Protection Measures Under Different Agricultural Policies. *Agricultural Water Management* , 147, 54-66.

Gonzalez-Redin, J., Luque, S., Poggio, L., Smith, R. & Gimona, A. (2016). Spatial Bayesian Belief Networks as a Planning Decision Tool for Mapping Ecosystem Services Trade-Offs on Forested Landscapes. *Environment Research*, 144, 15–26.

Haimes, Y.Y. (2006). On The Definition of Vulnerabilities in Measuring Risks to Infrastructures. *Risk Analysis*, 26(2), 293-296.

Haimes, Y.Y., Horowitz, B.M., Lambert, J.H., Santos, J.R., Lian, C. & Crowther, K.G. (2005). Inoperability Input-Output Model (IIM) for Interdependent Infrastructure Sectors: Theory and Methodology. *Journal of Infrastructure Syst*em, 11(2), 67–79.

Haines-Young, R. (2011). Exploring Ecosystem Service Issues across Diverse Knowledge Domains Using Bayesian Belief Networks. *Progress in Physical Geography*, 35(5), 681–699.

Hosseini, S. & Barker, K. (2016). Modeling Infrastructure Resilience Using Bayesian Networks: A Case Study of Inland Waterway Ports. Computers & Industrial Engineering, 93, 252–266.

John, A., Yang, Z., Riahi, R. & Wang, J. (2016). A Risk Assessment Approach to Improve The Resilience of A Seaport System Using Bayesian Networks. *Ocean Engineering*, 111, 136–147.

Kabir, G., Demissie G., Sadiq, R. & Tesfamariam, S. (2015). Integrating Failure Prediction Models for Water Mains: Bayesian Belief Network Based Data Fusion. *Knowledge Based System*, 85, 159-169.

Kongar, I., Esposito, S. & Giovinazzi, S. (2015). Post-Earthquake Assessment and Management for Infrastructure Systems: Learning from the Canterbury (New Zealand) and L'Aquila (Italy) Earthquakes. *Bull Earthquake Engineering*, 15(2), 589-620.

Landuyt, D., Broekx, S., D'hondt, R., Engelen, G., Aertsens, J. & Goethals, P. (2013). A Review of Bayesian Belief Networks in Ecosystem Service Modelling. *Environmental Modelling & Software*, 46, 1–11.

Leopardi, M. (2012). Gli Effetti Prodotti Dal Sisma Del 6 Aprile 2009 Sul Sistema Idrico Della Conca Aquilana, *XXXIII Convegno Nazionale Di Idraulica E Costruzioni Idrauliche* Brescia. (*In Italian*).

Marcot, B.G. (2012). Metrics for Evaluating Performance and Uncertainty of Bayesian Network Models. *Ecological Modelling*, 230, 50– 62.

Pagano, A., Giordano, R., Portoghese, I., Fratino, U. & Vurro, M. (2014a). A Bayesian Vulnerability Assessment Tool for Drinking Water Mains Under Extreme Events. *Natural Hazards*, 74, 2193–2227.

Pagano, A., Giordano, R., Portoghese, I., Vurro, M. & Fratino, U. (2014b). Emergency Management of Drinking Water Infrastructures Based on A Bayesian Decision Support System. Vulnerability, Uncertainty, and Risk: Quantification, Mitigation, and Management. *Proceedings of the 2nd International Conference on Vulnerability and Risk Analysis and Management ICVRAM 2014 and the 6th International Symposium on Uncertainty Modeling and Analysis ISUMA 2014*.

Pagano, A., Giordano, R., Pluchinotta, I. & Vurro, M. (2017). Drinking Water Supply in Resilient Cities: Notes from L'Aquila Earthquake Case Study. *Sustainable Cities and Society*, 28, 435-449.

Phan, T.D., Smart, J.C.R., Capon, S.J., Hadwen, W.L. and Sahin, O. (2016). Applications of Bayesian Belief Networks in Water Resource Management: A Systematic Review. *Environmental Modelling Software*, 85, 98-111.

Refsgaard, J.C., Van Der Sluijs, J.P., Højberg, A.L. & Vanrolleghem, P.A. (20071). Uncertainty in the Environmental Modelling Processes. A Framework and Guidance. *Environmental Modelling Software*, 22(11), 1543-1556.

Rossetto, T., Peiris, N., Alarcon, J.E., So E., Sargeant, S., Free, M., Sword-Daniels, V., Del Re D., Libberton , C., Verrucci, E., Sammonds, P. & Walker, J.F. (2011). Field Observations from The Aquila, Italy Earthquake of April 6, 2009. *Bulletin of Earthquake Engineering* 9, 11-37.

Shabarchin, O. & Tesfamariam, S. (2016). Internal Corrosion Hazard Assessment of Oil & Gas Pipelines Using Bayesian Belief Network Model. *Journal of Loss Prevent Proceedings*, 40, 479-495.

Uusitalo, L. (2007). Advantages and Challenges of Bayesian Networks in Environmental Modeling. *Ecological Modelling*, 203(3-4), 312–318.

Uusitalo, L., Lehikoinen, A., Helle, I. & Myrberg, K. (2015). An Overview of Methods to Evaluate Uncertainty of Deterministic Models in Decision Support. *Environmental Modelling Software*, 63, 24-31.

Zhang, L., Wu, X., Qin, Y., Skibniewski, M.J. & Liu, W. (2016). Towards A Fuzzy Bayesian Network Based Approach for Safety Risk Analysis of Tunnel-Induced Pipeline Damage: Risk Analysis of Tunnel-Induced Pipeline Damage. *Risk Analysis*, 36(2), 278-301.

Zhou, Y., Li, N., Wu, W., Wu, J. & Shi P. (2014). Local Spatial and Temporal Factors Influencing Population and Societal Vulnerability to Natural Disasters. *Risk Analysis*, 34(4), 614-639.

WATER ALLOCATION MODELLING: A COMPARISON OF RANKING AND PENALTY APPROACHES IN MIKE HYDRO BASIN

BERTRAND RICHAUD[1], ROAR JENSEN[2], EDUARDO MUNOZ[3], KEIKO YAMAGATA[4] & MICHAEL BUTTS[5]

[1,2,3,5] DHI Denmark, Agern Alle 5, DK 2970, Hoersholm, Denmark,
ber@dhigroup.com, raj@dhigroup.com, ejq@dhigroup.com, mib@dhigroup.com
[4] DHI Australia, 3A02-0, Suite 8.01, 50 Clarence Street, Sydney, NSW 2000, Australia
kya@dhigroup.com

ABSTRACT

The global demand for water continues to grow, driven by population growth, urbanization and rising standards of living, food and energy security. To achieve and maintain sustainable water resources under these unprecedented demands requires both careful management and protection of the resource and efficient allocation of water to match the demands in both space and time. In this paper, we compare two methods of modelling water allocation for water resources management, applying MIKE HYDRO Basin to a highly modified and simplified system based on an actual case study in Sri Lanka. The first is a commonly used global ranking algorithm, based on the assumption that the water user demands can be assigned a priority, irrespective of their location in the river basin and water is distributed according to this global priority. The second uses penalties rather than ranks. Penalties are assigned to units of water user and hydropower deficit as well as the reservoir storage depletion and the water allocation problem solved using linear programming. The initial results show that both methods appear to be efficient in solving the water allocation problem posed. The global ranking approach is easily understood and can be applied in a straightforward manner, once the priorities amongst the different users are identified. The penalty approach requires calibration of the penalties, which may be tedious for practitioners and may well influence the overall results. We propose using the ranking approach to perform an initial screening of water allocation options and constraints that could then be refined by using an optimization method such as the linear approach with penalties evaluated in this study.

Keywords: Water allocation; optimization; global ranking; linear programming; penalty function approach.

1 INTRODUCTION

As the demand for water continues to grow, because of population growth, urbanization and rising standards of living, the sustainable development of water resources requires both careful management and protection of the resource and efficient allocation of water. In river basins or countries where the water resources are scarce and new permits can only be assigned by revoking others, a global priority solution is needed. In other places, where the water is distributed according to priority of importance (e.g. water supply is more important than irrigation) or based on equitable sharing (e.g. where a shortage of water is evenly distributed among competing users), more complex algorithms are required.

With the increasing complexity of water resources management and planning projects, practitioners and decision-makers use hydrological models to assess allocation options and consequences. In many cases, reservoirs or systems of reservoirs are central to the management of surface water resources and at the same time, the most complex element of the water resources system. Reservoirs allow the spatial and temporal redistribution of the water but their operation must often address multiple and conflicting demands for water, such as industrial, municipal, and agricultural water supply, flood control, hydropower, etc. Simonovic (1992) has comprehensively described the challenges of reservoir systems operation in water allocation models. There is, therefore, an increasing need to deal with more complex water allocation modelling in generic manner.

Such water allocation problems can be solved by either simulation, optimization or combination of both – the optimisation-simulation approach. Simulation models solve the flow distribution as a water balance problem. Reservoir operation is modelled via a set of rule curves, which guide the release of the reservoir by restricting supply to some users under certain conditions of low storage. Optimisation models require that the water allocation problem, to be solved, can be expressed in the form of an objective function. The application of optimisation models has been widely documented in the literature (Labadie, 2004; Loucks, 1992).

The most common approach has been to use linear programming (LP) for finding the optimal flow distribution in a river system given a set of constraints defined by the network, allocation rules, etc. This approach requires that the penalties (also referred to as “costs”) are assigned correctly. The process of identifying the correct penalty or cost for each elements of the system can become very difficult when dealing with systems of complex networks and allocations, especially for practitioners with less theoretical knowledge. Chou and Wu (2014) describe a variant of the linear programming, network flow programming (NFP) and concluded that it could become an efficient alternative to the simple LP approach, where the possibly time-consuming and difficult trial and error process of identifying penalties can be avoided. However, non-NFP constraints, such as water transmission losses and flow routing, must be handled by using iterative methods. Ilich (2009) has described the limitations of such approaches.

Cai et al. (2001) described the use of genetic algorithms (GA) in combination with linear programming, where they stated that “The key idea is to identify a set of complicating variables in the model, which when fixed, render the problem linear in the remaining variables”. This approach can be quite complex in terms of selecting these complicating variables, and more generally GA algorithms are computationally demanding, with the risk of finding only a local optimum.

Loucks et al. (2005) recommended the use of optimization methods as a screening tool and then further refine the selection by using the simulation approach. However, applying optimisation and then simulation model on the same system might be subject to inconsistencies, due to the different approaches. As mentioned above, combined optimisation-simulation approaches have also been proposed. Sechi & Sulis (2009) concluded that methods using simulation-optimisation approaches are not “truly general-purpose tools”, since a “tuning phase is needed to when using the proposed approach” on real case applications.

There appears to be a gap between the methods presented in the research literature and results achieved in real-world applications (Labadie, 2004). This discrepancy was already recognised in earlier literature. Loucks (1992) identified that communication as the key element in the successful implementation of water resource planning. This is supported by Simonovic (1992), who concluded that utilizing knowledge-based technologies could be one solution in reducing the gaps between theory and practice. In the meantime, applications of decision support systems have become more widespread (e.g. Sørensen et al., 2016) and been implemented around the world and are part of many models (Assaf et al., 2008). Nevertheless, difficulties remain in the application and generalisation of theoretical models.

To address the complexity of real-world water allocation for water resources management, we present a ranking based model approach, which does not require any tuning of penalties for computing the water balance and reservoir operation. This approach is compared to a more commonly applied method to solve the flow distribution that uses linear programming. The two methods are evaluated for a test case, using the water resource systems modelling tool, MIKE HYDRO Basin (DHI, 2014).

2 METHODOLOGY

MIKE HYDRO Basin is a general water resources modelling tool developed specifically to assess water resources and constraints and the impact of water resources management measures. This tool represents the water resource system as a network of branches and nodes. The branches represent, for example, river reaches, while the nodes represent confluences or a location where certain water activities occur (Figure 1). These activities can include multipurpose reservoirs, withdrawals for water supply and irrigation, effluent discharges, diversion canals, gauging stations or low flow control points. The tool supports rainfall-runoff modelling, different routing methods along the branches and multiple, multipurpose reservoirs. Individual reservoirs can simulate the performance of specified policies using associated operating rule curves or the actual performance based on measured data. Applications of MIKE HYDRO Basin, previously MIKE BASIN, including climate changes impact assessments (Butts et al., 2016), economically efficient ways to meet WFD requirements (Riegels et al., 2011) and seasonal forecasting (Butts et al. 2016).

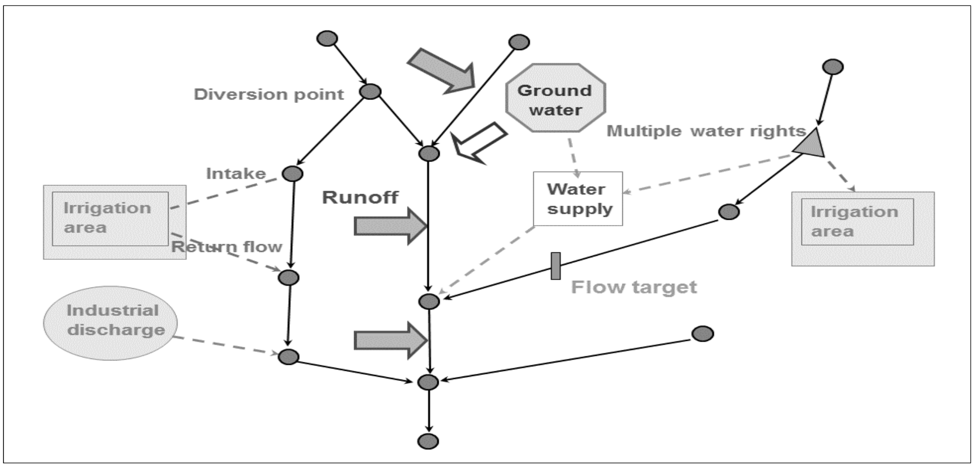

Figure 1. Schematic of the MIKE HYDRO Basin model for different water users, reservoirs, water activities and hydrological processes.

2.1 Global ranking

The global ranking algorithm is based on the assumption that the water user demands, irrespective of their location in the river basin, can be assigned the priority and water should be distributed according to this priority. In some countries, this is a common water allocation paradigm, based on the date they were given a particular water right (first in time), also called "riparian rights". This is distinct from the simpler method, which solves the water allocation problem from upstream to downstream (first in line). This means that when high priority users are located downstream of a low priority user, the latter may take the water as it passes the node and might potentially leave no water to the high priority users.

In the global ranking algorithm, also called global priority, as implemented in MIKE HYDRO Basin, each user (or demand point) is assigned a rank and the model solves for the water distribution by first assigning water to the user marked with the highest priority, and the amount of water flowing in upstream nodes is then earmarked (DHI, 2014). The algorithm then checks the next highest ranked user and so forth. Essentially, a priority parameter is set for each user. This process is repeated for each time step.

In this ranking concept, the water users (including hydropower plants) are assigned a unique rank. The highest priority user is assigned the first rank. Actually, the supply connections to users are assigned a rank rather than directly to the user itself. In cases where a user has several sources, each supply connection can be assigned a different source. Reservoir storages are divided into several zones with different ranks. The users with rank lower or equal to the rank of the zone will be supplied by the reservoir storage. As shown in Figure 2, the reservoir is divided into five zones:

- Above flood control level, water is not stored,
- Above “Level #2” (guide curve with ranking priority 2), storage will be used to supply users with ranks inferior or equal to 2,
- Above “Level #1” (guide curve with ranking priority 1), storage will be used to supply users with ranks inferior or equal to 1,
- Above the top of dead storage and until “Level #1”, no supply,
- Below the top of dead storage, no supply.

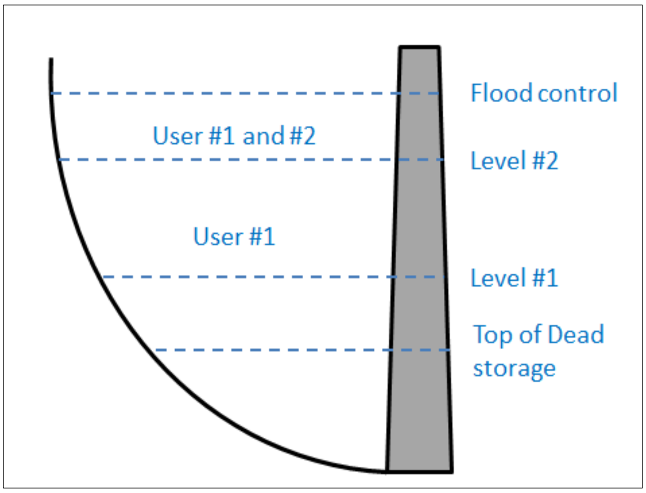

Figure 2. Reservoir allocation zones.

The steps for solving the water allocation model are as follows:

- Naturalised flow: The naturalised flow of the network corresponds to the flow in the river network without any intake from users. The naturalised flow gives information about the water available at any node in the network;
- Allocated water to users: After calculating at each river node (calculation point) of the naturalised flow, the user with the highest priority will be assigned water based on its demand. If necessary, reservoirs will be forced to release water if the ranking guide curve allows supplying such a user. When several reservoirs can supply to the same user, the closest upstream reservoir (in number of calculation points) will be asked first.

Then the following sequence is calculated, as shown in Figure 3:

1. Assign water based on the demand and availability at extraction node,
2. Flush return flows,
3. Comply downstream flow by updating the flow available and unallocated water at all downstream nodes of the extraction point,
4. Update unallocated water at all nodes upstream of the extraction point,

5. Fix unallocated water, so it is a monotone non-decreasing function of the stream flow network. This mechanism handles ambiguities that could arise upstream of confluences, where both branches (*i.e.* the chain of upstream reaches) could support a demand downstream of the confluence.

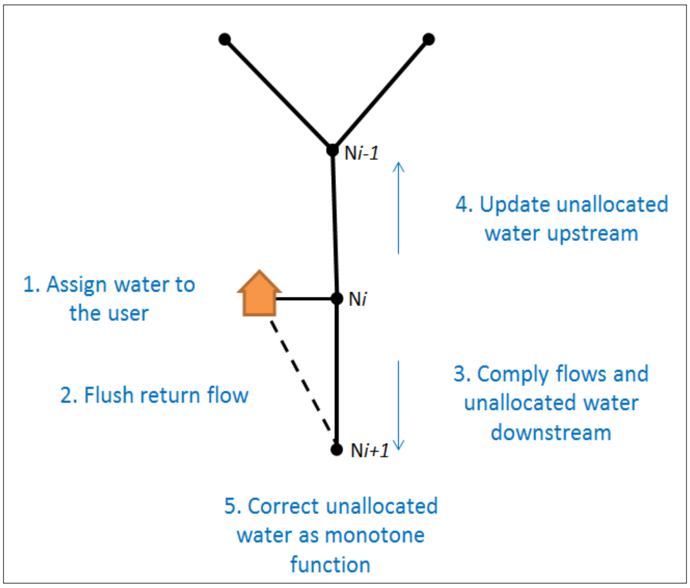

Figure 3. Calculation steps for water allocation at each calculation point processes.

2.2 Penalty approach with linear programming

Penalties are assigned to units of water user and hydropower deficit as well as reservoir storage depletion. The aim of water allocation optimisation model is to minimize the total penalties in the entire system at each time step. The problem is formulated as a linear problem where the objective functions are solved under given constraints. The objective function are minimised by optimising a set of decisions variables (DHI, 2013). The linear solver, *lp_solve,* has been tailored to be accessed from Excel (Buttrey, 2005). At each time step, the decision variables are optimised. The decision variables are divided into two groups, reach flow at each simulation time, q_k and reservoir storage in each zone at the end of each simulation time step, $S_{i,j}$; where k is the reach number, i the node number and j the penalty zone number.

Reach flows are sufficient to determine water distribution in the system. However, these cannot control storage change in the reservoirs. They do not have any influence in determination of how much water should remain in each reservoir at the end of this time step. Therefore, the second type of decision variable was introduced. Each reservoir is divided into several penalty zones and storages in each penalty zones at the end of this simulation time step are selected as another set of decision variables.

The solver shall minimize the total penalty at each time step for the entire system. Penalties are split into two groups, water users and reservoirs. For water users, the water user deficit at each time step is multiplied by the water user penalty. The deficit is calculated as the difference between the amount of water demanded and the amount supplied. For reservoirs, the depletion in storage in each reservoir's penalty zone is multiplied by the associated penalty. The depletion in storage is the difference between the reservoir outflow and the sum of the inflow from the river network and the catchment runoff.

The objective functions are:

$$OF = Min\{[\sum_i^{WU}(Demand_i - Qin_i) * Penalty_i] + [\sum_i^{Res}(Qout_i - Qin_i - catinflow_i) * Penalty_i]\} \quad [1]$$

where $Penalty_i$ is the penalty at node i, $Demand_i$ is the demand at node i, Qin_i is inflow at node i, $Qout_i$ is the outflow from node i, and $catinflow_i$ is the catchment inflow at node i. The nodes are either water user nodes or reservoir nodes.

The objective function formulation can be simplified by removing the constant terms (water user demand and catchment runoff), as shown in Eq. [2]. By reversing the signs, the objectives can be formulated in term of obtaining a maximum rather than a minimum, as represented by Eq. [3].

$$OF = Min\{[\sum_i^{WU} - Qin_i * Penalty_i] + [\sum_i^{Res}(Qout_i - Qin_i) * Penalty_i]\} \quad [2]$$

$$OF = Max\{[\sum_i^{WU} Qin_i * Penalty_i] + [\sum_i^{Res}(Qin_i - Qout_i) * Penalty_i]\} \quad [3]$$

Finally, the reservoir storage is divided into several penalty zones. Hence, the equation of the objective function can be reformulated as follows:

$$OF = Max\{[\sum_i^{WU} Qin_i * Penalty_i] + [\sum_i^{Res} \sum_j^{zone}(S_{i,j} - CurrentS_{i,j})/\Delta t * Penalty_{i,j}]\} \quad [4]$$

where $Penalty_i$ is the penalty at node i, $Penalty_{i,j}$ is the penalty for zone j at reservoir node i, $S_{i,j}$ is the storage for zone j at reservoir node i, $CurrentS_{i,j}$ is the current storage penalty for zone j at reservoir node i, and Δt is the simulation time step.

The set of optimal decision variables are found subjected to the system constraints. The system constraints are used to ensure: (a) the mass balance at each river node, water user, hydropower node or reach, (b) the operational rule at reservoir that the water level shall not be below the dead storage or exceed the dam crest, and (c) meet the capacity limitation in reaches or at the outlet of reservoirs.

3 TEST CASE

To obtain a realistic test case we have taken, as a starting point, a highly complex model setup developed in MIKE BASIN, an earlier version of MIKE HYDRO Basin. As shown in Figure 4, the original model, developed in a separate study, covered a large part of Sri Lanka (DHI, 2013). This system is clearly too complex, for this study if we are to properly understand how the two approaches perform. We therefore focused on a smaller subsystem within the eastern part of the system, the inset as shown in Figure 4. This subsystem was then further simplified and modified so that we have complete control on the water budget. In this simplified version of the subsystem, six major water users and two active reservoirs are included. Penalties and corresponding ranks have been assigned to the six water users of the system. A higher penalty corresponds to a lower rank. For water users with identical penalties, it has been necessary to arbitrarily assign a rank. Unlike penalties, the ranks have to be unique.

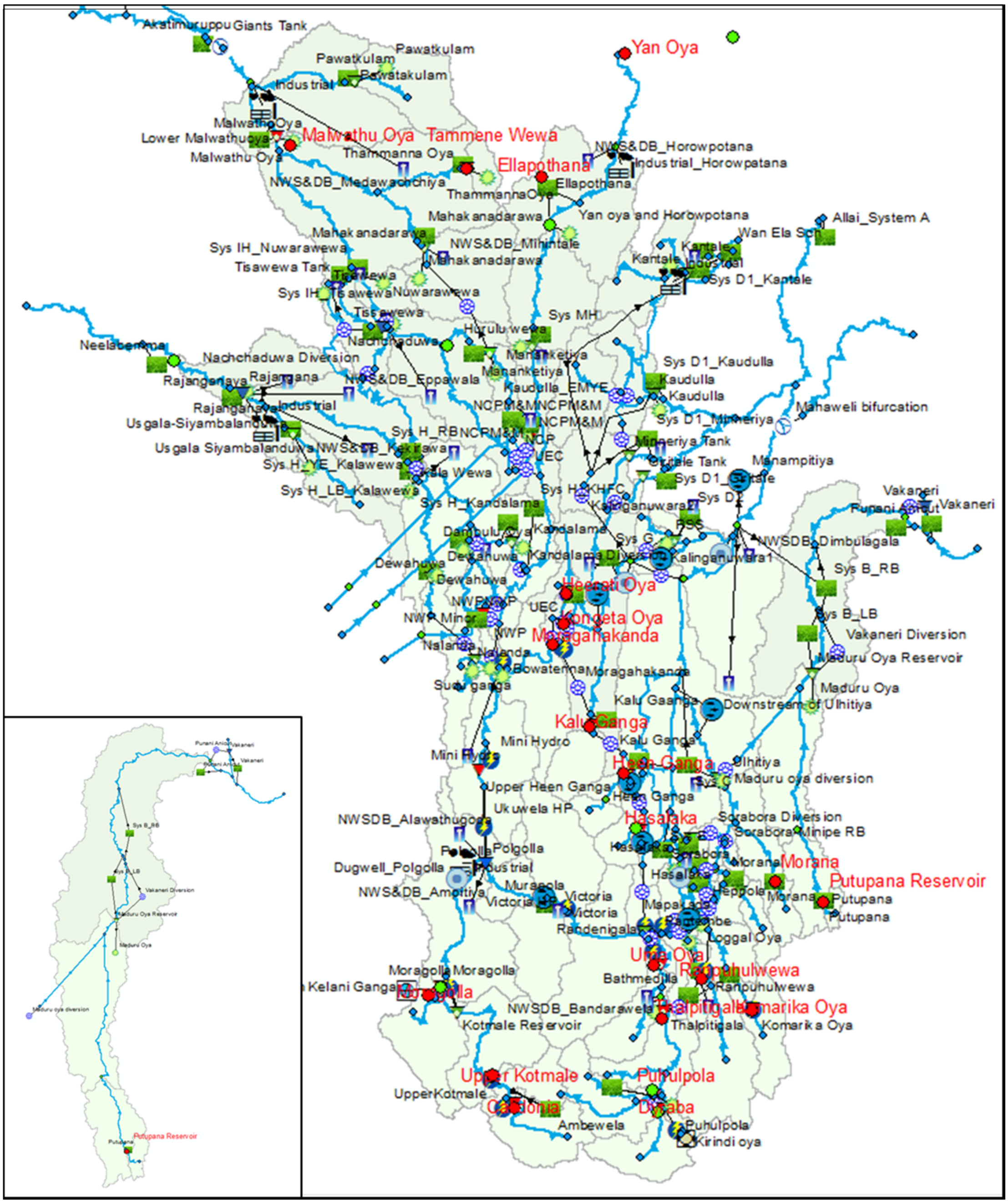

Figure 4. A schematic of the realistic but simplified model subsystem used in this study (inset in the bottom-left corner). This modified subsystem was derived from part of a complex water allocation carried out in another study.

To assess the performance of the two models, it is necessary to compare how water users are supplied based on the water availability. Rules to prioritize the water allocation using the two approaches were setup by translating the penalties to ranks used in the global ranking approach. Several scenarios have been performed.

The active reservoirs are represented by a set of guide curves or penalty curves as illustrated in Figure 5. Li are the penalty levels used by the linear programming, CGi are the guide curves used by the global ranking algorithm, R is the ranks of the users in the global ranking algorithm and P is the penalty in the linear programming. As an illustration, the storage between L3 and L2, will be for user with a rank inferior or equal to 5 in the ranking approach and will be applied a penalty of 2 in the penalty approach. Both models can handle seasonal variation of the guide/penalty curves. Curves are parameterised with monthly values. Figure 6 illustrates the seasonal variation of the curves, where the penalty curves are shown in blue and the guide curves for the ranking approach are shown in red.

  / ISSN 1562-6865 (Online) - ISSN 1063-7710 (Print)

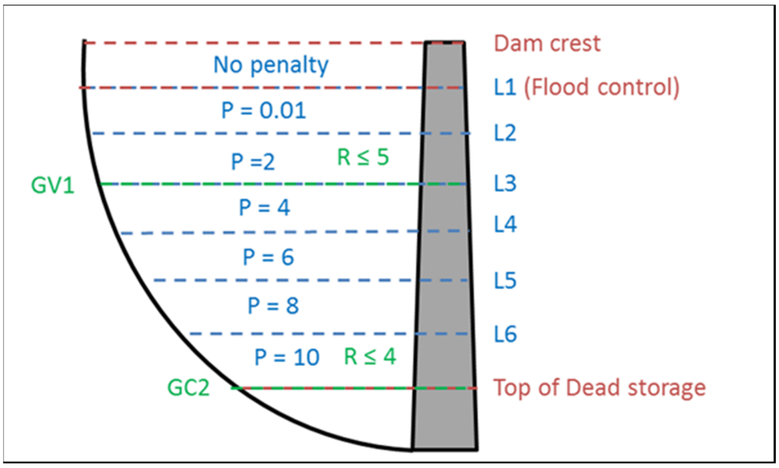

Figure 5. Guide/Penalty curves in one of the subsystem reservoirs.

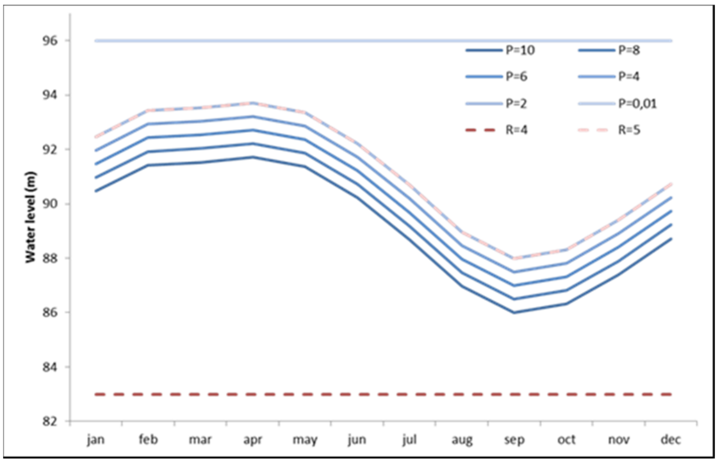

Figure 6. Seasonal variation of Guide/Penalty curves for the reservoir shown in Figure 5.

4 RESULTS

To assess the performance of the two models, it is necessary to compare how the water users are supplied based on the water availability. Rules to prioritize the water allocation using the two approaches were setup by translating the penalties to ranks used in the global ranking approach. Several scenarios have been performed. The first or baseline scenario is used to verify that there were no discrepancies in the application of the two methods. In this scenario, a simple upstream/downstream (inline) approach could be applied as the users with the highest priority are located upstream and those with the lowest downstream.

The results of the two approaches for the baseline scenario are compared in terms of water user deficit, the amount of water that was not delivered to the user and used water, the water delivered and consumed by the users (return flow has been subtracted), as shown in Figure 7. The seasonal water user deficitand average deficit for each month is compared in Figure 8. These results show the two approaches are very similar, as would be expected in this baseline scenario. This provides a verification of two methods and demonstrates consistency in the way we have parameterized the two methods in this simple case. In the second scenario, presented here, referred to as scenario A, the ranks and the corresponding penalties of the highest priority users located upstream have been modified to become the lowest priority user. The results for scenario A, in terms of water user deficit and used water, are shown in Figure 9 and the corresponding seasonal water user deficit in Figure 10. The same deficit occurs for the water user with rank 1. This is due to its location upstream in the river network, where no resource is available even with highest priority. However, in contrast to the baseline scenario, differences can be observed in the seasonal variation of the water user deficit of the lowest priority (rank 5.1).

Figure 11 shows the simulated reservoir levels for scenario A, in one of the active major reservoirs. Small differences are also observed here for the results from the two approaches. The likely explanation is that the ranking approach appears to be stricter when it comes to the reservoir operation, since no deviations from the guide curves are permitted. The differences in the simulated behaviour of the reservoirs to slightly different water deficits for the lowest priority users, which are the last ones to be affected by lack of water.

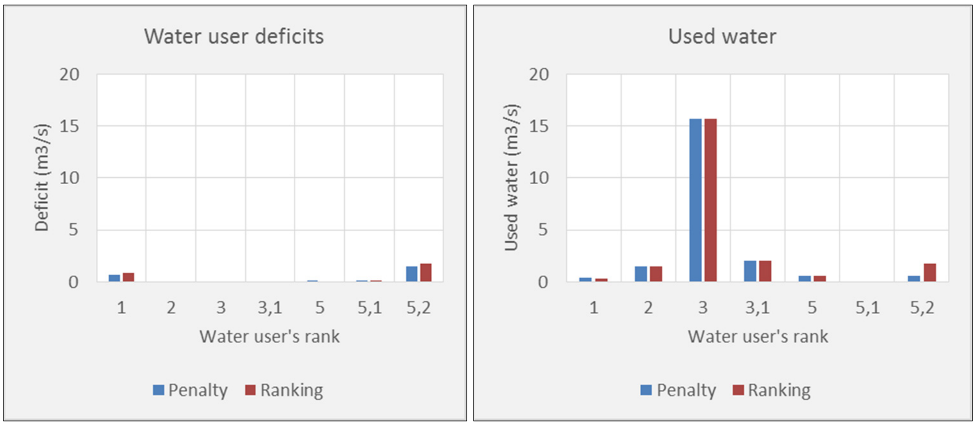

Figure 7. Results of the baseline scenario in terms of water user deficit (a) and used water (b).

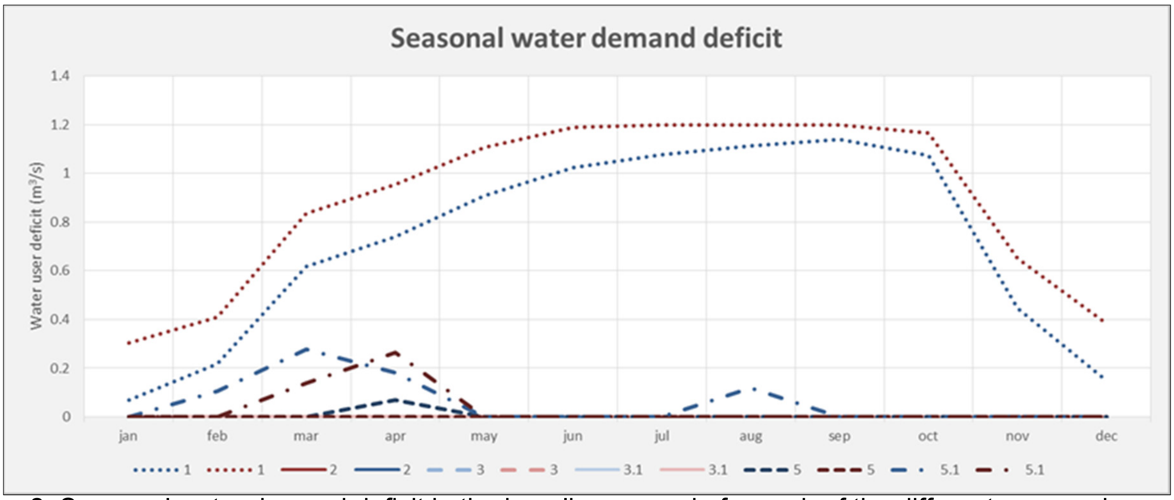

Figure 8. Seasonal water demand deficit in the baseline scenario for each of the different users using ranking (red) and penalty (blue) methods.

(a) (b)

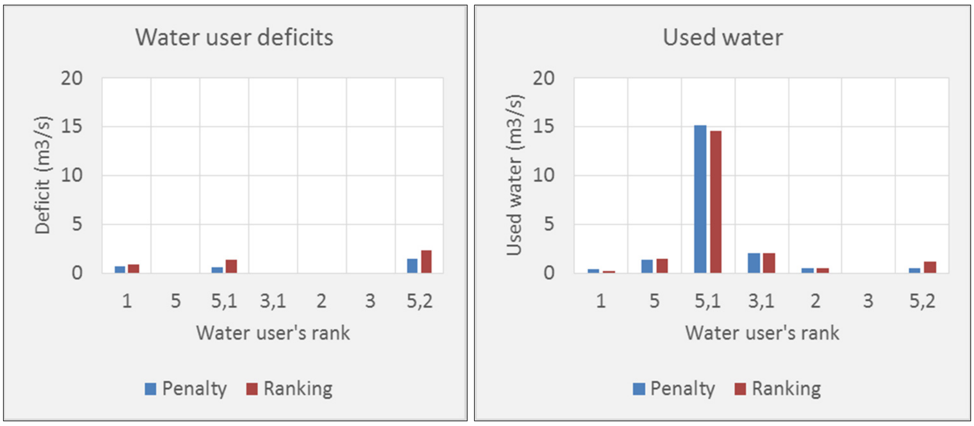

Figure 9. Results for scenario A in terms of water user deficit (a) and used water (b).

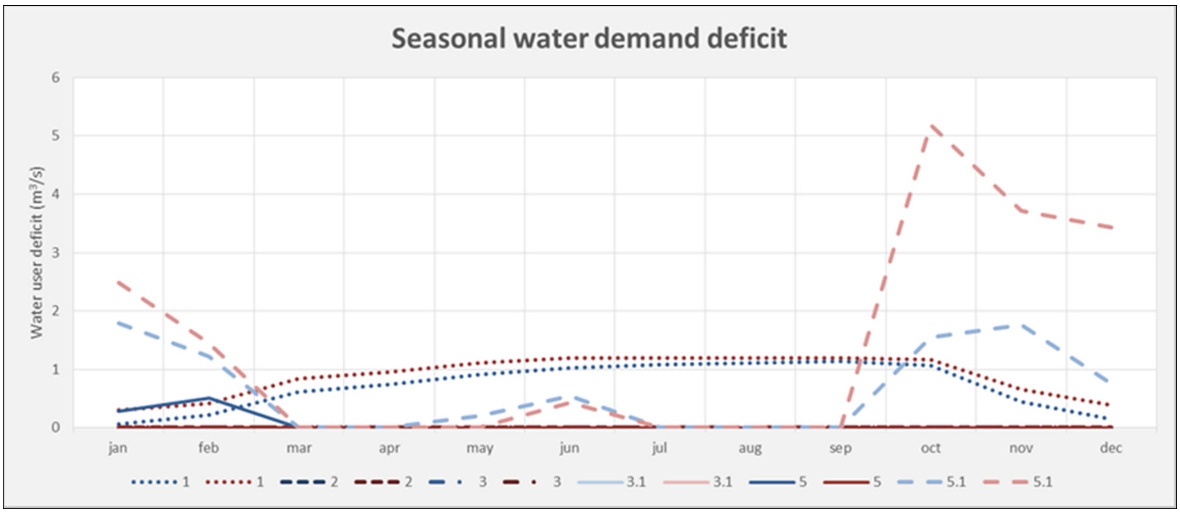

Figure 10. Seasonal water demand deficit in the scenario A for each of the different users using ranking (red) and penalty (blue) methods.

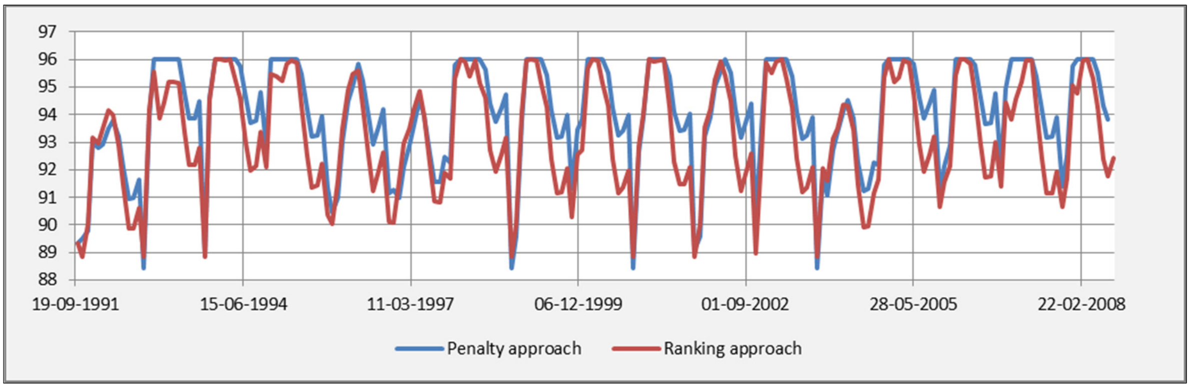

Figure 11. Reservoir levels for scenario A obtained using both the penalty and ranking approach.

5 CONCLUSIONS

In this study, we have developed a global ranking approach for water allocation with the MIKE HYDRO Basin water resources modelling tool. This approach is compared to a more commonly applied method to solve the flow distribution that uses linear programming with penalties. To provide test that is realistic, on the other hand, straightforward to be understood and analysed on the other, the two methods were evaluated for a highly modified and simplified test case, based on a subsystem of a more comprehensive water resource study in Sri Lanka. Both methods appear to be efficient for solving water allocation problems. The global ranking approach is easy to understand and can be applied in a straightforward manner once the priorities between users have identified. The penalty approach requires calibration of the penalties, which may influence the overall results and can be a tedious task for practitioners.

Therefore, the ranking approach appears to be a more efficient method for an initial screening of the water allocation. This could then be refined by applying an optimization method, such as the linear programming approach, which seems to be better at solving more complicated systems, for example, with very complex networks including diverted and reconnected networks. On the other hand, the linear programming approach will only be able to solve linear problems, which could limit the use of hydropower calculation based on energy units. In future work, we intend to investigate the applicability of these two approaches in an actual water allocation problem.

REFERENCES

Assaf, H., Van Beek, E., Borden, C., Gijsbers, P., Jolma, A., Kaden, S. & Sieber, J. (2008). Chapter Thirteen Generic Simulation Models for Facilitating Stakeholder Involvement in Water Resources Planning and Management: A Comparison, Evaluation, and Identification of Future Needs. *Developments in Integrated Environmental Assessment*, 3, 229-246.

Buttrey, S.E. (2005). Calling the Lp Solve Linear Program Software from R, S-PLUS and Excel. *Journal of Statistical Software*, 14(4), 1-13.

Butts, M.B., Buontempo, C., Lørup, J.K., Williams, K., Mathison, C., Jessen, O.Z. & Jones, R. (2016a). A Regional Approach to Climate Adaptation in the Nile Basin. *Proceedings of the International Association of Hydrological Sciences*, 374, 3.

Butts, M.B. Xu, Y., Mueller, H.G. Jensen, R.A., Larsen, J.K., Godiksen, P.N. Richaud, B., Larsen, P.T. & Corcuera Barrera. M.A. (2016b). Seasonal Forecasting for Water Resource Management: Reservoir Inflows and Uncertainties. *XXI International Conference Computational Methods in Water Resources, CMWR 2016*, University of Toronto, Canada.

Cai, X., McKinney, D.C. & Lasdon, L.S. (2001). Solving Nonlinear Water Management Models using a Combined Genetic Algorithm and Linear Programming Approach. *Advances in Water Resources*, 24(6), 667-676.

Chou, F.F. & Wu, C.W. (2014). Determination of Cost Coefficients of a Priority-Based Water Allocation Linear Programming Model–A Network Flow Approach. *Hydrology and Earth System Sciences*, 18(5), 1857-1872.

DHI (2013). *Multi-Sector Water Resources Planning Project Sri Lanka – Seasonal Operation Model Technical Reference*. DHI Report.

DHI (2014). *MIKE HYDRO User Guide*. MIKE by DHI.

Ilich, N. (2009). Limitations of Network Flow Algorithms in River Basin Modeling. *Journal of Water Resources Planning and Management*, 135(1), 48-55.

Labadie, J.W. (2004). Optimal Operation of Multireservoir Systems: State-of-the-Art Review. *Journal of Water Resources Planning and Management*, 130(2), 93-111.

Loucks, D.P. (1992). Water Resource Systems Models: Their Role in Planning. *Journal of Water Resources Planning and Management*, 118(3), 214-223.

Loucks, D.P., Van Beek, E., Stedinger, J.R., Dijkman, J.P. & Villars, M.T. (2005). *Water Resources Systems Planning and Management: An Introduction to Methods, Models and Applications*. Paris: UNESCO.

Riegels, N., Jensen, R., Bensasson, L., Banou, S., Møller, F. & Bauer-Gottwein, P. (2011). Estimating Resource Costs of Compliance with EU WFD Ecological Status Requirements at the River Basin Scale. *Journal of Hydrology*, 396(3), 197-214.

Sechi, G.M. & Sulis, A. (2009). Water System Management through a Mixed Optimization-Simulation Approach. *Journal of Water Resources Planning and Management*, 135(3), 160-170.

Simonovic, S. P. (1992). Reservoir Systems Analysis: Closing Gap between Theory and Practice. *Journal of Water Resources Planning and Management*, 118(3), 262-280.

Sørensen, H.R., Beyene, M. & Ammentorp, H.C. (2016). The Nile Basin Decision Support System. *International Association of Hydro-environment Engineering and Research (IAHR). Hydrolink* 4, 117-119.

PREPARATION OF POMEGRANATE PEELS DERIVED ACTIVATED CARBONS BY CHEMICAL AND PHYSIO-CHEMICAL ACTIVATION FOR THE SUCCESSIVE TREATMENT OF HAZARDOUS ACETAMINOPHEN

ZARROUG MANEL[(1)], KENG YUEN FOO[(2)], SOUAD NAJAR SOUISSI[(3)] & ABDELMOTTALEB OUEDERNI[(4)]

[(1,3,4)] LR: Process Engineering & Industrial Systems, National School of Engineers of Gabes, University of Gabes, St Omar Ibn El-Khattab, 6029 Gabes, Tunisia
zarrougmanel@yahoo.fr; Souad.Najar@enig.rnu.tn; Mottaleb.ouederni@enig.rnu.tn
[(2)] River Engineering and Urban Drainage Research Centre (REDAC),
Universiti Sains Malaysia, Engineering Campus, 14300 NibongTebal, Penang, Malaysia.
k.y.foo@usm.my

ABSTRACT

In this work, pomegranate peel (PP), the by-products that abundantly available from the fruit processing industries, has been applied as the renewable resources for the preparation of low cost, eco-friendly and high quality activated carbons. A comparison of the activating conditions, phosphoric acid and phosphoric acid/steam assisted activation on the physical and chemical properties of PP derived carbon adsorbents has been evaluated. The prepared adsorbents were featured as a mean of nitrogen adsorption-desorption curve and Fourier Transform Infrared Spectroscopy (FTIR). The adsorptive behavior was examined with respect to the innovative treatment of acetaminophen, a widely applied pharmaceutical, characterized by the acute toxicity, carcinogenic and mutagenic effects. These newly prepared activated carbons showed the high BET surface area and total pore volumes of 1354 m^2/g and 0.705 cm^3/g; and 1819 m^2/g and 1.040 cm^3/g, respectively. The adsorption performance illustrated an encouraging result towards the adsorptive removal of acetaminophen. The equilibrium data were best confronted to the Langmuir isotherm model, with the monolayer adsorption capacities of 85.49 mg/g and 189.61 mg/g for PAC and PSAC, respectively. The obtained findings supported the high economical and technical feasibility of PP derived activated carbons as a viable solution for the effective treatment of pharmaceutical contaminants.

Keywords: Acetaminophen; activated carbon; adsorption; phosphoric acid; pomegranate peel; steam.

1 INTRODUCTION

Concerning about environmental protection has increased over the year from a global view point, today, the emission of pharmaceutical residues on the surface and subsurface water is a serious agenda among the environmental scientists (Jennifer et al., 2017; Ashfaq et al., 2017). In particular, acetaminophen, or commonly known as paracetamol, is the most widely applied analgesic and anti-inflammatory drug for the relief of fever, severe pain and flu remedies (Andreozzi et al., 2003; Yang et al., 2008). Acetaminophen is commonly detected in the water streams, notably rivers, wells and groundwater tables (Roshanfekr et al., 2015; Kummurer, 2009). As an essential resource of daily life and ecosystems, the issue of water pollution is allied to the aesthetic attention by the environmental protection authorities, with the continuous exploration of efficient water treatment technology as a convenient response to the new emerging contaminants. Among all, activated carbon adsorption process has prevailed to be an effective treatment method for the effective control of water pollutants, mainly ascribed to the large accessible surface area and pore volume, and the great regenerative potential (Ruiz et al., 2010). However, the wide scale application is hampered by the high operating cost associated with the available commercial activated carbons. Extensive researches have been devoted to the development of agricultural biomass derived carbonaceous adsorbents (Ghaedi et al., 2012). The abundant availability of agricultural by-products makes them the good sources of raw precursors for preparation of low cost activated carbons (Foo and Hameed, 2012a). In such perspective, pomegranate is an important fruit crop grown in the Mediterranean countries, which are commonly consumed as fresh, or processed as juice, jams and wine. Pomegranate peel, a major by-product emitted from the pomegranate processing industry would serve as a potential alternative raw precursor for the preparation of low cost activated carbons (Radaei et al., 2014; Ghaedi et al., 2012; Amin, 2009).

The preparation of activated carbons is usually implemented by the physical or chemical activation or a combination of both (Klijanienko et al., 2008). Physical activation involves the pyrolysis (carbonization) of the initial raw precursor under inert atmosphere, subsequently by the activation at relatively high temperatures of above 800 °C under the flow of carbon dioxide or steam (Budinova et al., 2006). Chemical activation is conducted with the presence of chemical reagents at a much lower temperature of 400 to 600 °C (Lupul et al., 2015). In particular, phosphoric acid assisted chemical activation has been related to the formation of phosphate and polyphosphate bridges, leading to the connection and cross linking with the biopolymer fragments (Mestre et al., 2011). In contrast, phosphoric acid activation under steam flow has been associated with a better development of porous structure, a wider pore size distribution range, and greater yield and resistance to attrition. In this sense, this study was undertaken to evaluate the viability of pomegranate peel as a renewable precursor for the preparation of eco-friendly activated carbon by both phosphoric acid and phosphoric acid/steam assisted activation. The structural, functional and surface characterizations were performed. Moreover, the novel application for the adsorptive removal of acetaminophen, with the modeling analysis was elucidated.

2 MATERIALS AND METHODS

2.1 Adsorbate

Acetaminophen, also known as N-(4-hydroxy- phenyl) ethanamide, was selected as the model adsorbate in this work. The standard stock solution was prepared by dissolving the adsorbate in ultra-pure water, and the working solutions were prepared by serial dilutions. The physico-chemical properties of acetaminophen are given in Table 1.

Table 1. Physico-chemical properties of acetaminophen.

Properties	Description
Molecule structure	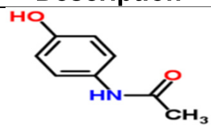
Molecular formula	$C_8H_9NO_2$
Molecular weight (g/mole)	151.16
pKa	9.86
Molar volume (cm^3/mole)	120.90

2.2 Preparation of activated carbons

Pomegranate peels (PP) used in the present study was acquired from a local plantation area in Gabes, Tunisia. The initial raw precursor was washed extensively with distilled water, dried, grinded and sieved to a particle fraction of 2 to 5 mm. The preparation of activated carbons was performed by the impregnation of PP with phosphoric acid (50%) at the predetermined weight ratio of 4:1. The impregnated samples were carbonized in a tubular furnace under inert condition and activated at 400 °C for 2 h under the flow of nitrogen or nitrogen/steam. These activated products were rinsed with deionized water until the pH of the filtrate solution reached to the neutral pH. These newly prepared PP derived adsorbents via phosphoric acid and phosphoric acid/steam induced activation are defined as PAC and PSAC, respectively.

2.3 Physical and chemical characterizations

The initial PP was analyzed with respect to the carbon content using an elemental analyzer (LECO-CHNS-932) and thermogravimetric analyzer (DSC Q600).The surface physical properties of the newly prepared PAC and PSAC were examined using an Autosorb surface area analyzer (Quantachrome) with N_2 as the adsorbate at -196 °C. The Brunauer–Emmett–Teller (BET) surface area, total pore volume, mesopore and micropore volumes were deduced using the *t*-plot method. The surface functional groups were detected by the Fourier Transform Infrared (FTIR) spectroscopy (FTIR-100, Shimadzu) using the KBr pellet method within the scanning range of 4000 to 400 cm^{-1}.

2.4 Bach equilibrium studies

The batch adsorption experiments were carried out in a set of Erlenmeyer flasks containing 0.01 g of carbon adsorbents and 50 mL of acetaminophen solutions (ACP) with the initial concentrations range of 10 to 300 mg/L in a water bath shaker at 30 °C and 120 rpm. The concentration of ACP was withdrawn at predetermined time intervals, and was measured using a UV-vis spectrophotometer (Shimadzu UV-1700) at the optimum wavelength of 243 nm. The equilibrium uptake of ACP, q_e (mg/g) was given by Eq [1]:

$$q_e = \frac{(Co - Ce) \times V}{m} \qquad [1]$$

where C_0 (mg/L) and C_e (mg/L) are the initial and equilibrium concentrations of ACP, respectively, V (L) is the volume of solution, and m (g) is the mass of carbon adsorbent.

3 RESULTS AND DISCUSSION

3.1 Physical and chemical characterizations

Table 2 provides a summary of the ultimate and proximate analysis of the initial raw precursor, PP. The selected precursor showed a relatively high volatile matter and fixed carbon content, but with a lower ash content, demonstrating the high suitability for the preparation of high quality activated carbon (Das et al., 2015). The economic feasibility of different raw precursors, oak and birch (Klijanienko et al., 2008), sisal waste (Mestre et al., 2011), and hemp stem (Lupul et al., 2015) with a comparative elemental content have been reported by previous researchers.

Table 2. Elemental and proximate analysis of PP.

Elemental analysis	**(wt%)**
Carbon	46.7
Oxygen	47.2
Hydrogen	5.5
Nitrogen	0.5
Sulphur	0.2
Proximate analysis	**(wt%)**
Moisture	1.7
Volatile matter	71.9
Fixed carbon	21.2
Ash	5.2

Nitrogen adsorption isotherm is a standard procedure for the determination of porosity of the carbonaceous adsorbents. From Figure 1, it can be deduced that these PP derived carbon adsorbents belong to the type I isotherm according to the International Union of Pure and Applied Chemistry (IUPAC) classification, with a significant increase of N_2 adsorption at low relative pressures, and a long plateau extended to $P/P_0 \approx 1$. The results revealed that these carbonaceous adsorbents are essentially microporous, and the small adsorption-desorption hysteresis illustrated the presence of mesoporous structure (Klijanienko et al., 2008). Interestingly, the adsorption isotherm of PSAC displays a higher slope, indicating a wider distribution of microporous texture.

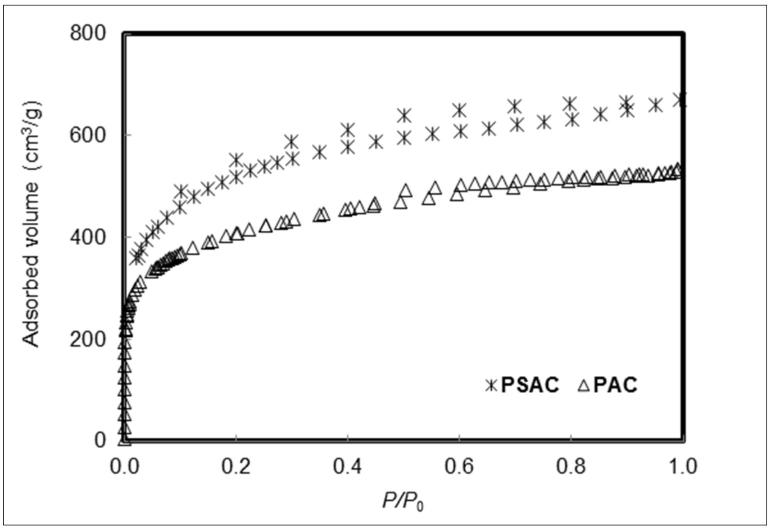

Figure 1. Nitrogen adsorption-desorption curves of PAC and PSAC.

Similarly, the surface physical properties were substantially affected by the activating conditions. The BET surface areas, total pore volumes, and average pore diameters of PAC and PSAC were identified to be 1354 m^2/g, 0.705 cm^3/g and 20.82 Å; and 1819 m^2/g, 1.040 cm^3/g, and 22.86 Å, respectively. It is evident that phosphoric acid may induce significant chemical alteration at low temperatures in the initial raw precursor to promote the pyrolytic decomposition of PP, with the formation of cross-linked structure. This cross-linking structure is governed by the bond cleavage reactions between the acid and organic materials in the raw precursor, leading to the formation of phosphate linkages between the fragments in the biopolymer. Conversely, steam pyrolysis showed an extra ability to penetrate into the porous surface to facilitate the distillation, desorption and efficient removal of volatiles, resulting in the significant improvement of the BET surface area and total pore volume (Budinova et al., 2006). This finding could also be explained by the excessive presence of activating agent, leading to the collapse of the extended weak structure, as a result of the enhanced elimination of phosphate compounds during the phosphoric acid induced activation, which did not occur under the steam flow. Therefore, a greater BET surface area and higher total pore volume were obtained during the phosphoric acid assisted activation under steam flow (Lupul et al., 2015).

Table 3. Surface textural properties of the PP derived activated carbons.

Properties	**PSAC**	**PAC**
BET surface area (m^2/g)	1819	1354
Micropore volume (cm^3/g)	0.983	0.684
Mesopore volume (cm^3/g)	0.057	0.021
Total pore volume (cm^3/g)	1.040	0.705
Average pore diameter (Å)	22.86	20.82

Table 4 exhibits a comparison of the BET surface area and total pore volume of a wide range of activated carbons derived from different precursors. The activated carbons prepared in this work showed relatively high BET surface areas and total pore volumes as compared to some previous works reported in the literature.

Table 4. Comparison of textural properties of different agricultural biomass derived activated carbons.

Precursor	**Activated agent**	**BET surface area (m^2/g)**	**Total pore volume (cm^3/g)**	**References**
Pomegranate peels	H_3PO_4/Steam	1819	1.040	Present study
	H_3PO_4	1354	0.684	
Pomegranate peels	KOH	941	0.470	Azmier et al. (2014)
Pomegranate seeds	$ZnCl_2$	988	0.568	Uçar et al. (2009)
Date stone	KOH	856	0.468	Foo and Hameed (2011a)
Oil palm fiber	KOH	708	0.380	Foo and Hameed (2011b)
Woody biomass birch	H_3PO_4/Steam	1290	0.939	Budinova et al. (2006)
Grap seeds	H_3PO_4	1139	0.730	Al Bahri et al. (2012)
Green Coconut Shell	$ZnCl_2$	996	0.449	Das et al. (2015)
Sisal waste	H_3PO_4	1008	0.450	Dizbay-Onat et al. (2017)
Tea waste	H_3PO_4	880	0.680	Kan et al. (2017)

The FTIR spectra of the PP derived activated carbons are depicted in Table 5. The broad band at 3391–3368 cm^{-1} is the primarily characteristic of the hydrogen bond (–O–H) in carboxyl, phenols, alcohols, and the absorbed water molecules (Nahil and Williams, 2012). The sharp peak at 2917 cm^{-1} is attributed to the symmetric or asymmetric stretching in aliphatic –C–H. The signal at 1703 cm^{-1} is assigned to the C=O vibration in ketones, aldehydes, lactones and carboxylic groups. This peak disappearance in PSAC suggested the excessive presence of carboxylic group did not take place during the phosphoric acid/steam assisted activation (Budinova et al., 2006). The intensity at 1599/1598 cm^{-1} is related to large condensed aromatic skeletons in the carbonaceous system. The weak signal at 1384 cm^{-1} may be due to the C-C vibration of aromatic ring. The small shoulder peak at 1248/1216 cm^{-1} is corresponded to C–O stretching of C–O–P in acids, alcohols, phenols, ethers and esters, while the presence of P–O–P derivatives showed the transmittance at 1051/1044 cm^{-1}. At the low wavenumber district, the broad band at 565 /544 cm^{-1} indicates the out-of-plane deformation mode of the C-H vibration in aromatic rings (Zhu et al., 2016; Tounsadi et al., 2016).

Table 5. FTIR analysis of PAC and PSAC.

No.	**Wavenumber (cm^{-1})**		**Assignment**
	PAC	**PSAC**	
1	3391	3368	–O–H
2	2917	2917	C–H
3	1703	-	C=O
4	1384	1384	C-C
5	1248	1216	C-O
6	1044	1051	P-O-P
7	565	544	C-H

3.2 Adsorption equilibrium study

Figure 4 displays the curve adsorption equilibrium, q_e versus equilibrium concentration of ACP, C_e onto the PP derived activated carbons. Initial concentration exerted an important driving force for alleviating the mass transfer resistance between the liquid phase and the carbon adsorbents. By increasing the initial concentration from 10 to 200 mg/L, an increasing q_e from 19.15 to 75.10 mg/g, and from 16.31 to 122.70 mg/g, for PAC and PSAC, respectively, were shown.

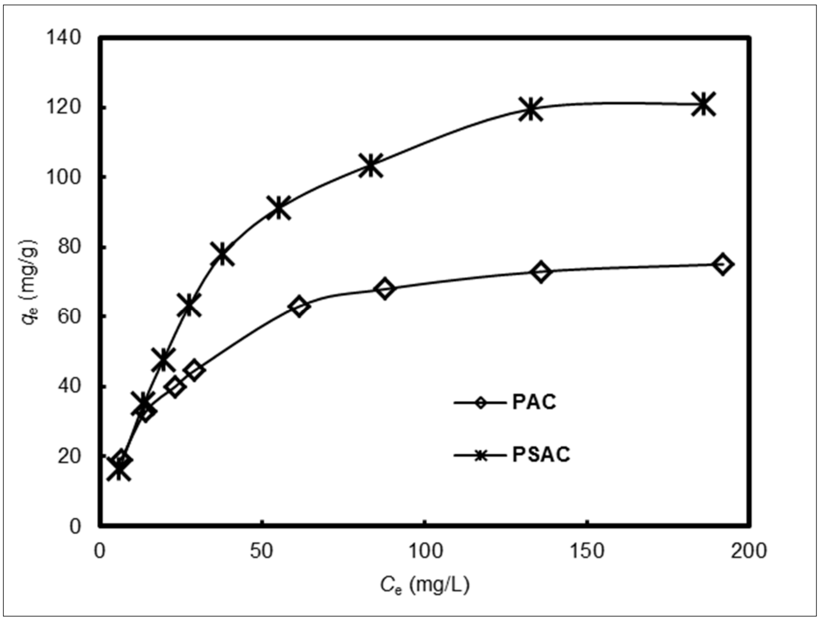

Figure 2. Adsorption equilibrium, q_e versus equilibrium concentration of ACP, C_e onto PAC and PSAC.

Adsorption isotherm is an essential data source for the practical design and fundamental understanding of the carbonaceous adsorbents. Typically, the mathematical correlation is accessed by linear regression analysis. Due to the inherent bias resulting from linearization, alternative isotherm parameter sets were determined by non-linear regression (Foo and Hameed, 2010). In this study, three isotherm models: Langmuir, Freundlich and Temkin equations were established. Langmuir isotherm model (Langmuir, 1916) assumes monolayer adsorption with adsorption occur only at a finite number of definite localized sites, which are identical and equivalent. The Langmuir isotherm model is defined as:

$$q_e = \frac{Q_0 K_L C_e}{1 + K_L C_e} \qquad [2]$$

where Q_0 (mg/g) and K_L (L/mg) are the Langmuir isotherm constants related to the adsorption capacity and energy of adsorption, respectively. The Freundlich isotherm model (Freundlich, 1906) is an empirical equation describing the non-ideal and reversible adsorption, with non-uniform distribution of heat adsorption and affinities over the heterogeneous surface, and is given by:

$$q_e = K_F C_e^{1/n} \qquad [3]$$

where K_F (mg/g)/(L/mg)$^{1/n}$ and 1/n are Freundlich parameters related to the adsorption capacity and adsorption intensity, respectively. The Temkin isotherm model (Tempkin an Pyzhev, 1940) elucidates the indirect interactions between the adsorbate molecules based on the assumption that the heat of adsorption of all molecules in the layer would decrease linearly rather than logarithmically with surface coverage. It has the predictive power over a wide range of concentrations, and is commonly expressed as:

$$q_e = B\ln(AC_e) \qquad [4]$$

where B=RT/b and b (J/mole) is Temkin isotherm constant related to the heat of adsorption, A (L/g) is the equilibrium binding constant, R (8.314 J/mole.K) is the universal gas constant, and T(K) is the absolute temperature.

The applicability of the isotherm models was determined by judging the correlation coefficients, R^2 value derived as:

$$R^2 = \frac{(q_{e,exp} - \overline{q_{e,calc}})^2}{\sum (q_{e,exp} - q_{e,calc})^2 + (q_{e,exp} - q_{e,calc})^2} \quad [5]$$

The validity of the models was further verified by the root-mean-square deviation (*RMSD*), the commonly used statistical tool to measure the predictive power of a model and is derived as:

$$RMSD = \frac{\sqrt{\sum_{i=1}^{n} (q_{exp} - q_p)^2}}{n - 1} \quad [6]$$

where q_{exp} (mg/g) and q_p (mg/g) are the experimental and theoretical adsorption capacity, respectively.

The detailed parameters obtained from these isotherm models are tabulated in Table 6. The experimental analysis showed strong positive evidence that the adsorption of ACP onto PAC and PSAC was best fitted to the Langmuir isotherm model, with the highest R^2 of 0.994 and 0.996, and the lowest *RMSD* of 0.579 and 0.690, respectively. This implied that the adsorption of ACP onto these newly prepared activated carbons from the aqueous solutions proceeds by a monolayer formation. The findings also suggested that the adsorption takes place on the homogeneous sites that are identical and energetically equivalent (Foo and Hameed, 2012b). The present results are in agreement with the previous researches for the adsorption of ACP onto sludge (Llado et al., 2015) and dende coconut (Ferreira et al., 2015) derived activated carbons.

Table 6. Langmuir, Freundlich and Tempkin isotherm model parameters for the adsorption of ACP onto PAC. and PSAC.

Adsorbent	Langmuir K_L (L/mg)	Langmuir Q_0 (mg/g)	Langmuir R^2	Langmuir *RMSD*	Freundlich K_F (mg/g)/(L/mg)$^{1/n}$	Freundlich *n*	Freundlich R^2	Freundlich *RMSD*	Temkin *A* (L/g)	Temkin *B* (J/mole)	Temkin R^2	Temkin *RMSD*
PAC	0.0395	85.49	0.994	0.579	15.58	3.325	0.933	1.698	16.54	0.514	0.987	1.741
PSAC	0.0175	189.61	0.996	0.690	6.19	1.466	0.976	1.442	34.81	0.231	0.973	1.517

Table 7 lists a comparison of the monolayer adsorption capacity of ACP onto activated carbons derived from different precursors. It can be concluded that the monolayer adsorption capacities of ACP onto the PP derived activated carbons obtained in this work were comparable with the previous researches. The present findings demonstrated the potential of pomegranate peel as a valuable precursor for preparation of high quality activated carbons via phosphoric acid and phosphoric acid/steam assisted activation for environmental applications.

Table 7. A comparative evaluation of monolayer adsorption capacities of ACP onto activated carbons derived from different precursors.

Precursor	Activating agent	Adsorption capacity (mg.g^{-1})	References
Pomegranate peels	H_3PO_4	85.49	This study
	H_3PO_4/Steam	189.61	
sisal waste	K_2CO_3	124	Mestre et al. (2011)
Dende coconut mesocarp	-	90	Ferreira et al. (2015)
Sludge	Steam	53	Lladoa et al. (2015)
Commercial activated carbon	-	130	Saucier et al. (2017)

4 CONCLUSIONS

The present research revealed the great technical and economic feasibility of pomegranate peels as renewable resources for preparation of activated carbon by a single step, phosphoric acid or phosphoric acid/steam assisted activation. These newly prepared carbonaceous adsorbents showed the high BET surface areas and total pore volumes of 1354 m^2/g and 0.705 cm^3/g; and 1819 m^2/g and 1.040 cm^3/g respectively. The novel application for the innovative treatment of acetaminophen has been attempted. The equilibrium data were best fitted to the Langmuir isotherm model, with the monolayer adsorption capacities of 85.49 mg/g and 189.61 mg/g, respectively.

ACKNOWLEDGEMENTS

The authors acknowledge the financial support provided by Universiti Sains Malaysia, Malaysia and University of Gabes, Tunisia under the RUI (Project no.: 1001/PREDAC/814272) and Research Travel (LR: GPSI-LR11ES54) grant schemes.

REFERENCES

Al Bahri, M., Calvo, L., Gilarranz, M.A. & Rodriguez, J.J. (2012). Activated Carbon from Grape Seeds Upon Chemical Activation with Phosphoric Acid: Application to the Adsorption of Diuron from Water. *Chemical Engineering Journa*l, 203, 348–356.

Amin, N.K., (2009). Removal of Direct Blue-106 Dye from Aqueous Solution using New Activated Carbons Developed from Pomegranate Peel : Adsorption Equilibrium and Kinetics. *Journal of Hazardous Materials*, 165(1), 52–62.

Andreozzi, R., Caprio, V., Marotta, R. & Vogna, D. (2003). Paracetamol Oxidation from Aqueous Solutions by Means of Ozonation and H_2O_2 / UV System. *Water Research*, 37(5), 993–1004.

Ashfaq, M., Khan, K.N., Saif, M., Rehman, U., Mustafa, G., Nazar, M.F., Sun, Q., Iqbal, J., Mulla, S.I. & Yu, C. (2017). Ecological Risk Assessment of Pharmaceuticals in the Receiving Environment of Pharmaceutical Wastewater in Pakistan. *Ecotoxicology and Environmental Safety*, 136, 31–39.

Azmier, M. A., Nur Azreen, A. P. & Bellos, O. S. (2014). Kinetic , Equilibrium and Thermodynamic Studies of Synthetic Dye Removal using Pomegranate Peel Activated Carbon Prepared by Microwave-Induced KOH Activation. *Water Resources and Industry Journal*, 6, 18–35.

Budinova, T., Ekinci, E., Yardim, F., Grimm, A., Björnbom, E., Minkova, V. & Goranova, M. (2006). Characterization and Application of Activated Carbon Produced by H_3PO_4 and Water Vapor Activation. *Fuel Processing Technology*, 87(10), 899–905.

Das, D., Samal, D.P. & Bc, M. (2015). Preparation of Activated Carbon from Green Coconut Shell and its Characterization. *Jouranl of Chemical Engineering & Process Technology*, 6(5), 1-7.

Dizbay-onat, M., Vaidya, U.K. & Lungu, C.T. (2017). Preparation of Industrial Sisal Fiber Waste Derived Activated Carbon by Chemical Activation and Effects of Carbonization Parameters on Surface Characteristics. *Industrial Crops and Products*, 95, 583–590.

Ferreira, R.C., Junior, O.M.C., Carvalho, K.Q., Arroyo, P.A. & Barros, M.A.S.D. (2015). Effect of Solution pH on the Removal of Paracetamol by Activated Carbon of Dende Coconut Mesocarp. *Chemical and Biochemical Engineering Quarterly*, 29(1), 47–53.

Foo, K.Y. & Hameed, B.H. (2012a). Potential of Jackfruit Peel as Precursor for Activated Carbon Prepared by Microwave Induced Naoh Activation. *Bioresource Technoloy*, 112, 143–150.

Foo, K.Y. & Hameed, B.H. (2012b). Adsorption Characteristics of Industrial Solid Waste Derived Activated Carbon Prepared by Microwave Heating for Methylene Blue, *Fuel Processing Technology*, 99, 103-109.

Foo, K.Y. & Hameed, B.H. (2011a). Microwave-Assisted Preparation of Oil Palm Fiber Activated Carbon for Methylene Blue Adsorption . *Chemical Engineering Journal*,166, 792–795.

Foo, K.Y. & Hameed, B.H. (2011b). Preparation of Activated Carbon From Date Stones by Microwave Induced Chemical Activation : Application for Methylene Blue Adsorption, *Chemical Engineering Journal*,170(1), 338–341.

Foo, K.Y. & Hameed, B.H. (2010). Insights into the Modeling of Adsorption Isotherm Systems. *Chemical Engineering Journal*, 156(1), 2–10.

Freundlich, H.M.F. (1906). Over the Adsorption in Solution. *Journal of Physical Chemistry*, 57, 385-471.

Ghaedi, M., Tavallali, H., Sharifi, M., Nasiri, S. N. & Asghari, A. (2012). Preparation of Low Cost Activated Carbon from Myrtus Communis and Pomegranate and Their Efficient Application for Removal of Congo Red from Aqueous Solution. *Spectrochimica Acta Part A: Molecular and Biomolecular Spectroscopy,* 86, 107–114.

Jennifer, A., Abdallah, M.A. & Harrad, S. (2017). Pharmaceuticals and Personal Care Products (Ppcps) in the Freshwater Aquatic Environment. *Emerging Contaminants*,1-16.

Kan,Y., Yue, Q., Li, D., Wu, Y. & Gao, B. (2017). Preparation and Characterization of Activated Carbons from Waste Tea by H_3PO_4 Activation in Different Atmospheres for Oxytetracycline Removal. *Journal of Taiwan Institute of Chemical Engineers,* 71, 494–500.

Klijanienko, A., Lorenc-grabowska, E. & Gryglewicz G. (2008). Development of Mesoporosity During Phosphoric Acid Activation of Wood in Steam Atmosphere. *Biosourse technology*, 99(15), 7208–7214.

Kummurer, K. (2009). The Presence of Pharmaceuticals in the Environment Due to Human Use-Present Knowledge and Future Challenges. *Journal of Enviromental Managemen,* 90(8), 2354–2366.

Llado, J., Lao-Luque, C., Ruiz, B., Fuente, E., Solé-Sardans, M. & David Dorado, A. (2015). Role of Activated Carbon Properties in Atrazine and Paracetamol Adsorption Equilibrium And Kinetics . *Process Safety and Environmental Protection*, 95, 51–59.

Langmuir, I. (1916). The Constitution and Fundamental Properties of Solids and Liquids. *Journal of American Chemical Society*, 38(11), 2221-2295.

Lupul, I., Yperman, J., Carleer, R. & Gryglewicz G. (2015). Tailoring of Porous Texture of Hemp Stem-Based Activated Carbon Produced by Phosphoric Acid Activation in Steam Atmosphere. *Journal of Porous Materials*, 22(1), 283–289.

Mestre, A.S., Bexiga, A.S., Proença, M., Andrade, M., Pinto, M.L., Matos, I., Fonseca, I.M. & Carvalho, A.P. (2011). Activated Carbons from Sisal Waste by Chemical Activation with K_2CO_3 : Kinetics of Paracetamol and Ibuprofen Removal from Aqueous Solution. *Bioresource Technology*, 102(17), 8253–8260.

Nahil, M.A. & Williams, P.T. (2012). Pore Characteristics of Activated Carbons from the Phosphoric Acid Chemical Activation of Cotton Stalks. *Biomass and Bioenergy*, 37, 142–149.

Radaei, E., Reza, M., Moghaddam, A. & Arami, M. (2014). Removal of Reactive Blue 19 from Aqueous Solution by Pomegranate Residual-Based Activated Carbon : Optimization by Response Surface Methodology. *Journal of Environmental Health Sience and Engineering*, 12(1), 1-8.

Roshanfekr, L., Haririan, I. & Divsar, F. (2015). Comparison of Adsorption and Photo-Fenton Processes for Phenol and Paracetamol Removing from Aqueous Solutions : Single and Binary Systems. *Spectrochimica Acta Part A : Molecular and Biomolecular Spectroscopy*,136, 423–428.

Ruiz, B., Cabrita, I., Mestre, A.S., Parra, J.B., Pires, J., Carvalho, A.P. & Ania, C.O. (2010). Surface Heterogeneity Effects of Activated Carbons on the Kinetics of Paracetamol Removal from Aqueous Solution. *Applied Surface Science*, 256(17), 5171–5175.

Saucier, C., Karthickeyan, P., Ranjithkumar, V. & Lima, E.C. (2017). Efficient Removal of Amoxicillin and Paracetamol from Aqueous Solutions using Magnetic Activated Carbon. *Environmental Science and Pollution Research,* 1-15.

Tempkin, M.I. & Pyzhev, V., (1940). Kinetics of Ammonia Synthesis on Promoted Iron Catalyst. *Acta. Physico Chemica USSR*, 12, 327-356.

Tounsadi, H., Khalidi, A., Machrouhi, A. & Farnane, M. (2016). Highly Efficient Activated Carbon from Glebionis Coronaria L. Biomass : Optimization of Preparation Conditions and Heavy Metals Removal using Experimental Design Approach. *Journal of Environmental Chemical Engineering*, 4(4), 4549–4564.

Uçar, S., Erdem, M., Tay, T. & Karago, S. (2009). Applied Surface Science Preparation and Characterization of Activated Carbon Produced from Pomegranate Seeds by $Zncl_2$ Activation. *Applied Surface Science,* 255(21), 8890–8896.

Yang, L., Yu, L.E. & Ray, M.B. (2008). Degradation of Paracetamol in Aqueous Solutions by Tio_2 Photocatalysis. *Water Research*, 42(13), 3480–3488.

Zhu, G., Deng, X., Hou, M., Sun, K., Zhang, Y., Li, P. & Liang, F. (2016). Comparative Study on Characterization and Adsorption Properties of Activated Carbons by Phosphoric Acid Activation from Corncob and its Acid and Alkaline Hydrolysis Residues. *Fuel Processing Technology*, 144, 255–261.

INTEGRATED HYDRO-ENVIRONMENT ASSESSMENT WITH LATITUDE (IHEAL): A FRAMEWORK FOR CONCEPTUALIZING AND QUANTIFYING WATER USE SUSTAINABILITY IN IWRM

CARTER BORDEN[1], PETER GOODWIN[2] & DARREN SWANSON[3]

[1] Centered Consulting International, LLC, Boise, Idaho, USA,
carterbwater@gmail.com
[1,2] University of Idaho, Boise, USA,
pgoodwin@uidaho.edu
[3] Novel Futures Corporation and Associate-International Institute for Sustainable Development, Winnipeg, Canada,
dswanson@novelfutures.com

ABSTRACT

As the anthropogenic footprint increases on Earth, the wise use, maintenance, and protection of freshwater resources is key for sustainable development and integrated water resource management (IWRM). Methodologies supporting IWRM implementation have largely focused on the overall process, paying limited attention to evaluation methods of ecologic, economic, and social conditions. To assist in assessing water resource sustainability, the Integrated Hydro-Environment Assessment with Latitude (IHEAL) has been developed. IHEAL merges the driver-pressure-state-impact-response (DPSIR) framework used by the United Nations Global Environment Outlook, the ecosystem services and human wellbeing framework used by the Millennium Ecosystem Assessment, and sustainability criteria for water resource systems to better understand spatiotemporal interactions between hydrologic, socio-economic, and ecologic systems and evaluate impacts of disturbances on ecological goods and services (EGS) and human well-being. IHEAL comprises a Conceptual Template (IHEAL-CT), for assessing basin conditions and guiding indicator selection, and an Assessment Interface (IHEAL-AI) for organizing, processing, and assessing analytical results. IHEAL-CT connects water use directly, or through EGS, to constituents of human well-being. Disturbance Templates for eight pressure types (e.g. land use change, climate change, population growth) are provided to guide users regarding potential changes to landscape elements in the hydrological cycle, impacts to EGS, and societal implications to human well-being. IHEAL-AI organizes the output data from hydrologic, ecologic, economic, and social analyses with respect to time and space, computing the reliability, resilience, and vulnerability of the sustainability indicators for various water use scenarios. Results are presented as a time series of sustainability indicators and a star plot for comparison of management alternatives. IHEAL-CT was applied to the Lemhi River Basin, Idaho. IHEAL supports the IWRM process by providing a structured means to frame and analyze water related issues and select appropriate indicators to assess the contribution of water programs and policies to sustainable development in river basins.

Keywords: Integrated water resources management; conceptual model; sustainability indicators; ecosystem goods and services.

1 INTRODUCTION

The sustainable management of water resources is critical to the long-term viability of the ecologic, economic, and social systems in a basin on which people rely (GWP, 2004). Efforts to promote sustainable and responsible use of water have given rise to integrated water resource management (IWRM) (GWP, 2004; GWP, 2008). IWRM involves understanding the current hydrologic conditions and water resource issues, identifying and assessing limiting factors, developing and implementing solutions, and monitoring for success. Supporting the implementation of IWRM is a broad base of literature covering general concepts, philosophies, methodologies, guidance, and applications. The IWRM methodology and guidance literature has largely focused on the overall process: creating participatory organizations, building institutional capacity, financing programs, developing legal frameworks, outlining components of a plan, and identifying management instruments (GWP, 2004; 2008; UNESCO, 2009a; 2009b). While a significant aspect of IWRM is participatory and management oriented, analytical tools can assist water managers and participants in assessing the current situation as well as developing solutions to address and mitigate identified limitations.

Water management has traditionally focused on the distribution of water given the available supply and demand of water within a basin (ASCE, 1998). Yet, by IWRM principles, assessment of water management decisions needs to also evaluate how water distribution affects the sustainability of the ecological, economic, and social systems within a basin (GWP, 2004; 2008). By ‘sustainability’ or ‘sustainable development’ we are referring to the definition provided by the Brundtland Commission as ‘development that meets the needs of the present without compromising the ability of future generations to meet their needs (WCED, 1987) and as implemented through the 2030 Agenda for Sustainable Development (UN, 2015). To date, the information necessary to make effective management decisions with respect to the sustainability of ecological, economic, and social systems has been limited by its complexity and fragmentation. In addition, the general lack of knowledge regarding the holistic assessment of sustainable water resources can result in less than optimal management strategies. Absent are the methodologies and frameworks necessary to make effective, efficient, and timely decisions and support the IWRM process. To assist in illuminating the connectivity between the drivers/pressures of change and the impact on the ecological, economic, and social systems, the Integrated Hydro-Environment Assessment with Latitude (IHEAL) was developed (Borden, 2014). IHEAL supports the IWRM process by providing a structured and transparent means to understand how water related issues influence these systems, guiding the selection of discipline specific analytical techniques, and assessing the sustainability of the systems' analytical results. IHEAL is intended to address two audiences: 1) non-scientific participants (decision makers, water user associations, non-technical stakeholders; and 2) technical participants (scientist and engineers). Note, this document provides a high-level overview of IHEAL. A more complete description of the fundamental logic, methodology, and case study description can be found in Borden (2014).

2 INTEGRATED HYDRO-ENVIRONMENT ASSESSMENT TOOL WITH LATITUDE (IHEAL)

IHEAL has been developed to evaluate the sustainability of water resources in river basins with respect to current and future ecologic, economic, and social systems conditions. IHEAL's analytical and process framework provides a systematic foundation for understanding changes in sustainability due to natural and/or anthropogenic disturbances altering the hydrologic system. IHEAL is the marriage of three analytical foundations: i) the DPSIR framework used by the UN's Global Environment Outlook (UNEP, 2007; Pintér et al., 2008) to help users identify cause-effect relationships; ii) the Millennium Ecosystem Assessment framework (MA, 2003) for describing linkages between changes in the state of water resources and ecological systems, the services they provide, and links to human well-being; and iii) the water resource systems sustainability criteria which encompass aspects of resilience, reliability, and vulnerability as defined by the American Society for Civil Engineers (ASCE, 1998). Additionally, IHEAL is organized to help facilitate multi-stakeholder dialogue and partnerships among policy-makers, analysts, and interested stakeholders; an important principle set forth in the 2030 Agenda for Sustainable Development (UN, 2015). Together these frameworks provide users a straightforward method for identifying the drivers of change, the associated change in the state, and the impacts on the hydrologic systems which influences the delivery of ecological goods and services (EGS) and affect human well-being. The framework is intended to support analysis by experts as well as in facilitated participatory settings for planning and adaptation within a basin; bridging the perspectives of the analyst with the needs of the policy-maker and interested stakeholders.

For incorporating the IHEAL analysis into IWRM, Giupponi et al. (2006) identified five steps: problem framing, indicators and measures, conceptual frameworks, analysis, and assessment (Figure 1). IHEAL supports this process using the Conceptual Template (IHEAL-CT) to frame water resources issues with respect to sustainability and identify relevant indicators, and using the Assessment Interface (IHEAL-AI) to organize, process, and assess results from the hydrologic, ecologic, economic, and social systems analyses. More specifically, IHEAL-CT is a screening tool for identifying the relevant uses of water throughout a basin and how these uses influence sustainability. In IHEAL, water use includes both direct and indirect usage through EGS provided by hydrologic landscape elements (e.g. rivers, groundwater, wetlands). Within the IHEAL-CT, water use is represented as provisioning EGS (direct consumption, production, navigation, food, fiber,), regulating EGS (water regulation, erosion control, water purification, storm protection), and cultural EGS (spiritual, educational, aesthetic, social relations, cultural, recreation/ecotourism). Once baseline conditions have been screened, Disturbance Templates qualitatively predict how disruptions to the hydrologic system impacts hydrologic landscape elements, direct and indirect water use, and human well-being. This screening provides users with a holistic overview of water use and potential impacts to sustainability in a basin given current condition and future scenarios. Finally, based on water use and predicted impacts, relevant indicators are identified which can help establish monitoring systems and select analytical methods for the hydrologic, ecological, economic, and social systems.

IHEAL-AI quantitatively assesses the ecological, economic, and social systems related to the current water resources conditions in a river basin (including the magnitude of water resources issues) and tests potential scenarios with respect to the ASCE's Sustainability Criteria for resilience, reliability, and vulnerability, and the results are expressed as Sustainability Indicators (refer to Section 2.2).

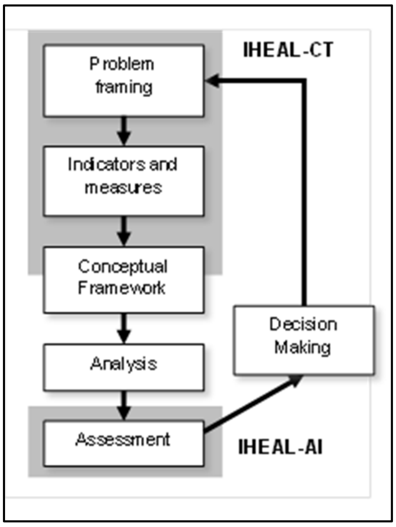

Figure 1. Steps to incorporate analytics into IWRM (modified from Giupponi et al., 2006). The grey boxes represent the steps that IHEAL supports.

2.1 IHEAL-CT process and outcomes

The general procedure for applying IHEAL-CT involves delineating the basin into sections, developing baseline conditions of water use for each section, creating scenarios that depict impacts from drivers and pressures, and post-processing the analysis to cull irrelevant information and consolidate important factors. The specific process, as depicted in Figure 2, involves:

A. Basin Delineation into sections representing distinct hydrologic landscape elements (e.g. lakes, river reaches, wetlands) and where the significant disturbances to the hydrologic regime are likely to occur (e.g. introduction of a reservoir, increased withdrawals from a river to accommodate greater irrigation requirements).

B. Screen Sections to identify water uses and associated constituents of human well-being for each hydrologic landscape element. IHEAL-CT includes a matrix to guide this process. Within each section, users select from 8 possible hydrologic landscape elements, each with up to 24 EGS, as outlined in the MA (2003), and their relevant constituents of human well-being. Providing guidance to the user, the matrix limits selection to only EGS and constituents of human well-being relevant to a landscape element being considered. Once users select relevant hydrologic landscape elements, EGS, and constituents of human well-being, the unselected options are hidden thus highlighting only relevant water use in the basin. The results are 1) outline of the hydrologic landscape elements per section throughout the basin and 2) a baseline understanding of where and how water is used and its influence on human well-being.

C. Apply Disturbance Templates to the baseline results to predict changes associated with drivers and pressures acting on the hydrologic system. Disturbance Templates have been developed to represent changes in supply, demand, land use, and climate as well as the introduction of water infrastructure or a change in its operation. Given the disturbance type, these templates predict alteration in the basin hydrology, impacts to hydrologic landscape elements, and delivery of EGS. The Disturbance Templates are applied to the hydrologic landscape elements and they include two types: active and altered disturbance. Active disturbances represent landscape elements where the pressure is being directly applied and altered disturbances represent landscape elements that are being impacted, but are spatially removed from the pressure. For example, a river reach experiencing increased withdrawals to satisfy population growth is classified as “active”. If the water satisfying the population growth is supplied by an upstream reservoir. New operations in the reservoir and flow in the intervening river system would alter hydrologic regime in these landscape elements and thus be classified as “altered”. When several different disturbances are evaluated, relevant Disturbance Templates are applied to each disturbance separately as a “Scenario” and the results are aggregated in the Reporting Score Card.

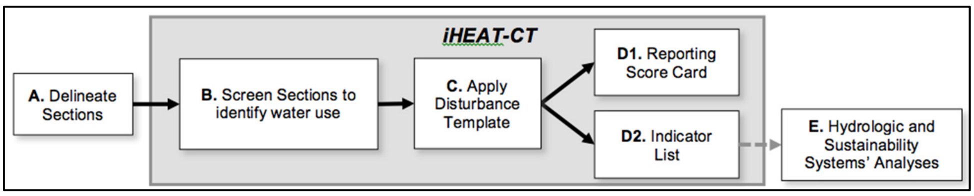

Figure 2. Processing steps in the IHEAL-CT.

Once these steps are completed, IHEAL-CT generates:

D1 Reporting Score Card that identifies active and altered landscape elements and, in each landscape element throughout the basin, qualitatively predicts trends in water use (EGS) as well as constituents of human well-being. Multiple scenarios can be plotted to show the impacts from multiple disturbances.

D2 Indicator List of relevant hydrologic, ecologic, economic, and social indicators to guide monitoring programs and selection of analytical methods supporting the sustainability assessment in IHEAL-AI. Indicators are drawn from over 550 water related indicators from 11 water resource indexes and are linked to the UN Sustainability Development Goals.

IHEAL-CT has been developed in MS EXCEL and contains macros to consolidate the information into the Reporting Score Card and generate the Indicator List. The summary output can be translated into conceptual models of the river basin that clearly delineates connections between the physical landscape features, the stressors and factors important to the environment and communities. These conceptual models are developed in collaboration with stakeholders and can be used to prioritize quantitative models and studies.

2.2 IHEAL-AI process and outcomes

Using hydrologic, social, economic, and ecological analytical results, IHEAL-AI quantitatively assesses the sustainability of current and proposed water resources conditions in a river basin. The process by which IHEAL-AI performs the assessment involves converting analytical output to sustainability indicators, aggregating these indicators using a decision tree, and reporting the results. The specific process, as depicted in Figure 3, involves:

E Hydrologic, Ecologic, Economic, and Social Systems' Analyses. Using discipline specific methods, analytical results of the current water resources conditions in a river basin (including the magnitude of the problem) and tests potential scenarios. This step is outside of the IHEAL-AI framework, but the results inform the IHEAL-AI interface.

F Sustainability Indicators (SI) are computed from the hydrologic, ecologic, economic, and social systems' analytical results. SIs are a function of a system's resilience, reliability, and vulnerability of an indicator (ASCE 1998). Resilience is a measure of a system's ability to withstand and recover from changes from drivers or pressures. Reliability is defined as the probability that an indicator is within an acceptable range during the time period considered. Vulnerability is the extent to which change from a driver or pressure may damage or harm a system and reflects on a system's sensitivity to perturbations and ability to adapt to new conditions. In other words, a system's vulnerability is the evidence of the buffering capacity to adjust to perturbations or susceptibility to tipping points or thresholds of harmful change. In general, with greater reliability and resilience and lower vulnerability, a system becomes increasingly sustainable. The computations for these terms are presented in ASCE (1998).

Additionally, show-stopper (SS) flags highlight when systems are critically limited by a parameter or condition based on expert knowledge in a discipline. For example, 40ºC is lethal for many fish species, irrespective of how suitable the water depth or velocity conditions are in the river system. If water depth, velocity, and temperature are combined to evaluate fish habitat quality in a river reach, the fish habitat SI may appear acceptable because water depth and velocity are favorable despite the water temperature making the reach inhospitable. In this situation, fish habitat would be tagged with a SS flag to identify the limitation.

Much like the sections and hydrological landscape elements identified by the IHEAL-CT, the SI and SS flags are calculated at user-defined locations throughout the basin. The types and spatio-temporal distribution of SI and SS flags are a function of the ecological, economic, and social systems' analyses. The Sustainability Indicator Module in IHEAL-AI contains algorithms for computing the SI and identifying SS flags.

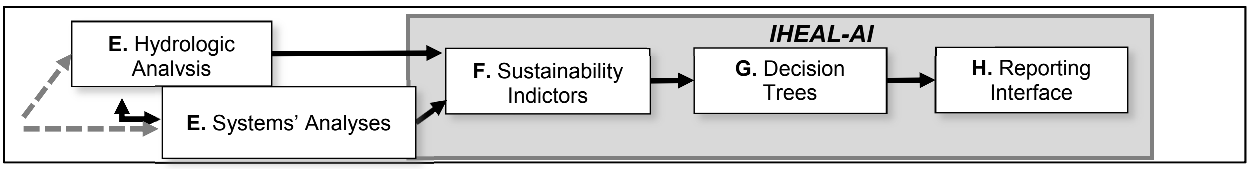

Figure 3. Processing steps in the IHEAL-AI.

G Decision Trees aggregate disparate and spatially distinct SIs into the Hydrologic, Ecologic, Economic, and Social Sustainability Indexes used to evaluate water resource sustainability. IHEAL-AI decision trees are defined in 4 levels that start with local characteristics (termed Indicators) and are up-scaled at several levels to represent the entire basin. The Indicator Level combines a single or several SIs from output data to form a local SI that represents a zone, site, or reach. For example, SI values of stream velocity, water depth, and temperature are combined to compute SI values of spawning, rearing, migration, and adult habitats for salmon. The Component Level combines the Indicator SIs into a single value representing zones, sites, or reaches. For example, the Component Level combines the Indictor SI values of spawning, rearing, migration, and adult salmon habitats to a single SI representing general habitat quality for the reach. The Theme Level aggregates spatially distinct Component SI values from zones, sites, or reaches into a single SI value for the basin. In our example, the Component Level SI values for salmon habitat from all the reaches would be combined to represent the salmon habitat quality throughout the river system. Finally, the Index Level combines the Theme SI values of different basin-wide Themes. In this example, the Theme SI for salmon habitat quality and the Theme SI for another aquatic species such as bull trout are aggregated into the Ecological Sustainability Index value representing all the species of concern in the basin.

The Decision Tree is also applied to the SS flags, but only at the Theme Level where spatially disparate sites or zones are aggregated. At the Theme Level, the number of sites or zones that have a “Fail” status are compared against an “acceptable” criteria to determine if the system as a whole is impaired. For example, if 20% of the reaches in a basin have SS flags and impairments is considered 30% of reaches having SS flags, the SS flag assessment for that system would be “Pass”. The SS flag designation in the Theme Layer is carried through to the Index Level. A user is able to disaggregate these SS or indices to discern the spatial coverage.

H Reporting Interface displays the resulting Hydrologic, Ecologic, Economic, and Social Sustainability Indexes as well as the SS flags. For the overall comparison between scenarios, the Reporting Interface uses a star plot of the Index values and a table of SS flags (Figure 6). To review the impacts of water availability, an annual time series of the Hydrologic, Ecologic, Economic, and Social Sustainability Indexes and percentage normal precipitation are plotted for each scenario. Below that is a corresponding table of annual SS flags for the ecological, economic, and social systems.

3 ASSESSING WATER RESOURCE SUSTAINAIBITY IN THE LEMHI RIVER BASIN

IHEAL was applied to the Lemhi River Basin (LRB), a rural basin in northeast Idaho, USA, to assess the water resources sustainability associated with a change in irrigation practices. The following provides a brief description of the application with a full description by Borden (2014).

3.1 Lemhi River Basin background

The basin covers 3,149 km^2 and is flanked by the Bitterroot Range and Beaverhead Mountains to the east and the Lemhi Range to the west. Elevations range from an average of 1,585 m and 2,745 m amsl along the valley floor to the ridges, respectively. The Lemhi River flows 97 km to the northwest where, at the confluence, the minimum, average, and maximum daily average discharge of the Lemhi River is 0.02 m^3/s, 7.11 m^3/s, and 73.91 m^3/s, respectively. The LRB has cold, wet winters and warm, dry summers. Annual precipitation ranges from 230 mm on the valley floor to 1016 mm in the mountains, with 70% falling during the winter months (November – April).

Stream flow is important for agricultural irrigation and the fishery. Economically, the LRB community is heavily tied to the land. Cattle ranchers, the primary economic sector, have traditionally flood irrigated alfalfa hay crops and pastures to support cattle production, requiring large quantities of water to be diverted from the river system. Irrigation waters are largely taken from surface water sources, thus dewatering the stream network. Though instream flow is decreased when applying flood irrigation early in the irrigation season, a portion of the diverted water recharges the shallow groundwater system, enhancing baseflow later in the summer. Ecologically, the basin’s river system maintains resident and migratory fish populations by providing spawning and rearing habitat for anadromous steelhead and Chinook salmon, as well as habitat for the resident bull trout. Reducing stream flows stresses the aquatic ecosystems by fragmenting habitat, creating fish migration barriers and inducing warmer water temperatures. Steelhead, Chinook salmon, and bull trout are listed as endangered species under the U.S. Endangered Species Act.

The competing demands between agricultural irrigation requirements and adequate stream flow to support fish habitat creates a contentious setting for water use in the LRB. To ease the competition for water, conversion from flood irrigation to more efficient sprinkler irrigation is being promoted to leave more flow in the river system. Due to its efficiency, sprinkler irrigation reduces recharge to the shallow aquifer system, reducing baseflow in the river later in the summer. Thus, questions arise as to the water resource sustainability associated with the conversion to sprinkler in the basin. Will the reduction in flood irrigation diminish shallow groundwater and reduce instream flows later in the season? Will the increase in the sprinkler use benefit or impair the ranching economy? How will this conversion impact the aquatic habitats supporting the steelhead, Chinook salmon, and bull trout populations and what will be the effect on the recovery of the species? What are the social impacts of converting to sprinklers? IHEAL was applied to the LRB to demonstrate its applicability in framing and analyzing these questions (Borden, 2014).

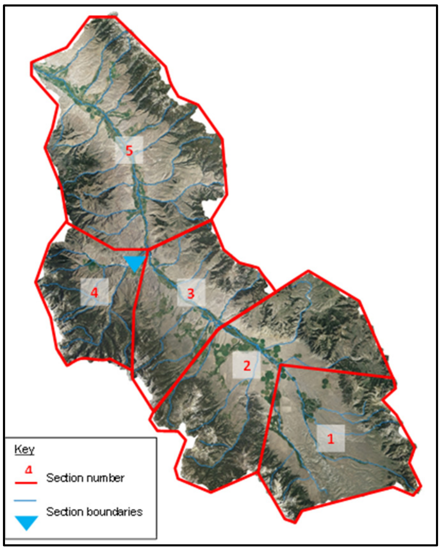

Figure 4. Sectional delineation of the LRB. Flow in the basin is from southeast to northwest (Borden, 2014).

3.2 Water resource use screening of the LRB

Four scenarios and the baseline conditions (B) were evaluated using IHEAL-CT: S1 - change in irrigation in Section 2 with short-term minimum conversion, S2 - change in irrigation in Section 2 with long-term significant conversion, and S3 – construction of the proposed Hayden Creek Reservoir in Section 4. For Scenarios 1-2, less water is required for sprinkler irrigation resulting in decreased diversion rates, more water in the Lemhi River, and a less disturbed flow regime. This more natural flow regime has higher peak stream flows and a more varied hydrograph that is responsive to snowmelt throughout the river system. However, the conversion may decrease the late season stream flows as the shallow groundwater is not supplemented by flood irrigation infiltration during the spring and early summer resulting in less water for both fish and ranchers later in the summer. This hydrologic trend will become more pronounced as conversion to sprinkler irrigation increases from S1 to S2.

Construction of the Hayden Creek Reservoir (Scenario 3) will inundate part of the existing river system and floodplain habitats to create a lake/reservoir habitat. Reservoir storage and releases will decrease peak flows and augment lower flows thus reducing flow variability in the lower basin Section 5. Water temperatures will lower in Section 5 as the reservoir is designed for bottom release. However, if the cold-water pool is exhausted in dry years, it is possible that released water temperature could return or be elevated above pre-reservoir conditions. Reservoir releases will be required to maintain sufficient flows at the L-6 diversion to ensure it does not become a migration barrier. Hydrologically, the reservoir will have no impact on Sections 1-3.

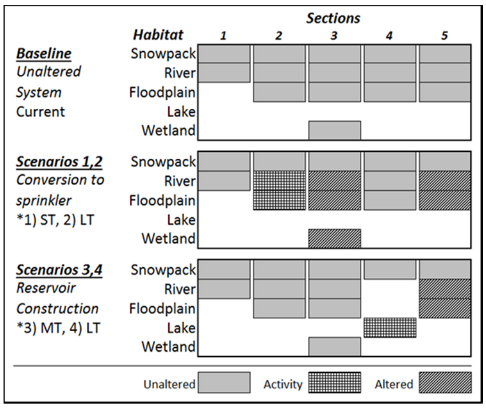

Figure 5. Mapping of hydrologic landscape element per basin sections for baseline conditions and 3 scenarios in the LRB case study (Borden, 2014).

For the screening, the LRB was delineated into five sections based on hydrologic characteristics and management alternatives (Figure 4). The freshwater habitats (Figure 5 Baseline), primary EGS and associated constituents of human well-being for each habitat (Table 1 "B") were identified within each section. Note that although Lake/Reservoir habitat is not currently present in the LRB, it has been included in the Baseline analysis as it was introduced in the S3 scenario. Based on the change in irrigation diversions in S1 and S2, Section 2 will be directly impacted and Sections 3 and 5 will be indirectly impacted due to a change in downstream flow (Figure 5). For the S3 scenarios, introduction of the reservoir will have direct impact in Section 4 and indirectly impact Section 5. This analysis provides users with a rapid overview of potential impacts throughout the basin given the location of the disturbance.

Applying the IHEAL-CT screening matrix, the Baseline freshwater habitats are mountain snowpack, riverine, floodplain, and wetland. EGS provided by these include provisioning (irrigation water), regulating (flood protection, water supply), and cultural (aesthetics, cultural) (Table 1). The associated constituents of human well-being include security (resilience to ecological stresses, access to EGS), basic needs (access to the resource for making a living), health (adequate food and nutrition), and good social relations (realization of aesthetic and recreational values). For Scenarios S1 and S2, the provisioning services of freshwater production in Section 2 will likely increase throughout most of the irrigation season with the exception of the late summer, when stream flow may drop below current levels (Table 1). Therefore, the provisioning services of freshwater production in Sections 3 and 5 will also drop for late summer. The increased high water lessens the chance of migration barriers being created in Section 5 and connections of tributaries to the mainstem in Section 2 during the early spring before snowmelt (an important time for steelhead migration). However, late summer low flow conditions may degrade valuable rearing habitat in the lower reaches of Section 2 and 3, thus impacting the supporting services associated with habitat and cultural opportunities associated with recreational fishing. Wetlands, partially recharged by subsurface irrigation return flow, will likely decrease in function with the increased use of sprinklers. Human well-being associated with the increased access to resources for a viable livelihood will go up in Section 2, but may have adverse effect on irrigators in Sections 3 and 5 later in the season.

Table 1. Examples of the EGS and constituents of human well-being trends in Sections 3 and 5 resulting from the IHEAL-CT screening of the LRB. “B” is Baseline and “S1”, “S2”, and “S3” are Scenarios 1, 2, and 3, respectively.

Habitat	EGS	EGS Trend* I	S1	S2	S3	Impacted Zones	Human Well-Being Trend* B	S1	S2	S3
***Section 3:* Riverine**		·	↕	[illegible]	**–**	**5,X**	**–**	↘	↘	**–**
Provisioning	Freshwater Production	·	↘		–	5,X	–	↘	↘	–
Cultural	Aesthetic, Recreation	·	↔	[illegible]	–	X	–	↔	↔	–
Supporting	Natural Cycles*, Habitat & Biodiversity	·	↕	[illegible]	–	5,X	–	↔	↔	–
Floodplain		·	↕	[illegible]	**–**	**5,X**	**–**	↗	↑	**–**
Provisioning	Freshwater Production	·	↗	[illegible]	–	5,X	–	↗	↑	–
Regulating	Water Regulation	·	↘		–	5,X	–	↔	↔	–
Cultural	Recreation	·	↔	[illegible]	–	X	–	↔	↔	–
Wetlands		·	**↘**	[illegible]	**–**	**5,X**	**–**	**↘**	↓	**–**
Regulating	Water Regulation, Storm Protection	·	↘	[illegible]	–	5,X	-	↘	↓	-
Cultural	Recreation	·	↘	[illegible]	–	X	-	↘	↓	-
***Section 5:* Riverine**		·	↕	[illegible]	↑	**X**	**–**	↔	↔	↑
Provisioning	Freshwater Production	·	↘		↑	X	–	↘	↘	↑
Cultural	Aesthetic, Recreation	·	↑	[illegible]	←	X	–	↔	↔	↔
Supporting	Natural Cycles*, Habitat & Biodiversity	·	↕	[illegible]	↑	1,2,3,4, X	–	↔	↔	↑
Floodplain		·	↕	[illegible]	↑	**X**	**–**	↗	↑	↑
Provisioning	Freshwater Production	·	↗	[illegible]	↑	X	–	↗	↑	↑
Regulating	Water Regulation	·	↔	[illegible]	←	X	–	–	–	↔
Cultural	Recreation	·	↔	[illegible]	↑	X	–	↔	↔	↑

* ↕ Positive and negative trends will occur, ↑ Definite positive trend, ↗ Weak positive trend, ↔ Either positive or negative trend could occur, ↘ Weak negative trend, ↓ Definite negative trend, − No change

The EGS lost in Section 4 due to the Hayden Creek Reservoir includes the provisioning services of the floodplain and natural riverine habitat and the migration barrier created by the structure. Section 5 will likely see an increase in provisioning services associated with freshwater production due to the water regulation associated with the reservoir in Section 4. In terms of human well-being, recreational benefits increase in Section 4 and expected increased reliability of water supply enhances livelihood in Section 5. However, with the loss of the floodplains available for irrigation in Section 4, the local ranchers have lost access to resources for a viable livelihood. Factoring in the cost of reservoir construction, the benefits associated with the increased access to resources for a viable livelihood in Section 5 are likely insignificant and, in fact, cost more when looking at area inundated and EGS lost.

Based on the screening of freshwater habitats and the relevant EGS highlighted, a recommended indicator list was generated for the ecological, economic, and social systems (Table 2). Pressures indicators identified are change in water demand for agriculture (hydrologic system) and change in production (economic system). State indicators for the hydrologic system center around water supplied to the irrigators (demand, supply, and deficit) and the ecological functions that are sustained by the flow regime in the river. For the proposed dam, state indicators also include water level and storage volume. Economic indicators include costs, and revenues of crop production and construction, operations, and maintenance costs for the proposed reservoir. Ecological state indicators are the bull trout and salmon aquatic habitat for the spawning, rearing, migration, and adult (bull trout only) life stages. Social state indicators include average annual income for the residents and the recreational use of the reservoir. Hydrologic impact indicators include total delivery, demand, deficit, and reliability of delivery and for S3, the reservoir average annual storage and likelihood of filling. For economics, the change in net revenue per acre for each irrigation method and section as well as the change in production were considered. Ecological impacts were measured by the change in habitat for both listed species and the social impact was the trend in household income and recreational access.

Table 2. Indicator list from the IHEAL-CT screening of the LRB scenarios. Italicized parameters were used in the IHEAL-AI assessment.

PSI	Hydrologic System	Ecologic System	Economic System	Social System
Pressure	•Change in water demand •Reservoir construction	•None	•Change from sprinkler to flood irrigation	•None
State	•Water flow in river system •Irrigation demands •Water delivery •Water deficit •Area irrigated •Consumptive use •Reservoir storage •Reservoir water levels	•Aquatic habitat quality for salmon: rearing, migration, spawning •Aquatic habitat quality for bull trout: rearing, migration, spawning •Minimum stream flow requirements	•Production from irrigation •Cost of production •Revenue generated by crops •Land under irrigation •Crops grown •Recreational dollars •Reservoir construction costs •Reservoir O & M	•Average household income •Days of recreational use of river system •Days of recreational use of reservoir
Impact	•Reliability of water supply •Average annual supply	•Change in salmon aquatic habitat •Change in bull trout aquatic habitat	•Trend in net revenues •Trend in land under production	•Trend in household income •Recreational use of reservoir

3.3 Water Resource Sustainability Assessment of the LRB

A preliminary hydro-economic modeling study was conducted to determine the optimal distribution of flood and sprinkler irrigation to produce the maximum economic benefit (Borden, 2014). Unlike screening of S2 and S3, this analysis looked at impacts throughout the LRB. Hydrologic, ecologic, economic, and social systems analyses were conducted on the Baseline Scenario and Optimized Irrigation Scenario conditions. These analytical results were synthesized using IHEAL-AI with impact indicators (Table 2) and evaluation methods described in Table 3.

Table 3. Summary of analytical methods used in LRB (Borden, 2014).

SC Discipline	Analytical Method	Analytical Output Evaluated	Processing Method
Hydrologic	Lemhi River Basin Model (LRBM): a water allocation model developed in MIKE BASIN (Borden, 2016) that accounts for daily catchment inflows; routing of water in the stream network; and diversion operation, consumption, and return flows for irrigation. Results include time series of any computational component (e.g. river flows, water delivery, and deficits for water users). The LRBM simulated flow on a daily time step over a 13-year period.	Reliability of water delivery	The LRB was divided into 5 sections, similar to sections in IHEAL-CT (Figure 4). For each section, the daily water deficit for all nodes representing flood irrigation and all nodes sprinkler irrigation was computed.
Ecologic	The USGS conducted 12 PHABSIM sites throughout the LRB. For each site, a discharge-weighted usable area (WUA) relationship was developed per species and life stage (Sutton & Morris, 2004, 2005, 2006)	WUA for steelhead: •rearing habitat, •spawning habitat	At each PHABSIM site, the daily discharge from the LRBM was applied to the discharge-WUA relationships from the PHABSIM studies. The result was a daily WUA for each PHABSIM site throughout the simulation period.
Economic	Cost-benefit analysis of hay and alfalfa production (Contor, 2008). Revenues linked to production based on water delivery through FAO33. Water delivery was taken from the LRBM output. Note, as the majority of the PHABSIM sites were in the upper basin, the results include this bias.	Net revenue Reliability of water delivery	The LRB was divided into 5 sections, similar to sections in IHEAL-CT (Figure 4). For each section, the daily water delivery for all nodes representing flood irrigation and all nodes sprinkler irrigation was computed. Per irrigation method per zone, calculated crop yield based on water delivery for each cutting. Based on crop yield, computed the economic production based on cost-benefit analysis.
Social	No correlation could be found between existing social indicators and discharge in the LRB.	None	None

The analytical results and assessment using IHEAL-AI for the Baseline Scenario and Optimized Irrigation Scenario are presented in Reporting Interface (Figure 6). The Radar Plot (top graph in the Reporting Interface) indicates that increasing sprinkler use to optimize economic output in the LRB will result in an *increase* in the Hydrology and Economic SI Indexes by 0.11 and 0.10, respectively, and a *decrease* in the Ecologic Index by 0.21. SS flags are green for all systems in both scenarios indicating that overall the systems do not exhibit critical conditions in most years.

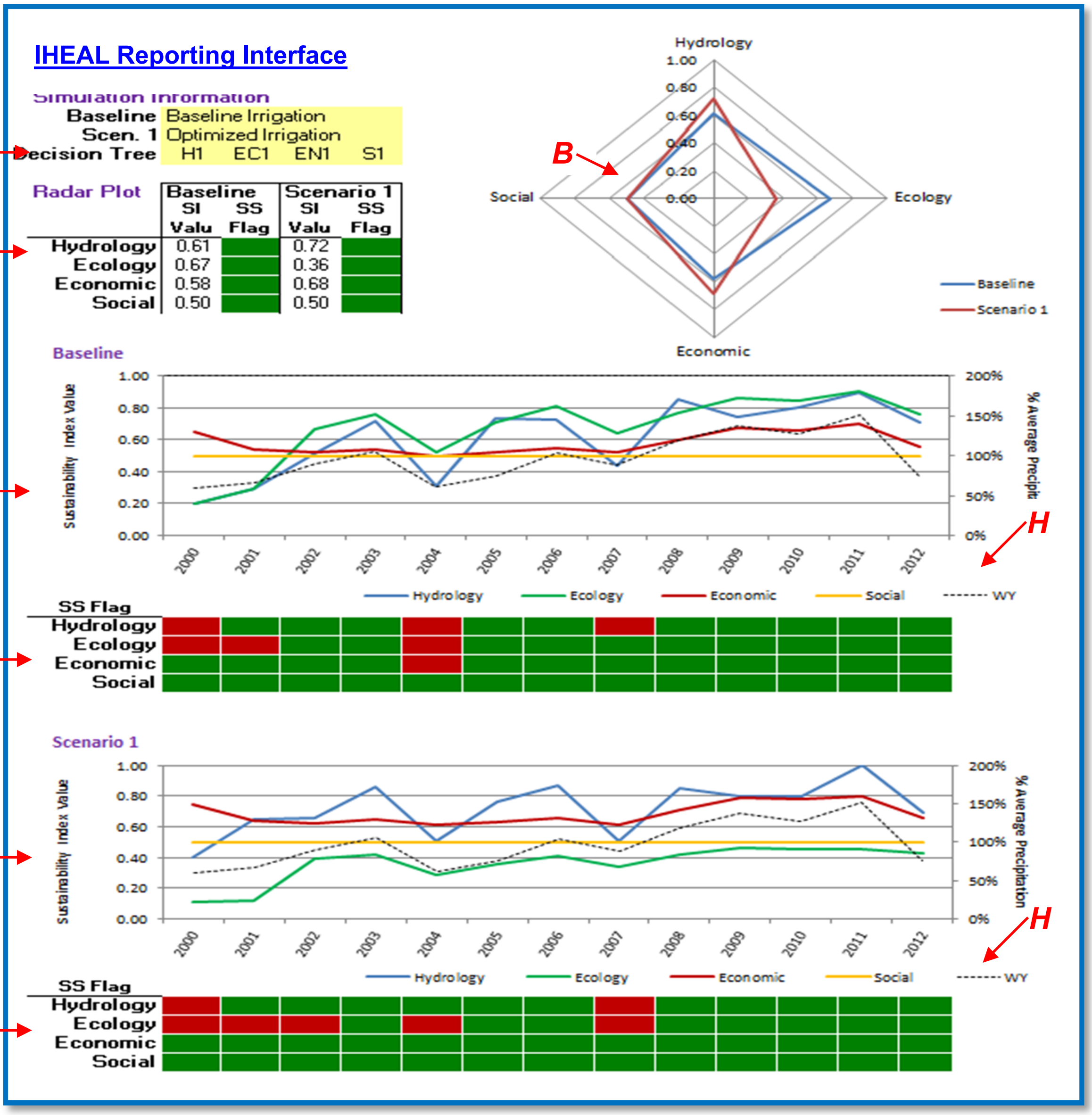

Figure 6. IHEAL-AI Reporting Interface assessing the sustainability of water resources for the Baseline Scenario and Optimized Irrigation Scenario (Scenario 1). The simulation information (*A*), radar plot (*B*) and accompanying data table (*C*) provide the overall system performance of the Hydrologic, Ecologic, Economic, and Social Sustainability Indexes and SS flags (green denotes passing, red denotes failing). In the lower half, the Baseline and Scenario 1 time series provide the annual Hydrologic, Ecologic, Economic, and Social Sustainability Indexes (*D,F*) and SS flags (*E,G*). The percentage of average precipitation (denoted “WY”) (*H*) enables users to compare the SI Indexes and SS flags with respect to water availability.

The Reporting Interface also reports the annual values of the Hydrology, Ecologic, Economic, and Social SI indexes and SS flags as well as the percentage of annual precipitation in the LRB (time series in Figure 6). The SI indexes for all systems show improved conditions with greater annual precipitation. That said, the Hydrology and Ecological SI indexes are more sensitive to annual precipitation while the Economic SI index is relative stable. Comparing the scenarios, the Ecological SI index showed a marked decrease in the sustainability of quality habitat. The Hydrology SS flags dropped from 3 to 2 and Economic SS flags from 1 to 0 reflecting fewer critical conditions in the reliability of water delivery and net revenue between the Baseline and Optimized Irrigation Scenarios. Conversely, Ecological SS flags increased from 3 to 5, which indicates that the critical conditions in the sustainability of habitat will increase with increased sprinkler conversion. The results presented in the Reporting Interface allow those concerned with water management in the LRB to holistically assess the water resources sustainability given a change in irrigation practice.

4 CONCLUSIONS

The Integrated Hydro-Environment Assessment with Latitude enables a conceptual framework to be developed identifying critical components and linkages within a river basin that can be influenced by management decisions. This framework facilitates analytical assessments of water resource sustainability and policy alternatives in a structured, reliable, and transparent manner. IHEAL merges the DPSIR and ecosystem services/human well-being frameworks, and sustainability criteria for water resource systems to enable users to better understand spatiotemporal interactions between hydrologic, socio-economic, and ecologic systems. IHEAL supports the IWRM process by providing a structured means to frame and analyze water related issues and select appropriate indicators to assess the sustainability of water programs and policies in river basins. IHEAL- CT (Conceptual Template) is used for appraising the situation and guiding indicator selection and IHEAL-AI (Assessment Interface) for organizing and processing analytical results. The Lemhi River Basin application demonstrates how the framework can be used to setup and assess water resource issues in basins.

REFERENCES

ASCE (1998). *Sustainability Criteria for Water Resource Systems.* Task Committee on Sustainability Criteria, Water Resources Planning and Management Division, ASCE and the Working Group of UNESCO/IHP IV Project M-4.3, D.P. Loucks, (committee chairman), Reston, VA: American Society of Civil Engineers, 253.

Borden, C. (2014). Flexible Framework for Assessing Water Resources Sustainability in River Basins, Dissertation *for Center of Ecohydraulics Research*. University of Idaho, Boise, Idaho, USA, 230.

Borden, C. (2016). *Lemhi River Basin Model Supporting Documentation,* Centered Consulting International Report prepared for the State of Idaho Office of Species Conservation, 88.

Brundtland Commission (1987). *Our Common Future,* Report of the World Commission on Environment and Development, 8. Oxford University Press: Oxford, New York.

Contor, B. (2008). Demand-PriceEffects.xls. Spreadsheet, Idaho Water Resources Research Institute (USA), Idaho.

Giupponi, C., Jakeman, A.J., Karssenberg, D. & Hare, M.P. (2006). *Sustainable Management of Water Resources: An Integrated Approach.* Edward Elgar Publishing, 384.

GWP (2004). *Global Water Partnership Strategy 2004-2008.* Global Water Partnership Report. Available at: http://www.gwp.org/About-GWP/Publications/Strategy-Documents/.

GWP (2008). WRM toolbox. Available at: http://www.gwp.org/en/ToolBox/ [Accessed June 2008].

MA (2003). *Ecosystems and Human Well-being: A Framework for Assessment*. Island Press, Washington, DC, 266.

Sutton, R. & Morris, C. (2004). *Flow Characterization Study Instream Flow Assessment Big Timber Creek, Idaho*. US Bureau of Reclamation Report, Boise, Idaho, June 2004, 119.

Sutton, R. & Morris, C. (2005). *Flow Characterization Study Instream Flow Assessment Big Eightmile Creek, Bohannon Creek, and Hayden Creek, Idaho*. US Bureau of Reclamation Report, Boise, Idaho, June 2005. 183.

Sutton, R. & Morris, C. (2006). *Flow Characterization Study Instream Flow Assessment Upper Lemhi River and Canyon Creek, Idaho.* US Bureau of Reclamation Report, Boise, Idaho, July 2006, 167.

UN (2015). Transforming our world: the 2030 Agenda for Sustainable Development. United Nations. Available at: https://sustainabledevelopment.un.org/post2015/transformingourworld.

UNEP (2007). *Global Environment Outlook (GEO) 4 Environment for Development*. United Nations Environmental Programme (UNEP), Malta Program Press Company Ltd, Valletta, Malta 2007. 572.

UNESCO (2009a). *IWRM Guidelines at River Basin Level. Part 1: Principles*. UNESCO-International Hydrological Programme (IHP), World Water Assessment Programme (WWAP), Network of Asian River Basin Organizations (NARBO), 33.

UNESCO (2009b). *IWRM Guidelines at River Basin Level. Part 2-1: The Guidelines for IWRM Coordination*. UNESCO-International Hydrological Programme (IHP), World Water Assessment Programme (WWAP), Network of Asian River Basin Organizations (NARBO), 176.

WCED (World Commission on Environment and Development). (1987). *Our Common Future*, (“The Brundtland Report”), Oxford University Press, 383.

WATER BALANCE STUDY FOR A WATERSHED IN GODAVARI RIVER BASIN USING SWAT MODEL

AMEY BAGUL [(1)], VIJAYA S. PRADHAN [(2)] & PRACHI BAGUL [(3)]

[(1)]Research scholar, Civil Engineering Department, Jawaharlal Nehru Engineering College, Aurangabad, Maharashtra state, India
ameybagul@ymail.com
[(2)]Faculty, Civil Engineering Department, Jawaharlal Nehru Engineering College, Aurangabad, Maharashtra state, India
[(3)]Research scholar, Civil Engineering Department, PES College, Aurangabad, Maharashtra state, India
bprachi501@gmail.com

ABSTRACT

Increased human activity, growing demands and limitations in water supply have made it absolutely necessary to pay greater and closer attention to the management of water resources. Water engineers and scientists are confronted with challenges of sustainable development and have the responsibility to meet these challenges, both at the macro-level of overall demand and supply and at the micro-level, by designing, operating and maintaining water resources with the objective of local sustainability. The present study aims to study the water balance of a watershed located in Khuldabad, Aurangabad, and Maharashtra, India. Digital Elevation Model (DEM), boundary map, land use map, soil map and weather data of the study area are the inputs to QSWAT. QGIS 2.6.1 Brighton was used to developed DEM and thematic maps, such as soil map, Land use Land Cover map of study area. The analysis has been carried out by using QSWAT1.2 for time period of 33 year from 1979 to 2012. Daily data of precipitation, temperature, radiation, wind velocity and solar has been processed on monthly basis. The delineated watershed is divided into 14 sub basins. SWAT output gives the simulated result for hydrological parameter in graphical and numerical format. The SWAT output can be effectively visualized by SWAT Check 1.2. Hydrological components of sub basins are obtained on monthly basis using SWAT Check. The output of one sub basin is presented graphically and statistically. The total area under the 14 sub basins is 19.90 km^2. The average monthly basin values of rainfall, surface runoff, water yield, sediment yield, evapotranspiration and potential evapotranspiration are obtained for the basin using SWAT Check.

Keywords: Watershed; watershed development; Khuldabad; quantum geographic information system (QGIS); soil water assessment tool (SWAT).

1. INTRODUCTION

Water is a very essential resource for mankind. The availability of pure water is less in the region and one of the factors is dependent on rainfall, which is unevenly distributed. In the semi-arid region, rainfall is less and unpredictable, hence the demands of water for drinking and irrigation become critical. For any watershed development work, it is necessary to understand the relationship between the physical parameters of watershed and hydrological components and hence, the water balance approach is widely used for watershed management practices. SWAT is a basin-scale, continuous-time model that operates on a daily time step and is designed to predict the impact of management on water. The model is physically based, computationally efficient, and capable of continuous simulation over long time periods. In SWAT, a watershed is divided into multiple sub-watersheds, which are then further subdivided into hydrologic response units (HRUs) that consist of homogeneous land use, management, and soil characteristics. The HRUs represent percentages of the sub-watershed area and are not identified spatially within a SWAT simulation. Results from field-based HRU delineation may be quite different from the standard approach due to choosing a majority soil type in each farm field. This approach is flexible such that any land use and soil data prepared for SWAT can be used and any shape file boundary can divide HRUs.

2. LITERATURE REVIEW

Unde and Telore (2012) have mentioned that water is essential for the existence of the biotic world including human beings. Watershed is a hydrologic unit and is often used for the management and planning of natural resources. Watershed development is a need of hour for sustainable water resource development and management of rain shadow region. Mangrule and Kahalekar (2003) observed that recent technologies such as remote sensing and GIS support us to give a quicker and cost-effective analysis of various applications with accuracy for planning. It also gives a better perspective for understanding the problems and therefore helps Planners evolve a better solution for sustainable development. From the final output of these themes generate, Recharge wells, percolation tank and check dams are recommended for the study area, mainly to control sedimentation from the catchments. Jasorita et al. (2009) used the water balance assessment

 / ISSN 1562-6865 (Online) - ISSN 1063-7710 (Print)

approach to estimate the moisture deficit and moisture surplus for an entire watershed using Thornthwaite-Mather (TM) model along with remote sensing and GIS for the study. Jain et al (2011) applied SCS approach to each cell in a gridded rainfall map yielded a grid of expected runoff. Evapotranspiration has been estimated using an energy balance model. An advanced and very high resolution radiometer has been used for preparation of various maps required for runoff and ET analysis. Sathian (2009) used SWAT model to analyse and quantify the water balance of a river basin. The predicted water balance components were also been compared with their measured or alternately computed counterparts.

SWAT is a physically based and requires specific information about the meteorological parameters, soil type, topography, vegetation, and land use for a watershed. Physical processes associated with water movement can be studied. It is a hybrid model spatially based on hydrological response units (HRU) that includes both conceptual and physical approaches. A central part of SWAT is the general water balance equation. Surface runoff is determined by the SCS Curve Number approach. The simulated results are visualized statically, graphically and numerically in QSWAT output.

2.1 Object of study

To generate SWAT analysis over selected study area located in Khuldabad district. For SWAT analysis, the methodology is divided in to four stages. To execute objective above, the collection of satellite data and survey of India topographical maps, collection of weather data and other collateral data covering the study area is carried out. Also, the land use data and soil data of the study is collected.

3 METHODOLOGY

3.1 The study area

The study area is located in Khuldabad, Aurangabad, Maharashtra between the latitudes of 19° 57' 00" - 20° 13’48” North and longitudes 74° 58’12.00’’ - 75° 31’48” East. It is covered by survey of India toposheet no. (46 p/4, 46 p/8, and 47 m/1, 47 m/5) with scale of 1:50,000. The study area has an average elevation of 729 m MSL with gently sloping rolling lands. The area is having the average annual rainfall *i.e.* less than 625 mm. Location of study area is shown in Figure 1.

DEM of study area, boundary of study area, land use map, soil map, and weather data of the study area are the input data require to run the QSWAT. To develop the boundary map of study area, top sheets of scale 1:50,000 were collected from survey of India department and georeferenced in QGIS environment. Then, digitization of boundary map was done in QGIS.

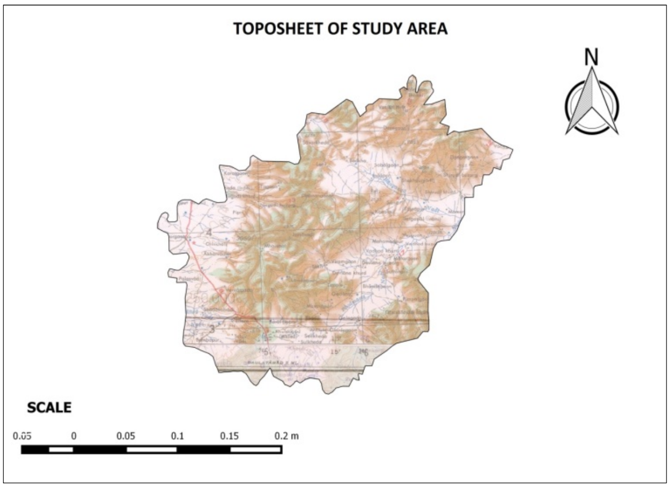

Figure 1. Toposheet of study area.

3.2 Digital elevation model

The DEM of study area was downloaded from Shutter RADAR Topography Mission (SRTM) of 90 m by 90 m resolution. After that, by using QGIS vector tool, the boundary was created and DEM of area was extracted. DEM of the study area is shown in Figure 2.

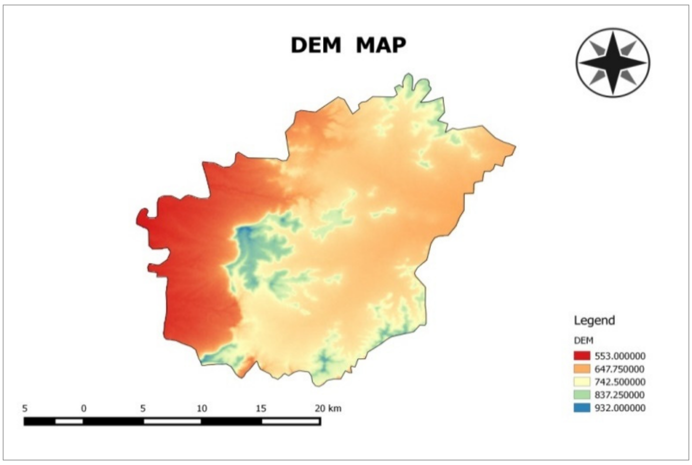

Figure 2. DEM of study area.

After this, DEM of the study area was processed to develop slope map and flow direction for watershed delineation.

3.3 Land use land covers map

By adding web map service (WMS), layer is provided by http://bhuvan.nrsc.gov.in in QGIS. The land use map of Khuldabad area was digitized and rasterized in QGIS. LULC map is shown in Figure 3.

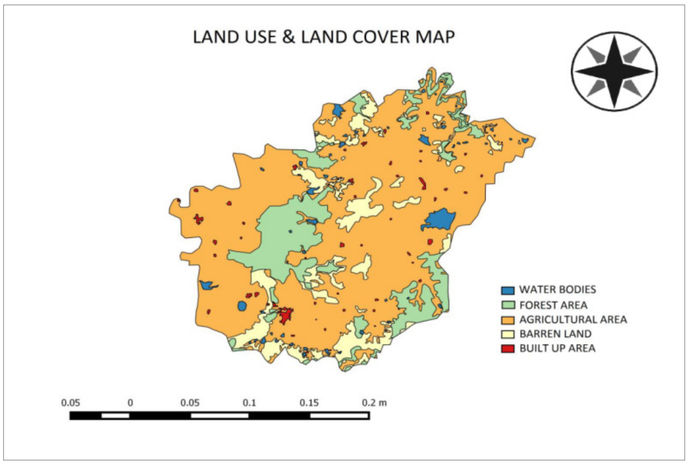

Figure 3. LULC map.

3.4 Soil map

Soil map of Maharashtra developed by NBSS, Nagpur was geo-referenced and used for digitized and rasterize soil map. The soil map for the area is shown in Figure 4.

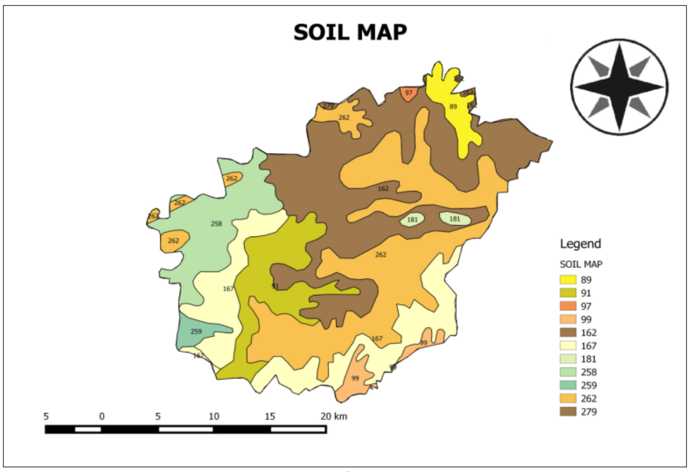

Figure 4. Soil map.

QSWAT Ref 2012.mdb file SWAT Code was edited by coping the usersoil.xls in excel. 33 years of daily weather data such as precipitation (mm), temperature (°C), wind velocity (m/s) and solar radiation (MJ/m²) for study area was downloaded from http://globalweather.tamu.edu site. The calculations of TMPMX, TMPMN, TMPSTDMX, SOLARAV, WNDAV have been carried out with the help of Microsoft Excel. The precipitation related parameters and dew point were computed using customized software called pcpSTAT.exe and dewpoint.exe. Then, all the results are copied to the WGEN_WatershedGan.xls file.
In SWAT model, the delineation watershed gets divided into multiple sub-basins, then for each sub-basin the water balance components were calculated.

4 RESULTS

After successful running SWAT, the simulated result is obtained. The results can be visualized on the basis of total, annually daily, monthly and yearly. It gives all type of hydrological components for each sub-basin.

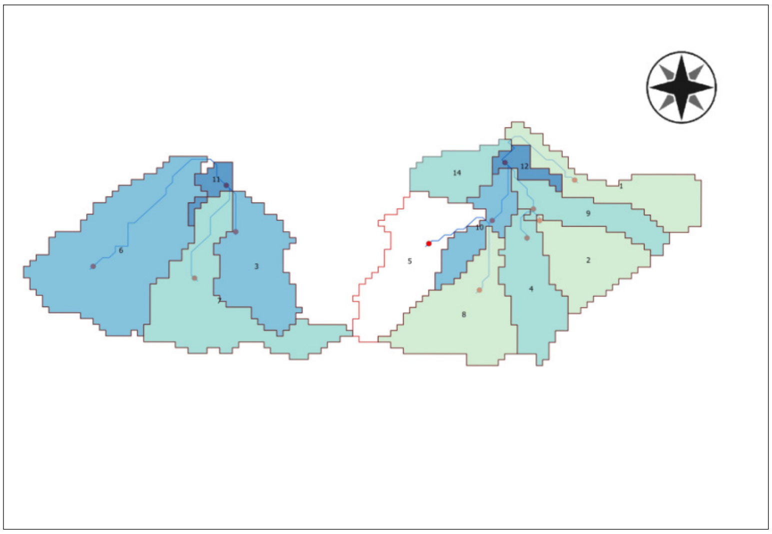

Figure 5. Obtained Sub-basins.

In the present study, the 14 sub-basins are obtained. The total watershed area under sub-basins is 19.90 km². The output can be visualized graphically, statically and numerically.

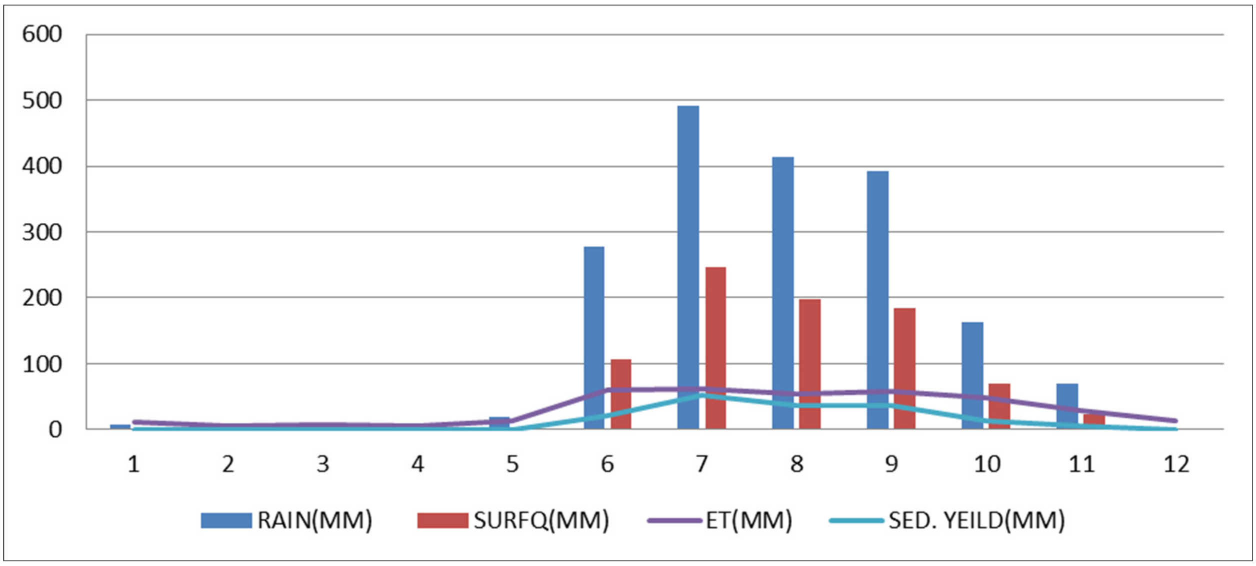

Graph 1. Graph of sub-basin for different parameter.

Potential evapotranspiration, actual precipitation, surface runoff, water yield, average amount of precipitation, groundwater contribution of sub-basins on monthly basis are visualized as follow in Figure 6.

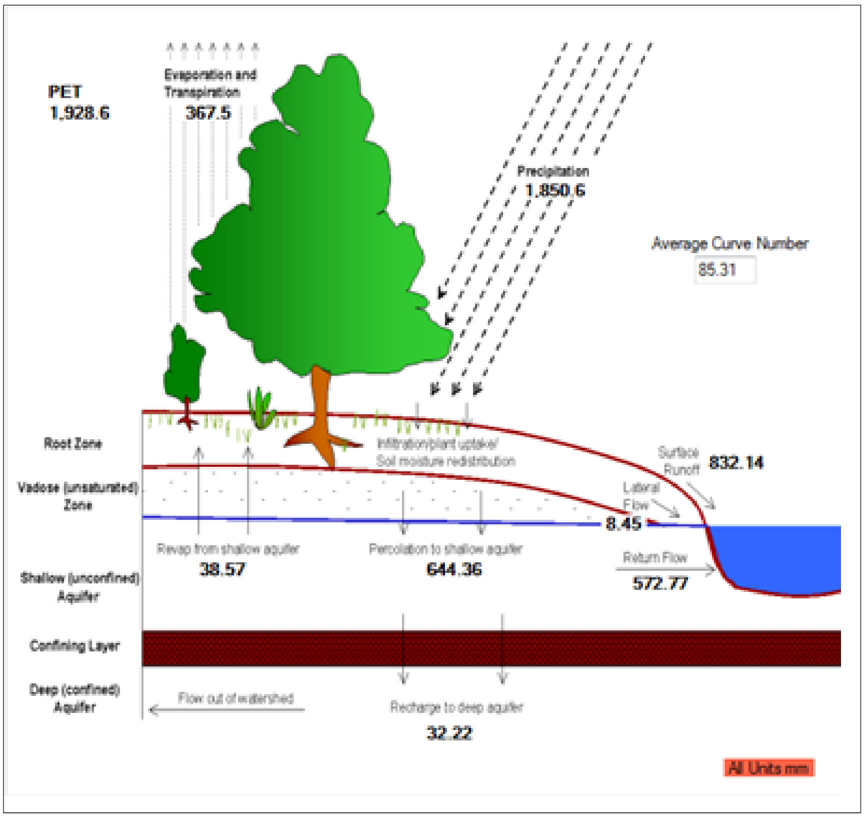

Figure 6. Hydrology of study area by SWAT checker.

The total area under the 14 sub-basins is 19.90 km^2. For sub-basin 1, the agricultural land is 53.75 ha and the forest area is 86.36 ha, which is 2.77 % and 4.45 % of the total watershed area, respectively. The average monthly basin values of rainfall, surface runoff, water yield, sediment yield, evapotranspiration and potential evapotranspiration are obtained for the basin using SWAT Check. The percentage area covered by the watershed of different land use area is obtained by the SWAT. It can be visualized by the report viewer. The HRU analysis for sub-basin 2 is as below.

Table1. Hydrological Response Unit analysis Output.

Land use pattern	Area(ha)	% Watershed area	% sub-basin area
Watershed	1939.09		
Barren area(BARR)	446.41	23.02	
Agricultural Land (AGRL)	1199.1	61.84	
forest area (FRST)	293.59	15.14	
Sub-basin 2			
Agricultural Land (AGRL)	43.19	2.23	31.55
forest area (FRST)	22.82	1.18	16.67
Barren area(BARR)	70.90	3.66	51.79

Table 2. Average monthly basin values.

Month	Rain (mm)	Snowfall (Mm)	Surfq (mm)	Lat Q (mm)	Water Yeild (mm)	Et (mm)	Sed. Yeild (mm)	Pet (mm)
1	6.52	0	0.16	0.11	19.28	10.38	0.09	134.12
2	2.35	0	0.01	0.07	4.1	5.82	0	152.89
3	6.62	0	0.14	0.06	1.94	8.24	0.05	237.4
4	6.02	0	0.19	0.05	1.45	5.93	0.09	301.5
5	18.48	0	2.18	0.07	3.18	13.05	0.53	375.99
6	278.21	0	106.04	0.66	109.63	59.77	21.56	144.5
7	490.8	0	246.14	1.71	294.37	62.51	52.11	70.97
8	414	0	198.25	1.79	306.25	53.23	36.33	57.98
9	392.03	0	184.46	1.87	321.3	58.26	35.88	67.38
10	162.28	0	70.23	1.24	211.06	47.64	13.03	125.21
11	70.56	0	23.75	0.58	116.68	28.38	5.14	123.1
12	2.75	0	0.59	0.24	55.06	14.19	0	136.07

From Table 2, it seems that the quantified values of rain, sediment yield, water yield, ET, and PET are the average annual monthly basin values. The result shows that there is increase in discharge during wet month and decrease during dry period.

5 CONCLUSIONS

SWAT model proves to be an effective tool in simulating the hydrology of large basins at watershed scale. This gives simulated results of each parameter. The estimated parameters can be used for many other purposes of study, such as agricultural water management climate change impact assessment, flow forecasting, water quality assessment, etc. This water balance study minimizes the risk of drought and mismanagement, and hence leading to a proper utilization of water resource available. The water balance is the best way of determining availability of water in different components of hydrological cycle and changes in between these components. The open-source geospatial techniques were used to prepare various thematic maps of study area that influences land use, soil, drainage, and slope used as input for SWAT model.

REFERENCES:

Jain, S.K., Jain, S.K., Hariprasad, V. & Choudhry, A. (2011). Water Balance Study for a Basin Integrating Remote Sensing Data and GIS. *Journal Indian Society of Remote Sensing*, 39(2), 259–270.

Jasrotia, S., Majhi, A. & Singh, S. (2009). Water Balance Approach for Rainwater Harvesting using Remote Sensing and GIS Techniques, Jammu Himalaya, India. Journal of Water Resource Management Springer, 23(14), 3035-3055.

Sathian, K.K. & Symala, P. (2009). Application of GIS Integrated SWAT Model for Basin Level Water Balance. *Indian Journal of Soil Conserv*, 37(2), 100-105.

REMOTE SENSING BASED CROP IDENTIFICATION AND ESTIMATION OF DISTRIBUTED CROP EVAPOTRANSPIRATION IN A CANAL COMMAND

DEEPAK KHARE[(1)], PRABHASH KUMAR MISHRA[(2)], ARUN MONDAL[(3)] & SANANDA KUNDU[(4)]

[(1,4)]Water Resources Development and Management Department, Indian Institute of Technology Roorkee, Roorkee, India
kharefwt@gmail.com; sanandakundu@gmail.com
[(2,3)]Water Resources Systems Division, National Institute of Hydrology, Roorkee, India
erprabhash@gmail.com; arun.iirs@gmail.com

ABSTRACT

To assess distributed crop water requirement in a canal command, identification of different crops becomes essential. This paper attempted to identify multiple crops grown in the *Rabi season* (Nov/Dec to Feb/Mar) in the Tawa canal command (Madhya Pradesh, India) utilizing temporal LISS III (24m x 24m) and AWiFS (60m x 60m) images. Initially, the interest class (irrigated agriculture) and non-interest class were segregated in developing land use land cover map. Then, irrigated crop pixels were masked prior to generating Normalized Difference Vegetation Index (NDVI) values of nine AWiFS images representing the Rabi crop season (23rd Oct'11, 11th Nov'11, 21st Nov'11, 10th Dec'11, 24th Dec'11, 12th Jan'12, 05th Feb'12, 20th Feb'12 and 10th Mar'12). Based on the NDVI profile and sample GPS points taken during field visits, four principal crops viz. wheat (74.68%), chick-pea (14.52%), sugarcane (2.42%), linseeds (2.32%) and others, mainly vegetables (6.06%) were identified in the command. In the study, apart from identification of crops, assessment of water availability in the Tawa canal command has also been made, wherein distributed (pixel-wise) evapotranspiration (ET) approach has been applied to estimate the crop water requirement. Regression equations between the NDVI values and corresponding crop coefficient of identified crops taken from literature (FAO 56) for the six consecutive months were developed. The coefficient of determination (R^2) obtained between Kc-NDVI relations were in the range of about 0.65-0.95. Using this empirical equation, pixel-wise crop coefficient values from the corresponding NDVI values for six months were computed, and represented as crop coefficient maps (Kc map). Daily reference evapotranspiration (ET_0) values for the six months were calculated using the FAO-56 Penman-Monteith equation, and were multiplied by the pixel-wise crop coefficient values, and thus, corresponding crop evapotranspiration maps (ETc map) were generated for six different months.

Keywords: NDVI; Kc map; ETc map; Tawa canal command; RS based crop identification.

1 INTRODUCTION

Optimal management of available water resources in a canal command primarily requires correct assessment of water requirement by different crops, i.e. crop water requirement. However, for sound management and planning of water resources, one requires good and reliable information on water use. With the development of aerial and space borne multispectral sensors, it is now possible to acquire multispectral data from a fairly large area in the narrow and discrete bands of the electromagnetic spectrum on a repetitive basis. Remote sensing data acquired from space-borne platforms, owing to their wide synoptivity and multispectral acquisition, offer unique opportunities for the study of soils, land use/land cover and other parameters required for water demand assessment of large command areas. Water demand assessment of an area requires a thorough understanding of the water balance components, to act as the basic information needed for efficient utilization and management of water (Ambast et al., 2002a; Panigrahy et al., 2009).

Evapotranspiration (ET) of a catchment is related to the systematic distribution of moisture and land cover over its extent. Knowing the way moisture and ET are distributed is a key factor in the successful use of water balance studies in a command. A large number of empirical and semi-empirical methods have been developed to estimate the component of the water balance attributable to ET. The standard methods use climatological data to estimate a potential ET that would occur if water were not limited, and use simple water balance methods to both modify the potential to an actual ET as well as to estimate the available water. However, in catchments with reasonable topographic variation, even if the regional potential ET based on the state of the atmosphere and intensity of solar radiation could be estimated accurately, the actual ET will not be uniform spatially. Most of the current water demand models are a non-spatial model, which uses point data of reference evapotranspiration and the crop coefficient values from available literature (Doorenbos and Pruitt, 1977). However, the climatic data used to measure ET are highly spatially variable. Also the land use and the crop condition can vary from field to field, thus affecting the crop coefficients and thereby crop evapotranspiration rates. Hence, using crop coefficient values from available literature may provide a practical guide for scheduling irrigation, but considerable error in estimating crop water requirement can occur due to their empirical nature (Jagtap and Jones, 1989; Panigrahy and Chakraborty, 1996). The advantage of remote sensing derived crop coefficient over traditional crop coefficient is that it represents a real-time crop coefficient that responds to actual crop conditions in the field and captures the field variability in between.

In this study, major crops were identified using satellite imageries and GPS sampling and then relationships were developed between crop coefficients of identified crops in the command and normalized difference vegetation Index (NDVI) from remote sensing data, as both are affected by leaf area index and fractional ground cover, before estimating the distributed crop evapotranspiration.

2 STUDY AREA

Tawa canal system, situated in the Narmada valley (Hoshangabad district) of Madhya Pradesh, India, with a gross command area of about 0.04 million square kilometer, comprises of two irrigation systems viz. Left bank canal (LBC) and Right bank canal (RBC). LBC is originated from the left bank of the Tawa dam running towards west and RBC towards east. It is a gravity based irrigation system draining north and north-west up to the Narmada River flowing east to west in the northern part of the command. The tail end of the LBC reaches Harda district irrigating about 1862 square kilometer of land. There are three distinct crop seasons practiced in the command. *Kharif* crop season is overlapped with the monsoon months and mainly rainfed. The sowing for the *Kharif* crops (*Kharif* paddy; *Kharif* soyabean) are generally started in the months of June-July and harvested by October-November. Immediately after harvesting of *Kharif* crops, people go for *Rabi* crops (Winter crops). The *Rabi* season starts by the months of October-November up to the months of February-March. Rainfall during this time is scanty in the command area, and hence, the *Rabi* crops are mainly dependent on the canal water supply and groundwater. Apart from the two major crop seasons, summer crops (vegetables) are grown in the command wherever provisions of irrigation are available. The design cropping intensity in the LBC is 138% of the Culturable Command Area (CCA) (*Kharif*-67%; *Rabi*-67%; Summer-4%), whereas the cropping intensity in the RBC is about 125% (*Kharif*-58%; *Rabi*-67%; Summer-nil) of the CCA. The existing cropping intensity in the LBC and RBC is about 165% and 154% of the CCA respectively.

3 SATELLITE DATA USED

Two LISS III (24 m x 24 m) images and Nine AWiFS (60 m x 60 m) images on-board IRS P6 were procured from NRSC, Hyderabad for generating land use/land cover map. Maximum likelihood supervised classification technique was used to separate the interest class (irrigated agriculture) and NDVI. One scene for each month of Rabi season was used for the development of spatially and temporally distributed ETc map. The dates of nine AWiFS images covering entire Rabi period are 23rd October 2011, 11th November 2011, 21st November 2011, 10th December 2011, 24th December 2011, 12th January 2012, 05th February 2012, 20th February 2012 and 10th March 2012. These images were used for NDVI profiling. The temporal dates have been considered based on quality image availability starting from pre-sowing period (23rd October 2011) to crop harvest (10th March 2012).

4 CONCEPT AND METHODS

4.1 Preparation of land use/land cover map

Two scenes of IRS P6 LISS III of 27th January 2011 were selected for the land use/land cover mapping of (*Rabi)* seasons for the command area. The Survey of India (SOI) topographical sheets covering the present study area were scanned and geometrically rectified. The satellite data were geometrically corrected with respect to the SOI toposheets to impart proper projection, uniform scale and orientation. Supervised classification technique with maximum likelihood algorithm was used for image classification. Here, the ground truth information was fed to the computer which is called training process. Ground Truth (GT) information acquired from field visits and topographical sheets was fed to the computer in the form of spectral signatures and there by the segmentation of the categories for the entire scene was performed.

4.2 Identification of crops

The methodology consisted of selection of the datasets, pre-processing of the satellite data, generating Land use land cover (LULC) map and NDVI map, Mapping NDVI profile, accuracy assessment of classified images, and finally crop map for discriminated crops. Flowchart showing broad methodology followed in the study is shown in Figure 1. The nine AWiFS scenes were pre-processed using image to image registration and atmospheric corrections. Nine temporal AWiFS images were stacked in chronological order of their dates (each image represents as a band in the stacked image) before generating NDVI map. Pixels of the interest class i.e. irrigated agriculture were masked to the stacked NDVI temporal image where every band represents to a particular temporal dates. Sample NDVI values were collected to develop the NDVI profile corresponding to the GPS points of sample crops collected during field visit. Finally, major crops were identified and discriminated based on the NDVI profile and crop calendar of different crops grown in the command area. The main principle of detecting vegetation using NDVI is the high absorptivity of vegetation pigments (chlorophyll) in the red spectral region and high reflectance in the near infrared spectral region. NDVI is highly correlated to the photosynthetic activity and indicates the greenness of the vegetation. Hence NDVI has been used for this temporal and multispectral data set for enhancement of the vegetation class and discriminating specific crops. The NDVI is calculated as given in Eq. [1] (Mishra et al., 2005):

$$NDVI = \frac{\rho_{NIR} - \rho_{RED}}{\rho_{NIR} + \rho_{RED}} \qquad [1]$$

where, ρ_{NIR} = near infra-red band of sensor, and ρ_{RED} = red band of sensor.

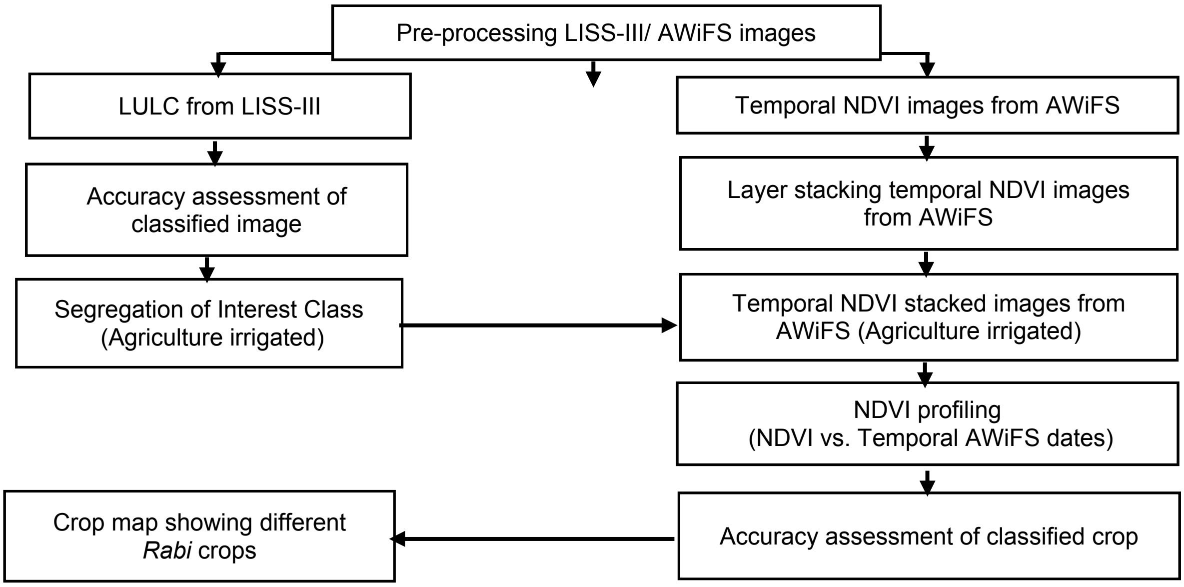

Figure 1. Flowchart showing methodology for the temporal crop discrimination.

4.3 Evapotranspiration estimation using RS and GIS

One scene(s) of AWiFS for six consecutive months of *Rabi* season were taken for estimation of evapotranspiration. From the classified scene representing the *Rabi* season, only the pixels representing the identified crops were chosen by a process called masking. NDVI values were calculated for each pixel representing identified crop (Ambast et al., 2002b; Morid et al., 2002; Gontia and Tiwari, 2008; Gontia and Tiwari, 2010; Panda, et al., 2010a; Mishra et al., 2015). For each scene(s), there were five-sample areas, and from each area, few pixels were chosen and corresponding NDVI values were noted down. The average of the NDVI values picked from each scene(s) was considered to be the representative value of NDVI for that scene(s). Thus, for nine scenes, nine NDVI values were obtained. Regression equations between the NDVI values and corresponding crop coefficients of identified crop taken from literature for the six consecutive months were developed. Using these empirical equations, crop coefficient maps (Kc map) were generated. Daily reference evapotranspiration (ET_0) values for the six months were calculated using the FAO-56 Penmann-Monteith equation (CROPWAT 8.0). Monthly average value of the ET_0 was multiplied with the crop coefficient maps developed, and thus corresponding crop evapotranspiration maps (ETc map) were generated for six different months involving nine scenes. The flowchart indicating steps to generate Kc and ETc map is shown schematically in Figure 2.

5 RESULTS AND DISCUSSION

5.1 Development of crop NDVI profile

NDVI profiling is the process of plotting mean NDVI values of different crops for different temporal dates during the entire crop period. In the study, temporal NDVI images from AWiFS data of different dates were generated for the interest class, i.e. irrigated agriculture. All the NDVI images were stacked chronologically to their dates such that every temporal dates becoming a respective band in the stacked image. GPS sample points of different crops collected during field visit on 25th November 2011 were superimposed over the image as shown in Figure 3. Sample NDVI values were collected from nine scenes from different probable crop signatures from the GPS superimposed images. Mean NDVI values was then derived as given in Table 1. NDVI values of different crops for different temporal dates have been plotted to develop the NDVI profile for the entire crop period during *Rabi* season (Figure 4). Major crops grown in the Tawa command with their crop period is presented in Figure 5.

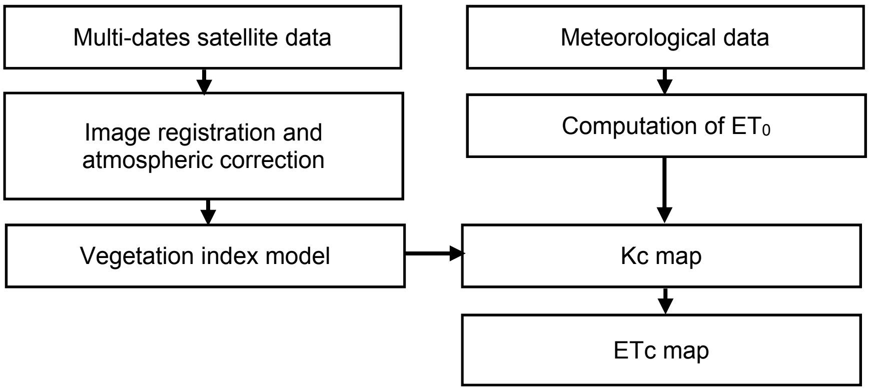

Figure 2. Flow chart for crop evapotranspiration (ETc) estimation using RS and GIS.

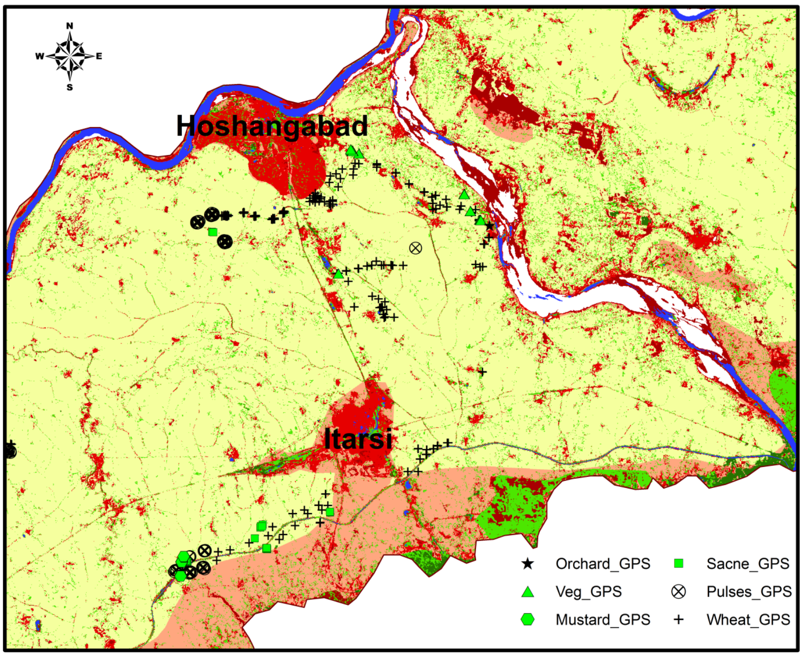

Figure 3. Sample crop points taken through GPS superimposed over LULC.

Table 1. Mean NDVI values of different crops.

Temporal AWiFS dates	Wheat	Pulses (Chick pea)	Oilseeds (Linseed)	Sugarcane	Others
23rd October 2011	0.1169	0.1766	0.2067	0.3560	0.2260
11th November 2011	0.1392	0.1707	0.2214	0.3585	0.1871
21st November 2011	0.1944	0.3285	0.4672	0.3660	0.2493
10th December 2011	0.2521	0.6895	0.6422	0.4136	0.3495
24th December 2011	0.5125	0.7787	0.7543	0.5522	0.5975
12th January 2012	0.7230	0.7851	0.7318	0.5764	0.3652
05th February 2012	0.6999	0.5771	0.6515	0.6438	0.3909
20th February 2012	0.6487	0.3402	0.5540	0.6519	0.5574
10th March 2012	0.5527	0.2395	0.2659	0.6142	0.3919

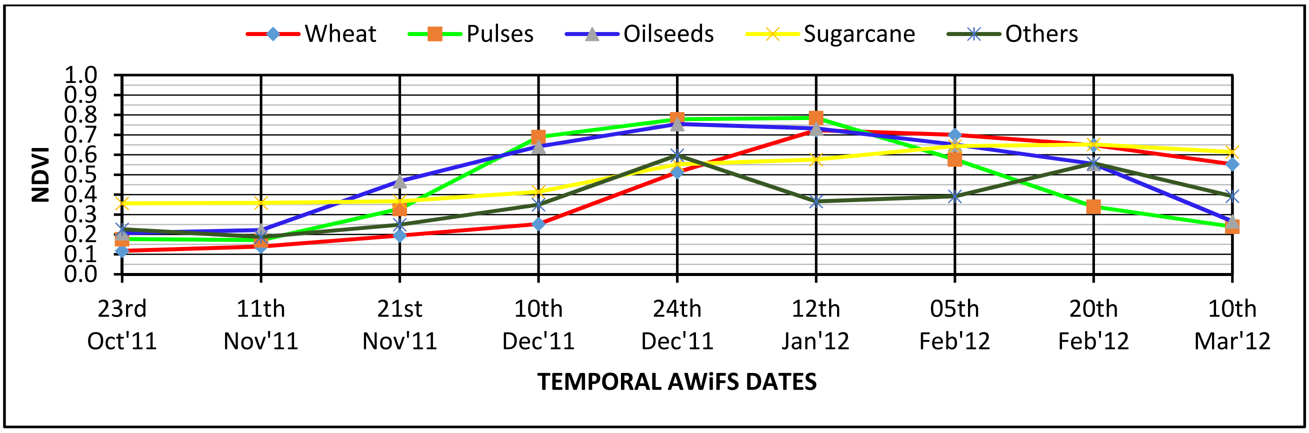

Figure 4. NDVI profile of different crops.

Crop type/ Crop period	October	November	December	January	February	March
Wheat						
Peas						
Linseed						
Mustard						
Vegetables						
Sugarcane						

Figure 5. Crop period for major crops during *Rabi* season in the command area.

5.2 Identification of crops for the *Rabi* season

Different crops exhibit different reflectance properties at different growing stages. Further, it is also true that short duration crops (pulses) will achieve early maturity than long duration crops (sugarcane). Keeping these points in mind, NDVI profile indicated following major crops in the command during *Rabi* season: (i) wheat, (ii) chick-pea, (iii) sugarcane, (iv) linseed and (v) crops such as vegetables and orchards. As can be seen in the NDVI profiling (Figure 6), short duration crops such as pulses and oilseed were attaining early maturity (higher mean NDVI values) then wheat and sugarcane. Sugarcane was exhibiting a rather straight profile. Spatial distribution of major crops (Figure 6) indicated highest coverage for wheat (75%) followed by chick-pea (15%), sugarcane (2.42%) and linseed (2.32%). The details on the spatial distribution of different crops are presented in Table 2.

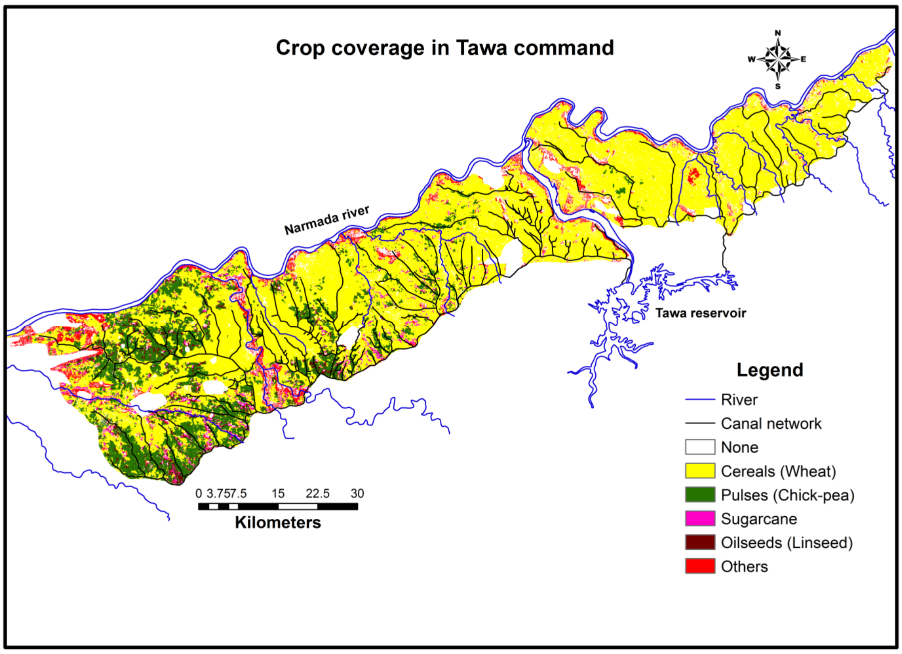

Figure 6. Crop map showing major *Rabi* crops.

Table 2. Area coverage of identified crops.

Crop type	Area (km^2)	% cover
Cereals (Wheat)	1166.15	59.33
Pulses (Chick-pea)	561.87	28.59
Sugarcane	55	2.80
Oilseeds (Linseeds)	36.82	1.87
Others (mainly vegetables, orchards, etc.)	145.73	7.41
Total	**1965.57**	**100.00**

5.3 NDVI based ETc Estimation

5.3.1 Development of Kc map and ETc map

The Kc map and ETc map for different months were generated by the digital image analysis of 2011-2012 agricultural season of IRS-P6 AWiFS data of dated 23rd October 2011, 11th November 2011, 21st November 2011, 10th December 2011, 24th December 2011, 12th January 2012, 05th February 2012, 20th February 2012 and 10th March 2012. The average of the NDVI values picked from each scene was considered to be the representative value of NDVI for that scene for a particular crop. Thus, for nine scenes, nine NDVI values were obtained for each crop (Table 1). The corresponding crop coefficients of each crop were taken from literatures. NDVI values obtained in the month of October and November were minimum since crops were in its initial phase of development. It then increased linearly and touched maximum in the month of January-February signifying maximum crop coverage over the ground. It was also observed that NDVI values decreased as the crop attains maturity.

5.3.2 Relationship between Kc and NDVI

Regression equations between the NDVI values and corresponding crop coefficient of identified crops taken from literature (FAO 56) for the six consecutive months were developed. The Kc and NDVI values for different scenes used in regression relationship are given in Table 3. The regression equations developed for each crop are presented in Figure 7. The coefficient of determination (R^2) obtained between Kc-NDVI relations were in the range of about 0.65-0.95. The analysis of regression showed that the equations were highly significant with high R^2 values.

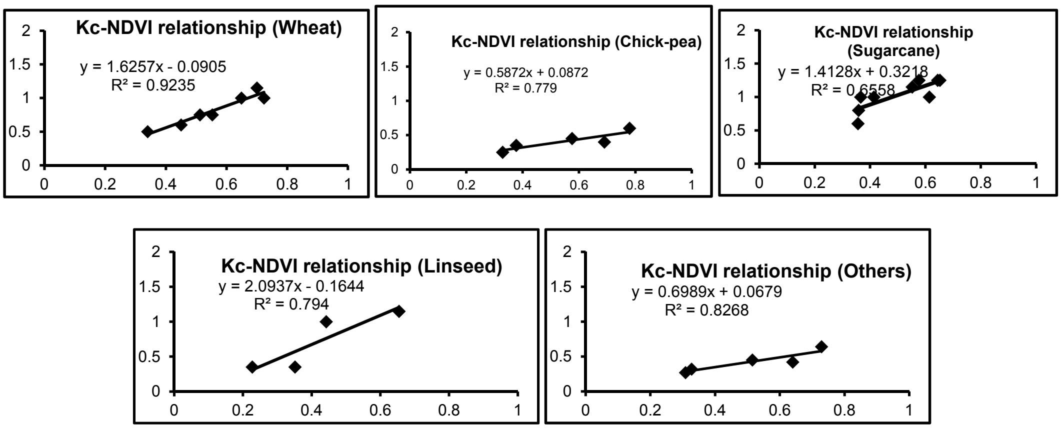

Figure 7. Regression curves between Kc and NDVI values for different crops.

Table 3. Kc* and NDVI values for different scenes used in regression relationship.

Months	Kc wheat	NDVI wheat	Kc chick pea	NDVI chick pea	Kc sugarcane	NDVI sugarcane	Kc linseed	NDVI linseed	Kc Others	NDVI Others
23-Oct					0.60	0.36				
11-Nov	0.50	0.34	0.25	0.33	0.80	0.36			0.27	0.31
21-Nov	0.60	0.45	0.40	0.69	1.00	0.37	0.35	0.23	0.42	0.64
10-Dec	0.75	0.51	0.60	0.78	1.00	0.41	1.00	0.44	0.64	0.73
24-Dec	1.00	0.72	0.45	0.58	1.15	0.55	1.15	0.65	0.45	0.52
12-Jan	1.15	0.70	0.35	0.38	1.25	0.58	0.35	0.35	0.32	0.33
5-Feb	1.00	0.65			1.25	0.64				
20-Feb	0.75	0.55			1.25	0.65				
10-Mar	0.67	0.53			1.00	0.61				

**Source: FAO 56*

Using this empirical equations, pixel-wise crop coefficient values from the corresponding NDVI values for six months were computed. Crop coefficient maps (Kc map) generated for different months based on NDVI is given in Figure 8. Climatic data collected from nearest weather station were used to compute the reference evapotranspiration. Daily reference evapotranspiration (ET_0) values for the six months were calculated using the FAO-56 Penmann-Monteith equation. Monthly average value of the reference evapotranspiration was multiplied with the pixel-wise crop coefficient values, and thus corresponding crop evapotranspiration maps (ETc map) were generated for six different months. Crop evapotranspiration map (ETc) generated for six months based on NDVI are presented in Figure 9. The range of crop coefficient and crop evapotranspiration values (scene wise) based on NDVI are given in Table 4.

Table 4. Scene wise range of Kc values and ETc values (mm) of different crops.

Months	Wheat		Pulses		Sugarcane		Oilseeds		Others	
	Kc	ETc	Kc	ETc	Kc	ETc	Kc	ETc	Kc	ETc
23rd October 2011					0.3-1.05	2.25-3.15				
11th November 2011	0.25-0.77	1.35-2.25	0.35-0.45	1.15-2.35	0.4-1.15	1.57-4.19			0.11-0.45	1.0-2.3
21st November 2011	0.68-0.89	1.86-2.38	0.40-0.75	1.55-2.89	0.37-1.18	1.65-5.11	0.15-0.75	1.05-2.65	0.32-0.78	1.34-2.89
10th December 2011	0.93-1.17	2.10-2.75	0.61-0.98	1.87-3.5	0.55-1.25	1.18-5.28	0.33-1.05	1.55-3.25	0.51-0.98	1.37-4.5
24th December 2011	1.03-1.32	2.17-3.10	0.41-0.84	1.74-3.89	0.71-1.25	1.5-5.55	0.61-1.15	1.81-3.87	0.39-0.86	1.24-5.36
12th January 2012	1.10-1.16	2.55-3.76	0.31-0.78	1.35-3.15	0.61-1.31	1.87-5.76	0.3-0.74	1.74-3.39	0.31-0.78	1.35-4.15
05th February 2012	0.89-1.11	2.67-4.98			0.38-1.18	1.45-4.67				
20th February 2012	0.30-1.13	1.27-4.87			0.31-0.97	1.57-4.49				
10th March 2012					0.29-0.89	1.15-4.55				

It is observed from Table 4 that crop evapotranspiration values have an increasing trend as the season progress. It was minimum in the month of October-November and maximum in the month of February-March. Sometimes, the harvesting season extended to April also. The spatial resolution of AWiFS sensor is 60 m, that means a pixel represents 60×60 m^2 in the real ground situation. Spatially distributed pixel-wise crop evapotranspiration computed from satellite image when multiplied with the pixel area gives the total volume of water requirement for that particular pixel. Thus total demand (in volume unit) in the command for each scene was estimated. The scene-wise ETc values (total demand) obtained for nine scenes based on NDVI are presented in Table 5.

Table 5. Scene wise ETc values based on NDVI.

Months	Wheat ETc (mm)	Pulses ETc (mm)	Sugarcane ETc (mm)	Oilseeds ETc (mm)	Others ETc (mm)
23rd October 2011			2.25-5.15		
11th November 2011	1.35-2.25	1.15-3.35	1.57-4.19		1.15-4.3
21st November 2011	1.86-3.38	1.55-3.89	1.65-5.11	1.05-2.65	1.34-4.89
10th December 2011	2.10-2.75	1.87-4.50	1.18-5.28	1.55-3.95	1.37-4.5
24th December 2011	2.17-3.10	1.74-3.71	1.5-5.55	1.81-3.87	1.24-5.36
12th January 2012	2.55-3.76	1.35-3.15	1.87-5.76	1.74-3.39	1.35-4.15
05th February 2012	2.67-4.98		1.45-4.67		
20th February 2012	1.27-4.87		1.57-4.49		
10th March 2012			1.15-4.55		

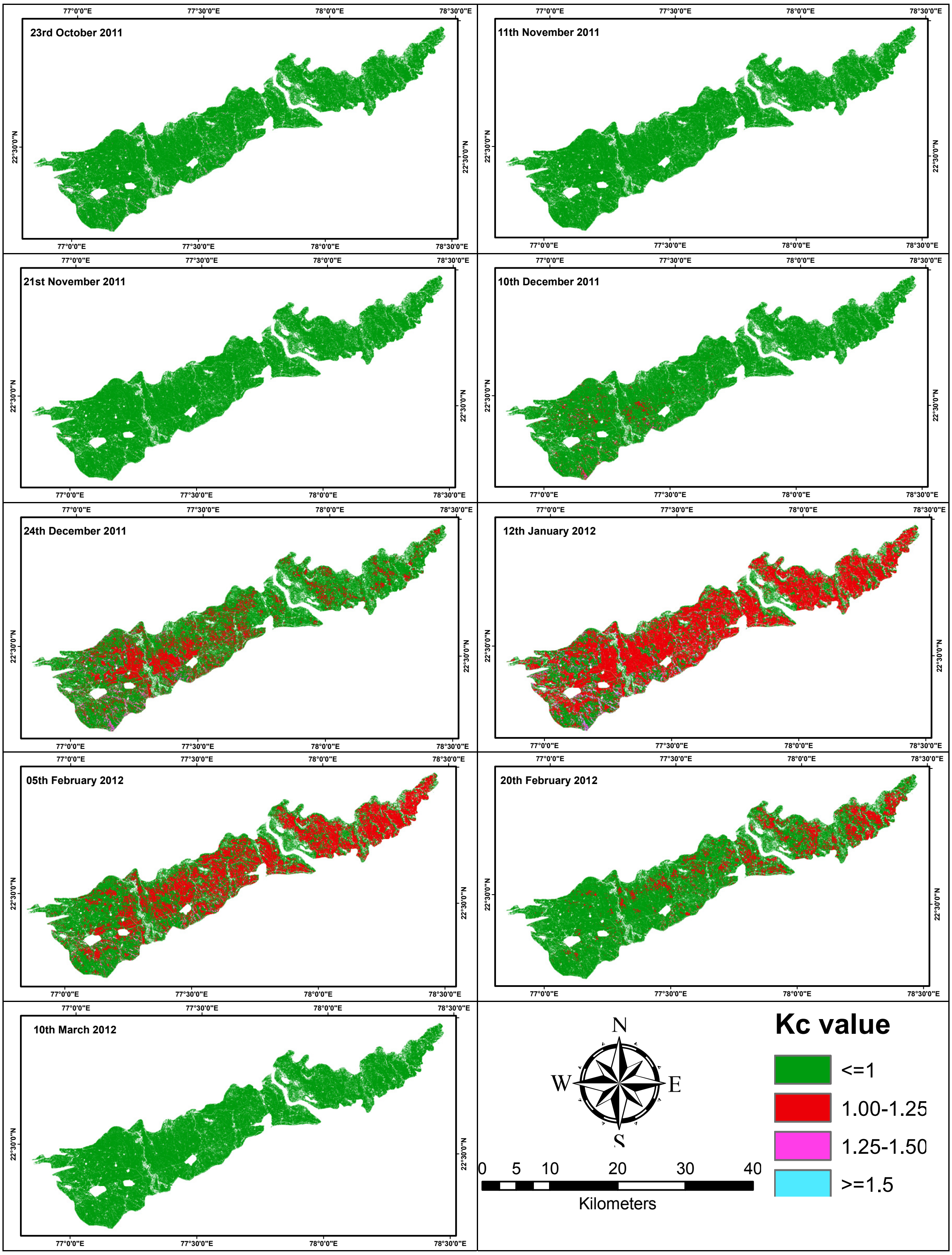

Figure 8. NDVI based spatially and temporally distributed Kc map.

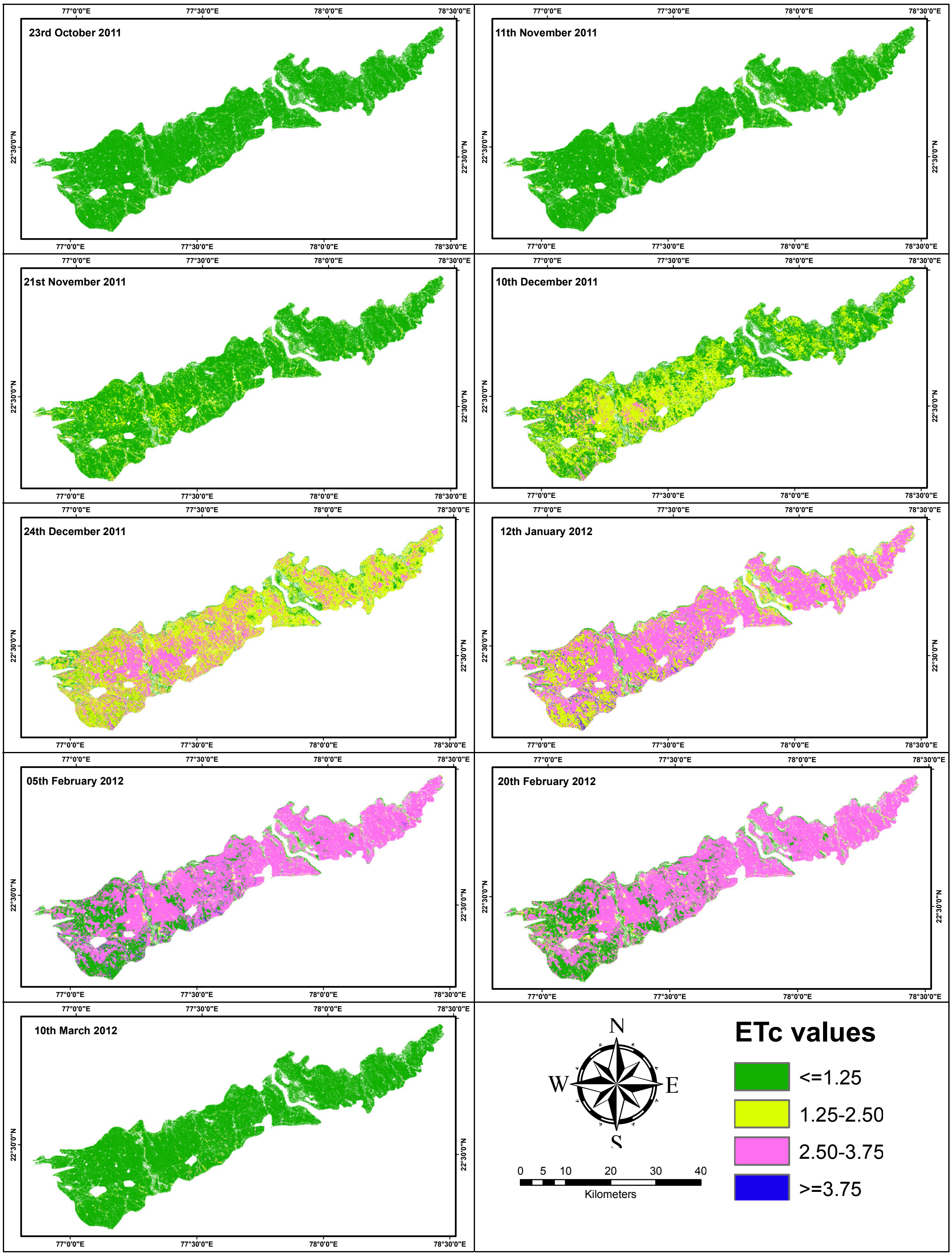

Figure 9. NDVI based spatially and temporally distributed ETc map.

6 CONCLUSIONS

Crop management at command level requires considerable efforts in terms of crop planning, water management, pest management, etc. When the area encompasses by the command is large, the task becomes more difficult to the command area authority for proper planning and decision making. With the arrival of technologies such as remote sensing and geographical information systems, NDVI based crop identification and discrimination in large areas helps planners in multiple ways. In the preset study, utility of LISS-III and multi-dates AWIFS images have been demonstrated for identifying and discriminating different crops during *Rabi* season in the Tawa command. Based on the NDVI profile and sample GPS points taken during field visits, four principal crops viz. wheat (74.68%), chick-pea (14.52%), sugarcane (2.42%), linseeds

(2.32%) and others mainly vegetables (6.06%) are identified in the command. Also in the study, demonstration has been made on how distributed crop evapotranspiration (ETc map) is prepared based on the relationship between crop coefficient and NDVI. This helps in estimating the demand and supply scenario in the canal command.

ACKNOWLEDGEMENTS

The authors, thankfully, acknowledge the *Tawa Command Authority* for providing various data and extending supports during the field visit. The authors are also thankful to the Ministry of Human Resources Development (MHRD), GoI for financial assistance in terms of fellowship during the study period.

REFERENCES

Ambast, S.K., Keshari, A.K. & Gosain, A.K. (2002). Satellite Remote Sensing to Support Management of Irrigation Systems: Concepts and Approaches. *Irrigation and drainage*, 51(1), 25-39.

Ambast, S.K., Keshari, A.K. & Gosain, A.K. (2002b). An Operational Model for Estimating Regional Evapotranspiration through Surface Energy Partitioning (RESEP). *International Journal of Remote Sensing*, 23(22), 4917-4930.

Doorenbos, J. & Pruitt, W.O. (1977). Background and Development of Methods to Predict Reference Crop Evapotranspiration (ETo). *Appendix II in FAO-ID-24*, 10, 108-119.

Gontia, N.K. & Tiwari, K.N. (2008). Development of Crop Water Stress Index of Wheat Crop for Scheduling Irrigation using Infrared Thermometry. *Agricultural Water Management*, 95(10), 1144–1152.

Gontia, N.K. & Tiwari, K.N. (2010). Estimation of Crop Coefficient and Evapotranspiration of Wheat (Triticum Aestivum) in an Irrigation Command using Remote Sensing and GIS. *Water resources management*, 24(7), 1399-1414.

Jagtap, S.S. & Jones, J.W. (1989). Stability of Crop Coefficients under Different Climate and Irrigation Management Practices. *Irrigation Science*, 10(3), 231-244.

Mishra, P.K., Khare, D., Shukla, R., Mondal, A. & Kundu, S. (2015). Utility of LISS III and AWiFS Data in Identifying Rabi Crops in a Canal Command. *Proceeding of International Conference HYDRO 2015 jointly organized by IIT Roorkee and ISH, Mumbai*.

Mishra, P.K., Tiwari, K.N., Chowdary, V.M. & Gontia, N.K. (2005). Irrigation Water Demand and Supply Analysis in the Command Area using Remote Sensing and GIS. *Hydrology Journal*, 28(1-2), 59-69.

Morid, S., Gosain, A.K. & Keshari, A.K. (2002). Solar Radiation Estimation using Temperature-based, Stochastic and Artificial Neural Networks Approaches. *Hydrology Research*, 33(4) 291-304.

Panda, S.S., Ames, D.P. & Panigrahi, S. (2010a). Application of Vegetation Indices for Agricultural Crop Yield Prediction using Neural Network Techniques. *Remote Sensing*, 2(3), 673-696.

Panigrahy, R.K., Ray, S.S. & Panigrahy, S. (2009). Study on the Utility of IRS-P6 Awifs SWIR Band for Crop Discrimination and Classification. *Journal of the Indian Society of Remote Sensing*, 37(2), 325-333.

Panigrahy, S. & Chakraborty, M. (1996). A Case Study for Burdhaman District of West Bengal. In *Indo-US Workshop on Remote Sensing and its Applications*.

FORECASTING OF RIVER DISCHARGE BY USING ARTIFICAL NEURAL NETWORK MODEL: CASE STUDY, LATYAN DAM BASIN, IRAN

MOZAFAR ANSARI(1), FARIDAH OTHMAN(2) & AHMED EL-SHAFIE(3)

(1,2,3) Department of Civil Engineering, Faculty of Engineering,
University of Malaya, Kuala Lumpur, Malaysia
m.ansari@siswa.um.edu.my; faridahothman@um.edu.my; elshafie@um.edu.my

ABSTRACT

Predicting and modeling river discharge is one of the most important issues for any hydrological studies. Accurate discharge prediction leads to better performance in other operation or studies such as reservoir operation or flood plain mapping. Due to this importance, many studies have been done to improve the performance of hydrological models. Among of these models, artificial intelligences (AIs) are the state-of-the-art methods which bring proper results with limited variety of data. In this study, ANN model was applied on Jajrood River at Latyan Dam basin in Iran. Sixteen years of daily precipitation and discharge were the main inputs of the model. Beside these, due to seasonal rainfall in arid and semi-arid area, months of the year were also applied in the model. Four scenarios of inputs, which had different elements, were determined and results of these states were compared. Results showed that in the first one, which had months of the year and three days of rainfall and six days lagged data of previous discharge had the lowest root mean square error (RMSE) and the highest correlation coefficient (R) result among other scenarios. Therefore, months of the year could be alternative data for all elements which change during the year such as wet season, soil moisture condition, and etc. which are not available or not easy to be obtained.

Keywords: River discharge prediction; artificial neural network (ANN); Jajrood River; Latyan Dam; Iran.

1 INTRODUCTION

River discharge is one of the most important data in water resources engineering. Predicting the river flow rate is very important for planning and developing the civilized area which can be affected by the river. Precise predicting multi-scale inflow discharge (such as daily, weekly, monthly and seasonal) is very critical and helps to plan or operate many structures such as bridge, channels, reservoir, hydropower generation, flood protection, irrigation management and other hydrological applications efficiently (Araghinejad et al., 2006; Solomatine and Shrestha, 2009; Othman & Naseri, 2011; Danandeh Mehr et al., 2014; Yaseen et al., 2016). In addition, accurate short-term forecasted data are valuable in developing flood warning systems and risk control beforehand (Chiang et al., 2004; Guven, 2009; Szolgayová et al., 2014; Yaseen, 2015).

Researchers are always trying to develop and apply various methods to receive an accurate prediction of river discharge. Scientists tried to predict the peak flow by using empirical methods such as Dicken's formula (1865), Fuller's method (1914), Curve Number (CN) and etc. Among these methods, the CN method which was developed by the Soil Conservation Service (SCS) hydrologists in 1969, was considered one of the most accurate empirical methods because a lot of environmental parameters are involved in estimating the watershed runoff such as soil cover, hydrological soil group and condition, and etc. Researchers found those models are not accurate enough to meet their expectations, therefore they developed some physically-based models to model and predict the flow rate and erosion such as The Water Erosion Prediction Project (WEPP), Soil Water and Analysis Tools (SWAT), Système Hydrologique Européen TRANsport (SHETRAN), and etc. These models need a vast variety of environmental data such as soil type, evaporation, temperature, land use, Digital Elevation Model (DEM) and etc. To predict reliable flow rate easier and faster than aforementioned comprehensive models, hydrologists applied Artificial Intelligences (AI) methods such as ANN, Adaptive Neural-Fuzzy Inference System (ANFIS), Support Vector Machine (SVM), Extreme Learning Machine (ELM) and many other AI algorithms.

Many researchers applied Multilayer Perceptron (MLP) models to predict flood discharge of a river because the model is easy to use and there are much proper software that runs MLP model. However, new AI methods and algorithms have become more complicated and more accurate. Ghorbani et al. (2016) compared the results of MLP, Radial Basis Function (RBF) and SVM models to predict river flow rate of Zarrinehrud river in Iran. They found that the SVM model provided more accurate results than MLP and RBF models. Although the high performance of the new AI algorithms, many researchers have tried to use rainfall and previous time stepped discharge data as the model inputs (Kerh and Lee, 2006; Ghorbani et al., 2016; Tayyab et al., 2016) to model the river discharge. On the other hand, there are many parameters which are as important as rainfall such as evaporation, temperature, soil hydrological condition, land cover, and etc., should be considered in the model training. The aim of this research is to increase the prediction accuracy in a model by including other environmental parameters and finding the easiest and cheapest way to apply these parameters to the model. In this research, the performance of ANN model with different conditions will be compared to find out the effectiveness of other environmental parameters as the input to the model.

2 STUDY AREA

Jajrood River, which origins from Alborz Mountain range and ended to Namak Lake, is one of the longest rivers in Tehran province, Iran. The drainage area of Latyan Dam catchment up to Roodak hydrometric station was chosen as the study area. It is spread from 51.40 to 51.70 longitudes and 35.83 to 36.05 latitudes and covers 435.3 square kilometers (Zeinivand and De Smedt, 2009). This region has the semi-arid climate with annual precipitation 330mm and the average discharge of 7.53 (m^3/s). All hydrometric and precipitation data were provided by Tehran Regional Water Organization and Iranian Water Resources Research Organization (TAMAB Co). Topography map was provided by National Geographical Organization. Figure 1 shows the position of the study area.

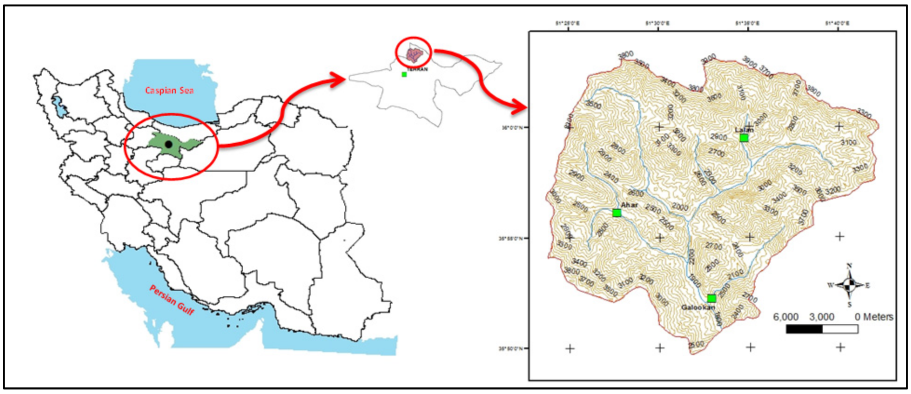

Figure 1. The study area, Latyan dam drainage in Tehran, Iran.

3 MATERIALS AND METHODS

Artificial Intelligence (AI) models are used to forecast hydrological phenomena. Unlike physically-base models which need more detailed information, they operate like a black-box model (Kalogirou, 2001). ANN is one of AI algorithms which models data by the learning process, memorizing, and creating the relationship between data. It finds the relationship between inputs and outputs by finding optimum weight between them (Kalogirou, 2000; Shahverdi et al., 2015). A schematic structure of a typical multilayer feedforward neural network is represented in figure 2.

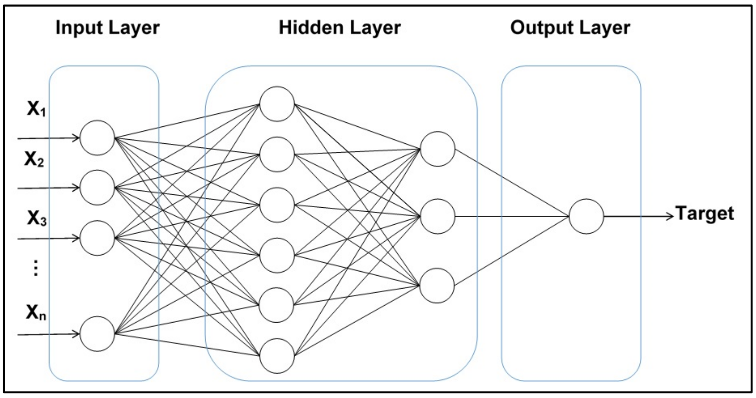

Figure 2. Schematic of neural network architecture.

Most of the meteorological parameters such as evaporation, temperature, rainfall pattern and etc., and environmental conditions such as plant canopy, are fluctuating during a year. These parameters are difficult and costly to collect. Whereas in each month of every year, these parameters are almost steady, based on month order, month number of the year was applied as a coefficient to the model.

Sixteen years daily stream flow and rainfall records from 1991 to 2007 were used in the study. Since most of the records in Iran are stored based on Iranian official calendar, which starts from first day of spring, in this research, number of the month is applied in scale of 1 to 12, i.e. the first month of the year is 1 and the last month is 12, based on month order in the Iranian Solar calendar. To cover hydrological soil condition, rainfall data was lagged for 2 days.

Before the ANN process starts, outliers of the records were detected and replaced by mean of previous and next reliable records. To develop inputs of the models, 4 scenarios were designed to evaluate the effect of month coefficient on the model accuracy by comparing the performance of the ANN model. Only in two scenarios, month coefficient was applied as one of the model inputs. In one pair of scenarios with different month coefficient status, two-day lagged precipitation was used. Stream discharge was lagged for 6 days and used as input for all scenarios. Summary of each scenario is given in Table 1.

Table 1. Summary of inputs at each scenario.

Scenario No.	No. of Inputs	Month Coeff.	Precipitation	Discharge
S1	10	Yes	$R_{(t-2)}$, $R_{(t-1)}$, $R_{(t)}$	$Q_{(t-6)}$, $Q_{(t-5)}$, $Q_{(t-4)}$, $Q_{(t-3)}$, $Q_{(t-2)}$, $Q_{(t-1)}$
S2	8	Yes	$R_{(t)}$	$Q_{(t-6)}$, $Q_{(t-5)}$, $Q_{(t-4)}$, $Q_{(t-3)}$, $Q_{(t-2)}$, $Q_{(t-1)}$
S3	9	None	$R_{(t-2)}$, $R_{(t-1)}$, $R_{(t)}$	$Q_{(t-6)}$, $Q_{(t-5)}$, $Q_{(t-4)}$, $Q_{(t-3)}$, $Q_{(t-2)}$, $Q_{(t-1)}$
S4	7	None	$R_{(t)}$	$Q_{(t-6)}$, $Q_{(t-5)}$, $Q_{(t-4)}$, $Q_{(t-3)}$, $Q_{(t-2)}$, $Q_{(t-1)}$

To minimize the errors of the model, the scaling of inputs and output were generalized to have the smaller numerical range (between 0 and 1) by using Eq. [1]:

$$V_{i,normalised} = \frac{V_i - V_{min}}{V_{max} - V_{min}} \qquad [1]$$

where, $V_{i,normalised}$ is the normalized value, V_i, V_{min}, and V_{max} are the current value, minimum and maximum values in the dataset, respectively.

In the next step, in MATLAB software, an MLP algorithm was applied to train, test, and validate the data. Each scenario was divided into two states. In the first state, an MLP with one hidden layer was applied and in the second state, the MLP was done with two hidden layers algorithms. The MLP model was evaluate with different size of hidden layers. The size of hidden layers for the first layer started from 1 to 4 times greater than the number of inputs in both state 1 and 2, and second layer size started from one to the number of inputs. To find the best hidden layer size, Mean Square Errors (MSE) of the model, based on generalized data, were calculated and their results were compared to the best model which has minimum errors, in each scenario.

Subsequently, after the suitable model in each state were defined, the model was run and then results were converted to their scale and compare with the original data. Two model performance indicators, namely Correlation coefficient (r), and Root Mean Square Error (RMSE), were applied to score the performance of each scenario (Legates and McCabe Jr, 1999).

4 RESULTS AND DISCUSSIONS

Figure 3 displays the monthly average rainfall and discharge of the study area.

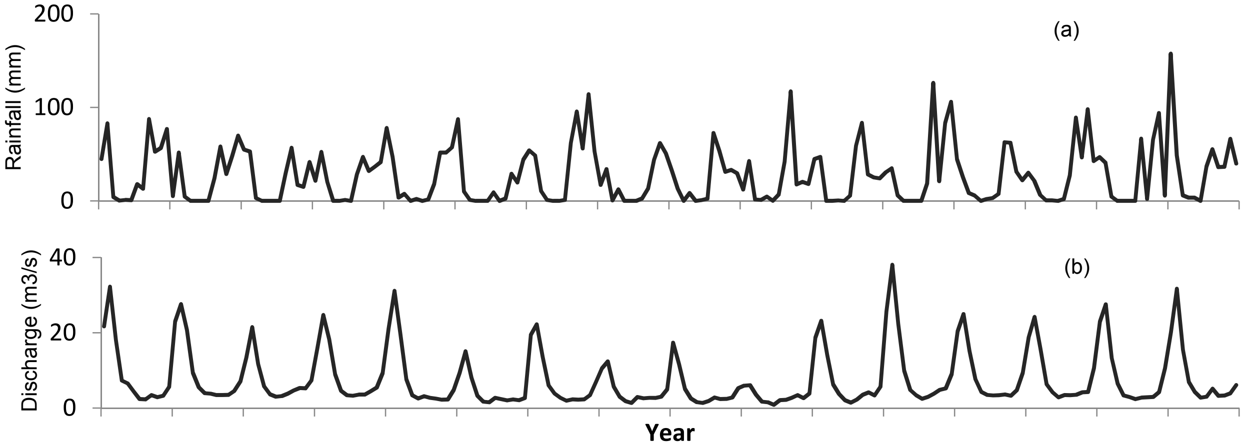

Figure 3. (a) Cumulative monthly rainfall and (b) monthly average stream discharge of Roodak.

Scatter-plots of observed and predicted discharge for each state of all scenarios are presented in figure 4. The correlation coefficient which indicates the accuracy of the model shows the performance and reliability of the model.

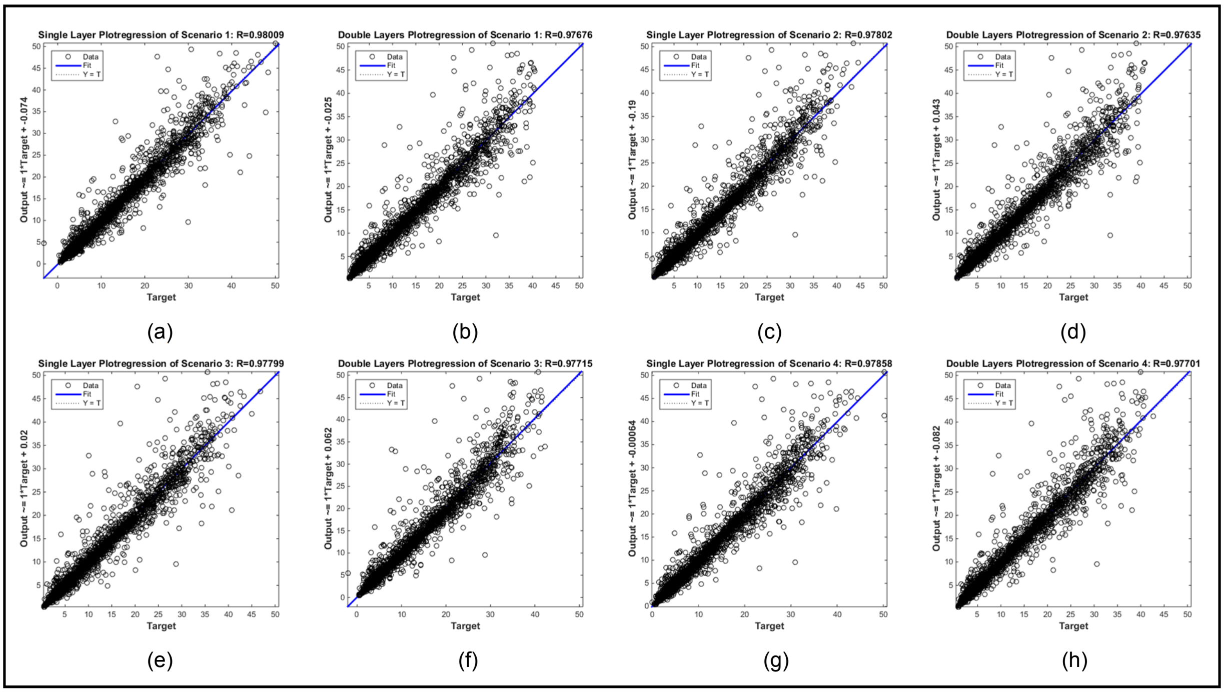

Figure 4. Scatter-plots of observed (Target) and predicted (Output) by ANN model of (a) single layer, (b) two-layer for scenario 1; (c) single layer, (d) two-layer for scenario 2; (e) single layer, (f) two-layer for scenario 3; (g) single layer, (h) two- layer for scenario 4.

Evaluation indices result of the first scenario, which month of the year and 3 times lagged rainfall were applied to the model, showed the best performance of the model. A comparison of model assessment for all scenarios as well as optimum hidden layer size is briefly given in table 2 and table 3. In this table, ANN algorithm calculated MSE results based on generalized data.

Table 2. Summary of ANN results for all single layer ANNs.

Scenarios	Optimal size	MSE	RMSE	R
S1	33	0.001028	1.616309	0.980086
S2	29	0.001143	1.704549	0.978018
S3	18	0.001129	1.693906	0.977992
S4	13	0.001099	1.671474	0.978576

Table 3. Summary of ANN results for all double layers ANNs.

Scenarios	Optimal size Layer 1	optimal size Layer 2	MSE	RMSE	R
S1	29	3	0.001037	1.741032	0.976756
S2	29	8	0.001047	1.755729	0.976346
S3	14	3	0.00111	1.729587	0.977147
S4	16	6	0.001049	1.732273	0.977014

By comparing the RMSE and R of all the scenarios, single hidden layer algorithms have better results than multi hidden layer ones. MSE results showed that there are some exceptions to consider all the mono hidden layers to be more accurate than multi-layer one. Figure 5 illustrates a comparison between predicted results and existing records of stream flow for the best model in each scenario.

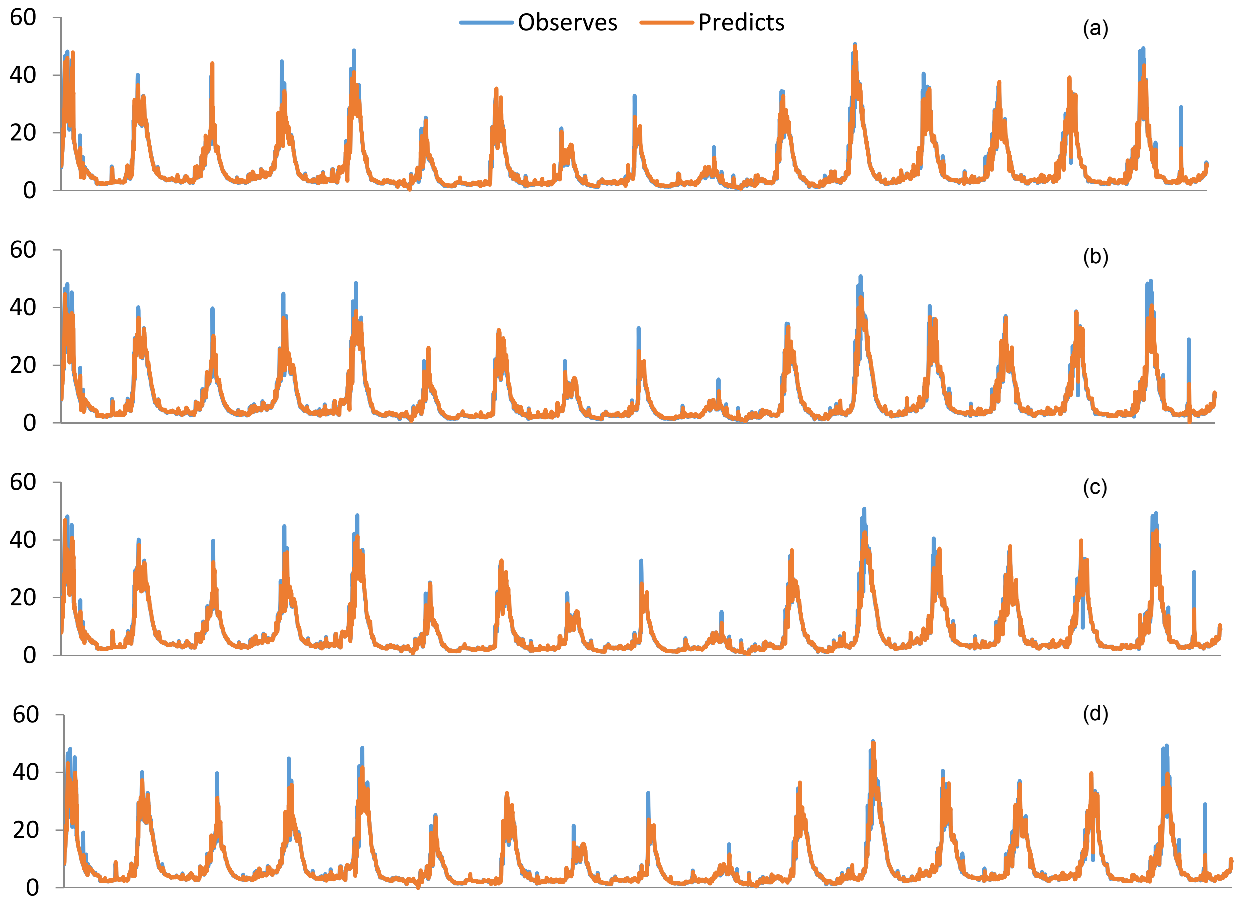

Figure 5. Observed stream discharge and predicted discharges for: (a) scenario 1; (b) scenario 2; (c) scenario 3; (d) scenario 4.

5 CONCLUSIONS

In this research, ANN model was applied with different inputs to compare their accuracies. In all models, a set of 6 times lagged discharge was the constant input. Moreover, two important factors, precipitation and seasonal effects, were compared by designing 4 different scenarios. Lagging the rainfall data up to 3 days was aimed to represent the soil moisture condition and month number of the year represented the weather conditions, for example as precipitation pattern or mean temperature and evaporation, as well as land canopy coverage in semi-arid area which mostly covered the study area by seasonal herbs that grows up in spring and summer.

The research aims was applying environment parameters besides the precipitation and discharge data as the model inputs as cheap and easy as possible. The model assessment results prove that both 3 days rainfall data and month deficient data together provide more accurate results than other situations. Therefore, these 2 parameters can be a good representative of environmental conditions. However, by comparing scenarios 3 and 4, using the month coefficient without the lagged rainfall data do not provide precise result. Thus, month coefficient exclusively cannot be a good representative for all environmental factors. As the results show, a three-day precipitation records provide a better forecasting than only one day record and even one day records besides the month number.

By comparing this research results with the results of other studies, the model performance is better than other methods which did not consider the seasonal or soil conditions and have been applied on the study area or similar areas.

In conclusion, besides improving prediction algorithm by using state-of-the-art AI methods, providing adequate inputs that describe the system can bring better results. It is recommended to apply these inputs in any more accurate AI algorithms especially for the models problem in predicting some peak flows and compare the results with the results of this research.

ACKNOWLEDGEMENTS

The data of research was provided by TAMAB Co. in Tehran, Iran. And also the essential facilities including software and hardware were provided by Fundamental Research Grant Scheme (Project code: FP016-2014A), faculty of Engineering in University of Malaya. The authors would like to thank TAMAB and FRGS for their involvement in this project.

REFERENCES

Araghinejad, S., Burn, D.H. & Karamouz, M. (2006). Long-Lead Probabilistic Forecasting of Streamflow using Ocean-Atmospheric and Hydrological Predictors. *Water Resources Research,* 42(3), 1-11.

Chiang, Y.M., Chang, L.C. & Chang, F.J. (2004). Comparison of Static-Feedforward and Dynamic-Feedback Neural Networks for Rainfall-Runoff Modeling. *Journal of Hydrology,* 290(3-4), 297-311.

Danandeh Mehr, A., Kahya, E., Şahin, A. & Nazemosadat, M.J. (2014). Successive-Station Monthly Streamflow Prediction using Different Artificial Neural Network Algorithms. *International Journal of Environmental Science and Technology*, 12(7), 2191-2200.

Ghorbani, M.A., Zadeh, H.A., Isazadeh, M. & Terzi, O. (2016). A Comparative Study of Artificial Neural Network (MLP, RBF) and Support Vector Machine Models for River Flow Prediction. *Environmental Earth Sciences,* 75(6), 1-14.

Guven, A. (2009). Linear Genetic Programming for Time-Series Modelling of Daily Flow Rate. *Journal of Earth System Science,* 118(2), 137-146.

Kalogirou, S.A. (2000). Applications of Artificial Neural-Networks for Energy Systems. *Applied Energy,* 67(1–2), 17-35.

Kalogirou, S.A. (2001). Artificial Neural Networks in Renewable Energy Systems Applications: A Review. *Renewable and Sustainable Energy Reviews,* 5(4), 373-401.

Kerh, T. & Lee, C.S. (2006). Neural Networks Forecasting of Flood Discharge at an Unmeasured Station using River Upstream Information. *Advances in Engineering Software,* 37(8), 533-543.

Legates, D.R. & McCabe, G.J. (1999). Evaluating the use of “Goodness-Of-Fit” Measures in Hydrologic and Hydroclimatic Model Validation. *Water resources research*, 35(1), 233-241.

Othman, F. & Naseri, M. (2011). Reservoir Inflow Forecasting using Artificial Neural Network. *International Journal of Physical Sciences,* 6(3), 434-440.

Shahverdi, K., Khodaei, K. & Shokohi, A. (2015). Prediction of Monthly Inflow to Dam Reservoir using ANN and ANFIS: A Case Study of Latyan Dam. *International Bulletin of Water Resources and Development (IBWRD),* 3(3), X-XVIII.

Solomatine, D.P. & Shrestha, D.L. (2009). A Novel Method to Estimate Model Uncertainty using Machine Learning Techniques. *Water Resources Research,* 45(1), 1-16.

Szolgayová, E., Arlt, J., Blöschl, G. & Szolgay, J. (2014). Wavelet based Deseasonalization for Modelling and Forecasting of Daily Discharge Series Considering Long Range Dependence. *Journal of Hydrology and Hydromechanics,* 62(1), 24-32.

Tayyab, M., Zhou, J., Zeng, X. & Adnan, R. (2016). Discharge Forecasting by Applying Artificial Neural Networks at the Jinsha River Basin, China. *European Scientific Journal,* 12(9), 1-20.

Yaseen, Z.M. (2015). RBFNN versus FFNN for daily river flow forecasting at Johor River, Malaysia. *Neural Computing and Applications*, 27(6), 1533-1542.

Yaseen, Z.M., Jaafar, O., Deo, R.C., Kisi, O., Adamowski, J., Quilty, J. & El-Shafie, A. (2016). Stream-Flow Forecasting using Extreme Learning Machines: A Case Study in a Semi-Arid Region in Iraq. *Journal of Hydrology,* 542, 603-614.

Zeinivand, H. & De Smedt, F. (2009). Hydrological Modeling of Snow Accumulation and Melting on River Basin Scale. *Water Resources Management,* 23(11), 2271-2287.

COMBINING AN IMPROVED SNOW MODEL WITH ABOVE-GROUND NEUTRON SENSING AND REMOTE SENSING

PAUL SCHATTAN[1], GABRIELE BARONI[2], SASCHA E. OSWALD[3], JOHANNES SCHÖBER[4], CHRISTINE FEY[5], TILL FRANCKE[6], MATTHIAS HUTTENLAU[7], ROBERT KIRNBAUER[8] & STEFAN ACHLEITNER[9]

[1,5,7] alpS Centre for Climate Change Adaptation, Innsbruck, Austria,
schattan@alps-gmbh.com
[1] Institute of Geography, University of Innsbruck, Innsbruck, Austria,
[2] UFZ – Helmholtz Centre for Environmental Research, Leipzig, Germany,
[2,3,6] Institute of Earth and Environmental Science, University of Potsdam, Potsdam, Germany,
[4,5] TIWAG Tiroler Wasserkraft AG, Innsbruck, Austria,
[8] Institute of Hydraulic Engineering and Water Resource Management, Vienna University of Technology, Vienna, Austria
[9] Unit of Hydraulic Engineering, University of Innsbruck, Innsbruck, Austria,

ABSTRACT

The knowledge of the state of snow water resources is crucial for managing water resources in mountain regions and beyond. Thereby, snow covered area (SCA) can be retrieved operationally from remote sensing data but available water in terms of snow water equivalent (SWE) can still vary substantially. Traditional methods to retrieve SWE have severe drawbacks like a lack of representativeness, labor-intensity or discontinuity in time. In this study, an approach of combining satellite based SCA maps and different types of in-situ SWE measurements is proposed. Based on that, the hypothesis that the predictive capability of an improved distributed snow model is improved by integrating this combined information is tested. In particular, the objectives are to test (i) whether a combination of remote sensing and in-situ data improves the model results and (ii) whether there are differences in the choice of the in-situ data. The state of the snowpack was monitored over two winter seasons by several measurement techniques with contrasting spatial and temporal characteristics. Measurements included (i) continuous point-scale measurements, (ii) several campaigns during the snow accumulation and melting season (terrestrial laser scanning and snow pits) and (iii) continuous above-ground cosmic-ray neutron sensing (CRNS) at an intermediate scale (footprint around 250 m in radius). While continuous point-scale SWE data largely overestimated the snowpack, CRNS based SWE data represented values derived from TLS measurements quite well. Measured in-situ SWE data and SCA area maps (Landsat8 and Sentinel-2A data) were combined within a multi-objective model calibration. The objective functions varied with regard to the used in-situ SWE data, where runoff and SCA was used throughout. The results showed that including intermediate scale CRNS data clearly outperforms the version with conventional point-scale data underlining the importance of the choice of in-situ data.

Keywords: Cosmic-ray neutron sensing (CRNS); light detection and ranging (LiDAR); model coupling; alpine hydrology; water resources management.

1 INTRODUCTION

Snow represents an important component of the hydrological cycle, in particular, for mountain regions. On a seasonal scale, precipitation stored as snow in winter first and then contributes considerably to the total discharge and runoff generation in spring and early summer during snow melt.

The state of the snow water resources can be monitored using (i) ground observations, (ii) remote sensing and (iii) snow models with the best results are to be expected if these three approaches are combined (Sturm, 2015). These combinations have been used with respect to data assimilation (Thirel et al., 2013; Magnusson et al., 2014), inverse modelling of basin-wide precipitation (Shrestha et al., 2014; Rittger et al., 2016) and multi-objective model calibration (Kirnbauer et al., 1994; Finger et al., 2011, 2015; Revuelto et al., 2016).

Hydrological models can be classified according to their completeness of theoretical system description ranging from physically based to conceptual models. Snow hydrological models with different degrees of complexity exist (Essery et al., 2013; Avanzi et al., 2016) where individual (sub) modules can differ in the degree of physically meaningful process description. Often even physically-based models are partly based on "hidden parametrizations" (Kirnbauer et al., 1994). Physically based models can be more robust in the face of changing environmental conditions. There is, however, a trade-off between model complexity and the number of parameters (i.e. data requirements).

Remote sensing data are usually available for complete hydrological basins. In mountain regions, space-borne remote sensing products are limited to snow covered area (SCA) products from optical satellites with varying spatial and temporal resolution (Dozier, 1989; Dietz et al., 2012) or Synthetic Aperture Radar (SAR) satellites with high spatial resolution (Nagler et al., 2016; Rondeau-Genesse et al., 2016). Thereby, optical data are limited by cloud coverage, while SAR based data are not suitable for discriminating dry snow from snow-free ground.

Ground-based data is therefore needed to combine remote sensing data of snow extent with information on snow mass. Traditional ground observations like snow pits or snow core surveys (Proksch et al., 2016) are labor-intensive and suffer from other drawbacks such as low repeat frequency. Continuous measurements for obtaining snow depth (SD) or snow water equivalent (SWE) at index stations are potentially subjected to temporally varying biases as compared to a larger area (Winstral and Marks, 2014; Grünewald and Lehning, 2015). Terrestrial laser scanning (TLS) (Deems et al., 2013) has the potential of measuring the distribution of snow depth but is also usually limited to dedicated campaigns. Therefore, recent developments of techniques measuring at an intermediate spatial scale of several hectares like acoustic sounding (Kinar and Pomeroy, 2007), above-ground gamma-ray scintillators (Choquette et al., 2013) or above-ground neutron counters (CRNS) (Sigouin and Si, 2016; Schattan et al., 2017) are promising.

In the present study, we hypothesize that the predictive capability of snow models is improved by integrating SCA maps and snow measurements at intermediate spatial scale. In the frame of the operational flood forecasting system for the Inn River (Austria), the combination of an improved snow hydrological model with high resolution SCA products and SWE measured at different spatial scales were applied and evaluated.

2 STUDY AREA AND MONITORING ACTIVITIES

The study focuses on the headwater basin of the Fagge River, a major tributary to the Inn River in the Austrian Alps. The upper Fagge catchment drains an area of 51.85 km² at the main alpine ridge and is highly glacierized (Figure 1). The elevation ranges between 1,915 and 3,509 m.a.s.l. with an average elevation of 2,830 m.a.s.l.. As of 2006, 39 % of the basin was covered by glaciers. Forest cover at the basin outlet is very sparse with only a small number of individual trees occupying the lowermost parts of the basin. The basin is of high interest for water resource management as it comprises the main natural inflow to the Gepatsch reservoir with an installed capacity of 325 – 392 MW. An automated weather station (AWS) is operated within the area located at an elevation of 2470 m.a.s.l. which also measures a number of snow parameters including SD and SWE. Several TLS campaigns have been conducted to characterize the distribution of SD and SWE in an area of about 500 m around the AWS (see Figure 1). In addition, a CRNS was installed in 2014 providing continuous values of SD and SWE at the scale of ~ 200 x 200 m. For additional information about the experimental site and the monitoring activities, we refer to Schattan et al. (2017).

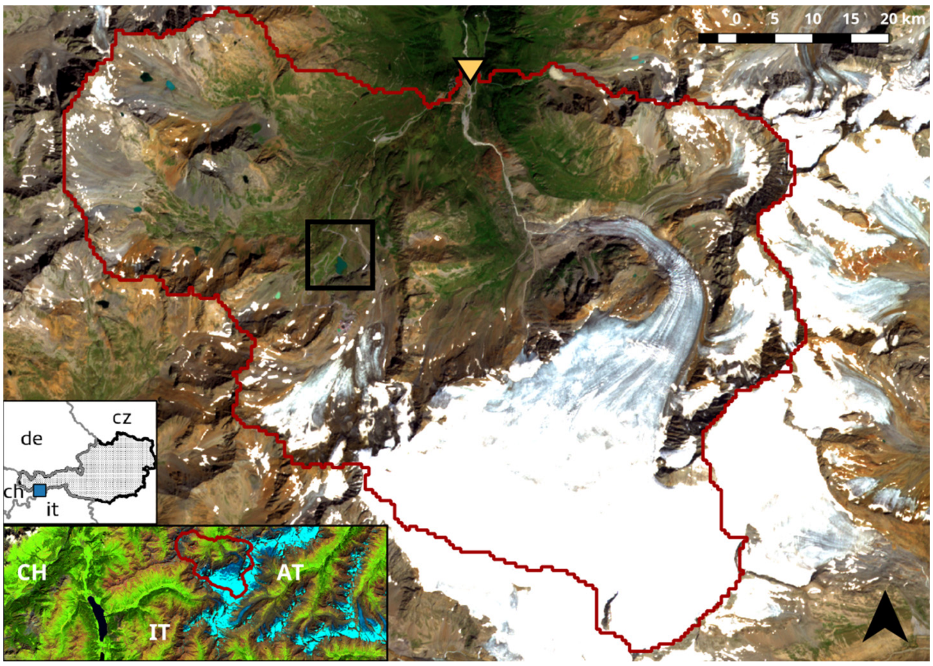

Figure 1. Sentinel-2A scene (Aug. 2015) of the study area (yell. triangle = gauge; black square = TLS area).

3 DATA AND METHODS

3.1 Available datasets and study design

The experiment included a model warm up period (10/2012 – 09/2013), a calibration period (10/2013 – 09/2015) and a following validation period (10/2015 – 09/2016). For the initialization of the firn and glacier storages, a deterministic model run from 10/2003 (low firn cover due to above-average summer temperatures) to 09/2012 (beginning of the warm up period) was used. The overall time-step for all simulations was one hour.

An improved snow model vertically coupling components from both models currently applied within the flood forecasting system of the Inn River (see section 3.3) is intended to describe the dominant processes of alpine basins in a physically more meaningful way. To ensure this, the model was evaluated against a number of different environmental datasets being available for a multi-objective model calibration and validation:

i. Discharge measurements at an hourly time-step at the basin outlet (for the complete time-series);
ii. Landsat-8 and Sentinel-2A derived binary SCA maps (16 scenes for calibration, 5 for validation);
iii. Continuous point-scale SWE measurements at the AWS with a footprint of approximately 1 m² (10/2014 – 09/2016);
iv. Continuous CRNS based SWE measurements at the AWS with a footprint of approximately 200 x 200 m (03/2014 – 06/2014 and 10/2014 – 06/2016);
v. Distributed TLS based SWE maps covering the area around the AWS (11 during the calibration period and 6 during the validation period).

The multi-objective calibration of the model includes discharge data, snow covered area maps and continuous ground based SWE measurements based on point-scale and CRNS data. TLS measurements were used for validating both the continuous SWE data and the model runs.

Point-Scale SWE data were obtained by a Snow-Pack-Analyzer (Stähli et al., 2004). CRNS based SWE was derived from neutron count rates [$N \cdot h^{-1}$] using Eq. [1] (Schattan et al., 2017). TLS based SWE were spatially weighted with respect to the distance to the AWS (Köhli et al., 2015). For areas with melting snow, SWE was limited to 200 mm to reflect the characteristics of the CRNS measurements (Schattan et al., 2017).

$$SWE(N) = \frac{12.571}{\left(\frac{N}{5307.466}\right) - 0.432} - 16.194 \qquad [1]$$

In Figure 2, point-scale SWE and CRNS SWE are compared to TLS based SWE values. The CRNS derived SWE values have a good agreement with TLS SWE campaigns. In contrast, point-scale SWE largely overestimates the snowpack during the 2014/15 winter season as compared to TLS measurements.

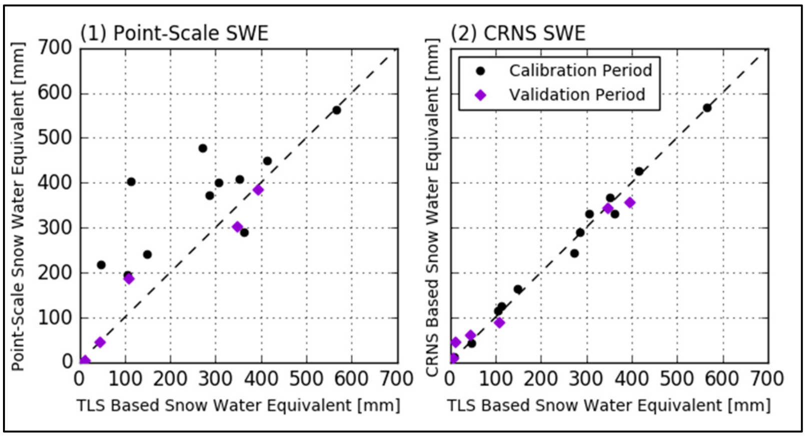

Figure 2. Comparison of (1) point-scale SWE and (2) CRNS SWE with TLS based SWE.

3.2 Model input data

The basic data for model setup were derived from the digital elevation model of Tyrol, which was resampled to a spatial resolution of 50 m, and the Corine Land Cover 2006 data. For a more detailed representation of the glacier borders, the Corine data was refined by the third Austrian Glacier Inventory (AGI-III) of the year 2006 (Fischer et al., 2015). Additional terrain data (e.g. LAI, roughness height, snow-free albedo) needed to calculate evapotranspiration were derived from the ECOCLIMAP II dataset (Faroux et al., 2013).

As meteorological model forcing the analysis data from the operational analysis and nowcasting system INCA (Integrated Nowcasting through Comprehensive Analysis) (Haiden et al., 2011) was used. The model requires temperature, precipitation, wind speed, relative humidity and global radiation. The 1 km centroids of the INCA Analysis data were interpolated to the target grid of the model by Inverse Distance Weighting (IDW). Additionally, a variable lapse rate from a moving window of the 24 nearest neighbors was applied to temperature and precipitation data. Default lapse rates were used if the r^2 of the regression model was below a defined threshold set of 0.3.

3.3 Improved Snow Model

In its current setup, the flood forecasting system for the Inn River uses a modular hybrid hydrological-hydraulic approach (Achleitner et al., 2009). Tributary catchments are modelled with two serially linked hydrological models. Highly glacierized headwater catchments are modelled with the fully distributed snow and ice melt model SES (Asztalos, 2004; Asztalos et al., 2007). Non-glacierized catchments are modelled with the semi-distributed water balance model HQsim (Achleitner et al., 2012). Both hydrological models include conceptual process representations without physical meaning resulting in potentially large structural uncertainties (Bellinger et al., 2012; Schöber et al., 2014).

The distributed snow and ice melt model SES (Asztalos, 2004; Asztalos et al., 2007) is a representative of a medium complexity energy and mass balance model, a model type which generally show a good trade-off between model performance in terms of runoff prediction in alpine terrain and complexity (Essery et al., 2013). The model is a single layer snow model solving energy and mass balances on a grid with a resolution of 50x50 m. Firn and glacier ice are represented as additional layers. The model inputs are (i) air temperature [°C], (ii) the total amount of solid and liquid precipitation [mm], (iii) relative humidity [%], (iv) wind speed [m s^{-1}] and (v) global radiation [W m^{-2}]. Preferential deposition and redistribution of snow due to gravity and wind transport are parametrized based on slope and curvature of the terrain (Blöschl et al., 1991a). The energy budget calculation explicitly accounts for terrain induced effects on shortwave irradiance like self-shading and terrain shading. Snow albedo is altered with solar angle and energy input into the snow pack (Asztalos, 2004). Incoming long wave radiation is calculated based on air temperature, relative humidity and cloudiness (Blöschl et al., 1991b). For outgoing long wave radiation a snow temperature of 0 °C and a high emissivity are assumed (Blöschl and Kirnbauer, 1991). A bulk parameterization is used for processes associated with thermal conductivity and liquid water storage capacity (Braun, 1985; Blöschl and Kirnbauer, 1991). Simulated snow melt is routed using five parallel Nash-cascades for (i) soil, (ii) snow-free rocks, (iii) snow-covered terrain, (iv) the snow-free firn area and (v) the bare part of the glacier (Asztalos et al., 2007).

The semi-distributed water balance model HQsim (Kleindienst, 1996) is a conceptual rainfall-runoff model for alpine environments based on the Hydrological Response Units (HRU) approach. HRU delineation follows elevation, aspect and vegetation type. The requirements for the model forcing data are parsimonious and include only air temperature [°C] and precipitation [mm]. The model lacks a module for snow redistribution. Snowmelt is calculated by a modified degree-day approach where self-shading is accounted for. In analogy to SES, the onset of snow melt is delayed by the concept of “cold content” (Braun, 1985; Blöschl and Kirnbauer, 1991) defined as the sum of negative temperature accumulated over previous days. Soil infiltration and surface runoff are separated by a parameterization of contributing area (Achleitner et al., 2012). A closed form equation is used to calculate hydraulic conductivity within the soils as a function of volumetric soil moisture and saturated hydraulic conductivity (van Genuchten, 1980). The runoff concentration is computed according to the time-area method and routing is based on a non-linear storage release with adaptive time-steps for each channel segment. Flow velocities are calculated using an equation for steep channels (Rickenmann, 1996).

The improved vertically coupled model uses approaches of both hydrological models. Following the “Dominant Process Concept” (Blöschl, 1999; 2001), distributed and semi-distributed modules were combined. All processes highly influenced by terrain and energy budget were calculated on a distributed domain with a resolution of 50x50 m. Accumulation and melt of snow, firn and ice were calculated using the routines implemented in SES. Water available for infiltration and runoff generation (i.e. melt water and rain) and potential evapotranspiration (Monteith, 1965) were aggregated for each HRU as input for the semi-distributed part of the model. Actual evapotranspiration, soil water storage, runoff concentration and routing were modelled based on the HQsim scheme.

3.4 Combining the model with remote sensing data and ground measurements

To combine the model with remote sensing data and ground measurements, a multi-objective calibration approach was applied. Therein, discharge, snow extent (SCA) and snow mass were used to assess different aspects of the model. The individual goodness of fit values used to derive a combined goodness of fit value E (Eq. [2]) are explained in the following:

The modeled discharge at the basin outlet was compared with measured discharge data using the Kling-Gupta-Efficiency (KGE) (Kling et al., 2012) as this measure combines the coefficient of variation, a coefficient of variation ratio and a bias ratio. A binary SCA map was derived from modelled SWE data using a threshold of 5 mm and was used to assess the accuracy of modeled against observed SCA (ACC) (Zappa et al., 2003). A KGE value was also calculated for evaluating modeled and observed SWE data. For point-scale SWE data, observed values were compared with the values of the grid cell where the AWS was located. To compare with CRNS SWE data the modeled SWE values of individual grid cells were spatially weighted with respect to the distance to the AWS (Köhli et al., 2015). For grid cells with melting snow, SWE was limited to 200 mm (Schattan et al., 2017).

In Eq. [2] the formulation follows the concept of KGE (Kling et al., 2012) where both the combined efficiency and its components have their maximum at unity and the combined efficiency is dominated by the component with the poorest fit. The index of the overall efficiency represents whether point-scale SWE (i = 1) or CRNS based SWE (i = 2) was evaluated. Both realizations were calibrated separately by a simulated annealing algorithm (Kirkpatrick et al., 1983) with 2,000 samples using the overall efficiency E as objective function.

$$E_i = 1 - \sqrt{(1 - KGE_Q)^2 + (1 - ACC)^2 + \left(1 - KGE_{SWE_i}\right)^2} \qquad [2]$$

where *i* refers to the respective SWE time series used (point-scale SWE or CRNS SWE)

4 RESULTS AND DISCUSSIONS

For both realizations, the best percent of model runs, i.e. the 20 best parameterizations in terms of model efficiency *E* in the calibration period, was evaluated regarding the model's capability to predict (i) discharge at the stream gauge, (ii) the spatial and temporal patterns of SCA and (iii) the temporal evolution of the snow storage in terms of SWE.

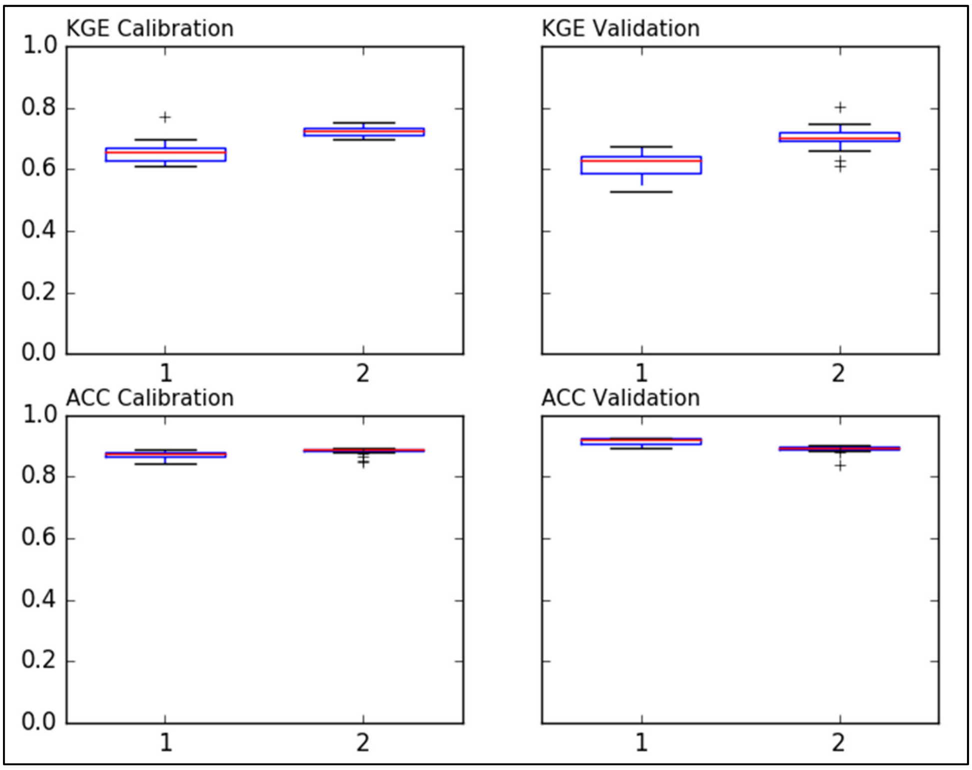

Figure 3. Model performance with regard to discharge (KGE_Q) and snow extent (ACC) using point-scale SWE (E_1) or CRNS SWE (E_2) in the objective function.

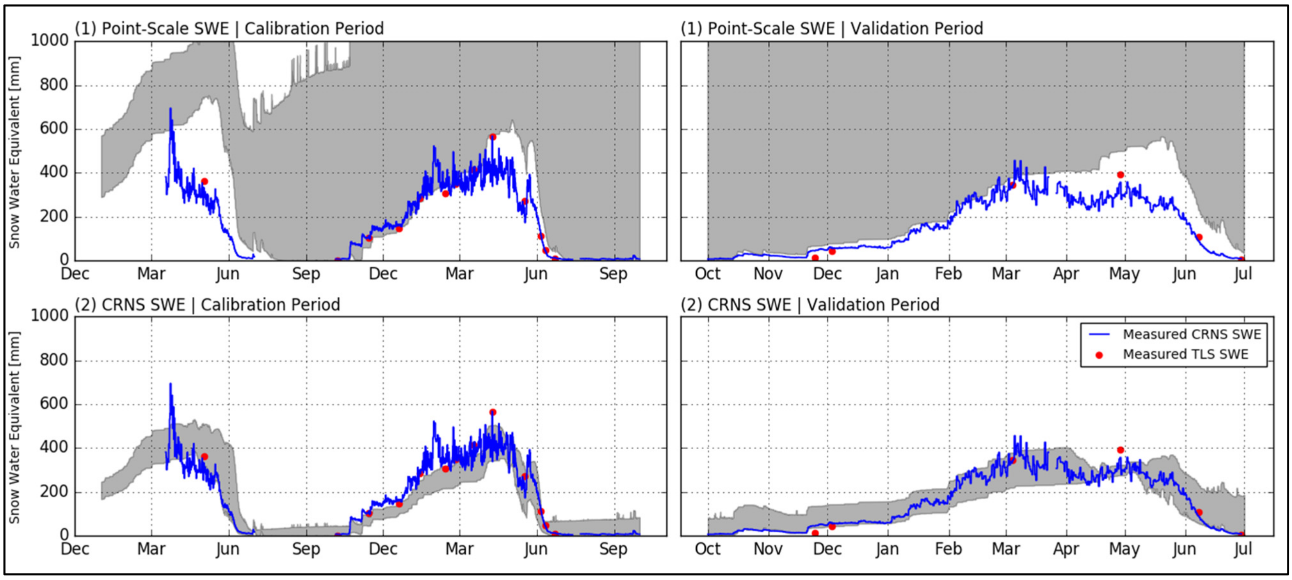

Figure 4. Model performance in terms of representing the temporal dynamic of the snow storage where (1) indicates using point-scale SWE in the *objective* function and (2) using CRNS SWE. The grey area represents the range of modeled SWE values based on a subset of the 20 best model runs.

The predictability of discharge and snow extent in the calibration and the validation period are shown in Figure 3 with boxplots of KGE_Q and *ACC* for both objective functions. In general, both performed reasonably well with regard to discharge and show a high agreement for snow extent. The calibration including CRNS based SWE, however, slightly outperformed the calibration with point-scale SWE data with regard to discharge.

Further insights on whether the parametrizations are physically meaningful, or discharge and snow extent are predicted well but for the wrong reasons, are given by evaluating the temporal evolution of the modeled snow storage. Time-series of SWE measured by CRNS and TLS were compared against model predictions (see Figure 4). This parameter is well represented for the realization including CRNS SWE data, showing a reasonable bound set by the best simulation runs. Both, the model results and the measured CRNS SWE time-series have a good agreement with TLS SWE campaigns. In contrast, simulations calibrated based on point-scale SWE largely overestimated the snowpack during the 2014/15 winter season in all runs. Furthermore, the spreads of simulated SWE were large for both, calibration and validation periods. The good overall performance of this realization seems not to be based on a sound representation of the principle physical processes, but the results from compensation by other model components.

5 CONCLUSIONS

A combination of a physically based model, remote sensing and ground observations shows high potential for building physically sound snow hydrological models. The results, however, also underline the importance of the choice of observation data for multi-objective model calibration.

Particularly, in highly heterogeneous environments like alpine headwater basins, the scale of the measurement matters. Measurements with a small footprint can result in temporally variable biases caused by small-scale heterogeneities. This in turn can lead to substantial model uncertainty. Therefore, for variables like SWE, intermediate-scale ground measurements like CRNS provide a promising information to improve the predictive capability of snow hydrological models.

ACKNOWLEDGEMENTS

This work was carried out as part of the project “W02 HoPI III – Runoff Forecasting System for the Inn River” at alpS – Centre for Climate Change Adaptation in Innsbruck, Austria. The K1-Centre alpS was funded through the Federal Ministry of Transport, Innovation and Technology (BMVIT), the Federal Ministry of Science, Research and Economy (BMWFW), as well as the Austrian Provinces of the Tyrol and Vorarlberg within the scope of COMET – Competence Centers for Excellent Technologies. The Programme COMET was managed by the Austrian Research Promotion Agency (FFG). The project was co-funded by TIWAG-Tiroler Wasserkraft AG. G. Baroni had financial support from the German Science Foundation (DFG) under CI 26/13-1 in the framework of the research unit FOR 2131 “Data Assimilation for Improved Characterization of Fluxes across Compartmental Interfaces”. We thankfully acknowledge the University of Potsdam for providing the CRNS for this study which was funded via EFRE-HIP-Brandenburg no. 80158356. The NMDB database (www.nmdb.eu), founded under the European Union's FP7 7th Framework Programme (contract no. 213007) and the University of Bern are acknowledged for providing neutron monitor data. Furthermore, the following institutions are thankfully acknowledged for the provision of environmental data of the study site: Hydrographic Survey of the Province of Tyrol, TIWAG-Tiroler Wasserkraft AG, European Environmental Agency (EEA), European Space Agency (ESA) and United States Geological Survey (USGS). We specially thank Sebastian Sprenger (master thesis, University of Innsbruck) for his support during the TLS campaigns in the season 2014/15.

REFERENCES

Achleitner, S., Rinderer, M., & Kirnbauer, R. (2009). Hydrological Modeling in Alpine Catchments: Sensing the Critical Parameters Towards an Efficient Model Calibration. *Water science and technology,* 60(6), 1507–1514.

Achleitner, S., Schöber, J., Rinderer, M., Leonhardt, G., Schöberl, F., Kirnbauer, R. & Schönlaub, H. (2012). Analyzing the Operational Performance of the Hydrological Models in an Alpine Flood Forecasting System. *Journal of Hydrology,* 412, 90–100.

Asztalos, J. (2004). Ein Schnee-und Eisschmelzmodell für vergletscherte Einzugsgebiete. Available at: http://www.hydro.tuwien.ac.at/fileadmin/mediapool-hydro/Diverse/Institutsseminar/DA_judit_041013-Abstr.pdf [Accessed 03/04/2013]

Asztalos, J., Kirnbauer, R., Escher-Vetter, H. & Braun, L. (2007). A Distributed Energy Balance Snow and Glacier Melt Model as a Component of a Flood Forecasting System for the Inn River. In *Alpine Snow Workshop*, Munich, 9-17.

Avanzi, F., De Michele, C., Morin, S., Carmagnola, C. M., Ghezzi, A. & Lejeune, Y. (2016). Model Complexity and Data Requirements in Snow Hydrology: Seeking a Balance in Practical Applications. *Hydrological Processes*, 30(13), 2106–2118.

Bellinger, J., Achleitner, S., Schöber, J., Schöberl, F., Kirnbauer, R. & Schneider, K. (2012). The Impact of Different Elevation Steps on Simulation of Snow Covered Area and the Resulting Runoff Variance. *Advances in Geosciences*, 32, 69-76.

Blöschl, G. (1999). Scaling Issues in Snow Hydrology. *Hydrological processes*, 13(1415), 2149-2175.

Blöschl, G. (2001). Scaling in Hydrology. *Hydrological Processes,* 15(4), 709–711.

Blöschl, G. & Kirnbauer, R. (1991). Point Snowmelt Models with Different Degrees of Complexity — Internal Processes. *Journal of Hydrology,* 129(1–4), 127–147.

Blöschl, G., Kirnbauer, R. & Gutknecht, D. (1991a). Distributed Snowmelt Simulations in an Alpine Catchment: 1. Model Evaluation on the Basis of Snow Cover Patterns. *Water Resources Research,* 27(12), 3171–3179.

Blöschl, G., Kirnbauer, R. & Gutknecht, D. (1991b). A Spatially Distributed Snowmelt Model for Application in Alpine Terrain. *IAHS-AISH Proceedings and Reports,* (205), 3–18.

Braun, L. (1985). Simulation of Snowmelt-Runoff in Lowland and Lower Alpine Regions of Switzerland. *Zürcher Geographische Schriften,* 21,1–166.

Choquette, Y., Ducharme, P. & Rogoza, J. (2013). CS725, An Accurate Sensor for the Snow Water Equivalent and Soil Moisture Measurements. In *Proceedings of the International Snow Science Workshop, Grenoble,* France, 7-11.

Deems, J.S., Painter, T.H. & Finnegan, D.C. (2013). Lidar Measurement of Snow Depth: A Review. *Journal of Glaciology,* 59(215), 467–479.

Dietz, A.J., Kuenzer, C., Gessner, U. & Dech, S. (2012). Remote Sensing of Snow–A Review of Available Methods. *International Journal of Remote Sensing*, 33(13), 4094-4134.

Dozier, J. (1989). Estimation of Properties of Alpine Snow from Landsat Thematic Mapper. *Advances in Space Research,* 9(1), 207–215.

Essery, R., Morin, S., Lejeune, Y.B. & Ménard, C. (2013). A Comparison of 1701 Snow Models using Observations from an Alpine Site. *Advances in Water Resources,* 55, 131–148.

Faroux, S., Kaptué Tchuenté, A.T., Roujean, J.L., Masson, V., Martin, E. & Moigne, P.L. (2013). ECOCLIMAP-II/Europe: A Twofold Database of Ecosystems and Surface Parameters at 1 Km Resolution based on Satellite Information for use in Land Surface, Meteorological and Climate Models. *Geoscientific Model Development*, 6(2), 563-582.

Finger, D., Pellicciotti, F., Konz, M., Rimkus, S. & Burlando, P. (2011). The Value of Glacier Mass Balance, Satellite Snow Cover Images, and Hourly Discharge for Improving the Performance of a Physically based Distributed Hydrological Model. *Water Resources Research*, 47(7), 1-14.

Finger, D., Vis, M., Huss, M. & Seibert, J. (2015). The Value of Multiple Data Set Calibration Versus Model Complexity for Improving the Performance of Hydrological Models in Mountain Catchments. *Water Resources Research,* 51(4), 1939–1958.

Fischer, A., Seiser, B., Stocker Waldhuber, M., Mitterer, C. & Abermann, J. (2015). Tracing Glacier Changes in Austria from the Little Ice Age to the Present using a Lidar-Based High-Resolution Glacier Inventory in Austria. *Cryosphere,* 9(2), 753–766.

van Genuchten, M.T. (1980). A Closed-form Equation for Predicting the Hydraulic Conductivity of Unsaturated Soils. *Soil Science Society of America Journal,* 44(5), 892.

Grünewald, T. & Lehning, M. (2015). Are Flat-Field Snow Depth Measurements Representative? A Comparison of Selected Index Sites with Areal Snow Depth Measurements at the Small Catchment Scale. *Hydrological Processes,* 29(7), 1717–1728.

Haiden, T., Kann, A., Wittmann, C., Pistotnik, G., Bica, B. & Gruber, C. (2011). The Integrated Nowcasting through Comprehensive Analysis (INCA) System and Its Validation over the Eastern Alpine Region. *Weather and Forecasting,* 26(2), 166–183.

Kinar, N.J. & Pomeroy, J.W. (2007). Determining Snow Water Equivalent by Acoustic Sounding. *Hydrological Processes,* 21(19), 2623–2640.

Kirkpatrick, S., Gelatt, C.D. & Vecchi, M.P. (1983). Optimization by Simulated Annealing. *Science,* 220(4598), 671–80.

Kirnbauer, R., Blöschl, G. & Gutknecht, D. (1994). Entering the Era of Distributed Snow Models. *Nordic Hydrology,* 25, 1–24.

Kleindienst, H. (1996). Erweiterung und Erprobung eines anwendungsorientierten hydrologischen Modells zur Gangliniensimulation in kleinen Wildbacheinzugsgebieten. *Institut für Geographie, Ludwig Maximilians Universität München, Germany*.

Kling, H., Fuchs, M. & Paulin, M. (2012). Runoff Conditions in the Upper Danube Basin under an Ensemble of Climate Change Scenarios. *Journal of Hydrology*, 424, 264-277.

Köhli, M., Schrön, M., Zreda, M., Schmidt, U., Dietrich, P. & Zacharias, S. (2015). Footprint Characteristics Revised for Field-Scale Soil Moisture Monitoring with Cosmic-Ray Neutrons. *Water Resources Research,* 51(7), 5772–5790.

Magnusson, J., Gustafsson, D., Hüsler, F. & Jonas, T. (2014). Assimilation of Point SWE Data into a Distributed Snow Cover Model Comparing Two Contrasting Methods. *Water,* 50, 7816–7835.

Monteith, J.L. (1965). Evaporation and Environment. *Symposia of the Society for Experimental Biology,* 19, 205–234

Nagler, T., Rott, H., Ripper, E., Bippus, G. & Hetzenecker, M. (2016). Advancements for Snowmelt Monitoring by Means of Sentinel-1 SAR. *Remote Sensing,* 8(4), 348.

Proksch, M., Rutter, N., Fierz, C. & Schneebeli, M. (2016). Intercomparison of Snow Density Measurements: Bias, Precision, and Vertical Resolution. *The Cryosphere,* 10(1), 371–384.

Revuelto, J., Vionnet, V., López-Moreno, J.-I, Lafaysse, M. & Morin, S. (2016). Combining Snowpack Modeling and Terrestrial Laser Scanner Observations Improves the Simulation of Small Scale Snow Dynamics. *Journal of Hydrology,* 533, 291–307.

Rickenmann, D. (1996). Fliessgeschwindigkeit in Wildbächen und Gebirgsflüssen. *wasser, energie, luft - eau, énergie, air,* 88(11), 298–304.

Rittger, K., Bair, E.H., Kahl, A. & Dozier, J. (2016). Spatial Estimates of Snow Water Equivalent from Reconstruction. *Advances in Water Resources,* 94, 345–363.

Rondeau-Genesse, G., Trudel, M. & Leconte, R. (2016). Monitoring Snow Wetness in an Alpine Basin using Combined C-Band SAR and MODIS Data. *Remote Sensing of Environment,* 183, 304–317.

Schattan, P., Baroni, G., Oswald, S.E., Schöber, J., Fey, C., Kormann, C., Huttenlau, M. & Achleitner, S. (2017). Continuous Monitoring of Snowpack Dynamics in Alpine Terrain by Above-Ground Neutron Sensing. *Water Resources Research*, 53, 1-20.

Schöber, J., Schneider, K., Helfricht, K., Schattan, P., Achleitner, S., Schöberl, F. & Kirnbauer, R. (2014). Snow Cover Characteristics in a Glacierized Catchment in the Tyrolean Alps - Improved Spatially Distributed Modelling by usage of Lidar Data. *Journal of Hydrology,* 519, 3492–3510.

Shrestha, M., Wang, L., Koike, T., Tsutsui, H., Xue, Y. & Hirabayashi, Y. (2014). Correcting Basin-Scale Snowfall in a Mountainous Basin using a Distributed Snowmelt Model and Remote-Sensing Data. *Hydrology and Earth System Sciences*, 18(2), 747-761.

Sigouin, M.J.P. & Si, B.C. (2016). Calibration of a Non-Invasive Cosmic-Ray Probe for Wide Area Snow Water Equivalent Measurement. *The Cryosphere,* 10(3), 1181–1190.

Stähli, M., Stacheder, M., Gustafsson, D., Schlaeger, S., Schneebeli, M, & Brandelik, A. (2004). A New In Situ Sensor for Large-Scale Snow-Cover Monitoring. *Annals of Glaciology,* 38(1), 273–278.

Sturm, M. (2015). White Water: Fifty Years of Snow Research in WRR and the Outlook for the Future. *Water Resources Research,* 51, 4948–4965.

Thirel, G., Salamon, P., Burek, P. & Kalas, M. (2013). Assimilation of MODIS Snow Cover Area Data in a Distributed Hydrological Model using the Particle Filter. *Remote Sensing,* 5, 5825–5850.

Winstral, A. & Marks, D. (2014). Long-Term Snow Distribution Observations in a Mountain Catchment: Assessing Variability, Time Stability, and the Representativeness of an Index Site. *Water Resources Research,* 50(1), 293–305.

Zappa, M., Pos, F., Strasser, U., Warmerdam, P. & Gurtz, J. (2003). Seasonal Water Balance of an Alpine Catchment as Evaluated by Different Methods for Spatially Distributed Snowmelt Modelling. *Nordic Hydrology,* 34(3), 179–202.

UPDATED PARTICLE SWARM OPTIMIZATION (PSO) ALGORITHM IN CALIBRATING RESERVOIR RELEASE POLICY

MD. SHABBIR HOSSAIN[(1)] & LARIYAH MOHD SIDEK [(2)]

[(1)] Universiti Tenaga Nasional (Putrajaya Campus), Kajang, Malaysia, 43000.
mdshabbir@uniten.edu.my
[(2)]Sustainable Technology & Environment Group, Institute for Energy Infrastructure, Universiti Tenaga Nasional, Selangor, Malaysia
Lariyah@uniten.edu.my

ABSTRACT

Particle swarm optimization is a very well-known method as it has a strong background in optimization field to solve different non-linear and complex problems. This study made a fine tuning in the particle updating process of standard PSO algorithm. The updated algorithm is used to develop and optimize a reservoir release policy for monthly basis. The historical data of inflow to the dam/reservoir has categorized in three different categories (high, medium and low). The problem formation has done on the basis of release and storage constraints. The objective function which was aimed to be minimized has been considered as the water deficit from the release. The monthly releases are taken as the main objective variables and are essentially control the water deficit of the process. The standard form of PSO is then compared with the updated version and the results are analyzed by adopting different performance measuring indicators such as reliability, vulnerability and resilience. These performance measuring indices are calculated from the outcome of the simulation process by feeding the optimization model with the actual historical data of inflow. From the results of the simulation and the value of the indicators, the study shows updated PSO algorithm performs significantly better in optimizing reservoir releases policy.

Keywords: Reservoir release policy; optimization; swarm intelligences; PSO; water resources management.

1 INTRODUCTION

Belonged to the Swarm Intelligence (SI) family, Particle Swarm Optimization (PSO) is a very popular tool in solving real life optimization problems. When the system is nonlinear and has several conflicting constraints, the PSO works very well and it is also relatively faster and easy to apply (Kennedy and Eberhart 2001). The simplicity and the applicability of PSO and the other SI techniques attracts many researchers to use it in solving different hydrological problems. This study was also intended to do same, including updating the key mechanism of the particle movement (velocity update) in the standard PSO algorithm. Both the standard and the updated PSO were formulated and tested to optimize the release policy of a reservoir system. The monthly releases were taken as decision variables bounded by release constraints. The formulation of the reservoir system was also considered to be subjected to the storage constraints and continuity equation. The problem has been formulated as a simple method that can be optimized by any improved population-based search techniques. Also, the representation of the release policy itself has been modified in such a way that the decision maker may have a clear understanding in deciding on the release amount. For verification of the model, simulation has been undertaken and the simulation results have been analyzed using the risk analysis approach to compare the models efficiency in minimizing water deficit. The Aswan High Dam (AHD) was considered as the case study in this case, which contributes as a major irrigation structure in Egypt. Some of the literature related to this study can are given here- Hossain MS. et al. (2016), Hossain MS. et al. (2015), Ahmed and Sharma (2005), El-Shafie and El-Manadely (2011).

The basic idea of PSO comes from the intelligent behavior of a flock of birds moving around in search of food. The choreography of the flight allows them to share all the information about the food once it is discovered. The direction and velocity of the flight change accordingly on the basis of this information. Kennedy and Eberhart (1995) first proposed the PSO algorithm. They described the social behavior of the flock on the phenomena of comparing two important decision properties named as “local best” and “global best”. Local best is the currently observed best decision for a particular food and the global best is the best decision found. Later, He et al. (2004) proposed passive congregation theory to improve the performance of standard PSO, inspired by the mathematical model of the social behavior of living organism.

2 PROBLEM FORMULATION FOR RESERVOIR SYSTEM OPERATION

In AHD, the operation policy has the flexibility of release no flow to maintain the storage bounds and specifications. 7.5 Billion Cubic Meter (BCM) has taken as the maximum release in a month. So, the release constraint is $0 \leq R_t \leq 7.5$ BCM. The water level for any time should be in the range of 147 to 183 m. So, in terms of the storage, this study has considered it to be $32 \leq S_t \leq 162$ BCM (for t = Jan, Feb, Dec). The actual natural inflow data is used to run the model and for simulation purposes. Eighteen years (Aug 1980 to Jul 1998) of historical data of monthly inflow was taken to discretize the whole inflow pattern into three states. Each inflow state, as well as the release curve generated from any optimization model, controls the release option.

Generally, in the reservoir operation, the authorities may face two types of constraints in deciding on the release amount, bounds on release volume and keeping the water level within a safe operational zone. In order to maintain these aspects, the problem has been formulated in the following form:

- Objective function / Fitness function:
- Minimization of water deficit (equation 1)

$$\text{Min } Z = \sum_{t=1}^{12} (D_t - R_t)^2 \quad [1]$$

- Subjected to:
- The releases (R) for any time period (t) must be within the upper and lower bounds,

$$R_t - R_{\min} \geq 0 \text{ and } R_{\max} - R_t \geq 0 \quad [2]$$

- Storages (S) for any time period (t) must be within the upper and lower bounds, [3]

$$S_t - S_{\min} \geq 0 \text{ and } S_{\max} - S_t \geq 0 \quad [3]$$

- Continuity equation should be satisfied for all time period, *t.*

$$S_{(t+1)} = S_t + Inflow_t - R_t - Losses_t \quad [4]$$

The concept of using a penalty function is based on adopting an extra parameter in addition to the objective function that controls the constraints and helps to eliminate the decision variables that cause violation of any constraints. As Equation 1 represents a minimization problem, the model always preferred to obtain the minimum value of *Z*. So, if any release policy caused the reservoir storage to violate the boundary condition (Equation 3), then the penalty term will increase the value of *Z* based on the violation magnitude. The variables that increase the value of *Z* have been denoted as weaker solutions and have been eliminated to reach an optimum state.

3 STANDARD PSO IN RESERVOIR SYSTEM OPTIMIZATION

Like the other heuristic approaches, PSO begins with generating a random decision variable set. The random variables are called "particles" and the variable set a "swarm" (given in Equation 5 and 6). So, in a random release string consisting of 12 values of water volume to be released (R) from January to December the 12 releases are considered to be particles and the population set of these particles is considered to be a swarm.

$$\begin{aligned} &particles = [R_{Jan}, R_{Feb}, ..., R_{Dec}] \\ &where,\ R_{\min} \leq R_i \leq R_{\max}\ for\ i = Jan,\ Feb, ..., Dec. \end{aligned} \quad [5]$$

$$\text{swarm} = \begin{bmatrix} particles_1 \\ particles_2 \\ ...... \\ .... \\ particles_{popsize} \end{bmatrix} \quad [6]$$

$$[\text{swarm}]_{(popsize \times nvar)} = (R_{\max} - R_{\min}) \times [r]_{(popsize \times nvar)} + R_{\min}. \quad [7]$$

where,

popsize = population or swarm size
nvar = total number of variables
r = random number between 0 and 1.

To generate the initial swarm for the PSO algorithm, Equation (7) has been used in this study. An equation (named the velocity update) controls the swarm in moving around the search space searching for the optimum. In each iteration, the algorithm saves the local optimum and compares it with the global (best yet) optimum values. Definitely, the criteria for being chosen as an optimum state depend on the fitness of the objective function.

The candidate solutions (decision variables: releases) of the particles calculate and remember their own fitness. The position of any particle is accelerated towards the global best position by using Equations (8) and (9). In any search step t, the i'th particle use to update its candidate solution's current position (xtij) by using local best (ptij) and global best (ptgj) position achieved yet.

$$v_{ij}^{t+1} = wv_{ij}^{t} + \phi_1 r_1^t (p_{ij}^t - R_{ij}^t) + \phi_2 r_2^t (p_{gj}^t - R_{ij}^t). \qquad [8]$$

$$R_{ij}^{t+1} = v_{ij}^{t+1} + R_{ij}^t. \qquad [9]$$

where

v_{ij}^{t+1} = velocity measures for the particles,

w = inertial weight; control the velocity direction,

ϕ_1 & ϕ_2 = acceleration coefficient; should be > 1 (mostly taken as 2),

r_1^t & r_2^t = random numbers; uniformly distributed between 0 and 1,

R_{ij}^t = position of any particle at t,

p_{ij}^t = best release options (providing lowest Z) at t,

p_{gj}^t = best release options (providing lowest Z) achieved yet.

After generating the initial population (randomly generated monthly release options), the velocity update provides a new direction to the particles. With a new velocity, a new position is reached, as given in Equation 9. The fitness (Z) is calculated by using the objective function (Equation 1) including the penalty for constraint violation and the best position of the particle is saved as the local best. The whole population (swarm) then turns towards the current best position until it finds another better solution than the current one. An iteration number need to be provided at the beginning of the algorithm. This iteration fixes the stopping criteria for the algorithm.

4 UPDATED PSO WITH PASSIVE CONGREGATION THEORY

In 2004, He et al. (2004) proposed to add the passive congregation factor with PSO velocity update. Based on the mathematical model of Parrish and Hamner (1997), the aggregation can be referred as grouping of the organisms (such as fish schooling and bird flocking) by external physical forces. On the other hand, congregation is defined as grouping by social forces where the attraction source is the group itself. In passive congregation theory, any individual group members attract the other but they may show no social behavior (global best). In these congregations, information may be transferred passively rather than actively (Magurran and Higham, 1988). To adopt this opportunity, we need to add information randomly from the population and make sure that the position is shifting accurately towards the global best.

In Equation 8, the third parameter, $\phi_2 r_2^t (p_{gj}^t - R_{ij}^t)$ is classified as active congregation (He et al., 2004). To adopt the passive aggregation theory, He et al. (2004) proposed by adding another term to keep the model simple and uniform. The modified velocity function is given in Equation 8:

$$v_{ij}^{t+1} = wv_{ij}^{t} + \phi_1 r_1^t (p_{ij}^t - R_{ij}^t) + \phi_2 r_2^t (p_{gj}^t - R_{ij}^t) + \phi_3 r_3^t (X_{gj}^t - R_{ij}^t). \qquad [10]$$

where

X_{ij}^{t+1} = randomly selected particle from the swarm,

ϕ_3 = passive congregation coefficient,

r_3^t = random numbers; uniformly distributed between 0 and 1

5 RESULT AND DISCUSSION

The release volume depends on the inflow category, operational time period (monthly) and current reservoir storage or water level. For each inflow category, the release policies have been given for every month to consider the storage condition as input parameter. With this release curve, one is able to decide on how much water release would be optimum for a particular month of the year to properly minimize the water deficit. The optimal release options for the month of April are given in Figure 1.

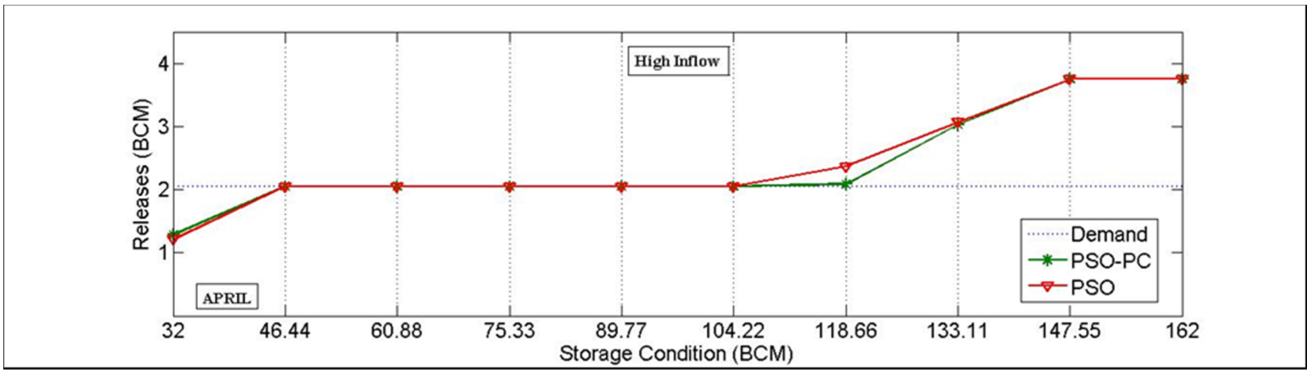

(a) High Inflow condition

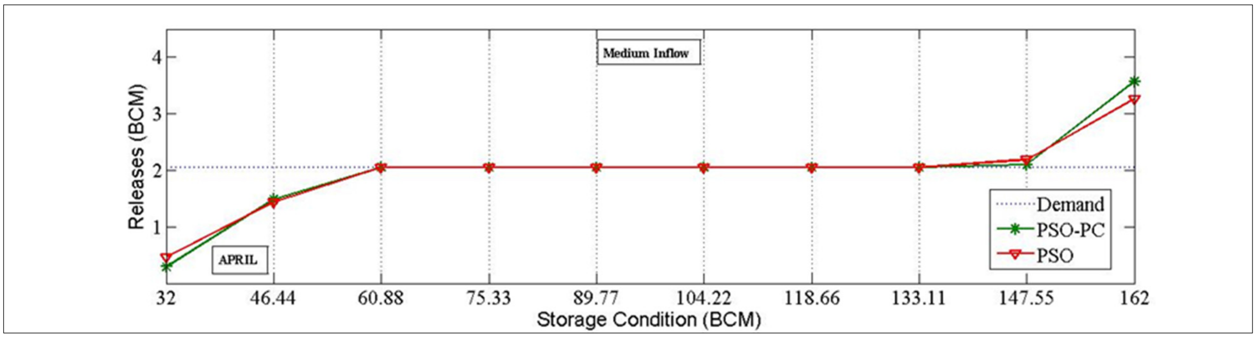

(b) Medium Inflow condition

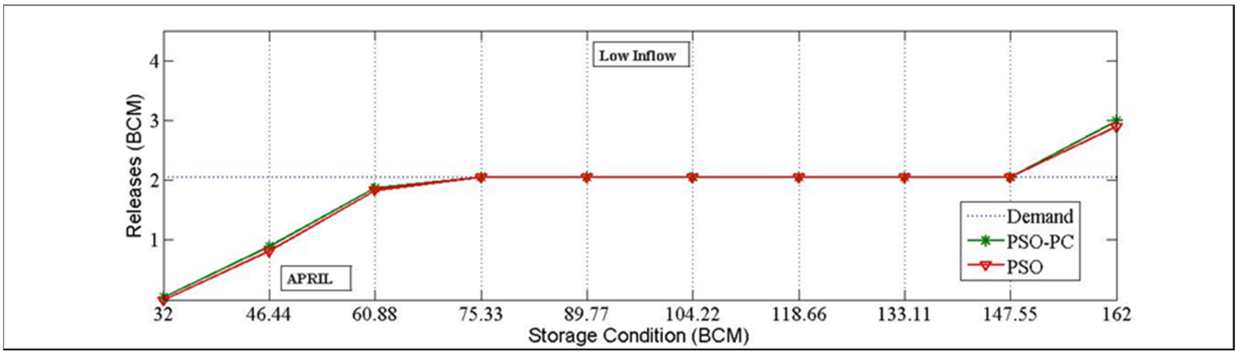

(c) Low inflow condition

Figure 1. Release curves for the month of April for High (a), Medium (b) and Low (c) inflow condition.

Each release curve provides the release amount under different storage conditions. The characteristics of the curves showed logical expressions with regard to the decision to release water. For the high and medium inflow categories, the release curves able to meet the demand line for low storage amounts, as there is adequate water available to release from inflow. With increasing storage capacity, the suggested releases are more likely to meet the demand and for extreme storage conditions it is suggested that more than demand is released to keep the storage levels in safe ranges.

To check the model efficiency, we adopted a very classical approach by measuring three measuring indices: Reliability (Wurbs 1996), Resiliency (Loucks et al., 2005) and Vulnerability (Loucks et al., 2005), from the simulated results. The equation for these indices are given in Table 1.

Table 1. Performance measuring indices.

Index	Equation	Variables
Volumetric (R_v) and Periodic (R_p) reliability	$R_v = (v/V) \times 100\%$; $R_p = (n/N) \times 100\%$	v = volume of water releases (model output) V = volume of targeted demand n = total no. of time period meeting the targeted demand (in months) N = total no. considered time period (in months)
Resilience (R_S)	$\mathrm{R}_S = \dfrac{NS}{NT}$	NS = no. of satisfied (zero deficit) time period followed an shortage NT = no. of total shortage period
Vulnerability (V)	$\mathrm{V} = \dfrac{1}{m} \times \sum_{t=1}^{N} [\max(0,\ D_t - R_t)]$ for $t = 1, 2, ...N$	m = no. of model failure period (water deficit ≠ 0) N = total time period considered for simulation (in months) D = targeted demand R = water release (model output)

For simulation, actual data of the reservoir (inflow and storage) was feed to the release curves and the results from the curves are recorded for that particular month. Then, the final storage was calculated by using the continuity equation and used as an initial storage for the next month. The simulation steps for a total considered time period (T) are given in Figure 2.

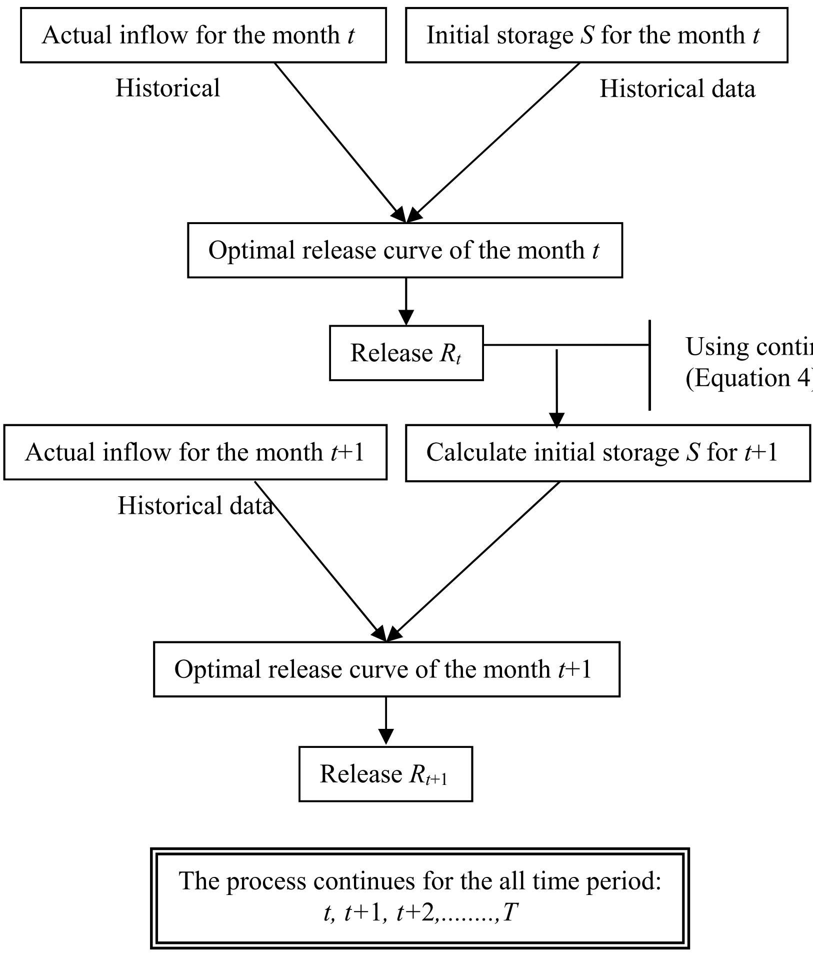

Figure 2. Simulation process by using historical data.

5.1 Reliability, Resilience and Vulnerability measures

Among 216 monthly (18 years) releases, the PSO-PC release policy provided the exact water release as per demand 137 times (63.4 %). The standard PSO algorithm provided the exact required release127 times (58.8 %). Table 2 reports the information on these issues, including the events of exceedance and shortage.

Table 2. Periodic reliability and Vulnerability for AHD.

Optimization techniques	More than demand	Meet the demand	Less than demand	Total no. of release	Vulnerability (V)
PSO-PC	35.1 % (76 times)	63.4 % 137 times	1.3 % 3 times	216	0.05
PSO	38.9 % (84 times)	58.8 % (127 times)	2.3 % (5 times)	216	0.07

The vulnerability (V) of each model has been calculated by using vulnerability equation (V from Table 1) and also given in Table 2. From the simulation results of both the models, PSO-PC is comparatively less vulnerable than PSO.

Table 3. Resiliency measures from the simulation.

Measures	ABC	PSO
Resiliency (R_s)	15.5	14
Max. no. of consecutive shortage period	1	1

The other effective performance indicator is resiliency, the recovering capability from a failure. The resilience equation (reported in Table 1) has been used to find out the resilience of both optimization model from the simulation results. Also, the maximum number of consecutive shortage (release less than demand) period has been calculated and saved for resilience measures. The resilience analysis of these two case studies is given in Table 3. In this case, PSO-PC performed slightly better as it shows larger R_s value. Also, the maximum number of consecutive shortage period is same in both cases.

From these analysis, it seems that PSO-PC is more capable of providing optimum release for a reservoir system than PSO. The standard PSO was also a very good optimizer but PSO-PC performed better in terms of reliability, resiliency and vulnerability.

6 CONCLUSION

The PSO-PC is the improvement of the standard PSO by adopting passive congregation theory in particle movement. The primary objective of this study was to use this both version of PSO to optimize the reservoir release of AHD and compare the results. To test the performance, three basic indicators were adopted: Reliability, Resilience and vulnerability. All three indicators are indicating that both PSO acted very well in handling reservoir system but PSO-PC is more capable (5% more reliable, 0.02 less vulnerable and 1.5 more resilience) in providing optimum results for a reservoir system.

REFERENCES

Kennedy, J.F., Kennedy, J., Eberhart, R.C. & Shi, Y. (2001). *Swarm Intelligence*. Morgan Kaufmann. 1-512.

Hossain, M.S., El-Shafie, A., Mahzabin, M.S. & Zawawi, M.H. (2016). System Performances Analysis of Reservoir Optimization–Simulation Model in Application of Artificial Bee Colony Algorithm. *Neural Computing and Applications*, 1-12.

Hossain, M.S., El-Shafie A. & Mohtar, W.W. (2015). Application of Intelligent Optimization Techniques and Investigating the Effect of Reservoir Size in Calibrating the Reservoir Operating Policy. *Water Policy*, 17 (6), 1143-1162.

El-Shafie, A.H. & El-Manadely, M.S. (2011). An Integrated Neural Network Stochastic Dynamic Programming Model for Optimizing the Operation Policy of Aswan High Dam. *Hydrology Research,* 42(1), 50–67.

Ahmed, J.A. & Sharma, A.K. (2005). Genetic Algorithm for Optimal Operating Policy of a Multipurpose Reservoir. *Water Resource Management*, 19(2), 145–161.

He, S., Wu, Q.H., Wen, J.Y., Saunders, J.R. & Paton,R.C. (2004). A Particle Swarm Optimizer with Passive Congregation. *Biosystems*, 78(1), 135-147.

Parrish, J.K. & Hamner,W.M. (1997). *Animal Groups in Three Dimensions*. Cambridge University Press, Cambridge, UK.

Magurran, A.E. & Higham, A. (1988). Information Transfer Across Fish Shoals under Predator Threat. *Ethology*, 78(2), 153–158.

Wurbs R.A. (1996). *Modelling and Analysis of Reservoir System Operations*. Prentice-Hall, Inc, Upper Saddle River, NJ, USA.

Loucks D.P., Beek, E.V., Stedinger, J.R., Dijkman, J.P. & Villars MT (2005). *Water Resources Systems Planning and Management: An Introduction to Methods, Models and Applications*. UNESCO Publishing, Paris.

Proceedings of the 37th IAHR World Congress
August 13 – 18, 2017, Kuala Lumpur, Malaysia

COPULA-BASED UNCERTAINTY ANALYSIS FOR THE IMPACT OF MULTI-WATER RESOURCES ON OPTIMAL ALLOCATION AND AGRICULTURAL SHORTAGE

YINZHU LIU(1), XUEPING GAO(2) & BOWEN SUN(3)

(1,2,3) State Key Laboratory of Hydraulic Engineering Simulation and Safety, Tianjin University, Tianjin 300072, China,
lyztju@163.com

ABSTRACT

This study presents a copula-based chance-constrained optimization approach for integrated agricultural water and water resources management. The construction of water transfer projects brings new challenges to water resources management, especially in water rational allocation and supply risk with multiple water resources. Transferring water and local surface water are both influence factors of water allocation and the individual effect, and their combination should be considered to assess water supply risk better. Besides, due to the growth of irrigated area and water diversion from agriculture to municipality and industry, the lack of agricultural water become the obstacle of urban development. It is necessary to determine the laws of the relationship between water ability and the loss in different combination of multi-water resources. A copula-based approach is proposed for estimating the joint probability of available multi-water and sampling from multivariate probability distribution. The multi-objective optimization model was employed to provide the optimal water allocation solution with multi-water resources. The relationship curves under the different multi-water resources supply conditions between the joint probability and the agricultural shortage were fitted to assess the impact of multi-water resources on the loss caused by conveyance. The study also offers an approach for effective and reliable identification of important allocation model influence factors, responding to the priorities of different water resources. It can improve the ability of multi-water resources overall distribution and the adaptation to uncertainty water resources, aiming to reduce the water supply risk and achieve sustainable development. Furthermore, the results of the study emphasize the importance to improve and update transferring and local water management and relevant countermeasures in order to ensure future water security.

Keywords: Uncertainty; joint probability; multi-water resources; water allocation optimization; agricultural shortage.

1 INTRODUCTION

The optimal allocation of available water resources is quite necessary in areas of severe water shortage in China. To solve the contradictions between the supply and demand of water resources and to mitigate losses, water resource diversion and allocation have been developed. However, several uncertain factors may affect the performance of water allocation(Li et al., 2008; Zeng et al., 2015). For natural impacts, the assumption that the characteristics of available water resources will follow a probability distribution, which is affected by the flows of rivers, streams, varied precipitation, and runoff levels, etc. On the other hand, due to the growth of irrigated area and water diversion from agriculture to life and industry, the lack of agricultural water become the obstacle of urban development. It is necessary to determine the laws of the relationship between water ability and the loss in different environment. Water allocation plan development is not straightforward due to the limited available water resources and uncertainties. Previous research into optimal water resources has mostly focused on embodying various characteristics in deterministic values and intervals(Zhou et al., 2015; Zhuang et al., 2015), but only a few works have been done to consider the various complexities in terms of relationship of multi-water resources. Correspondingly, more in-depth research to water resources allocation associated with available water resources probabilities and agricultural water shortage should be considered, depending on the origins of the uncertainties. The study aims to provide scientific, timely, quickly decision-making to inter-basin water transfer management, to provide risk evaluation and decision support for planning water allocation and agricultural activities.

2 MATERIALS AND METHOD

This paper assesses the implications of multi-water resources change on the water resource shortage for the Lunan water-receiving area (Figure 1) for a range of 800 scenarios from a combination of projected different water resources, demand and conveyance loss. The input data in this study come from historical literature review and statistical yearbooks.

The methodology described here is based on integrating the uncertainty analysis methods and mathematical modeling techniques, including a copula-based Monte Carlo simulation (MCS) and multi-objective optimization tools. The statistical copula function was adopted to obtain the joint probability distribution for water resources by separating their dependence from their marginal distributions. The most credible distribution was then used through the Monte Carlo simulation (MCS) to generate multivariate samples set for purpose of investigating the uncertainties of water resources. The ε-NSGA Ⅱ was used to estimate the water availability and shortage of different water users. The conclusion of the analysis is useful for the comprehension of the multi-water resources and consequently, the significance of certain water resources related management planning. The following subsections elaborate on the detailed description.

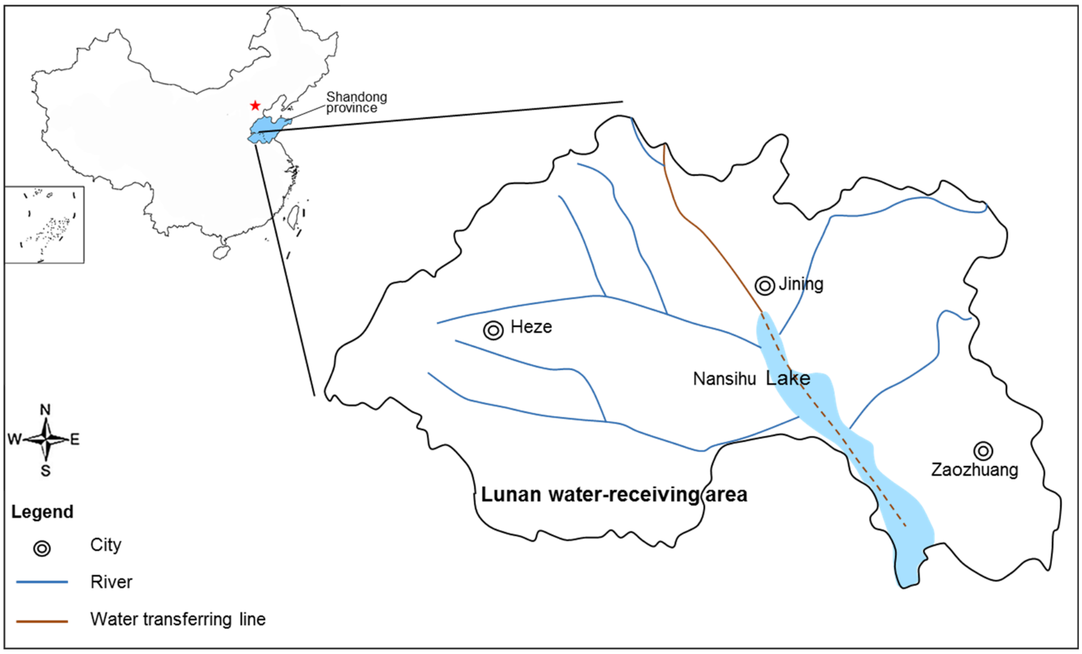

Figure 1. Diagram of the study area.

2.1 Copula function

In this study, copulas were used to describe the relevant relationships(Yazdi, 2014), which can make it easier to formulate multivariate models compared to other limited and complex models. Copulas are functions that link univariate marginal distribution to form a multivariate distribution. According to Sklar's theorem (Sklar, 1960), if the marginal distributions and are determined, the joint cumulative distribution function F with random variables x and y can be expressed with the function *C* as follows:

$$F(t,l) = C\left(F_T(t), F_L(l)\right) \equiv C_\theta(u,v) \qquad [1]$$

where $u = F_T(t)$, $v = F_L(l)$, *C* is the copula function that connects the marginal and joint distribution, θ is the parameter of copula function. If $F_T(t)$ and $F_L(l)$ are continuous functions, the joint distribution can be uniquely determined by the marginal distribution and structure correlation. Three widely used one-parameter Archimedean copulas, Clayton, Gumbel and Frank copula were compared to choose the best-fit one in the study(Nelsen, 1998) (see Table 1).

Table 1. Definition of the widely used one-parameter copula families.

Copula type	Copula function	Range of parameter
Clayton	$\left(u^{-\theta} + v^{-\theta} - 1\right)^{-1/\theta}$	$\theta \geq 0$
Frank	$-\frac{1}{\theta}\ln\left[1 + \frac{\left(e^{-\theta u} - 1\right)\left(e^{-\theta v} - 1\right)}{e^{-\theta} - 1}\right]$	$\theta \neq 0$
Gumbel	$\exp\left\{-\left[\left(-\ln u\right)^{\theta} + \left(-\ln v\right)^{\theta}\right]^{1/\theta}\right\}$	$\theta \geq 1$

The best family of copulas were determined by the maximum likelihood (ML) method. In the ML method, the copula function that has the greatest likelihood value is selected to fit over the data. Moreover, the copula parameter θ can be estimated by maximizing the following likelihood function:

$$\ln L(t,l;a_0,\alpha,\beta,a_{01},\alpha_1,\beta_1,\theta) = \ln L_C(F_T(t),F_L(L);\theta) + \ln L_T(t;a_0,\alpha,\beta) + \ln L_L(l;a_{01},\alpha_1,\beta_1) \quad [2]$$

where $\ln L_C$ is the log-likelihood function of copulas, $a_0,\alpha,\beta,a_{01},\alpha_1$ and β_1 are parameters of marginal distributions, the log-likelihood function $\ln L$ is maximized to obtain the copula parameter θ.

When the best-fit copula is chosen, the joint behavior that t and l both exceed specific values should be focused on. The joint impact of multi-water resources on the allocation was estimated using joint probability as the evaluation index. The joint probability is as follows:

$$P\cap(t,l) = P((T>t)\cap(L>l)) = 1 - F_T(t) - F_L(l) + F(t,l) \quad [3]$$

2.2 Generating synthetic multi-water resources

The inverse distribution function method was employed to generate a sample (t,l) from the most fitted joint distribution. According to the Sklar theorem, the conditional distribution function $c_u(v)$ for V given $U=u$ is presented as follows:

$$c_u(v) = P[V \le v | U=u] = \lim_{\Delta u \to 0} \frac{C(u+\Delta u,v) - C(u,v)}{\Delta u} = \frac{\partial C(u,v)}{\partial u} \quad [4]$$

For generating the sample (t,l) of a pair of random variables (transferring and local surface water resources), the steps are as follows:

(1) Generate two independent uniform (0,1) variates u and w;

(2) Set $v = c_u^{(-1)}(w)$, where $v = c_u^{(-1)}$ is the inverse function of c_u;

(3) For the pair (u,v), set $t = F^{-1}(u)$ and $l = F^{-1}(v)$. So, the sample point is (t,l).

In the first step, the Latin hypercube sampling (LHS) method (Mckay et al., 2000) was adopted to effectively reduce the unevenness and improve precision of sampling.

2.3 Optimization model

As a multi-objective optimal allocation problem, the implementation of optimization schemes is necessary. In this paper, the ε-nondominated sorted genetic algorithm II (ε-NSGAII) as a popular multi-objective evolutionary algorithm was introduced to solve the problems of optimal multi-water resources allocation. Compared with the other algorithm, ε-NSGAII can lead to less search failures and computation load for many engineering optimization problems. The appropriate allocation plans depend on their utilization efficiency and economic efficiency. Therefore, the regulated objectives in this paper included two objectives: the minimization of water shortage and allocation cost simultaneously.

Thus, the problem could be expressed as follows:

(1) Allocation cost:

$$\min f_1 = \sum_{i=1}^{I}\sum_{j=1}^{J} x_{ijt} c_{ij} \alpha_i \quad [5]$$

(2) Water shortage:

$$\min f_2 = \sum_{j=1}^{J}(D_j - \sum_{i=1}^{I}\alpha_i x_{ijt}) \quad [6]$$

where *i* denotes different water resources; *j* denotes water user; *t* represents the various scenarios of transferring and local surfer water resources, that is, *t* represents different joint probabilities; x_{ijt} is the amount of water supply of different water resource *i* distributed to different water users *j* under scenario *t*; c_{ij} is the water supply cost of different water resource *i* distributing to different water users *j*; α_i represent the different priority of water resources; D_{ij} is the fixed target needs of water. In the study the water demand was assumed to be the same in all scenarios.

These were subject to:
(1) Restriction of the water supply amount:

$$\sum_{j=1}^{J} x_{ijt} \le W_{i\max} \quad [7]$$

where $W_{i\max}$ is the maximum water supply amount of water resource *i*.
(2) Restriction of water demand amount:

$$D_{j\max} \ge \sum_{i=1}^{I} x_{ijt} \ge D_{j\min} \quad [8]$$

where $D_{j\max}$ and $D_{j\min}$ are the maximum and minimum water demand amount of water user *j*.
(3) Restriction of water-carrying capacity:

$$Pr\left\{\sum_{j=1}^{J} x_{ijt}\left(1+\lambda\right) \le W_{it}\right\} \ge 1-q \quad [9]$$

$$\lambda \sim \left(\mu, \sigma^2\right) \quad [10]$$

In the constraint condition, the constraints are satisfied at a certain probability $(1-q)$, where *q* stand for a predetermined probability set by managers, denoting the acceptable level to violate the constraint (Sun et al., 2013; Zhuang and Zeng, 2015). This constraint allows the spill of water conveyance. The water loss rate λ of the constraints was treated as a normally distributed random parameter (μ is the expectation and σ is the standard variation). The water loss rate was *N* (0.04, 0.062) in this study.
(4) Nonnegative constraint:

$$x_{ijt} \ge 0 \quad [11]$$

3 RESULTS AND DISCUSSIONS

3.1 Establishment of joint probability distribution

For transferring water resource *T* and local surface water resource *L*, the marginal distributions of $F_T(t)$ and $F_L(l)$ obeyed a Person type-III (P-III) distribution(Peng and Xu, 2010). For *T* and *L*, the parameters of the marginal distribution were estimated on the statistics reported in Table 2, and the distribution probability curves are shown in Figure 2. Based on the ML criterion (see Table 3), the Clayton copula function was chosen for synthetic multi-water resources during the MC process. The joint probability distribution of *T* and *L* is shown in Figure 3. A sensitivity analysis found that taking 200 samples from the fitted copula was sufficient for optimization.

Table 2. Estimated parameters of P-III distribution for annual water resource series.

Parameters	Transferring water	Local surface water
α_0	4.5948	10.5018
α	0.7991	0.3491
β	8.8642	10.3115

Table 3. Parameters and goodness-of-fit test of copulas.

	Clayton	Frank	Gumbel
Parameter θ	0.8571	2.9174	0.4548
Likelihood	-197.8271	-163.2077	-154.4219

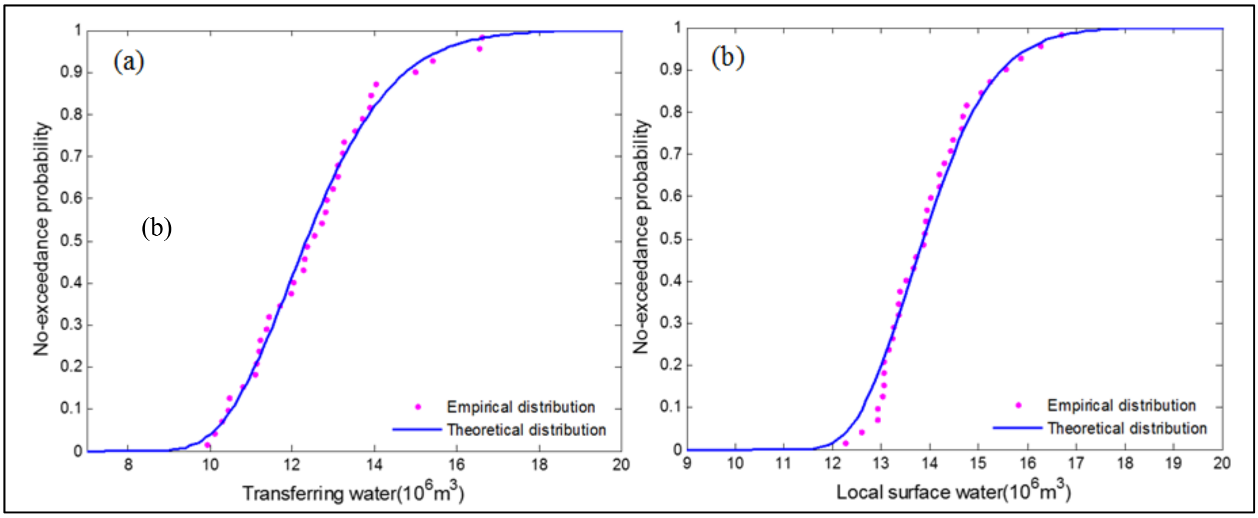

Figure 2. Comparisons of the empirical and theoretical marginal distributions: (a) transferring water resource; (b) local surface water resource.

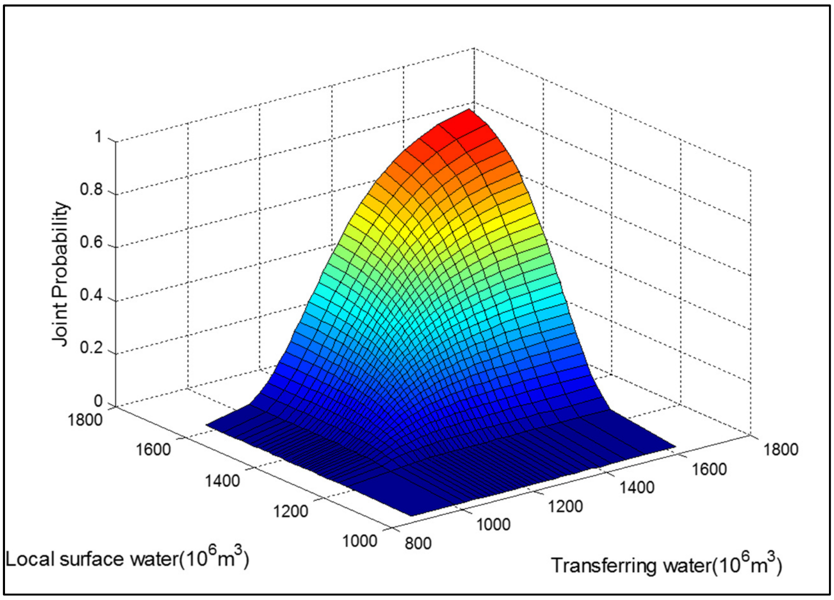

Figure 3. Joint probability distribution of transferring and local surface water resources.

3.2 Optimal water allocation

This model was used to research the optimal allocation of multi-water resources in the water-receiving area with a whole consideration of issues including growth, fairness and efficiency. The results showed that there will still be a degree of water shortage. In a water-receiving area, the water shortages and use of water resources can have a direct influence on the urban development. From the analysis and result of the multi-water resources system, it is considered that the rate of relative scarcity of water (Wang, 2006) can be an powerful tool to reveal the severity of water resource shortages and competitive water use. The water scarcity ratio is defined as the following equation:

$$\mathrm{SI}_j = \frac{D_j - \sum_{i=1}^{I} x_{ij}}{D_j} \qquad [12]$$

where SI_j is seen as the shortage index for water user *j* (municipal user when $j=1$, industry user when $j=2$, ecological user when $j=3$, agricultural user when $j=4$).

Table 4. The water scarcity ratio of water users under different conveyance loss.

	Municipal	Industry	Ecology	Agriculture
No conveyance loss	0	0.0059	0.0332	0.0432
q=10%	0	0.0065	0.0378	0.0483
q=5%	0	0.0068	0.0421	0.0573
q=1%	0	0.0148	0.0499	0.0735

It is obvious that water scarcity ratios of users increase given that violating probability decreases. This is because the CCP requires that the constraint should be satisfied with at least a probability level (1-*q*) when certain violating probability level is *q*. Higher violating probability represents relaxation of system constraint, and this can result in less water shortage. Taking agriculture water-using department as an example, the water scarcity ratios falls from 0.0735 to 0.0483 by violation probability from 1% to 10%. Hence, higher constraint violating probability leads to more water availability, correspondingly a higher water use efficiency and system cost. On the contrary, the optimistic managers would choose the higher violating probability to get lower water shortage and higher water use efficiency.

In addition, the water scarcity ratio of municipality is zero, which means the available water can meet the requirement of municipality. That is because the municipal allotment should be first guaranteed, regardless of available water levels. The water scarcity ratio of the others, however, is not zero, but shows variations between different users because of the cost of various water users. When *q* is 1%, the water scarcity ratios of industry, ecology and agriculture are 0.0148, 0.0499 and 0.0735 respectively, showing a trend of increase. High shortage mainly occurs for the agriculture because of the largest percentage of water demand and low benefit. Due to the large shortage of agriculture, it is necessary to determine the laws of the relationship between water ability and the loss in different combination of multi-water resources.

3.3 Risk assessment curves for agricultural water

From these results, it can be concluded that the scale of the agricultural shortage is significantly correlated with various combination of water supply. For agricultural water shortage, its occurrences, change characteristics and possible causes should be closely concerned because of its multiple uncertainties. The traditional method is only dependent on extensive farmland and irrigation surveys, rather than agricultural water shortage assessment in terms of various probabilities of occurrence. The curves of agricultural water shortage under different conveyance loss are fitted by using logarithmic functions with correlation coefficients from 0.9306~0.9387 shown in Figure 4.

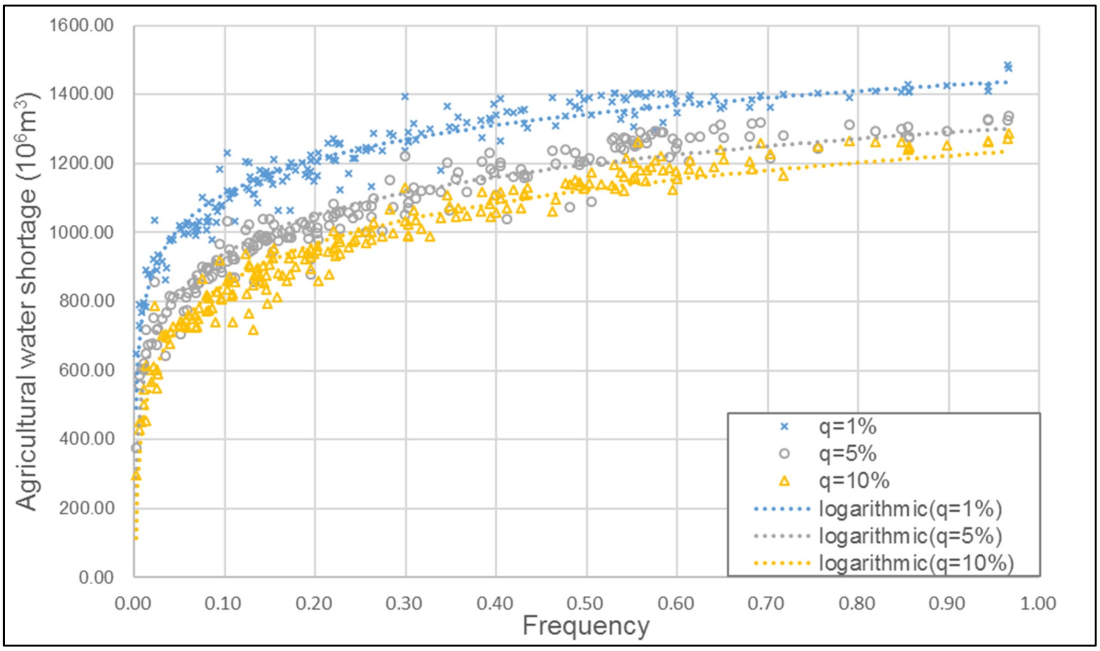

Figure 4. Relationship curves under different conveyance loss between the combination frequency of multi-water resources and agricultural water shortage.

From the three curves, we can infer that with the available water resources increasing, the water shortage of agriculture decrease. The lower combination frequency of multi-water resources, which means the more available water supply, the lower will be the shortage caused. At the same time, the high-frequency event will cause high shortage. Moreover, the figure also presents the trend of agricultural water shortage under different conveyance loss (different *q*). A conclusion could be made from comparing the water deficits in

  / ISSN 1562-6865 (Online) - ISSN 1063-7710 (Print)

three q levels: a greater water shortage would exist under lower q levels, while a smaller water shortage corresponded to high q levels. The constraint allowed the spillage of water during delivery in the model, and its acceptable level could be adjusted by managers. It can be explained that the relaxations (a higher q) of constraint would lead to raised available water resources and reduced water losses, correspondingly smaller water shortage. The laws from the three curves are almost the same with the objective facts, so the fitting curves can be used to analyze the impact of different combination of multi-water resources on the shortage of agriculture. In this way, different decision schemes would be obtained under different water availability levels and violating probabilities with focusing on extreme situation, in order to provide insights into agricultural shortage conditions and thus promote water-saving measures.

3.4 Sensitivity analysis

In order to clarify the impact factors of water shortage, the study made the sequences of the importance of all water resources. From there, it produces a variance-based global sensitivity measure with dependent inputs(Anstett-Collin et al., 2014; Mara and Tarantola, 2012), linking uncertainty and sensitivity analyses. The sensitive analysis indicate that the sensitivity index of groundwater water supply is the greatest (0.42), followed by transferring water (0.37) and local surface water (0.20). This indicates that the municipality and production supplies are mainly from groundwater, and that the transferring water resource plays an important role. Meanwhile, the total surface water supply composed of transferring and local surface water is greater than the groundwater supply. These can therefore be concluded that the goal of reducing the groundwater exploitation has been gradually achieved, and the water supply structure has been optimized.

4 CONCLUSIONS

This paper has presented a risk-based chance-constrained optimization approach for analyzing agricultural water and water resources management by integrating the copula method, MCS and multi-objective optimization. Considering the dependence structure of transferring and local surface water resources, the copula-based MCS methodology provided more realistic samples for evaluating the combination of multi-water resources, which reserved the uncertainty during the optimization process. The results showed that the water scarcity ratio of agriculture is the highest, meaning that different combinations of multi-water resources have the greatest influence on the agriculture. The agricultural shortage risk assessment curves were fitted by using joint probability and the water shortage of agriculture under different conveyance loss. Results showed that the two water resources had a common influence on water shortage. For a constant q, an increased joint probability means an increased crisis of water shortage, and more water shortage amounts would exist under lower q levels. Using this approach to research the impact of multi-water resources supply on agricultural shortage risk assessment is feasible. Overall, this model can help to reflect the uncertainty of agricultural using water. The study emphasizes the importance to improve and update transferring and local surface water management and relevant countermeasures in order to ensure future water security.

ACKNOWLEDGEMENTS

The research was supported by the National Science and Technology Support Program of China (2015BAB07B02), Science Fund for Creative Research Groups of the National Natural Science Foundation of China (Grant no. 51321065).

REFERENCES

Anstett-Collin, F., Mara, T. & Basset, M. (2014). Application of Global Sensitivity Analysis to a Tire Model with Correlated Inputs. *Simulation Modelling Practice and Theory*, 44, 54-62.

Li, Y. P., Huang, G. H., Nie, S. L. & Liu, L. (2008). Inexact Multistage Stochastic Integer Programming for Water Resources Management under Uncertainty. *Journal of Environmental Management*, 88(1), 93-107.

Mara, T. A. & Tarantola, S. (2012). Variance-Based Sensitivity Indices for Models with Dependent Inputs. *Reliability Engineering & System Safety*, 107, 115-121.

McKay, M. D., Beckman, R. J. & Conover, W. J. (2000). A Comparison of Three Methods for Selecting Values of Input Variables in the Analysis of Output from a Computer Code. *Technometrics*, 42(1), 55-61.

Nelsen, R.B. (1998). *An Introduction to Copulas (Lecture Notes in Statistics).* Optimal Mixture Experiments, 36.

Peng, D. Z. & Xu, Z. X. (2010). Simulating the Impact of Climate Change on Streamflow in the Tarim River Basin by using a Modified Semi-Distributed Monthly Water Balance Model. *Hydrological processes*, 24(2), 209-216.

Sklar, M. (1960). *Fonctions de Répartition À N Dimensions Et Leurs Marges*. Publinststatistunivparis, 8, 229-231.

Sun, W., Huang, G. H., Lv, Y. & Li, G. (2013). Inexact Joint-Probabilistic Chance-Constrained Programming with Left-Hand-Side Randomness: An Application to Solid Waste Management. *European Journal of Operational Research*, 228(1), 217-225.

Wang, D. (2006). Optimal Scheduling of Feeding Reservoir Based on Continuous Ant Colony Algorithm. *Water Resources & Power,* 24 (2), 77–78.

Yazdi, J., Lee, E. H. & Kim, J. H. (2014). Stochastic Multiobjective Optimization Model for Urban Drainage Network Rehabilitation. *Journal of Water Resources Planning and Management*, 141(8), 04014091.

Zeng, X. T., Li, Y. P., Huang, G. H. & Liu, J. (2015). Modeling Water Trading under Uncertainty for Supporting Water Resources Management in an Arid Region. *Journal of Water Resources Planning and Management*, 142(2), 04015058.

Zhou, Y., Guo, S., Xu, C. Y., Liu, D., Chen, L. & Ye, Y. (2015). Integrated Optimal Allocation Model for Complex Adaptive System of Water Resources Management (I): Methodologies. *Journal of Hydrology*, 531, 964-976.

Zhuang, X. W., Li, Y. P., Huang, G. H. & Zeng, X. T. (2015). An Inexact Joint-Probabilistic Programming Method for Risk Assessment in Water Resources Allocation. *Stochastic Environmental Research and Risk Assessment*, 29(5), 1287-1301.

